Online ISSN: 1920-3853

Vol. 11, No. 1, February 2017

Print ISSN : 1715-9997

Canadian Journal of pure & applied sciences

an International Journal

Published three times a year (Feb, June and Oct.)

SENRA
Academic Publishers
British Columbia

Print ISSN 1715-9997
Online ISSN 1920-3853

Volume 11, Number 1
February 2017

CANADIAN JOURNAL OF PURE AND APPLIED SCIENCES

The Canadian Journal of Pure and Applied Sciences (CJPAS) is a peer reviewed multi-disciplinary international journal aimed at promoting research in all field of science and technology on the basis of its originality. The CJPAS is indexed in major indexing databases of different indexing services and universities.

Every effort is made by the editors, board of editorial advisors and publishers to see that no inaccurate or misleading data, opinions, or statements appear in this journal, they wish to make clear that data and opinions appearing in the articles are the sole responsibility of the contributor concerned. The CJPAS accept no responsibility for the misleading data, opinion or statements.

The CJPAS is Abstracted/ Indexed in several indexing databases of different indexing services and universities.

Four Years Global Impact Factor
2012 2.657, 2013 2.756,
2014 2.845, 2015 2.988

Frequency:
3 times a year (Feb, June and Oct.)

Editorial Office
E-mail: editor@cjpas.ca, editor@cjpas.net

SENRA Academic Publishers
5919 129 B Street Surrey
British Columbia V3X 0C5 Canada
www.cjpas.net
E-mail: senra@cjpas.ca

Board of Editorial Advisors

The full text of all published articles published in Canadian Journal of Pure and Applied Sciences is also deposited in Library and Archives Canada which means all articles are preserved in the repository and accessible around the world that ensures long term digital preservation.

Member
CANADIAN ASSOCIATION OF LEARNED JOURNALS

Canadian Journal of pure&applied sciences

Volume 11, Number 1
February 2017

CONTENTS

LIFE SCIENCES

PHYSICAL SCIENCES

Canadian Journal of Pure and Applied Sciences
Vol. 11, No. 1, pp. 4053-4060, February 2017
Online ISSN: 1920-3853; Print ISSN: 1715-9997
Available online at www.cjpas.net

DISCRIMINATION OF MULTIDRUG RESISTANCE IN DIFFERENT OVARIAN CANCER CELLS USING A SINGLE-CELL BIOANALYZER

Haiyan Wang[1,2], Avid Khamenehfar[2], Michael Chung Kay Wong[2,4], James Lian Zhong Wang[4], *Paul Chi Hang Li[2,5], Da Zhou[3], Marinko Sarunic[3], Feng Feng[1], Hairong Cao[1] and King Leung Fung[5]
[1]Department of Chemistry and Environmental Engineering, Shanxi Datong University, Datong, Shanxi, China
[2]Department of Chemistry, Simon Fraser University, Burnaby, British Columbia
[3]School of Engineering, Simon Fraser University, Burnaby, British Columbia, Canada
[4] ZellChip Technologies Inc. Burnaby, British Columbia, Canada
[5]Laboratory of Cell Biology, Center for Cancer Research, National Cancer Institute, National Institutes of Health, Bethesda, Maryland, USA

ABSTRACT

A single-cell bioanalyzer (SCB) was presented to detect different ovarian cancer cells, i.e. to discriminate NCI/ADR-RES cells, which are multidrug resistant (MDR), from non-MDR OVCAR-8 cells. This discrimination has been achieved in the single-cell level by measuring drug accumulation in real-time, in which the accumulation is high in non-MDR single-cells without drug efflux, but is low in MDR single-cells with efflux. The SCB was constructed as an inverted microscope for optical imaging and fluorescence measurement of a cell that was retained in a microfluidic chip. The cell retained in the chip offers sufficient fluorescence signals for the SCB to measure the accumulation of daunorubicin (DNR) in a single ovarian cancer cell in the absence of the MDR inhibitor, cyclosporine A (CsA). The same cell allows us to detect the enhanced drug accumulation due to MDR modulation in the presence of CsA. The measurement of drug accumulation in a cell was achieved after it was captured in the chip, with the correction of background interference. The detection of accumulation enhancement due to MDR modulation by CsA was determined in terms of either the accumulation rate or enhanced amount of DNR in the same single-cell. It showed that with the effectiveness of efflux-blocking by CsA, DNR in a single-cell was increased by 3-fold against its same-cell control. For this single-cell bioanalyzer (SCB), it has the ability to discriminate MDR in different ovarian cells due to drug efflux in them by eliminating the interference of background fluorescence and by using the same-cell control.

Keywords: Single cell bioanalyzer, optical imaging, fluorescence measurement, microfluidic chip, same-cell control, multidrug resistance.

INTRODUCTION

It was proposed that highly integrated microdevices or microchips show great promise for basic biomedical and pharmaceutical research, and robust point-of-care devices could be developed for use in clinical settings (El-Ali *et al*., 2006). Since then, the microfluidic chip, which can be designed to contain features compatible with the size of human cells, has been used for the study of cell biology and analysis (Gómez-Sjöberg *et al*., 2007; Halldorsson *et al*., 2015; Lindström *et al*., 2010). Cell studies using microfluidic devices require low numbers of cell population down to a few hundred cells, or even a few cells, making it possible to measure perturbations of individual cells, increasing the spatial and temporal resolutions of the measurements for a given experimental setup. In 2008, the concept of same-single-cell analysis (SASCA) was proposed (Li *et al*., 2008), and the method was developed for the study of multidrug resistance (MDR) and its modulation in MDR cancer cells using real-time monitoring of drug efflux (Li *et al*., 2008), or of drug accumulation (Li *et al*., 2011), with the latter mode dubbed SASCA-A. Recently, this SASCA-A method was employed to measure drug accumulation and overcome MDR in murine melanoma B160VA cells (Khamenehfar *et al*., 2014a), human prostate 22Rv1 cells (Khamenehfar *et al*., 2015a), human leukemia patient cells (Khamenehfar *et al*., 2016) and non-small cell lung cancer H1650 cells (Khamenehfar *et al*., 2015b). In addition, to enhance drug accumulation, the SASCA method was used to identify various MDR modulators, such as the low-molecular-weight diblock copolymer, (Khamenehfar *et al*., 2014b), and ginsenosides (Chen *et al*., 2014).

*Corresponding author e-mail: paulli@sfu.ca

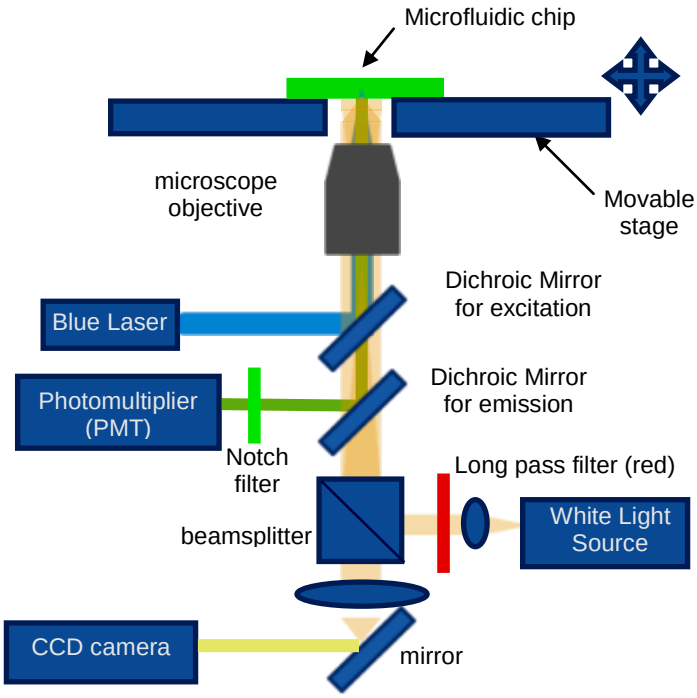

Fig. 1. Schematic diagram of the microscope-based single-cell bioanalyzer (SCB). The *microfluidic chip* is placed on a *movable stage*. There are 3 optical paths for the SCB conducting simultaneous optical imaging and fluorescence measurement of single-cells. The blue path represents the fluorescence excitation light provided by the *blue laser* and reflected on the *dichroic mirror for excitation* to pass through the *microscope objective* to excite drug molecules in a single-cell captured in the *chip*. The green path represents the fluorescence emitted from the drug molecules, which passed through the *microscope objective* and reflected on the *dichroic mirror for emission* to reach the *photomultiplier tube (PMT)* via a green *notch filter* for fluorescence measurement. The yellow path represents the red-colored light provided by the *white light source* and *long-pass filter* reflected on the *beam splitter* to the *chip*; then from the *chip* back and reflected on the *mirror* to the *CCD camera* for optical imaging.

In this study, the single cell bioanalyzer (SCB), which is an inexpensive and sensitive optical imaging/fluorescence measurement system, has been developed to measure multidrug resistance (MDR) in ovarian cells, discriminating the drug accumulation in these cells by using and not using cyclosporine A (CsA). A schematic diagram of the microscope-based imaging/measurement system of SCB is depicted in Figure 1. With the deduction of background fluorescence interferences accomplished by a previously reported method (Peng and Li, 2005), the corrected cellular fluorescence signals significantly distinguish drug accumulation between the test cell and its "same-cell control" in a convenient and fast manner. The optical parts and electronic components in the SCB are assembled with the mechanical parts that are fabricated in plastics by a 3-D printer, as depicted in Figure 2.

In terms of MDR, it is known that the permeability-glycoprotein (P-gp), a 170-kDa transmembrane drug transporter protein located in the cell membrane, plays a major role in cellular MDR (Sharom *et al*., 2008). This is resulted via the efflux of different classes of chemotherapeutic agents or drugs, lowering the accumulation of drugs in the cancer cells and hence reducing the effectiveness of chemotherapy (Thomas and Coley, 2003; Li *et al*., 2016). Cyclosporine A (CsA), which typically inhibits P-gp by interacting with its drug-binding domain (Marquez and Van Bambek, 2011), has been selected to enhance the accumulation of P-gp substrates in cancer cells in our experiments.

Using the single-cell bioanalyzer (SCB), we measured drug accumulation in the drug-resistant ovarian carcinoma cells (NCI/ADR-RES) and its parental control (OVCAR-8) quantitatively in a one hour time-frame. The electronic signals that are related to the fluorescence intensities of the single cancer cells significantly distinguish between two lines of ovarian cells, and by this real time

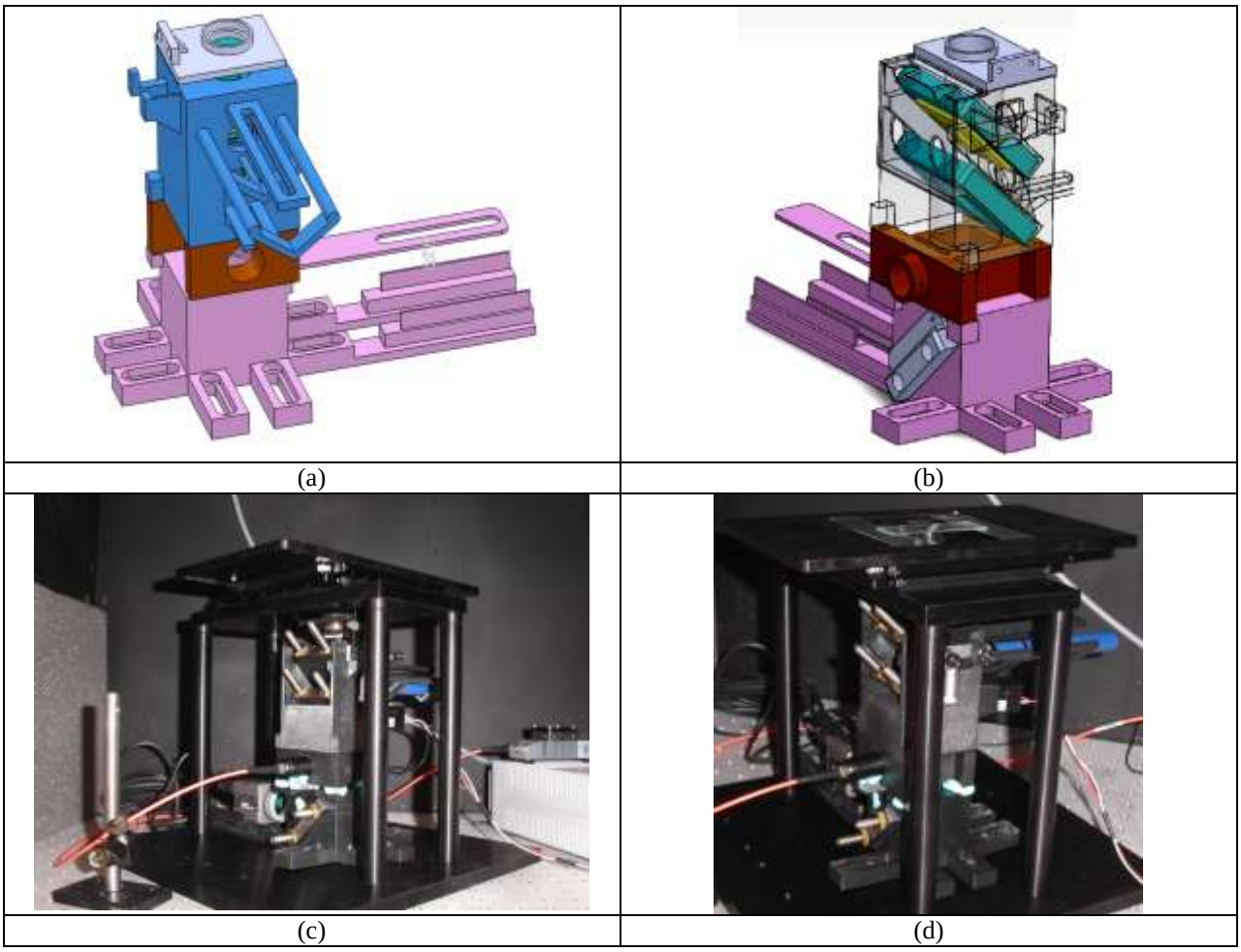

Fig. 2. Assembly of 3D-printed parts and optical/electronic parts. (a) and (b) are Solidworks drawing at two viewing angles to show the 3D-printed objective holder (grey), dichroic mirror holder (blue), beam splitter holder (brown) and holder for mirror and camera (purple). (c) and (d) are images showing the experimental set up that includes the 3D-printed plastic parts and associated optics and electronics as depicted in Figure 1. (c) reveals more clearly the camera, white light source with optical fiber (orange) and two dichroic mirrors; whereas (d) shows the chip, microscope objective and laser (blue) in a better viewing angle. The two dichroic mirrors and camera mirror are located on their respective mirror mounts with two thumb-adjustable screws.

monitoring system, the fluorescence drug's accumulation in single-cells could be quantified.

MATERIALS AND METHODS

Chip design

The layout of the microfluidic chip was designed using L-Edit (Tanners), and the chip design was sent to a printer (Coles Lithoprep) which produced the photomask on a plastic film. The microfluidic chip was made of polydimethylsiloxane (PDMS). As shown in the schematic diagram and image in Figure 3, the chip is composed of three channels, three reservoirs, and one chamber containing a cell retention structure. This chip was different from the ones described previously (Li *et al*., 2008; Li *et al*., 2011) in that it was made of polymeric plastics and it was simplified with two reservoirs less, making this new chip easier for the user to control the flow of reagents and capture the cells.

Reagents

Daunorubicin (DNR), calcein-AM ester (CaAM), cyclosporine A (CsA) and penicillin were obtained from Sigma-Aldrich (St Louis, MO). Fetal bovine serum (FBS) was obtained from ATCC (Manassas, VA). All reagents were of analytical grade.

Cell culture

Human ovarian carcinoma cell lines: NCI/ADR-RES and OVCAR-8 were generously provided by Michael M.

Gottesman of National Cancer Institute (NCI), USA. NCI/ADR-RES is an ovarian cell line, though its origin was previously mistaken as breast cancer (Ke *et al*., 2011). OVCAR-8 is the non-MDR parental control. All cell lines were cultured in RPMI 1460 medium supplemented with 10% fetal bovine serum, 2 mM L-glutamine, 100 I.U./mL penicillin, 100 µg/mL streptomycin in a 24-well cell culture plate (Greiner Bio One, Germany), and incubated at 37 °C and 5% CO_2. For cell passaging, confluent cells were washed with phosphate buffered saline (PBS) and incubated with 0.1% EDTA (Sigma) for detachment.

The single cell bioanalyzer (SCB)

The single cell bioanalyzer (SCB) was constructed by a microscope for optical imaging and fluorescence measurement of a cell, see Figure 1 and 2. The optical system (see Fig.1) has been employed for simultaneous fluorescence measurement and bright-field observation/imaging. The excitation light was provided by the blue laser, which was confirmed not to be critical to impact the cell membrane's permeability. The cell was captured in a microfluidic PDMS chip (Fig. 3). Figure 4 depicts the screenshots from the animation showing the principle of operation of the SCB. Briefly, when a group of cells is introduced into the single-cell chip, a desired cell is selected and retained near an arc slope opposite to a reagent channel of the chip. The cell's motion and selection was accomplished by using the hydrodynamic liquid flow. Reagents can be continuously delivered and switched. The measured voltage data were recorded by the Labview software. The cellular fluorescence intensity should be stable before the reagents were switched.

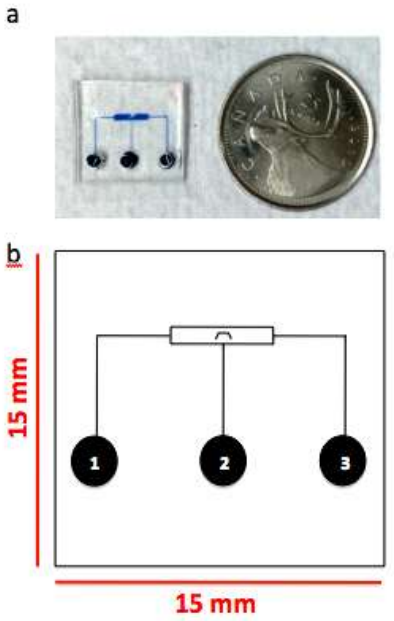

Fig. 3. The microfluidic chip consists of 3 solution reservoirs and 1 central chamber consisting of a cell retention structure. (a) The image shown a chip that is made of a 15mm×15mm (PDMS) slab that was sealed to a 0.17mm-thick glass slip. (b) The chip layout diagram shows the cell inlet reservoir 1, reagent reservoir 2, and waste reservoir 3 reach the microfluidic chamber that consists of a cell retention structure.

On-chip drug accumulation study on the same single cell

Calcein-AM ester (CaAM; λ_{ex}=470 nm; λ_{em}=535 nm) and daunorubicin (DNR; λ_{ex}=470 nm; λ_{em}=585 nm) were used as P-gp substrates for drug accumulation measurement.

Before use, the microfluidic chip was cleaned by LiquiNOX detergent, rinsed with purified water, and sterilized with 75% ethanol. When the cells were introduced from the left reservoir, they flowed from the left channel to the right. By adjusting the liquid levels of these reservoirs, a single cancer cell was led into the cell retention structure.

In order to identify DNR concentration in the cell, the effect of known amount of DNR standards were first tested in the cancer cell. After one cancer cell was selected and retained in the cell retention structure in the chip, cell media in all the reservoirs were removed, and then the drug inlet reservoir was filled with 5 µM DNR. Fluorescence measurement was started to monitor the increase in fluorescence intensity due to DNR accumulation in the cell. After the fluorescence intensity became stable, the procedure was repeated by treatment of the cell with DNR of higher concentrations (20, 35, 50, 65, and 80 µM). Since the fluorescence intensity was considered high enough at 35 µM, subsequent single-cell experiments were carried out at this DNR concentration.

For experiments, the key step was to measure the accumulation of the anticancer drug (i.e., DNR) in the absence and presence of the P-gp inhibitor, CsA. Different DNR concentrations were tested for measurements in the cell and outside the cell in the chip. To complete this function, the position of the chip was precisely controlled by a robotic arm to move the chip back and forth in three selected detection sites. Detection site 1 was on the PDMS chip wall; site 2 was focused on the chamber, in which the extracellular fluorescence intensity was detected; site 3 is on the cell, which provided the total fluorescence intensity. In principle, the fluorescence intensity from the PDMS chip wall should be zero. The fluorescence from detection site 2 was set as background. After deducting the background from the total fluorescence (measured from detection site 3), this corrected value was set to represent the amount of DNR accumulated in the cell.

RESULTS AND DISCUSSION

After ovarian cancer cells are introduced in the cell inlet

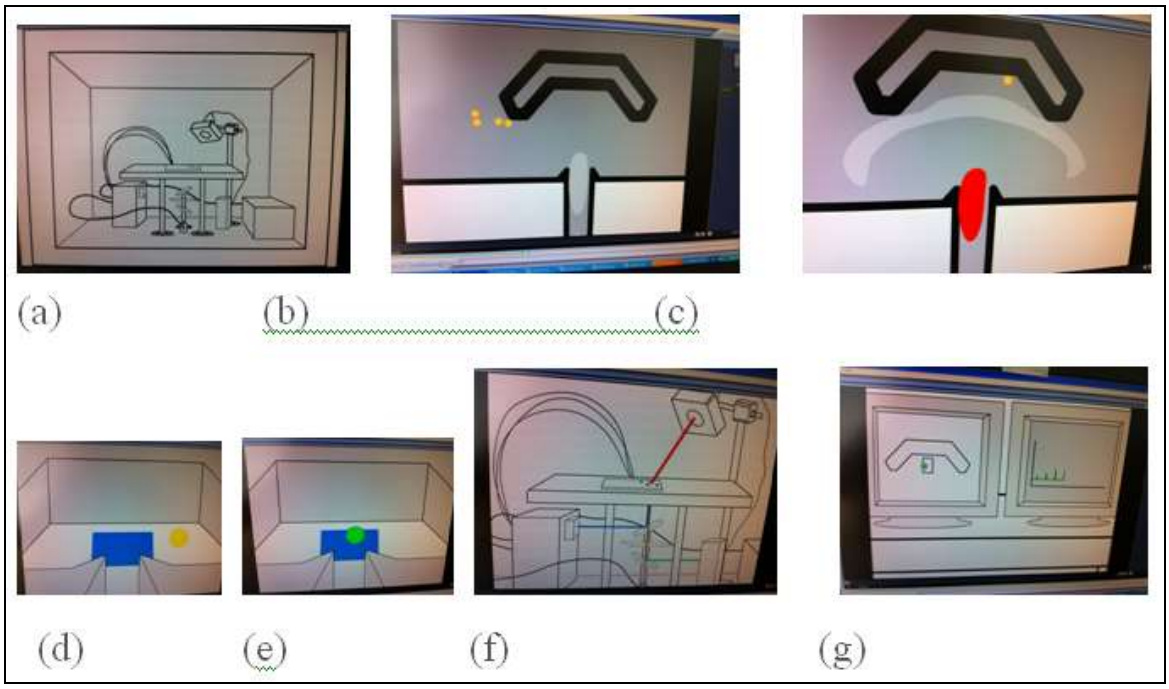

Fig. 4. Screen-capture of an animation illustrating the principle of operation of the single cell bioanalyzer (SCB) instrument. (a) overview of SCB with a single-cell chip placed on the movable stage (b) a group of 4 cells (yellow) arrived at the cell retention structure in the chip (c) a single-cell (yellow) was selected in the microfluidic flow (in grey) and the flow of drug (in red) was delivered to the cell (d) the background was measured when the cell (yellow) was moved outside the excitation region (blue) (e) the cell with the drug became fluorescent (green) when it was moved inside the excitation region (blue) (f) simultaneous fluorescence measurement (green) and optical imaging (red) occurred (g) optical image was shown on the left computer screen and fluorescence measurement shown on the right. For the video chip of this animation, see supplementary information.

reservoir in the microfluidic chip, Figure 4 depicts how the cell is selected and captured in the chip, and how the SCB is used to conduct simultaneous optical imaging and fluorescence measurement of the captured cell in the chip. Briefly, when a group of cells is introduced into the single-cell chip, a desired cell is selected and retained in the cell retention structure opposite to a reagent channel of the chip. Then, reagents can be continuously delivered and switched to treat the cell, and fluorescence measurement data are being recorded by the Labview software.

Figure 5 indicates the measurement of CaAM accumulation in the OVCAR-8 single-cell which does not express P-gp. After CaAM ester entered the cell, it was hydrolyzed to generate calcein. While the cell and the surrounding background are measured successively, the peaks and baseline are recorded. The baseline indicates the extracellular CaAM and the peaks represent the accumulated calcein after it was formed in the OVCAR-8 cell. The peak heights continue to increase until saturation and this occurs without using any MDR modulator, indicating that efflux due to P-gp does not occur in the cell, and the cell is non-MDR.

On the other hand, a P-gp expressing cell such as NCI/ADR-RES was measured. Figure 6 a, b and c indicate the image of a single NCI/ADR-RES cell captured in the retention structure of the chip before experiment, during experiment and after experiment, respectively. No matter how long the chip was moved for how many times, detection site 3 should always measure the cell, and the positions of these sites should never change. The distance among these three sites is more than 10 μm but less than 50 μm. During a cycle of 120 s, the chip was consecutively moved to detection sites 1, 2 and 3 to complete the fluorescence measurement on the PDMS background, outside the cell, and in the cell, respectively. We have demonstrated that the single-cell chip should have a wide and flat region for effective cell scanning and successful background correction.

The effect of cyclosporine A (CsA) on cancer cells in the SCB was determined. After one ovarian cancer cell was captured in the retention structure, the cell media in all the reservoirs were removed, and then the cell was first treated with DNR (35 μM) in the absence of CsA for about 1400 s for drug accumulation (control). Thereafter, the same cell was treated with a solution of 35 μM DNR

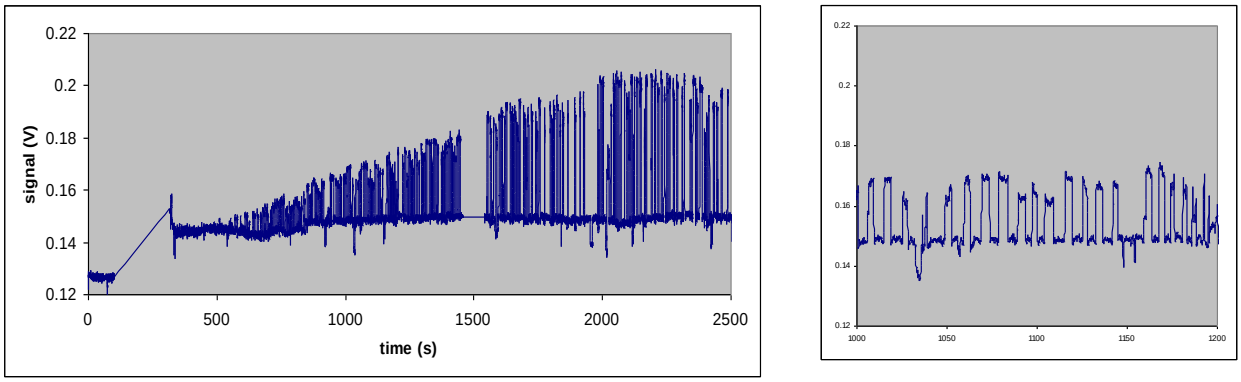

(a) (b)

Fig. 5. Measurement of a single non-MDR OVCAR-8 cell when calcein-AM (CaAM, 1 μM) is being accumulated. (a) fluorescence signal plotted against time, with DNR (35 μM) added (at 140 s); (b) expansion of graph in (a) during 1000-1200 s, showing the peaks (total fluorescence) and baseline (background interference due to extracellular DNR). The peaks keep increasing to a plateau when calcein is being accumulated in the non-MDR cell until saturation.

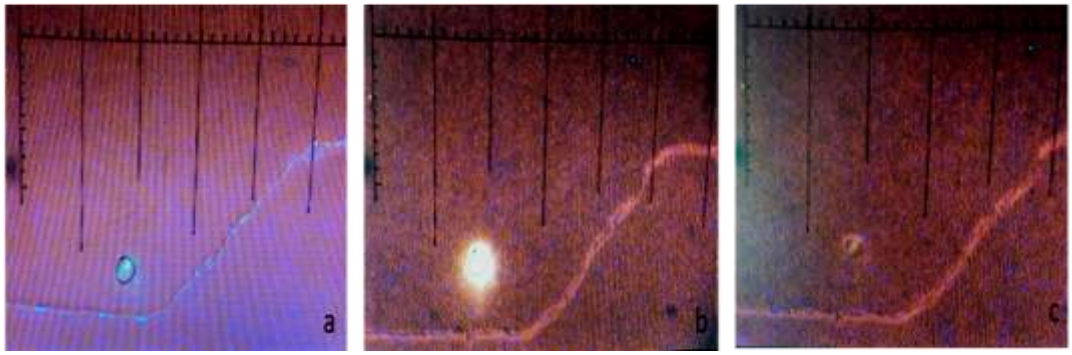

Fig. 6. Images of one P-gp expressing ovarian cancer cell (NCI/ADR-RES) retained in the cell retention structure of a microfluidic chip (a) after DNR (35 μM) was added (at 200 s); (b) after CsA (5 μM) together with DNR (35 μM) were added (at 1400 s); (c) after trypan blue was introduced to treat the cell when the test ended (at 3400 s). After CsA was added together with DNR, the cell turns brightly fluorescent (b), and since the cell was not stained after the test (c), it was still viable after measurement. The times listed can be referred to in Figure 7 which depicts the measurement data. The scale was marked on the screen for cell size measurement, with the smallest graduation indicating 10 μm.

containing 5 μM CsA (experiment). As the modulator has a positive effect, a higher drug accumulation is observed instantly; this enhancement is depicted as a bright cell in Figure 6 b and a high transition in the correction signal in Figure 7. It means that with the help of CsA, more DNR is accumulated in the cell than its control. From the corrected signal in Figure 7, the intracellular DNR concentration of the single NCI/ADR-RES cell was determined to increase by 3 folds against its same-cell control, i.e. 0.025/0.008 = 3.

The observation of CsA in enhancing the DNR accumulation was consistent with our previous studies by SASCA (same-single-cell analysis). With every test cell having two identities, one is the test cell, and the other is its same-cell control, this method allows background correction, which remove interference, essentially eliminating the effect of electrical noise and extracellular solution fluctuations.

This SCB instrument had completed the imaging analysis with simultaneous DNR accumulation measurement, and it also showed the effectiveness of MDR modulation by CsA, overcoming MDR in ovarian cells. Moreover, the collection of time-dependent fluorescence data can help understand the kinetics of drug accumulation in MDR cancer cells, without long-time and tedious tissue culture conducted conventionally.

CONCLUSION

In this study, it is found that the SCB is useful for the measurement of cellular fluorescence, which is unaffected by the presence of reagent switch and buffer fluctuations. Such a single-cell fluorescence measurement may have a potential to provide information about the response of ovarian cancer patient cells to chemotherapeutic drugs.

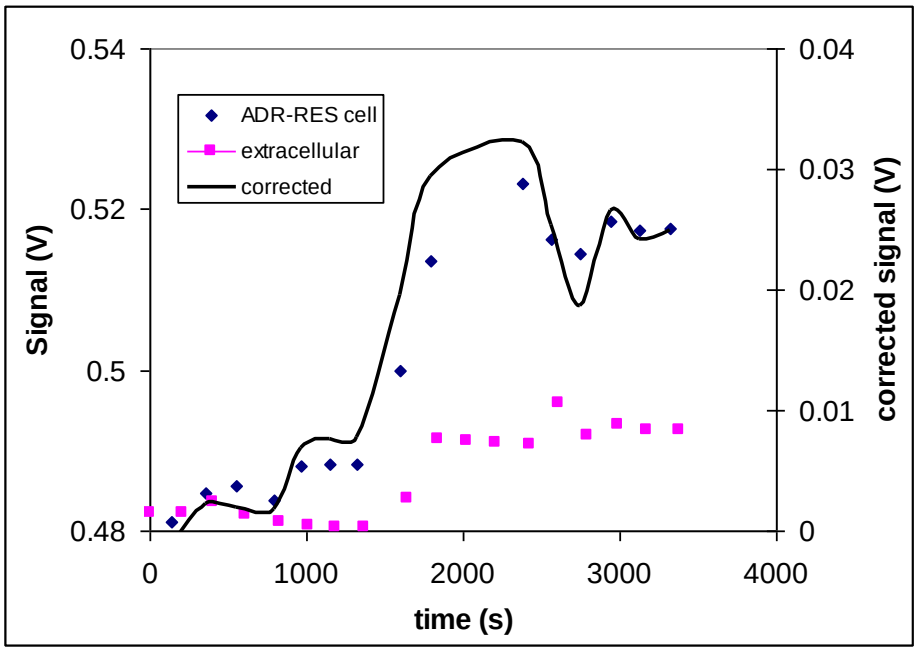

Fig. 7. DNR accumulation measured in a single P-gp expressing ovarian cancer cell (NCI/ADR-RES). The fluorescence intensity of DNR during its accumulation in the cell is plotted against time. At 1400 s, CsA (5 μM) together with DNR were added in the chip. Blue dots indicate the fluorescence intensity due to intracellular DNR, and pink dots represent the fluorescence intensity of extracellular DNR. The blue dots reach the first plateau at about 0.48 V after 1000 s and the second one at about 0.51 V after 3000 s. The corrected signal, which is obtained by subtracting the pink dots from the blue dots, is depicted as a black line, showing 0.008 V at 1300 s, and 0.025 V at 3300 s. The fold increase of DNR accumulation enhancement due to CsA is estimated by 0.025/0.008 = 3.

ACKNOWLEDGEMENTS

We are grateful to CMC Microsystems, Simon Fraser University, and Natural Sciences and Engineering Research Council (NSERC) of Canada for funding. We thank Justine Shillibeer for preparing the animation. We also thank Lukas-Karim Merhi, Eric Petersen, Byron Lim Yolanda Wu, Milad Bonakdar, Wilson Chim, Yueying Li and Scott Luu for technical assistance. We acknowledge the financial supports from NSFC of China (No. 21375083), training project of Shanxi University students' innovation and entrepreneurship (No. 2015348), and Shanxi Datong University (No. 2008K3).We thank Michael M. Gottesman and Suresh V. Ambudkar from the National Cancer Institute, National Institutes of Health, USA, for their support in this study. This research was also supported by the Intramural Research Program of the National Institutes of Health, Center for Cancer Research.

REFERENCES

Chen, YC., Kolesnyk, I., Li, PCH., Yue, PYK. and Wong, RNS. 2014. Microfluidic Single Cell Bioanalysis to measure drug uptake on single multidrug resistant cancer cell as enhanced by ginsenoside Rg 3. Proceedings of Science Plus International Conference, Nov. 14-15, 2014, Hong Kong. pp. 5-7.

El-Ali, J., Sorger, PK. and Jensen, KF. 2006. Cells on chips. Nature. 442(27):403-411.

Gómez-Sjöberg R., Leyrat AA., Pirone, DM., Chen, CS. and Quake, SR. 2007. Versatile, Fully Automated, Microfluidic Cell Culture System. Anal. Chem. 79(22):8557-63.

Halldorsson, S., Lucumi, E., Gmez-Sjberg, R. and Fleming, RMT. 2015. Advantages and challenges of microfluidic cell culture in polydimethylsiloxane devices. Biosens. Bioelectron., 63:218-231.

Ke, W., Yu, P., Wang, J., Wang, R., Guo, C., Zhou, L., Li, C. and Li, K. 2011. MCF-7/ADR cells (re-designated NCI/ADR-RES) are not derived from MCF-7 breast cancer cells: a loss for breast cancer multidrug-resistant research. Med. Oncol. Suppl 1:S135-41.

Khamenehfar, A., Wang, HY., Li, PCH., Schmidt, C. and Lopez, A. 2014[a]. Drug resistance of a single mouse melanoma cell and its interaction with a mouse dendritic cell studied using the microfluidic single cell bioanalyzer. 6th International Symposium on Microchemistry and Microsystems, Jul 30-Aug 1, Singapore. pp. 1-2.

Khamenehfar, A., Wan, CPL., Li, PCH., Letchford, K. and Burt, HM. 2014[b]. Same-single-cell analysis using the microfluidic biochip to reveal drug accumulation enhancement by an amphiphilic diblock copolymer drug formulation. Anal. Bioanal. Chem. 406:7071-7083.

Khamenehfar, A., Beischlag, TV., Russel, P., Ling, P., Nelson, C. and Li, PCH. 2015[a]. Label-free Isolation of a Prostate Cancer Cell among Blood Cells and the Single-Cell Measurement of Drug Accumulation Using an Integrated Microfluidic Chip. Biomicrofluidics. 9, 064104:1-18.

Khamenehfar, A., Li, PCH. and Leung, ELH. 2015[b]. Gefitinib enhanced cancer drug uptake in the same single non-small cell lung cancer cells observed in real-time in the microfluidic biochip. 2nd International Biotechnology, Chemical Engineering & Life Science Conference, July 20-22, 2015, Hokkaido, Japan. pp. 1-3.

Khamenehfar, A., Maher G., Chen, YC., Donna, H. and Li, PCH. 2016. Dielectrophoretic Microfluidic Chip Enables Single-Cell Measurements for Multidrug Resistance in Heterogeneous Acute Myeloid Leukemia Patient Samples. Anal. Chem. 88:5680-5688.

Li, XJ., Ling, V. and Li, PCH. 2008. Same-single-cell analysis for the study of drug efflux modulation of multidrug resistant cells using a microfluidic chip. Anal. Chem. 80:4095-4102.

Li, XJ., Chen, YC. and Li, PCH. 2011. A simple and fast microfluidic approach of same-single-cell analysis (SASCA) for the study of multidrug resistance modulation in cancer cells. Lab Chip. 11:1378-84.

Li, W., Zhang, H., Assaraf, YG., Zhao, K., Xu, X., Xie, J., Yang, D. and Chen, Z. 2016. Overcoming ABC transporter-mediated multidrug resistance: Molecular mechanisms and novel therapeutic drug strategies. Drug Resistance Updates. 27:14-29.

Lindström, S. and Andersson-Svahn, H. 2010. Overview of single-cell analyses: microdevices and applications. Lab Chip. 10(24):3363-72.

Marquez, B. and Van Bambek, F. 2011. ABC multidrug transporters: target for modulation of drug pharmacokinetics and drug–drug interactions. Curr. Drug Targets. 12:600-620.

Sharom, FJ. 2008. ABC multidrug transporters: structure, function, and role in chemoresistance. Pharmacogenomics. 9(1):105-127.

Peng, XY. and Li, PCH. 2005. Extraction of pure cellular fluorescence by cell scanning in a single-cell microchip. Lab Chip. 5:1298-1302.

Thomas, H. and Coley HM. 2003. Overcoming multidrug resistance in cancer: an update on the clinical strategy of inhibiting p-glycoprotein. Cancer Control. 10(2):159-165.

Received: Dec 27, 2016; Jan 20, 2017

Canadian Journal of Pure and Applied Sciences
Vol. 11, No. 1, pp. 4061-4066, February 2017
Online ISSN: 1920-3853; Print ISSN: 1715-9997
Available online at www.cjpas.net

DETERMINATION OF TIME OF INSECTICIDE APPLICATION AGAINST POTATO TUBER MOTH, *PHTHORIMAEA OPERCULELLA* ZELLER (LEP.: GELECHIIDAE) IN THE FIELD CONDITIONS IN TURKEY

*Pervin Erdogan[1] and Errol Hassan[2]
[1]Plant Protection Central Research Institute, 06172 Yenimahalle, Ankara, Turkey
[2]School of Agriculture and Food Sciences, University of Queensland, Gatton 4343, Queensland, Australia

ABSTRACT

The aim of this study was to determine the time of pesticides application to control potato tuber moth [*Phthorimae operculella* (Zeller) (Lep.: Gelechiidae)] in Turkish field conditions. For this purpose, the experiments were carried out in three provinces (Afyonkarahisar, Kirsehir and Bolu) of Turkey in 2013–2015. Sex pheromone traps were used to determine when adults first emerged in field and were checked at weekly intervals. During the experiments, all of the plant leaves and tubers were checked to determine any infestations. Three insecticides were used to determine against PTM. Five different pesticide schedules were tested although not in all provinces. In Bolu Province, the best schedule was achieved by a three spray technique with the first spray application being applied when adults are first identified in the field in pheromone traps, followed by a second application one month after the first application, with a third spraying 15 days before harvest. This schedule was no tested in Kirsehir and Afyonkarahisar Provinces where applications linked to pheromone trap detections and preharvest schedules were most effective.

Keywords: Potato tuber moth, application time, pheromone traps, insecticides.

INTRODUCTION

Potato (*Solanum tuberosum* L.) as a crop plant of international importance is subject to yield and quality losses by arthropod pests.Potato tuber moth (PTM) [*Phthorimae operculella* (Zeller) (Lep.: Gelechiidae)] especially causes the greatest losses. Currently PTM occurs wherever potatoes are cultivated and it is destructive especially under dry conditions in the warmer seasons. PTM also attacks tobacco (*Nicotiana tabacum* L.), tomato (*Solanum lycopersicum* L.), eggplant (*Solanum melongena* L.), Cape gooseberry (*Physalis peruviana* L.) and certain other broad-leaved weeds (Cunningham, 1969).

Fertilized female PTM lay eggs on foliage or tubers throughout the growing season, preferring foliage over tubers. When foliage has naturally or artificially senesced and tubers accessible, they deposit eggs in or near the eye buds. The larva mine leaves, stems, and petioles causing irregular galleries and excavate tunnels through tubers. Foliar damage to the potato crop usually does not result in significant yield losses. However infested tubers have reduced marketability and the losses in storage may be up to 100% especially in non-refrigerated systems (Nasser *et al*., 2012; Von *et al*., 1987; Bacon *et al*., 1971). Greatest tuber damage occurs immediately before harvest while the crop is left in the field prior to digging. Additional damage may occur in the storage if conditions are not maintained properly (Rondon *et al*., 2007; Rondon, 2010).

PTM control primarily relies on the use of insecticides to optimize production and minimize damage. Great benefits can be derived from insecticides if used judiciously, practically under emergency situations. Pesticide use must be scheduled appropriately to avoid the unnecessary applications. Well managed pesticide application also minimizes the development of resistance to pesticides, persistence of residues in food, emergence of new pests, destruction of beneficial organisms, human exposure and environmental contamination (Arnason *et al*., 1989).

To eliminate the negative effects of insecticides, researchers have conducted a number of studies to create an alternative to insecticides against PTM. For example, Steven *et al*. (2008) reported that *Bacillus thuringiensis* spp. kurstaki and granulovirus were significantly effective on PTM. Similarly, it was determined that granulovirus may be used to control Potato tuber moth under field conditions (Salah and Aalbu, 1992; Sporleder *et al*., 2005; Sporleder and Kroschel, 2008; Das, 1995; Chandel and Chandla, 2005). Additionally, researchers found that

*Corresponding author e-mail: pervinerdogan@gmail.com

Neem treatments afforded protection at acceptable levels against PTM in storage for several months (Hossein *et al*., 1994; Debnath *et al*., 1998) and Neem oil was as effective as the insecticide (Salama and Salem, 2000). Additionally, Gomaa and El-Nenaey (2006) also found that the application of Virotecto or GV infected larvae more effectively controlled PTM infestation than Bt-based insecticides. Abdel *et al*. (2014) reported that the application with Neem formulation could effectively reduce the PTM population. The main objective of this study was to determine the time of insecticide application against PTM under field conditions in Turkey.

MATERIALS AND METHODS

Experiments were carried out in three provinces in Turkey during 2013-2015. The potato fields were divided into randomized plots of 50 m^2. The experiments were made four times. The plots were equally assigned as either control or treatment. Sex pheromone traps were used to determine when adults first emerged in the field. Five pesticide application schedules were selected for evaluation. Three insecticides were used (Table 1).

Treatments were applied to in the fields in the morning. No other insecticides were used. Only water was sprayed into the control plot. The fields were irrigated weekly with a channel system. Each plot contained approximately 65 plants, producing 300 tubers. The five application schedules were as follows.

Schedule 1: One pheromone trap was placed onthe experiment field. It was checked weekly. When 15 to 20 adult PTMs were found on the pheromone trap, insecticides were sprayed. Depending on the plant's vegetation period, spray applications were carried out on all the plant and the soil surface (following Anonymous, 2010).

Schedule 2: Spray applications were made twice, one week and two weeks before the harvest. At this stage, all of the plant and the soil surface were subjected to spraying (following Salah and Aalbu, 1992).

Schedule 3: Spray applications were made 34 and 96 days after the emergence of the plants (following Steven *et al*., 2008).

Schedule 4: Spray applications were made when tubers were 4-5 cm in diameter (Rondon, 2010).

Schedule 5: Spray applications were made when the first adult was found in the trap, the first spray was applied and it was followed by a second spray one month later and a third spray 15 days prior to the harvest (Sannino *et al*., 2012).

During the course of the experiment, all of the plants and tubers were observedfrom each plot every week by the following parameters: (a) number of leaves and or stem with PTM damage, (b) number of tubers with visible PTM infestation, (c) number of tubers exposed, by soil cracking, to the sun and showing green chlorophyll areas. Potato tuber samples were gathered from the border areas of plots. At the harvest, PTM damage was assessed on 100 tubers per plot, harvest samples were taken only within the central 14 m^2 of the plots. Hundred tubers were selected as randomized from each application. These tubers were put in reinforced paper bags. Then they were placed in the laboratory and held at ambient temperature. The tubers which was found in the in reinforced paper bags were examined to determine damage of PTM. Observations were made at 10, 20 and 30 days intervals after storage. The number of tubers infested and no damage were recorded. The percentages tubers damaged by PTM after each treatment were compared to control. Effect was calculated according to Abbott (1925). The rate infestation of tubers were determined. Statistical analyses were conducted according to the SPSS program.

RESULTS AND DISCUSSION

Studies in Afyonkarahisar province

The pheromone trap was placed after plant emergence in the experiment field on 02.05.2013. The number of adult PTM determined on pheromone traps is presented in Table 2. First PTM adults emerged on 16.05.2013 and the highest number of adults appeared on 06.08.2013.

The results of experiments of insecticide applications are presented in Table 3. The highest the rate of infestation was 15.25% in the control. In spinoteram, the highest rate of infestation was 8.5% for schedule four. The lowest of rate infestation was obtained in schedule one. In deltamethrin treatment, infestation rates remained during the entire trail. Therefore a statistical analysis was performed only with the data obtained from the spinotoram applications. The highest rate of infestation was at schedule one.

Table 1. The name of the insecticides used

Commercial name	Active substance name and rate	Recommended dose
Radiant 120 SC	Spinetoram 120 gr/l	25 ml/1000 m^2
Coragen 20 SC	Chlorantraniliprole 200 g/l	20 ml/1000 m^2
Decis 2.5 EC	Deltamethrin 2.5 g/l	30 ml/1000 m^2

Table 2. The number of adults *Phthorima eoperculella* determined on pheromone trap and the dates of records in Afyonkarahisar province (2013).

Dates	The number of adults
16.05.2013	2
23.05.2013	4
27.05.2013	8
05.06.2013	5
14.06.2013	6
22.06.2013	6
30.06.2013	8
02.07.2013	25 (1. Spraying)
16.07.2013	18 (2. Spraying)
24.07.2013	5
01.08.2013	11
06.08.2013	29 (3. spraying)
13.08.2013	13
20.08.2013	12
29.08.2013	28 (4.spraying)
05.09.2013	23 (harvest)

Studies in Kirsehir province

The number of adult PTM detected in the pheromone trap are given in Table 4. The first PTM adult emerged on 05.06.2014. The highest number of adults was observed on 31.07.2014. The number of adults was below 15-20. Therefore spraying was not conducted during schedule one.

Table 4. The number of adults *Phthorima eoperculella* determined on pheromone trap and the dates of records in Kirsehir province (2014).

Dates	Thenumber of adults
25.04.2014	0
02.05.2014	0
11.05.2014	0
26.05.2014	0
05.06.2014	2
16.06.2014	8
23.06.2014	3
30.06.2014	4
08.07.2014	5
15.07.2014	7
22.07.2014	10
31.07.2014	11
10.08.2014	9
17.08.2014	7

The results of applications conducted are given in Table 5. The highest infection rates were in the control (11.77%). The spinotoram treatment had the lowest and the highest infection rates and effect were in schedule four. The chlorantraniliprole treatment also had the lowest and the highest infection rates and effects took place during schedule four. There was no significant difference in schedules between spinetoran and chlorantraniliprole treatments. Application times were important. While there was no difference between schedule two and schedule

Table 3. The rate of infestation (%) and effect (%) obtained from the experiments of *Phthorima eoperculella* in Afyonkarahisar province (2013).

The time of applications	Treatment			
	Spinetoram 120 gr/L		Deltamethrin 2,5 g/l	
	The rate of infestation (%)	Effect (%)	The rate of infestation (%)	Effect (%)
Schedule one (15-20 number of adults /per trap)	4.25	71.74±5.05a	8.75	42.56
Schedule two (Before two weeks harvest and one week)	5.75	61.57±3.09ab	8.50	44.66
Schedule three (After 34-96 days after plant emergence)	7.5	50,85±3.73 bc	9.00	43.69
Schedule four when tubers were 4-5 diameter cm	8.5	43.87±6.90 d	8.75	40.90
Control	15.25		15.25	

F=6.243; p=0.008

Table 5. The rate of infestation (%) and effect (%) obtained from the experiments of *Phthorimae operculella* in Kirsehir Province (2014).

The time of applications	Treatment			
	Spinetoram 120 gr/l		Chlorantraniliprole 200 g/l	
	The rate of infestation (%)	Effect (%)	The rate of infestation (%)	Effect (%)
Schedule two (One and two weeks before harvest)	7.00	39.97b	5.25	54.61 b
Schedule three (34-96 days after plant emergence)	6.25	46.95 b	7.50	35.26b
Schedule five (first adult trap, one month later, 15 days prior to harvest)	3.00	76.61a	2.50	81.09a
Control	15.25		15.25	

F=80,182; p=0,00

three, there was a large effect in schedule four for both spinetoran and chlorantranilip role.

Studies in Bolu province

Data on the number of adults PTM determined on pheromone trap are given in Table 6. The results clearly indicate that first adults of PTM emergency the date of 28.06.2015. The highest number of adults was on the date of 20.07.2015. It was noticed that the number of adults was less than 15-20. Therefore spraying was not conducted in application one. Statically analysis was performed by t-test at a rate of tuber infection.

Table 6. The number of adults *Phthorima eoperculella* determined on pheromone trap and the date of recorded Bolu province (2015).

Dates	Thenumber of adults
28.06.2015	3
05.07.2015	4
13.07.2015	4
20.07.2015	5
27.07.2015	1
03.08.2015	3
10.08.2015	4
17.08.2015	3
24.08.2015	4

The results given Table 7 indicated that the highest infection rate was in control. The smallest infestation rate was in schedule five.

According to observation of weekly intervals, it was determined that there were no infestation on leaves, stem and tubers visible with PTM damage. Moreover, it was found that there were few number of tubers exposed, by soil cracking, and to the sun and showing green chlorophyll areas.

When 15-20 adults/week/trap was detected, four different applications were conducted against PTM during the period of potato in the Province of Afyonkarahisar. It determined that the highest effect was in schedule one (15-20 adult/week/trap) to control PTM.

According to the results obtained from the applications in Afyon karahisar and Kirsehir, because schedule two and schedule three resulted in the lowest effects, these applications were not conducted in Bolu.

Experiments carried out in Kirsehir and Bolu found that the first spraying should occur when adults were first identified in the field in the pheromone traps followed by the second application, one month after the first application, with a third spraying 15 days before the harvest. These results are consistent with the findings reported by Anonymous (2010), who observed that the highest effect was during schedule one (15-20 adult/week/trap) to control PTM. However, this schedule was not as successful in Kirsehir and Bolu as in the experiments conducted in Afyonkarahisar, because the number of adult pheromone traps were below 15-20 adult/week/trap. Therefore, it was determined that schedule one (15-20 adult/week/trap) may not be appropriate in field conditions to control PTM in Turkey. Similarly, schedule two and schedule three were determined to be unsuccessful in field conditions to control PTM. However, Rondon (2010) revealed that these applications were successful in field conditions to

control PTM. Salah and Aalbu (1992) observed that schedule five was successful in field conditions to control PTM. However, this method appeared not successful in the experiments in Kirsehir and Bolu Provinces.

The studies were conducted in three provinces in Turkey, Afyon karahisar, Kirsehir and Bolu. According to the Bolu and Kirsehir results, we recommend that the first spraying should occur when adults were first identified in the field in the pheromone traps followed by the second application, one month after the first application, with a third spraying 15 days before the harvest. This is consistent with the results obtained by Sannino *et al*. (2012), who reported that applications of this method may be successful in field conditions to control PTM. However this schedule was not tested in Afyonkarahisar province.

CONCLUSION

This is the first study that was carried out regarding the effective spraying schedule to control PTM in Turkish field conditions. Given the different results in different provinces, one specific schedule may not be ideal for all of Turkey due to the different conditions in different provinces. More research is required to develop this initial study further.

ACKNOWLEDGEMENTS

The authors are grateful to Dr. Numan E. Babaroglu for statistical analysis. Plant Protection Central Research Institute Ankara-Turkey. Special thanks to Bernie Dominiak for reviewed and improved an earlier version of this manuscript (Australia). Thanks to the company of Dupont and Dow Agro for supplying insecticides (Turkey).

REFERENCES

Abbott, WS. 1925. A method of computing the effectiveness of an insecticide. Journal of Economic Entomology. 18(2):265-267.

Abdel, RAS., Salem, AE. and Ghany, NMA. 2014. Sustainable potato tuber moth, *Phthorimaea operculella* (Zeller), control using biopesticides of natural andm icrobialorigin. African Journal Scienceand Technology 2 (6):125-130.

Anonymous. 2010. Cropwatch.uni.edu/potato/tubermoth.

Arnason, JT., Philogene, BJR. and Moran, P. 1989. Insecticides of plants origin. ACS Symposium Series, American Chemical Society, Washington, DC, USA. 387: 1-213.

Bacon, OG., Calley, NF., Riley, WD. and James, RH. 1971. Evaluation of insecticides for control of the green aphid and tuberworm on Irish potatoes. American Potato Journal 48: 298.

Chandel, RS. and Chandla, VK. 2005. Integrated control of potato tuber moth (*Phthorimaea operculella*) in Himachal Pradesh. Indian Journal of Agricultural Science 75:837-39.

Cuningham, LC. 1969. Alternative host plants of tobacco leaf miners, *Phthorimae operculella* (Zell.) (Lepidoptera: Gelechiidae). Queenshed. Journal of Agriculture and Animal Science. 26:107-111.

Das, GP. 1995. Plants used in controlling the potato tuber moth, *Phthorimae operculella* (Zell.) (Lepidoptera:Gelechiidae) Crop Protection. 14:631-636.

Debnath, MC.,Khound, JN., Dutta, SK. and Sarmah, PC. 1998. Management of potato tuber moth, *Phthorimaea operculella* (Zeller) in potato storage. Journal of the Agricultural Science Society of North-East India. 11 (1): 55-60.

Gomaa, AE. and El-Nenaey, HM. 2006. Evaluation of certain controlling measures for *Phthorimaea operculella* (Zeller) (Lepidoptera, Gelechiidae) on potato in stores. The Egyptian Journal of Agricultural Research. 84 (1): 31-41.

Hossein, SMZ., Das, GP. and Alam, MZ. 1994. Use of various indigenous materals and insecticides in controlling potato tuber moth in storage. Bulletin of Institute of Tropical Agriculture Kyushu University 17: 79-84.

Nasser, SM., Ahmed, SA. and Atwa DH. 2012. The Integration between *Trichogramma evanescens* West (Hymenoptera:Trichogrammatidae) and selected bioinsecticides for controlling the potato tuber moth, *Phthorimae operculella* (Zell.) (Lepidoptera:Gelechiidae) of stored potatoes. Journal of Plant Protection Research. 52 (1):41-46.

Rondon, SI., Bano, SJ., Clough, GH., Hamm, PH., Jensen, A., Schreiber, A., Alvarez, JM., Thornton, M., Barbaur, J. and Dogramaci, M. 2007. Biology and management of the potato tuberworm in the Pacific Northwest. PNW. 594.

Rondon, SI. 2010. The Potato tuberworm: A literature Review of Its Biology, Ecology and Control. Journal Potato Research. 87:149-166.

Salah, H. and Aalbu, R. 1992. Field use of Granulosis virus to reduce initial storage infestation of the potato tuber moth, *Phthorima eoperculella* (Zeller), in North Africa. Agriculture, Ecosystems and Environment. 38:119-126.

Salama, HS. and Salem, SA. 2000. Bacillus thurungiensis and neem seed oil (*Azadirachta indica*) effects on the potato tuber moth *Phthorimae operculella* Zeller in the

field and stores. Archives of Phytopathology Plant and Protection. 33:73-80.

Sporleder, M., Kroschel, J., Hube, RJ. and Lagnaoui, A. 2005. An improved method to determine the biological activity (LC_{50}) of the granulo virus PoGV in its host *Phthorimaea operculella*. Entomologia Experimentaliset Applicata. 116:191-97.

Sporleder, M. and Kroschel, J. 2008. The Potato Tuber Moth Granulovirus (PoGV): Use, Limitations and Possibilities for Field Applications. In, Integrated Pest Management for the Potato Tuber Moth, Bio-pesticides for potato tuber moth control Potato J 40 (2): July - December, 2013 141 *Phthorimaea operculella* Zeller- a Potato Pest of Global Importance. Eds. Kroschel, J. and Lacey, L. Weikersheim, Germany, Margraf Publishers: 49-71.

Sannino, L., Piro, F., CrivellI, L. and Pasquini, S. 2012. Lottaalla Tignoladellapatata con Rynaxypyr e indoxacarb. Atti Giornate Fitopatologiche. 1:281-287.

Steven, PA., Lawrence, AL., Pruneda, HN. and Rondon, S. 2008. Semi-field evaluation of a granulovirus and *Bacillus thuringiensis* spp. kurstaki for seasen-long control of the potato tuber moth, *Phthorimae operculella.* Entomologia Experimentaliset Applicata. 129 (3):276-85.

Von, AR., Goueder, J. and Temime, AB. 1987. Integrated control of potato tubermoth, *Phthorimae operculella* (Zeller) in Tunusia. Insect Science and Application. 8:989-994.

Received: Dec 26, 2016; Accepted: Jan 20, 2017

Canadian Journal of Pure and Applied Sciences
Vol. 11, No. 1, pp. 4067-4077, February 2017
Online ISSN: 1920-3853; Print ISSN: 1715-9997
Available online at www.cjpas.net

EXTENT OF FISH AND MUSSEL SPECIES CONTAMINATED BY ENDOCRINE DISRUPTING CHEMICALS (EDCS) IN KARACHI COSTAL AREAS: ASSESSMENT USING AN *IN-VITRO* YEAST ESTROGENIC SCREENING (YES) TEST

*M Zaheer Khan[1**], Farhana Ali[1], Alvin Louie[1], Afsheen Zehra[2], Karim Gabol[2], Roohi Kanwal[2], Ghazala Yasmeen[2], M Asif Iqbal[2], Uzma Manzoor[2], Ubaid Ullah[2] and Francis CP Law[1]
[1]Environmental Toxicology Program, Department of Biological Sciences
Simon Fraser University, Burnaby, BC V5A 1S6, Canada
[2]Department of Zoology, University of Karachi, Karachi-75270, Pakistan

ABSTRACT

The objective of the present study was to screen for Endocrine Disrupting Chemicals (EDCs) contamination in fish (*Engraulis purava*) and mussel (*Mytilus*) in 10 selected areas of Karachi coast. After the baseline survey, we selected Paradise Point, Hawks Bay, Sandspit, Manora, Baba Island, and Korangi/Phitti Creek to collect fish samples where as Buleji point 1 & point 2, Paradise point 1 & point 2, and Manora point 1 & point 2 were selected for mussel samples. The YES bioassay was used in the present study to screen marine fish and mussel for EDC. According to findings the most contaminated area is Baba Island in which the Anchovy contained 95.78ngE_2 equivalents/g wet weight of fish tissue whereas the anchovy collected from Sandspit contained 20.70ng/g of fish tissue. The second most polluted area is Korangi/ Phitti Creek where the fish samples contain an average of 77.19ng/g, ww. In the mussel samples, Buleji point 1 area contains an average of 875.23ng/g, ww, and most polluted area for mussel as compared to other study areas. Further investigation such as chemical analysis has been recommended for identification of chemicals.

Keywords: Karachi, coastal areas, YES bioassay, *Engraulis purava*, *Mytilus*.

INTRODUCTION

Endocrine Disrupting Chemicals (EDCs) are present in hormones, pharmaceuticals, pesticides, and detergents and they are usually introduced into the aquatic ecosystem through industrial and municipal effluents along with urban and agricultural runoff. Exposures to EDCs may result in the disruption of normal functioning of hormones in vertebrates and invertebrates biodiversity. It is important to determine the levels of EDCs in different aquatic animals quantitatively using the yeast estrogen screen (YES) bioassay because the YES bioassay is an *in vitro* test that can be used to detect total EDC concentration in a sample in expensively and quickly.

In the aquatic environment some chemicals have been implicated as hormones or endocrine disruptors. The Endocrine disrupting chemicals (EDCs) are commonly used to describe environmental agents that alter the endocrine system. EDCs can be defined as an exogenous chemical that interferes with the synthesis, secretion, action transport, binding of natural hormones in the body. EDCs are responsible for behaviour, reproduction and development of animals and human (Crisp *et al*., 1998).

EDCs are a class of synthetic or natural compounds that are suspected of adversely affecting the populations of aquatic biodiversity and humans health. Estrogens are a main harmful source of EDCs that have been linked to feminization of biodiversity such as fish and reptiles (Gauillette *et al*., 1995; Sumpter and Jobling, 1995), and also the increasing incidence of testicular reduction in male fertility and breast cancer in humans (Toppari *et al*., 1996; National Research Council, 1999). Researchers Bolz *et al*. (2001), Ferguson *et al*. (2001), Peck *et al*. (2007), Stuart *et al*. (2005) and Houtman *et al*. (2006) have reported presence of EDCs in estuarine and river waters. The endocrine disrupting chemicals are thought to be especially important for development of fish, disrupting sexual development, fertility and behaviour (Rolland *et al*., 1997). Exposure to EDC's in the aquatic environment has been associated with abnormal thyroid function in fish, shellfish and birds (Moccia *et al*., 1981, 1986) and disturbed hatching in fish, turtles and birds

*Corresponding author e-mail: zaheer@scspkarachi.org
** Present address: Department of Zoology, University of Karachi, Karachi-75270

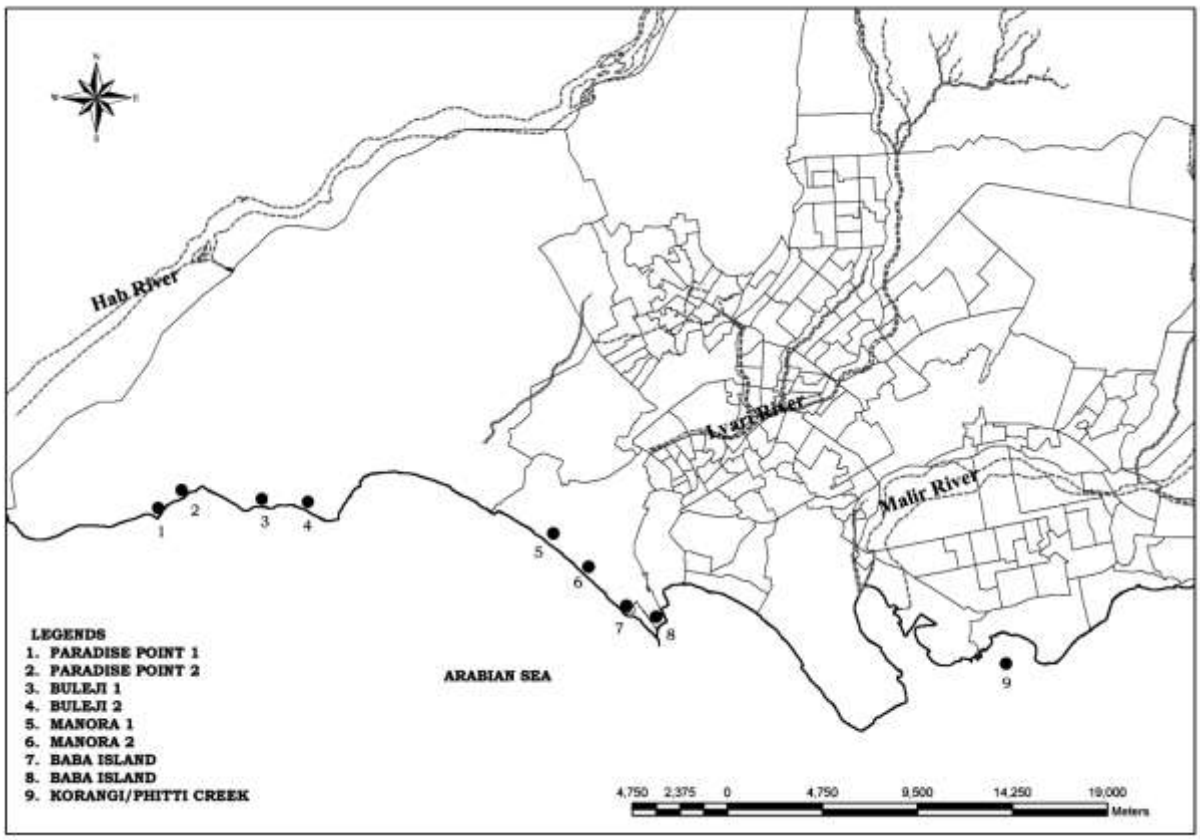

Fig. 1. Map of study areas of Karachi coast.

(Shugart, 1980; Leatherland, 1992; Mac *et al*., 1988; Bishop *et al*., 1991).

Pakistan's coastal areas have diverse rich marine biodiversity and coastal ecosystem is a complex array of creeks and delta of the Indus River. The environmental quality of coastline and marine ecosystem is continuously being degraded due to marine pollution arising from a combination of domestic and industrial activities.

Pakistan produced about 596,980 metric tons of marine fish and 25,000 metric tons of shrimp. About131,000 metric tons of fish is exported to Europe and other countries. Pollution in the coastal areas of Karachi are severely contaminating marine biodiversity (Govt. of Pakistan, 2016).

Karachi coastal areas receive 472,000m^3 domestic and industrial wastewater primarily through Lyari and Malir Rivers and from streams and drainages (KDA master plan1, 1990-2000). Presently, coastal areas of Karachi have high levels of organic pollutants and the presence of heavy metals (Ali and Jilani, 1995; Akhter *et al*., 1997; Jilani, 2014). A recent study revealed that toxic metals have been found in marine biodiversity and ecosystem in the coastal areas of Karachi. These metals include mercury, cadmium, chromium, lead, arsenic, and zinc. The mean concentration of cadmium in the fishes was found to be 0.06, 0.04, 0.06 ppm fresh weight in the fishes of Karachi harbour, Korangi creek and Gwadar East Bay, respectively. The highest concentration of cadmium was recorded both in Karachi harbour and Gwadar East Bay and obtain from Korangi creek fish. Highest concentration of metals in water and sediments was observed in Karachi Harbour area followed by Korangi creeks>Gizri creeks>Gwadar fish Harbour> Off Gwadar East Bay>Buleji (Saleem, 2002). The objective of the present study was to screen the extent of EDCs contamination in Fish (*Engraulis purava*) and Mussel (*Mytilus*) in selected areas of Karachi coast.

MATERIALS AND METHODS

Study Points

After the baseline survey and based study, we selected the following sites as study points:

For fish Anchovy sampling; Paradise Point, Hawks Bay, Sandspit, Manora, Baba Island, and Korangi/Phitti Creek, while Buleji point 1, point 2, Paradise point 1, point 2, and Manora point 1, point 2 for Sea mussel (Fig. 1).

Table 1.The dilution series for the standard curve. There are 11 dilutions and the 12th well is the methanol blank. The 100nM solution is diluted 1:3, 1:10, 1:17, 1:30, 1:50, 1:85, 1:150, 1:250, 1:1500, and 1:2500 for the assay.

Dilution Number	1	2	3	4	5	6	7	8	9	10	11	12
E2Dilution Factor	1	0.33	0.1	0.059	0.033	0.02	0.012	0.0067	0.004	0.00067	0.0004	methanol blank
Methanol volume (µL)	0	140	180	188	180	160	160	160	160	180	180	

We had hired professional fishermen for collection of live fish and mussels samples. Following collection of samples they were stored with ice and shifted to Wildlife Lab, Department of Zoology, University of Karachi for extraction.

Extraction

Three grams of Anchovy fish *Engraulis purava* / 2 gram of sea mussel *Mytilus* were cut, weighed, and placed into glass tubes separately. After 30 minutes, the fish/ mussel samples were placed in 5mL of methanol in a large glass test tube and homogenized with the Brinkmann Homogenizer (Polytron). The samples were centrifuged at 30rpm for 20 minutes. After centrifugation, the methanolic extract for each sample was removed and placed in a smaller test tube. After removing methanolic extract, the tissue sample was dissolved in 5mL of methanol and centrifuge at 30rpm for 20 minutes. After the centrifugation and the removal of the extract for the second time, the tissue pellet was extracted with 2mL of chloroform and centrifuge for 15 minutes at 30 rpm. The chloroform extract was then combined with previously removed methanolic extracts and then was centrifuged at 30rpm for 8 minutes, this allows the tissue particle to precipitate to the bottom of the extract (Peck *et al*., 2007).The final volume of the combined extract was measured before being evaporated to dryness in a rotator evaporator (Rotavapor RE 120, Büchi). The residues were reconstituted in 500µL of methanol and transferred to small vials then were sent to be dried again under a gentle stream of nitrogen. After nitrogen evaporation the residues were reconstituted in 500µL of ethanol and placed in a freezer at -40°C overnight.

Filtration Protocol

1) Samples were vacuum filtered through bond elute C18 extraction columns through the use of an extraction manifest.
2) C18 Extraction columns were pre-conditioned with 1mL methanol twice, followed by 1mL of distilled water twice.
3) Sample were then filtered through the extraction column with the filtrate being discarded.
4) 500 µL of methanol was then passed through the column to elute the sample. This portion was collected and evaporated by nitrogen gas.
5) Evaporated samples were re-constituted by adding 500µL of methanol

Sample extracts were mixed with methanol to 1, 1:5, 1:50, 1:500, 1:5000 and 1:50000 dilutions before being used in the YES assay.

Standard Dilution Series

E2 standard curves were prepared using 11 concentrations of the E2 standard solution. A pure methanol blank was also prepared. Thus, the E2 stock solution (0.01 M) was prepared by dissolving 27.24mg of estradiol in 10 mL of absolute ethanol. A 20µL aliquot of the stock solution was added to 980µL of methanol to make the substock solution. A 10µL aliquot of the substock was added to 990µL of methanol to make 100nM of working solution. A 200µL aliquot of the working solution was used as the first undiluted standard solution. From this 100 nm working solution, it was diluted with methanol to obtain 1:3, 1:10, 1:17, 1:30, 1:50, 1:85, 1: 150, 1: 250, 1:1500, 1:2500 dilutions (Table 1).

Yeast Preparation

Five days before the start of an experiment, transgenic yeast was spread on an agar plate and incubated at 30°C for 3 days. The plate was parafilmed and stored in a fridge at -10˚C. The procedure was described by Gaido *et al*. (1997) but modified for the present study according to Lorenzen *et al*. (2004). To prepare the yeast that would be used for the YES, the yeast was cultured in a 50mL polypropylene tube filled with 5mL of media on day one at 10:00 am. The culture was left in the incubation room on a shaker at 30°C overnight. On day two the yeast was diluted 1:10 by adding 45mL of media to the 5mL culture at 2:00 pm. On day 3 at 10 am the yeast culture was diluted 1:1 by re-suspending the yeast and transferring half the yeast to another 50mL propylene tube and adding 25mL of media.

Plate Preparation

10µL of the standard dilution series and the sample series were pipetted onto a 96 well plate. This is repeated twice for each standard dilution series and three times for each sample dilution. The plate was left to dry for 30-45 minutes. At 2:00 pm the yeast exposed to the estrogen on the plate by re-suspending the yeast and mixing 20mL of yeast with 200µL of copper sulphate. The copper

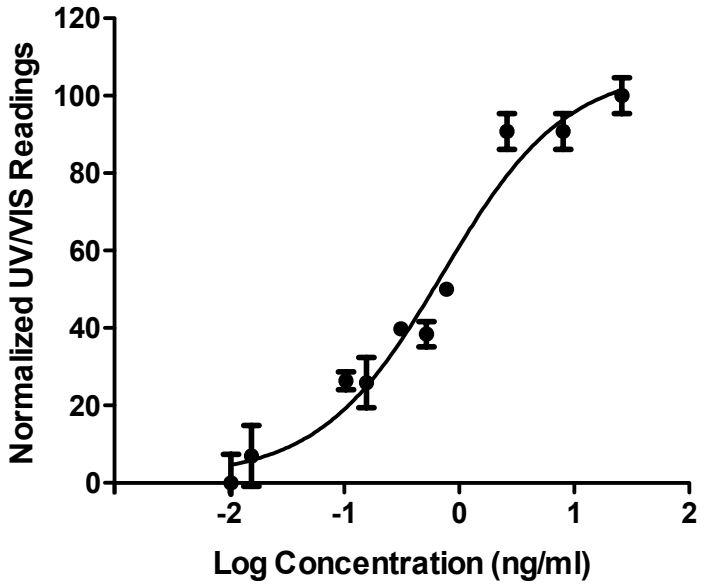

Fig. 2. This is a typical E2 standard dose-response curve. The concentration of E2 (log-transformed) is given on the x-axis; the response in percentage is given on the y-axis. Each data point is the mean ±SD of a duplicate assay. The curve shows a sigmoid shape with a maximum of 92.83%.

sulphate stimulates the production of hER in the yeast cells. 200µL of this mixture was added to each well by using a multi channel pipette. The plate is slightly shaken and parafilmed and kept in the incubation room at 30°C overnight. 2-Nitrophenyl β-D-galactopyranoside (ONPG) (0.022 grams) was dissolved in 10.9 g of Z-buffer and left in the shaker overnight. At 9:00am on the fourth day the yeast in each well was re-suspended and 100µL transferred to a new plate. Ten percent SDS (110µL) and 11 µL of oxalyticase, and 29.7µL of mercaptoethanol were added to the ONPG and then 100µL of the mixture were added to each well. Forty minutes after adding the ONPG, the plate was read by a UV/V was spectrophotometer at 415nm (over all colorimetric change) and 595 nm (for turbidity caused by yeast cells).

Data calculation and statistical analysis

Data was analyzed using Excel and Graph Pad Prism 5. The UV reading at 415 nm represents the overall colorimetric change of the sample and the reading at 595 nm represents the turbidity caused due to yeast growth. In order to obtain the colorimetric change specifically due to the reaction between ONPG and β-galactosidase, the reading at 595 nm was subtracted by 415 nm. To plot a dose response curve, the UV readings were normalized and the dilution factors were log-transformed for better data analyzing and plotting with Prism 5. The UV readings were used as the variables for y-axis and concentration factors as the variables for x-axis of the curve. The maximum of the standard curve was considered to be 100% and the sample dose-response curves were plotted compared to this maximum (Fig. 2).

The calculation of the E2 equivalence was done by using the following formula proposed by Lorenzen *et al.* (2004): E2 equivalent = [standard EC_{50} (ng/ml) / extract EC_{50}] * [volume of assay medium (ml) / (volume of extract tested (µl)] * [volume of stock extract (µl) / ww of sample (g)]. To further broaden the accuracy of our calculation EC_{20} and EC_{30} were also used in the calculation instead of just calculating using EC_{50}. To convert EC_{50} to EC_{20} and EC_{30} the following formula was used for the conversion: $EC_X = [X/(100-X)^{(1/H)}] * EC_{50}$, where the X is 20 or 30 and H is the hill slope of the dose response curve. The average of the E2 equivalence results calculated by using $EC_{20,}$ EC_{30} andEC_{50} were taken and used as the final representative of the E2 level in the samples.

RESULTS AND DISCUSSION

Exposures to endocrine-disrupting chemicals are currently regarded as the most serious anthropogenic threats to aquatic biodiversity and ecosystems.

The Malir and Lyari Rivers in the metropolitan city of Karachi are contributing about 25% and 59% of the total pollution load of Karachi City respectively, while 15% of

Table 2. The average EDC levels shown in study points (Fish samples) 2011.

Fish Sample locations	Sample I.D.	EDC (ng E2 equivalents/g fish)
Baba Island	BI 1	13.34
	BI 2	410.81
	BI 3	26.72
	BI 4	2.38
	BI 5	1.20
	BI 6	120.21
	Average	**95.78**
Hawks Bay	H 1	0.00
	H 2	0.00
	H 3	0.00
	Average	**0**
Manora	MA 1	0.00
	MA 2	23.74
	MA 3	0.00
	MA 4	326.95
	MA 5	24.53
	Average	**75.04**
Paradise point	P 1	0.00
	P 2	0.00
	P 3	0.00
	P 4	98.62
	Average	**24.66**
Sandspit	S 1	1.43
	S 2	105.61
	S 3	0.00
	S 4	0.00
	S 5	1.77
	S 6	15.39
	Average	**20.70**
Korangi/Phitti Creek	F1	63.41
	F2	134.56
	F3	0.00
	F4	0.00
	F5	399.75
	F6	0.00
	Average	**77.19**

the pollution load is directly discharged through Gharo, Gizri and Korangi Creek (Amjad and Rizvi, 2000).

Industrial toxic waste, and organic waste from the nearby cattle colony comprising of liquid dung mix with the blood from slaughterhouses are also drained into the Korangi Creek areas. Several studies Rizvi *et al*. (1988), Saifullah *et al*. (2002), Saleem and Kazi (1995) and Saleem and Kazi (1998) have already reported high levels of contaminants in the coastal areas of Karachi.

In the present work, Yeast Estrogenic Screening (YES) tests were conducted for the evaluation of Endocrine Disrupting Chemicals (EDCs) levels in the fish and mussel samples from the selected study areas of Karachi Coast. All fish samples were collected from Paradise Point, Hawks Bay, Sandspit, Manora, Baba Island, and Korangi/Phitti Creek areas, where as Sea mussel samples obtained from Buleji point 1 and point 2, Paradise point 1 and point 2, and Manora point 1 and point 2.

Study areas were surveyed and samples of fish Anchovy (*Engraulis purava*) and Sea mussel (*Mytilus*) were collected in Oct/Nov 2010 and March/April 2011. *In-Vitro* Yeast Estrogenic Screen (YES) assay techniques were used to evaluate the ECDs level in the fish and mussel samples. The most potent EDCs found in the environment are the natural and synthetic hormones such

Table 3. The average EDC levels shown in study points (Mussels samples) 2011.

Mussel Sample locations	Sample I.D.	EDC (ng E2 equivalents/g mussel)
Manora point 1	1	#
	2	876.41
	3	#
	4	364.71
	5	918.52
	6	#
	7	38.96
	8	0.00
	9	0.00
	10	0.00
	11	1306.53
	12	0.00
	13	23475.73
	14	614.56
	15	#
Manora point 2	16	0.00
	17	711.93
	18	0.00
	19	0.00
	20	0.00
	21	0.00
	22	0.00
	23	0.60
	24	0.00
	25	0.61
	26	1.00
	27	0.00
	28	47.61
	29	54.10
	30	0.00
	31	0.00
	32	0.00
	33	0.00
	34	0.00
	35	0.00
	36	33.98
Buleji Point 1	B1 A	0.00
	B1 B	27.23
	B1 C	2598.45
	Average	**875.23**
Buleji Point 2	B2 A	0.00
	B2 B	22.97
	B2 C	0.00
	Average	**7.66**
Paradise Point 1	P1 a	#
	P1 b	0.00
	P1 c	81.87
	Average	**40.94**
Paradise Point 2	P2 a	99.14
	P2 b	0.00
	P2 c	6.55
	Average	**35.23**

= No result due to sample contamination

Table 4. The average EDC levels shown in study points - 2009.

Plate and Location	Experiment	Sample	EC50+EC30+EC20/3
P1 Buleji Point 1	Sea Mussel *Mytilus*	1	60.53976
		2	4.689243
		3	14.46198
		4	7.573719
			21.81618
P2 Korangi/Phitti Creek	Anchovy *Engraulis purava*	5	213.6048
		6	12.09747
		7	1.260946
		8	0.556322
			56.87988
P3 Manora	Anchovy *Engraulis purava*	9	0.831914
		10	2.284097
		11	0.420291
		12	0.63614
			1.04311
P4 Paradise Point 1	Sea Mussel *Mytilus*	13	0.925197
		14	1.629437
		15	3.040487
		16	2.61711
			2.053058
P5 Paradise Point 2	Sea Mussel *Mytilus*	17	1.625567
		18	0.211116
		19	0.000946
		20	6.75E-05
			0.459424
P6 Buleji Point 2	Sea Mussel *Mytilus*	21	0.009465
		22	3199.153
		23	0.002393
		24	52031065
			13008566

as 17β-estradiol (E2), estrone (E1), and 17α-thynylestradiol (EE2). We used E2 as the chemical standard in our bioassay, as it is one of the most potent EDCs. E2 is produced in the ovaries, gonads, and, to a lesser extent, in the arterial walls, the brain, and adrenal cortex. E2 also acts as a growth hormone for the female reproductive organs (Hertz, 1985). The YES bioassay is an efficient and inexpensive method of detecting EDCs in aquatic samples. To find the E2 equivalents in our fish and mussel samples, the dose-response curves were compared to E2 standard curve from every experimental plate.

The average EDC levels found in the fish samples of Baba Island were found to be 95.78ng/g, 75.04ng/g in Manora, 24.66ng/g in Paradise points, 20.70ng/g in Sandspit and 77.19ng/g in Korangi/Phitti creek (Table 2).

The average EDC levels found in mussels samples were as follows, 200.91ng/g in Manora point 1, 40.46ng/g in Manora point 2, 875.23ng/g in Buleji point 1, 7.66ng/g in samples of Buleji point 2, 40.94ng/g in Paradise point 1and 35.23ng/g in samples of Paradise point 2 (Table 3).

According to present study's findings the most contaminated area is Baba Island in which the Anchovy is shown to contain 95.78ng E_2 equivalents/g wet weight of fish tissue whereas the anchovy collected from Sandspit contains 20.70ng/g of fish tissue. The second most polluted area is Korangi/ Phitti Creek where the fish samples contain an average of 77.19ng/g, ww.

In the mussel samples, Buleji point 1 area contains an average of 875.23ng/g, ww, and most polluted area for mussel as compared to other study areas. These findings are consistent with the report that the Korangi/Phitti Creek area is a polluted area of the Karachi coast because wastewaters are discharged into the sea from Korangi, Landhi, Karachi Export Processing Zone, Bin Qasim industrial areas, and Pakistan Steel Mill (Shahzad *et al*., 2009). Also, there are several tanneries, textile factories, insecticide and pesticide factories, and slaughterhouses in the area (Rizvi *et al*., 1988).

Further analysis of samples by HPLC or GC/MS have been recommended for identification of chemicals.

According to our 2009 study (Table 4), the most contaminated area was Korangi/Phitti Creek in which the anchovy is shown to contain 56.9ng E_2 equivalents/g wet weight of fish tissue whereas the anchovy collected from Manora contains only 1.04 EEQ ng/g of fish tissue. The second most polluted area was Buleji Point 1 where the mussel samples contain an average of 21.8 EEQng/g, ww. While remaining three mussel sampling sites show little or no EEQ.

Karachi city generates approximately 8,700 tons of domestic solid wastes per day (Alam, 2010). Pakistan has 17 Creeks in Sindh Coastal areas, Korangi/ Phitti Creeks being one of them. The Korangi/Phitti creek area is a polluted area of Karachi coast because several tanneries of Korangi industrial area are disposing off their untreated wastes into the creek areas.

Several studies have reported that Korangi/ Phitti Creeks has been highly polluted and are impacting marine biodiversity and human health. Three power plants located at the Karachi coastal areas use large quantities of marine water cooling; they discharge heated effluent and other pollutants to sea. Among the creeks, the Korangi and Gizri creeks are the most affected from oil discharges as well as municipal and industries activities. The present study has confirmed that Korangi/ Phittii Creeks areas have high level EDCs contamination.

Pakistan Steel Mills are located on the Gharo Creek. Thus the entire Korangi/ Phitti Creek and Gharo Creeks from an interrelated system of creeks receive industrial waste from some sources of pollution in the Karachi city. According to study conducted by National Institute of Oceanography, Steel Mills discharge cooling waste water effluent to directly adjacent area of Gharo Creek, and these effluents contain heavy metals including Cd, Fe, Zn, Cu, Pb, iron oxide particles, chlorine, oil and grease etc (Rizvi, 1997).

EDCs are introduced into the aquatic environment through industrial and municipal effluents as well as urban and agricultural runoff (Nelson *et al*., 2007; Soto *et al*., 2004, Metcalfe *et al*., 2001). Once in the environment EDCs can have harmful effects as they are transported up the food chain. The presence of endocrine disrupting compounds in the environment can cause adverse effects such as reproductive abnormalities and impaired development in aquatic biodiversity and silent killers, threatening biodiversity on a huge scale. Several adverse effects of endocrine disruption have been reported in fish, mussels, crustaceans, birds, mammals and reptiles (Canesi *et al*., 2004; Waring and Harris, 2005).

Industrial toxic waste, organic waste from the nearby cattle colony comprising liquid dung mix with the blood from slaughterhouses are also drained into the Korangi Creek areas. Earlier studies Rizvi *et al*. (1988), Saifullah *et al*. (2002), Saleem and Kazi (1995), Saleem and Kazi (1998), Saleem (2002) and Hunter *et al*. (2012) have already reported the contamination from various pollutants in the coastal areas of Karachi and they are transported up the food chain.

Many studies have proved that some industrial and agricultural chemicals have the ability to interfere with endocrine systems and hormonal functions of aquatic wild animals including fish and mussels. These EDCs are thought to be important at the larval or developmental stages of fish, disrupting sexual development, and general behaviour (Rolland *et al*., 1997). These studies and our present study results have indicated that marine biodiversity may be threatened by industrial and municipal effluents pollution especially in Korangi/ Phitti Creek area.

One new evidence at molecular level has reported that the environmental deterioration can change the genetic structure and genetic polymorphism of trout populations by cytogenetic and allozymic analysis (Was and Wenne, 2002).

In connection with screening the levels of ECD's further studies are needed at large scale screening of the levels of ECD's in the marine water, sediment, fish, mussels and prawn of all coastal areas of Sindh and Balochistan. After screening we were able to find out the hot spots, determination of level of estrogenic contamination then controlling the estrogenic contamination, protecting the aquatic biodiversity and increasing the fisheries, prawn and mussels production and preparing the aquatic biodiversity conservation plan for the coastal areas.

Further chemical analysis in the identification of chemicals is recommended for samples with high levels quantified in the yeast assay.

ACKNOWLEDGMENTS

The authors would like to thank the Higher Education Commission (HEC) Pakistan for the Sabbatical Fellowship Program grant in supporting this research study conducted at the Toxicology Program, Department of Biological Sciences, Simon Fraser University, Canada . We also thank to Prof. Jamil Kazmi, Department of Geography, University of Karachi for preparation of study areas map.

REFERENCES

Akhter, W., Ali, I., Zaidi, SS. and Jilani, S. 1997. The State of Pollution Levels of Karachi Harbor and Adjoining Coastal Waters. Water, Air and Soil Pollution, Kluwer Academic Publishers, Netherlands. 94(1-2):98-107.

Ali, I. and S. Jilani, 1995. Study of Contamination in the Coastal Waters of Karachi. The Arabian Sea. Living Marine Resources and the Environment. Eds. Mary-Frances, T. and Tirmizi, NM. Vanguard Book Publisher, American Institute of Biological Sciences. 653-658.

Amjad, S. and Rizvi, SHN. 2000. Pakistan National Program of Action under the Global Program of Action for the protection of marine environment from land based activities. Ministry of Environment and Local Government/National Institute of Oceanography. Karachi.

Alam, M. 2010. Unsafe disposal of waste poses threat to public health. Daily Dawn Karachi, News publication.

Bishop, CA., Brooks, RJ., Carey, JH., Norstrom, RJ. and Lean, DRSJ. 1991. The case for a cause-effect linkage between environmental contamination and development in eggs of the common snapping turtle (*Chelydra s. serpentina*) from Ontario, Canada. J Toxicol Environ Health.33:521-548.

Bolz, U., Hagenmaier, W. and Körner. 2001. Phenolic xenoestrogens in surface water, sediment and sewage sludge from Baden-Württemberg, south-west Germany. Environ Pollut. 115:291-301.

Canesi, L., Lorusso, LC.,Ciacci, C., Betti, M., Zampini, M. and Gallo, G. 2004. Environmental estrogens can affect the function of mussel hemocytes through rapid modulation of kinase pathways. General and Comparative Endocrinology.138:58-69 (http://dx.doi.org/10.1016/j.ygcen.2004.05.004).

Crips, TM., Clegg ED., Cooper, RL., *et al*. 1998. Environmental endrocrine disruption: An effects assessment and analysis. Environ Health Perspect. 106 (suppl. 1):11-56.

Ferguson, PL., Iden, CR. and Brownawell, BJ. 2001. Distribution and fate of neutral alkylphenol metabolites in a sewage-impacted urban estuary. Environ Sci Technol. 35:2428-35.

Gaido, KW., Leonard, LS., Lovell, S., Gould, JC., Babai, D., Portier, CJ. and McDonnell, DP. 1997. Evaluation of chemicals with endocrine modulating activity in yeast-based steroid hormone receptor gene transcription assay. Toxicol. Appl. Pharmacol. 143:205-212.

Guillette, LJ Jr., Gross, TS., Gross, DA., Rooney, AA. and Percive, HF. 1995. Gonadal steroidogenesis in vitro from juvenile alligators obtained from contaminated or control lakes. Environ. Health Perspect. 103(4):31-36.

Government of Pakistan. 2016. http://environment.gov.pk. (accessed on August 11, 2016).

Hertz, R. 1985.The estrogen problem-retrospect and prospect. IN Estrogens in the Environment II-Influences on Development. Ed. McLachlan, JA. Elsevier, New York, USA. 1-11.

Houtman, CJ.,Booij, P., Jover, E., Pascual, del Rio D., Swart, K., van Velzen. M., *et al*. 2006. Estrogenic and dioxin-like compounds in sediment from Zierikzeeharbour identified with CALUX assay-directed fractionation combined with one and two dimensional gas chromatography analyses. Chemosphere. 65:2244-52.

Hunter, S., Khan, MZ., Ben, HHS., Doerr, B., Sara, A. and Law, FCP. 2012. Assessing Estrogenic Chemicals in Anchovy and Mussel Samples from Karachi, Pakistan with the Yeast Estrogen Screen Bioassay. Bulletin of Environmental Contamination and Toxicology. 89(5):990-994, DOI: 10.1007/s00128-012-0821-6.

Jilani, S. 2014. Status of Metal Pollution in the River and Coastal Areas of Karachi. Middle-East Journal of Scientific Research. 22 (9):1288-1293.

Karachi Coastal Recreation Development Plan 1990-2000. Karachi Development Authority Master Plan & Environmental Control Department. UNDP United Nations Center For Human Settlement. Doxiadis Associate International Group S.A Consultant on Development and Ekistics & Osmani and Company (pvt.) Limited. pp. 104.

Lorenzen, A., Hendel, JG., Conn, KL., Bittman S., Kwabiah, AB., Lazarovitz, G., Massé, D., McAllister, TA. and Topp, E. 2004. Survey of Hormone Activities in Municipal Biosolids and Animal Manures, Inc. Environ.Toxicol. 19:216-225.

Leatherland, J. 1992. Endocrine and reproductive function in Great Lakes salmon. In: Chemically induced alterations in sexual and functional development: the wildlife/human connection. Eds. Colborn, T. and Clement, C. Princeton Scientific Publishing, Princeton, NJ. 129-145.

Moccia, R., Fox, G. and Britton, AJ. 1986. A quantitative assessment of thyroid histopathology of herring gulls (*Larus argentatus*) from the Great Lakes and a hypothesis on the causal role of environmental contaminants. J Wild Dis. 22:60-70.

Moccia, RD., Leatherland, JF. and Sonstegard, RA. 1981. Quantitative interlake comparison of thyroid pathology in Great Lakes coho (*Oncorhynchus kisutch*) and chinook (*Oncorhynchus tschauytscha*) salmon. Cancer Res. 41:2200-2210.

Mac, MJ., Schwartz, T. and Edsall, CC. 1988. Correlating PCB effects on fish reproduction using dioxin equivalents. Presented at the Ninth Annual Society of Environmental Toxicology and Chemistry Meeting, Arlington, Virginia, USA.

Metcalfe, CD., Metcalfe, TL., Kiparissis, Y., Koenig, BG., Khan, C., Hughes, RJ., Croley, TR., March, RE. and Potter, T. 2001. Estrogenic potency of chemicals detected in sewage treatment plant effluents as determined by in vivo assays with Japanese medaka (*Oryzias latipes*). Environ.Tox. and Chem. 20(2):297-308.

National Research Council. 1999. Hormonally active agents in the environment. National Academy Press, Washington, DC., USA.

Nelson, J., Bishay, F., van Roodselaar, A., Ikonomou, M. and Law, FCP. 2007. The use of *in vitro* bioassays to quantify endocrine disrupting chemicals in municipal wastewater treatment plants effluents. Sci. of the Total Environ. 374:80-90.

Peck, MR., Labadie, P., Minier, C. and Hill, EM. 2007. Profiles of environmental and endogenous estrogens in zebra mussel *Dreissena polymorpha*. Chemosphere. 69:1-8.

Rizvi, SHN., Saleem, M. and Baquer, J. 1988. Steel mill effluents: Influence on the Bakran Creek environment. In: Proceedings of Marine Science of the Arabian Sea. Eds. Thompson, MF. and Tirmizi, NM. American Institutes of Biological Sciences, Washington, DC., USA. 549-569.

Rizvi, SHN. 1997. Status of marine pollution in the context of coastal zone management in Pakistan. Coastal Zone Management Imperative for Maritime Developing Nations. Eds. Haq, BU., Haq, SM. and Stel, JM. Kluwer Academic. 347-371.

Rolland, RM., Gilbertson, M. and Peterson, RE. (Eds.). 1997. Chemically Induced Alterations in Functional Development and Reproduction of Fishes: Proceedings from a Session at the 1995 Wingspread Conference, SETAC, Pensacola, Florida, USA.

Saleem, M. 2002. Study of Heavy Metal Pollution Level and Impact on the Fauna and Flora of the Karachi and Gwadar Coast. Final Project Report, WWF Pakistan. pp. 32.

Saifullah, SM., Khan, SM. and Ismail, S. 2002. Distribution of nickel in a polluted mangrove habitat of the Indus Delta, Marine Pollution Bulletin. 44:551-576.

Saleem, M. and Kazi, GH. 1995. Distribution of trace metals in the seawater and surficial sediments of the Karachi harbor. In: Proceedings of the Arabian Sea, living Marine Resources and the Environment. Eds. Thompson, MF. and Tirmizi, NM. Vanguard Books (pvt) LTD, Lahore, Pakistan. 659-666.

Saleem, M. and Kazi, GH. 1998. Concentration and distribution of heavy metals (Lead, Cadmium, Copper, Nickel, Zinc) in Karachi shore and offshore sediments, Pakistan Journal Marine Science 7:71-79.

Shahzad, A., Khan, Shaukat, MA. and Ahmed, W. 2009. Chemical Pollution Profile of Rehri Creek Area, Karachi (Sindh). J ChemSoc Pak 31:592-600.

Shugart, G. 1980. Frequency and distribution of polygony in Great Lakes herring gulls in 1978. Condor 82:426-429.

Stuart, JD., Capulong, CP., Launer, KD. and Pan, X. 2005. Analyses of phenolic endocrine disrupting chemicals in marine samples by both gas and liquid chromatography–mass spectrometry. J Chromatogr A.1079:136-45.

Soto, AM., Calabro, JM., Prechtl, NV., Yau, AY., Orlando, EF., Daxenberger, A., Kolok, AS., Guilette, LJ., le Bizec, B., Lange, IG. and Sonnenschein, C. 2004. Andorgenic and Estrogenic Activity in Water Bodies Receiving Cattle Feedlot Effluent in Eastern Nebraska, USA. Environ. Health Perspect. 122(3):346-352.

Sumpter, JP. and Jobling, S. 1995. Vitellogenesis as a biomarker for estrogenic contamination of the aquatic environment. Environ. Health Perspect.103(7):173-8.

Toppari, J., Larsen, JC., Christiansen, P., Giwercman, A., Grandjean, P., Guillette, LJ Jr., Jégou, B., Jensen, TK., Jouannet, P., Keiding, N., Leffers, H., McLachlan, JA., Meyer, O., Müller, J., Rajpert-De Meyts E., Scheike, T., Sharpe, R., Sumpter, J. and Skakkebaek, NE.1996. Male reproductive health and environmental xenoestrogens. Environ. Health Perspect. 4:741-803.

Was, A. and Wenne, R. 2002. Genetic differentiation in hatchery and Wild sea trout (*Salmo trutta*) in the Southern Baltic at microsatellite loci. Aquaculture.204:493-506.

Waring, RH. and Harris, RM. 2005. Endocrine disrupters: A human risk? Molecular and Cellular Endocrinology.244 2-9 (http://dx.doi.org/10.1016/j.mce.2005.02.007).

APPENDIX

Four Hours Yeast Based Estradiol (E2) Receptor Bioassay

Day 1

1) Culture 1 colony of DSY-219 (E2 assay) into 5mL of SC-UW Media
2) Put on shaker and allow to grow overnight at 30^{o}C

Day 2

1) On the morning of day 2, dilute the yeast culture down to an optical density (OD) of 0.08 with SC-UW media
2) Allow the yeast to regrow to an OD of 0.10 on the shaker at 30^{o}C (Typically, the yeast regrows in 1.5-2 hours)
3) When the yeast is at an OD of 0.1, plate 1 µL/well of the sample to be tested on a white bottom 96 well plate
4) Add 100 µL yeast/well and incubate at 30^{o}C for two hours
5) Several minutes before the two hour incubation is complete, prepare the Tropix Gal-Screen buffer and put on ice (The buffer is prepared by diluting the substrate with B Buffer at a ratio of 1:24)
6) Add 100 µL buffer/well parafilm to prevent evaporation and incubate at room temperature for 2 hours
7) At the end of the 2 hour incubation, read the plate on the Perkin Elmer 2030 multilabel reader luminometer (The light intensity is usually the highest between 1.5 - 2.5 hours after addition of the buffer).

Received: Aug 22, 2016; Revised: Nov 24, 2016;
Accepted: Dec 16, 2016

Canadian Journal of Pure and Applied Sciences
Vol. 11, No. 1, pp. 4079-4085, February 2017
Online ISSN: 1920-3853; Print ISSN: 1715-9997
Available online at www.cjpas.net

FEED AND TROPHIC MORPHOLOGY OF YELLOW HAKE *CYNOSCION ACOUPA* (LACÈPEDE, 1801) IN THE NORTHEAST BRAZIL

Francisca Edna de Andrade Cunha[1,2, 3]
[1]Universidade Federal do Piaui. Av. São Sebastião, 2819
Reis Veloso – CEP: 64.202-020 – Parnaíba – PI – Brazil
[2]IMAT – Grupo de Ictiologia Marinha Tropical
[3]LAPICE - Laboratório de pesquisa em Ictiologia, Conservação e Ecologia

ABSTRACT

The stomach contents analysis revealed 72.4% of the items as fishes, 4.56% as crustaceans, 23.0% of organic matter and 0.1% as seagrass. The item Teleostei was featured as essential in feeding followed by fish Ariidae Family and the crustaceans, especially Penaeidae. The morphology of the digestive tube is characterized by presented short and tubular esophagus, stomach cecal form "Y" may be divided into cardiac (greater proportion), fundic and pyloric regions. The sphincter pyloric marks the transition from the stomach to the intestine. The intestine presented coefficient of 0.87 showed medium intestine and rectum portion separated by an ileo-rectal valve.

Keywords: Stomach contents, diet, carnivorous, characteristics anatomic, digestive system.

INTRODUCTION

Several species of Teleost fish in Brazil are marketed under the trade name of Hake, most belonging to Order Perciform, Family Sciaenidae, especially of the genus Cynoscion (Matos e Lucena, 2006). The Yellow Hake (*C. acoupa*) is part of this family considered of great commercial importance (Menezes e Figueiredo, 1980) and environmentally friendly food chains, being considered prey to some marine mammals such as sea-lion in South America, seals and franciscana dolphin (*Pontoporia blainvillei*), and seabirds (Waessle, 2003).

Fishes of the Family Sciaenidae are among the most fish in the Brazilian continental shelf, mainly in southern and southeastern Brazil (Vazzoler *et al*., 1999) representing one of the main fishery resources of shallow waters in many tropical and temperate regions of the world (Nelson, 1994) and intense fishing activity target held by the commercial fleet in these regions (Braga, 1990). To determine the sustainable potential of a fishing resource is necessary a comprehensive study involving, among other things, fish feed characteristics is essential for a better understanding of other subjects such as nutrition, wildlife surveys, trophic ecology where equal attention is given to both the predator or the prey and also for energy transfer studies, both in the individual and the ecosystem (Zavala-Camin, 1996) and thus subsidize management plans aimed at the rational exploitation of fish stocks and other marine organisms. The present work presents new information about natural feeding data and morphological features of *C. acoupa* through the examination your gastric system.

*Corresponding author e-mail: f_edna@yahoo.com.br

MATERIALS AND METHODS

Sample Collection

The specimens of *C. acoupa* were captured in the shallow continental shelf in Piaui coast, at medium depths of 10m (02º51'28'' S; 41º49'15''W), monthly from July 2013 to January 2014, by the artisanal fisheries. The fishing gear used was gill nets, anchored positioned in the background with mesh opening of ranging from 12-15 cm. After a realization biometrics we performed a longitudinal incision in the abdominal cavity for extracting for the digestive tract. The material was packed in individual plastic bags containing a paper label with the information of total length (cm), weight (g), Sex (Male/Female), date and place of collection and subsequently frozen.

Study of Diet and Morphology

The degree of repletion (DR) of the stomachs was verified by visually estimating, according Santos (1978) and the degree of digestion of the item proposed by Zavala-Camin (1996) adapted by Vaske-Jr. *et al*. (2003).

The stomachs content were examined under a stereomicroscope and food items were identified to the

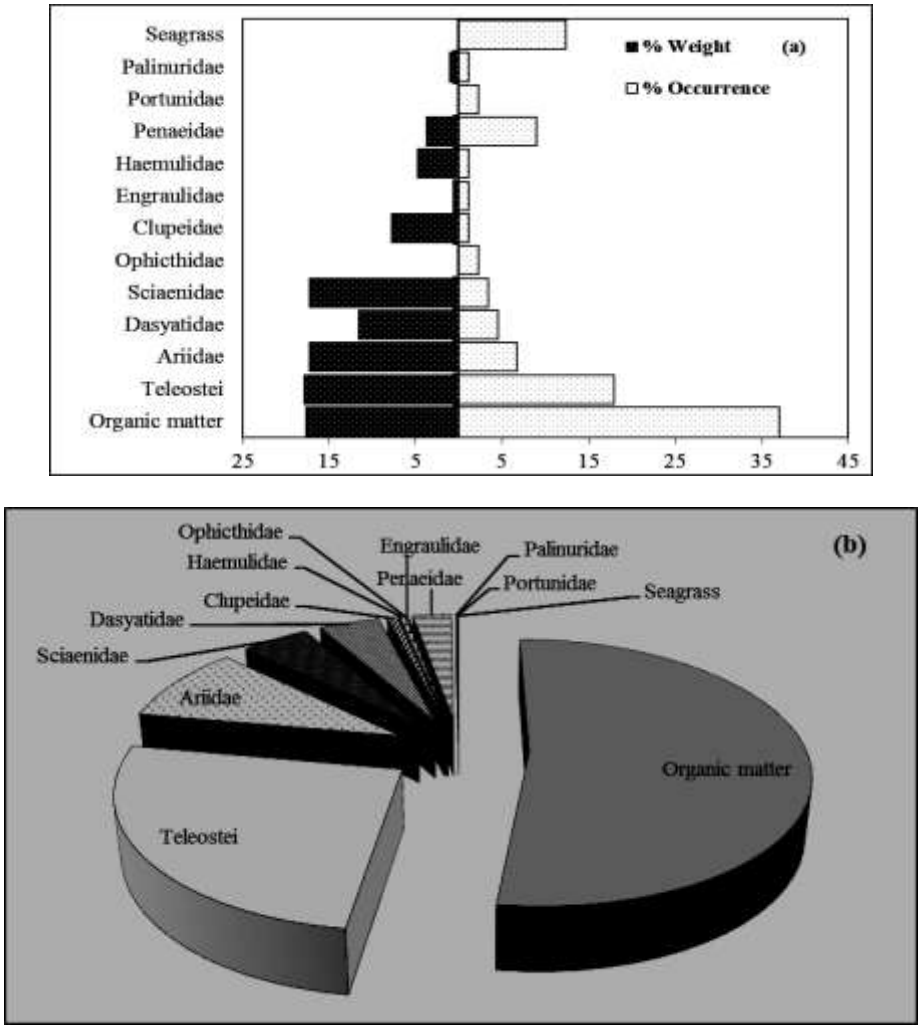

Fig. 1**. (a)** Participation in weight (% W) and Frequency of Occurrence (% FO) and **(b)** Food Index (% IAi) of food items found in the stomachs of *C. acoupa* captured in the Piaui coastline from July 2013 to January 2014.

lowest possible taxonomic level with the help of specialized literature, subsequently they were quantified and weighed (g) in digital scale with precision of 0.01g. During the counting of the items were considered only whole bodies or parts that clearly allowed the identification and quantification of the item.

Data analysis was across the frequency of occurrence according Hyslop (1980) and the gravimetric methods proposed by Hynes (1950). These data were combined in an alimentary index (IAi) proposed by Kawakami and Vazzoler (1980). Fifteen individuals of different sizes were taken at random for morphological characterization.

RESULTS AND DISCUSION

Overall Diet

The study was based on a lot of 83 specimens of *C. acoupa*, of these 53.9% were males and 46.1% females presenting overall length between 30 and 104 cm, with an average of 66 cm. Body weight ranged from 2.5 to 11.7 kg with an average of 6.4 kg. Among the stomachs analyzed seven were damaged, 30 were empty and 46 were considered for the analysis because it had some content.

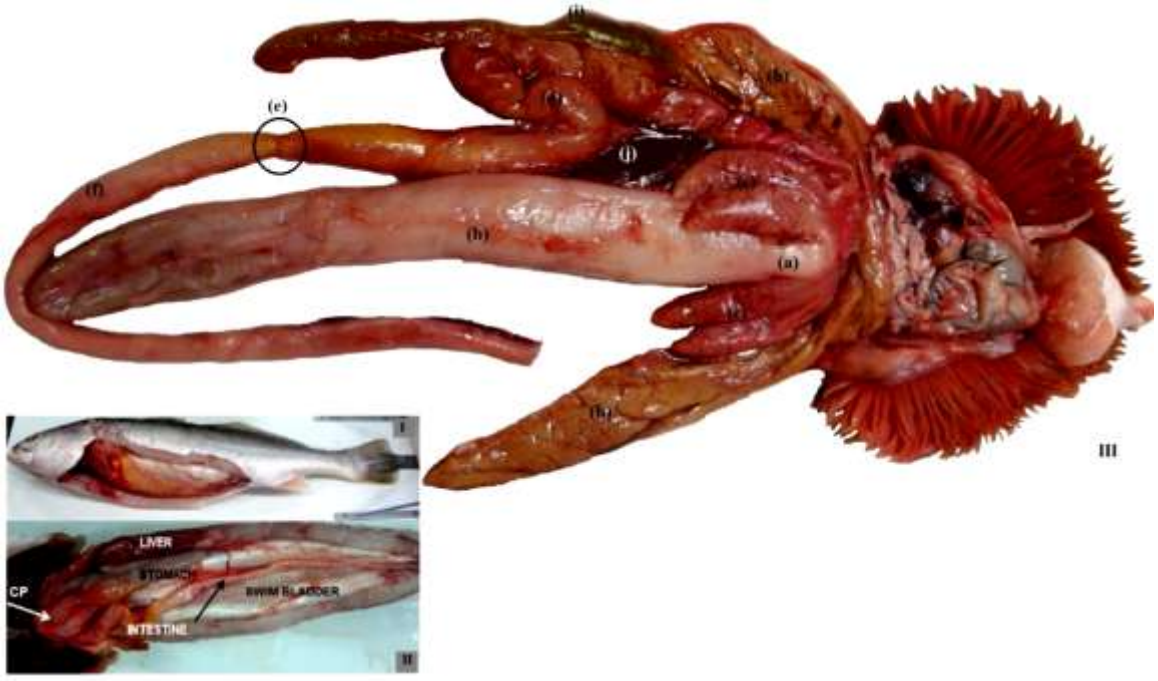

Fig. 2. **(I)** - Ventral view of the coelomic cavity *C. acoupa*, **(II)** Location stomach and swim bladder; **(III)** (a) esophagus; (b) stomach; (c) Pyloric caecum (CP); (d) intestine; (e) ileo-rectal valve; (f) Rectum; (h) Liver; (i) biliar vesicle; (j) Pancreas.

Table 1. Frequency of occurrence (FO) Volume (W) and feed index (IAi) of food items present in the stomachs of *C. acoupa* of Piaui coastline from July 2013 to January 2014.

Items	FO	%FO	W	%W	IAi
FISHES					
Dasyatidae	4	4.49	114.08	11.58	4.15
Teleostei	16	17.98	176.14	17.87	25.63
Ariidae	6	6.74	170.38	17.29	9.30
Sciaenidae	3	3.37	170.58	17.31	4.65
Ophicthidae	2	2.25	1.65	0.17	0.03
Clupeidae	1	1.12	76.80	7.79	0.70
Engraulidae	1	1.12	6.25	0.63	0.06
Haemulidae	1	1.12	46.77	4.75	0.43
CRUSTACEAN					
Penaeidae	8	8.99	36.36	3.69	2.65
Portunidae	2	2.25	1.35	0.14	0.02
Palinuridae	1	1.12	10.30	1.05	0.09
Organic matter (OM)	33	37.08	173.93	17.65	52.20
Seagrass	11	12.36	0.93	0.09	0.09
Total		100	985.52	100	100

The analysis on the degree of digestion indicated that most of the identified items found in the range III, followed by scale items II and to a lesser extent on the scale I, while the degree of repletion found in the stomachs with content revealed that 40.8% with 25% of the stomach occupied, 11 (14.5%) had between 25% and 75% of the occupied stomach, and only 4 (5.3%) degree of fullness 75-100%. The rest (39.5%), totaling 30 individuals presented degree of repletion 0, with empty stomach.

The food spectrum of *C. acoupa* presented an essentially carnivorous diet, with 4 food categories: Pisces, crustaceans (Decapod), OM (organic matter) and

seagrass. The obtained food items were represented by the following taxonomic groups: Teleostei, Ariidae, Sciaenidae, Ophicthidae, Clupeidae, Engraulidae, Haemulidae, Dasyatidae (Elasmobranchii), Penaeidae, Palinuridae, Portunidae, OM (organic matter) and seagrass (Table 1 and Fig. 1). In the fish category the families and species were identified: Ariidae (*Sciadeichthys luniscutis*), Sciaenidae (*Macrodon ancylodon*), Ophicthidae (*Ophichthus ophis*), Clupeidae (*Ophisthonema oglinum*), Haemulidae (*Genyatremus luteus*), Dasyatidae (*Dasyatis guttata* and *Dasyatis* spp.); while in the shellfish category occurred families and species: Palinuridae (*Panulirus laevicauda*), Portunidae (*Callinectes* spp.) and Penaeidae.

The largest proportion was in the category fish totaling 72.4% of the total weight of the items, the main were Teleostei (16.7%), and the Ariidae and Sciaenidae families, both with (16.2%) (Table 1 and Fig. 1a). Crustaceans showed 4.56% of highlighting the family Penaeidae (3.5%) (Table 1 and Fig. 1a). The plant represented solely by seagrass (0.1%) were considered incidental to present small proportion or weight (% W) (Table 1 and Fig. 1a).

The frequency of occurrence method (Table 1 and Fig. 1a) showed there was dominance of Teleostei (35.54%) and by family Penaeidae with (17.77%), followed by Family Ariidae (13.33%), Dasyatidae (8.89%), Sciaenidae (6.66%), Ophicthidae and *Callinectes* spp., both with 4.44% (Table 1 and Fig. 1a). Families Clupeidae, Engraulidae, Haemulidae and *Panulirus laevicauda* presented FO = 2.22% (Table 1 and Fig. 1a).

The Food Index express preferred food. The items essential were Teleostei (2722.76) followed by Family Ariidae with 734.99 (Table 1 and Fig. 1b). The taxonomic group of crustaceans with almost all belonging to the Family Penaeidae with 475.77, even though they have contributed significantly in the diet were classified as prey of secondary importance (Table 1 and Fig. 1b).

Trophic Morphology

The peritoneal cavity *C. acoupa* is relatively small (Fig. 2 I) as compared to the muscle mass of the fish. The digestive tract while extending along the cavity does not completely fill in due to the large volume occupied by the swim bladder and gonads that also extend throughout the peritoneum from the anterior third to the rectum (Fig. 2 II).

Most organs are in the anterior third of the celomatic cavity providing up sequentially the esophagus and stomach, pyloric caeca, liver and gallbladder, and in the middle portion occurs the intestine with shaped "N", and ends with the last intestinal segment that ends at the rectum and anus, located caudally (Fig. 2 III).

The esophagus is a relatively short, tubular and distensible with thick walls having folds 10 on average continuously to the pharynx and terminates at the cardiac region of the stomach, measuring approximately 3 cm in length.

The stomach is well developed with an average length of 17 cm; with linear format in "Y" shaped the cecal type presenting 3 well defined regions: cardiac (tube), fundic (shaped bag) and pyloric (tube). The cardiac and fundic regions are aligned in the same plane, responsible for food storage and in the stomach emptying, respectively, while the pyloric region is perpendicular to this plane, proportionately lower (Fig. 2 IIIb). The cardiac region is the largest portion of the stomach, accounting for about 60% of the total size (10.2 cm average), with large folds with average thickness of 3.6 mm in the longitudinal direction parallel, continuous folds with fundic or cecal region (thickness 1.8 mm), which represents 40% (6.5 cm) on average the total size of the stomach. The pyloric region is the minor, having an average length of 1.4 cm, with thin folds (1.7 mm thick) with a pyloric sphincter, which marks the transition from the stomach to the intestine.

The pyloric caeca are presented in the form of four small blind end tubes measuring on average 6.6 cm, project him from pyloric sphincter at the beginning of the midgut. The pattern of folds similar to the intestine, networked, with thickness 0.8 mm average (Fig. 2 IIIc). The intestine is relatively short, tubular shape, measuring 44.7 cm in total length, on average, formed by midgut and rectum, proportionally representing 60% (± 26.64 cm) and 40% (± 1.18 cm) of total length (Fig. 2 IIId). Among these there is the presence of a constriction characterized by a thickening of the muscle that forms the ileo-rectal valve enabling to make distinction between posterior intestine and rectum (Fig. 2 IIIe). Intestinal coefficient considered low with an average value of 0.87, indicating their carnivorous feeding habit.

The specimens examined in this study were derived from fishing and had sex ratio with a predominance of males (1.2 M: 1 F) and also observed that 63.6% of subjects were above the length of 1st maturity according to determining Chao (1978) which indicated that this maturity is achieved in individuals with 53 cm in total length. These characteristics are positive indications of the sustainability of the fishery yellow hake in Piaui coast.

It was possible to register a high incidence of empty stomachs (39.5%) among the samples used in this study. This feature can be associated to the characteristics of fishing gear used (network-in-waiting) as characteristics of the fishery. After being caught in the fishing gear, fish remain for a long period without food (Zavala-Camin, 1996), about 4 hours reported in this study. Fish caught

remain trapped on the network until they came on board and die quickly after capture, aspects that contribute to the advanced state of digestion of items observed in the stomachs. These observations are in line with Zavala-Camin settings (1996), where it comments that the fishing techniques with long periods of exposure influence in different ways in the obtained sample, including states, the de-expected net kill the fish quickly. However, when fishing a fish will postmortem digestion, while others will continue digesting alive and others will have to opportunity to continue to feed. Another contributing factor reported by fishermen is the fact regurgitation occur at the time of fishing, which claim that it is common to identify this process at the time of evisceration by the occurrence of prey in the mouth and esophagus yellow hake. According to Fonteles-Filho (2011), the fish may regurgitate stomach contents when hoisted aboard from great depths. The regurgitation process is described by Zavala-Camin (1996) as the partial or complete expulsion of stomach contents through the esophagus and is recognized by the occurrence of distended stomachs, empty or with little stomach contents. The incidence of empty stomachs is also a feature of carnivorous species (Gerking, 1994), as ingest trapped relatively large, high nutritional value and easily digestible, reducing the time to satiation (Hahn *et al*., 1999).

The plant food intake exclusively represented by seagrass in *C. acoupa* diet was considered accidental, because some aspects such as: the rapacious character of the species to snatch the prey ends up ingesting fragments of nearby vegetation and also the kind of behavior search for the next food in the background, due to its nekton-benthic habit, as it actively moves and lives most of the time in association with the substrate, dwelling sludge areas, sand or gravel, is coastal shallow water, brackish estuaries , estuarine lagoons and mouths of rivers, at depths ranging from 1-35 meters, and may also enter into the freshwater (Carvalho Filho, 1999). Finally, the species does not show anatomical adaptations required to use this feature (Zavala-Camin, 1996), evidenced by the fact that this item remain intact until the intestine.

In this analysis, the gravimetric method was used to measure the volume of food items to best suit the biological and anatomical characteristics of the species, the large size of the found items. The percentage of weight or volume has been considered by some authors as the most suitable approach to describe the importance of prey in the diet (Liao *et al*., 2001). The food index applied in this study proved to be appropriate in the context of the study and predator characteristics, combined with the objectives and work of the questions (Hahn and Delariva, 2003).

The power of Yellow hake (*C. acoupa*) was similar to hake-do-Piaui (*Plagioscion squamosissimus*) both of Sciaenidae, with a fish-based diet and shrimp (*Macrobrachium amazonicum*) (Santos *et al*., 2014) except for the presence of aquatic insects, absent in *C. acoupa*, concluding that it is a species of carnivorous feeding habits, prone to piscivory.

Several species of the Sciaenidae family were the subject of studies regarding its feed. Among them we can mention *Ctenosciaena gracilicirrhus*, *Macrodon ancylodon* and *Bairdiella ronchus*, whose studies showed no resemblance to the composition of the diet of *C. acoupa.* The species *C. gracilicirrhus* revealed broad food spectrum, comprising 15 food items, mainly consists of crustaceans (Gammaridae and Penaeidae) and Polychaete, other items were found fish scales, eggs and diatoms, foraminifera and bivalve (Cunningham, 1989). Studying the power *Macrodon ancylodon* verified as food items, crustaceans for young fish specimens to mature specimens (Juras and Yamaguti, 1985) although there is similarity between the items, you cannot relate to *C. acoupa* diet to maturation stages because they were not addressed their reproductive aspects in this study. Was registered in the diet of *B. ronchus* mainly crustacean decapod, and copepod and isopod, and other items were identified as fish, algae, higher plants, bivalves and gastropods (Vendel and Keys, 1998).

The species under study presents the carnivorous trend similar to other large species such as Common snook (*Centropomus undecimalis*) studied in the lagoon complex Mundaú in Alagoas (Teixeira, 1997) where it fed mainly on fish and secondarily crustaceans while the Golden (*Salminus brasiliensis*) fed into adulthood, preferably fish (Rodrigues and Menin, 2008).

Wootton (1990) emphasizes that fish are good samplers of the environment and their stomach contents reflect the availability of food. Thus, the species of carnivore habits reveal the fish fauna in the area and this top-down effect has been called trophic cascade (Carpenter and Kitchell, 1993). In this context, analyzing the *C. acoupa* of dietary components that inhabits the area of influence of the Parnaiba River estuary reveals the availability of prey in the area, at least related to fish fauna, as from the first ichthyofauna surveys conducted by Oliveira (1974), Families Scianidae and Ariidae are presented dominant with high numbers of species. Thus, the species appears as a balance of maintaining indicator of local fish populations and contributes to environmental health by their position in the food chain.

REFERENCES

Braga, FMS. 1990. Estudo da mortalidade de *Paralonchurus brasiliensis* (Teleostei, Sciaenidae) em área de pesca do camarão-sete-barbas (*Xiphopenaeus kroyeri).* Boletim do Instituto de Pesca. 17:27-35.

Carpenter, SR. and Kitchell, JF. 1993. The trophic cascade in lakes. Cambridge University Press, Cambridge. pp. 385.

Carvalho Filho, A. 1999. Peixes: costa brasileira. Editora Melro, São Paulo. pp. 320.

Chao, LN. 1978. Sciaenidae. In: FAO Species Identification Sheets for Fishery Purposes, West Atlantic (Fishing Area 31). Ed. Fischer, W. FAO, Rome. 4:94.

Cunningham, PTM. 1989. Observações sobre o espectro alimentar de *Ctenosciaena gracilicirrhus* (Metzelaar), Sciaenidae. Revista Brasileira de Biologia. 49(2):335-339.

Fonteles-Filho, AA. 2011. Oceanografia, biologia e dinâmica populacional dos recursos pesqueiros. Expressão Gráfica e Editora, Fortaleza. pp. 460.

Gerking, SD. 1994. Feeding ecology of fish. Academic press, San Diego, California. pp. 416.

Hahn, NS., Loureiro, VE. and Delariva, RL. 1999. Atividade alimentar da curvina *Plagioscion squamosissimus* (Heckel, 1840) (Perciformes, Sciaenidae) no rio Paraná. Acta Scientiuarum. 21:309-314.

Hahn, NS. and Delariva, L. 2003. Métodos para avaliação da alimentação natural de peixes: o que estamos usando? Interciencia 28:100-104.

Hynes, HBN. 1950. The food of freshwater sticklebacks (*Gasterosteus aculeatus* and *Pygosteus pungitius*) with a review of methods used in studies of the food of fishes. Journal Animal Ecology. 19:36-58.

Hyslop, EJ. 1980. Stomach contents analisys; a review of methods and their application. Journal of Fish Biology. 17:411-429.

Kawakami, E. and Vazzoler, G. 1980. Método gráfico e estimativa do índice alimentar aplicado no estudo de alimentação de peixes. Boletim do Instituto Oceanográfico. 29(2): 205-207.

Juras, AA. and Yamaguti, N. 1985. Food and feeding habitats of king weakfish, *Macrodon ancylodon* (Bloch and Schneider, 1801) caught in the southern coast of Brazil (Lat.29° to 32° S). Boletim do Instituto Oceanográfico. 33(2):149-157.

Liao, H., Pierce, CL. and Larscheid, JG. 2001. Empirical assessment of indices of prey importance in the diets of predacious fish. Transactions of the American Fisheries Society. 130:583-591.

Matos, IP. and Lucena, F. 2006. Descrição da pesca da pescada-amarela, *Cynoscion acoupa*, da costa do Pará**.** Arquivo de Ciências do Mar. 39:66-73.

Menezes, NA. and Figueiredo, JL. 1980. Manual de peixes marinhos do sudeste do Brasil. IV. Teleostei (III). Museu de Zoologia da USP, São Paulo. pp. 110.

Nelson, JS. 1994. Fishes of the World. John Wiley and Sons Inc., New York, USA. pp. 600.

Oliveira, AME. 1974. Ictiofauna das Águas estuarinas do Rio Parnaíba (Brasil). Arquivo de Ciências do Mar. 14:41-45.

Rodrigues, SSN. and Menin, E. 2008. Anatomia do tubo digestório de Leporinus macrocephalus (Characiformes, Anostomidae) em relação a seu habitar alimentar. Bioscience Journal. 24(3):86-95.

Santos, EP. 1978. Dinâmica de populações aplicada à pesca e a piscicultura. HUCITEC, EDUSP, São Paulo. pp. 129.

Santos, NCL. Medeiros, TN. Rocha, AAF. Dias, RM. and Severi, W. 2014. Uso de recursos alimentares por *Plagioscion squamosissimus* - piscívoro não-nativo no reservatório de sobradinho-Ba, Brasil. Boletim do Instituto de Pesca. 40:397-408.

Teixeira, RL. 1997. Distribuition and feeding habitats of the young common snnok, *Centropomus undecimalis* (Pisces: Centropomidae) in the shallow waters of a tropical Brazilian estuary. Boletim do Museu Biologia Mello Leitão. 6:35-46.

Vaske-Jr., T. Vooren, CM. and Lessa, RP. 2003. Feeding Strategy of Yellowfin Tuna (*Thunnus albacares*) and Wahoo (*Acanthocybium solandri*) in the Saint Peter and Saint Paul Archipelago, Brazil. Boletim do Instituto de Pesca. 29:173-181.

Vendel, AL. and Chaves, PTC. 1998. Alimentação de *Bairdiella ronchus* (Cuvier) (Perciforme, Sciaenidae) na Baía de Guanabara, Paraná, Brasil. Revista Brasileira de Zoologia. 15:297-305.

Vazzoler, AEM. Soares, LSH. and Cunningham, PM. 1999. Ictiofauna da Costa brasileira. In: Estudos ecológicos de comunidades de peixes tropicais. Ed. Lowe McConnell RC. Editora da Universidade de São Paulo, São Paulo, Brazil. 424-467.

Waessle, JA., Lasta, CA. and Favero, M. 2003. Otolith morphology and body size relationships for juvenile Sciaenidae in the Rio de la Plata estuary (35-36ºS). Scientia Marina. 67(2):233-240.

Zavala-Camin, LA. 1996**.** Introdução aos estudos sobre alimentação natural em peixes. NUPELIA, EDUEM, Maringá. pp.129.

Wootton, RJ. 1990. Ecology of Teleost Fishes. Chapman & Hall, London. pp. 404.

Received: May 23, 2016; Revised: Oct 20, 2016;
Accepted: Nov 11, 2016

Canadian Journal of Pure and Applied Sciences
Vol. 11, No. 1, pp. 4087-4090, February 2017
Online ISSN: 1920-3853; Print ISSN: 1715-9997
Available online at www.cjpas.net

SURVEY OF TICK (ACARI: IXODIDAE) INFESTATIONS OF CATTLE IN FEDERAL COLLEGE OF WILDLIFE MANAGEMENT, NEW BUSSA, NORTH CENTRAL NIGERIA

*Simon MK[1], Saba M[2], Mohammed BR[1] and Agbede RIS[1]
[1]Department of Veterinary Parasitology and Entomology
Faculty of Veterinary Medicine, University of Abuja, Nigeria
[2]Federal College of Wildlife Management, New Bussa, Niger State, Nigeria

ABSTRACT

Ticks and Tick borne diseases are major constraints to the development of viable livestock industries in tropical and sub-tropical countries including Nigeria. Little is known about the incidence of ticks in New Bussa. This study was therefore carried out at the Federal College of Wild life Management to investigate the degree of tick infestation of cattle in the college farm. A total of eighteen (18) cattle from two breeds of cattle (Sokoto Gudali and Fulani breeds) were randomly sampled out and grouped into three viz Colored Fulani (A), Sokoto Gudali(B) and White Fulani (C). Ticks were collected using a manual picking method over a period of eight months covering both dry (Jan-April) and wet (May-August) seasons in 2014. Ticks collected were sorted out as hard (Ixodidae) and soft (Argasidae) ticks. Results revealed that the college farm is endemic with ticks especially the soft ticks (55.17%) than hard ticks (44.83%) and higher numbers were recorded during wet season (soft ticks, 93.39%; hard ticks 6.61%) than dry season (Soft ticks 14.29%; hard ticks 85.71%). Furthermore, Colored Fulani had more affinity to ticks than Sokoto Gudali and White Fulani. There is a significant difference between the dry and wet season as the calculated value was 18.68 against the tabulated value 5.19. Tick infestations are strategically controlled through acaricide application either by hand spray or bath on regular basis. This study has implication on sustainable beef production for human consumption.

Keywords: Acaricides**,** Ectoparasites, Sokoto Gudali, Fulani breeds, New Bussa, Incidence.

INTRODUCTION

Cattle are one of the major protein suppliers to human populace globally and have a population of about 13.9 million in Nigeria (Girei *et al*., 2013). In tropical countries including Nigeria, Cattle (*Bos indicus*) production is constrained by ecto and endo parasites (Tamerat *et al*., 2015; Patel *et al*., 2015; Abdela, 2016). Among the ectoparasites, ticks are typically known to cause losses in productivity through irritation, mortality due to blood loss, destruction to hides and skin of infested animals, injection of toxins and serve as vectors of important protozoa, rickettsial, bacterial and viral diseases (Mohammed and Agbede, 1980; Agbede, 1981; Tongjura et *al*., 2012; Brites-Neto *et al*., 2015; Periyaveeturaman *et al*., 2016). Ticks are therefore the most important ectoparasites of cattle and are responsible for severe economic losses in livestock production (Alemu *et al*., 2014; Eyo *et al*., 2014). In Nigeria, the suitable conditions such as climatic factors of rain and temperature favor tick development and growth (Mohammed and Agbede, 1989; Ahmed and George, 2002). The serious impact of ticks and tick-borne diseases (TBD) on cattle production and national economies necessitate application of appropriate tick control strategies (Eyo *et al*., 2014; Gedilu *et al*., 2014). Despite reported cases of tick infestations of cattle in the college farm, no significant research on the families of ticks and their seasonal variation have been reported. Monitoring of tick infestation is quintessential for the development of effective control strategies for ticks and tick-borne diseases. The present study therefore was undertaken to determine the incidence of ticks in relation to the family of ticks and seasons of the year of the cattle population.

Corresponding author e-mail: balarabemohammed161@yahoo.co.uk

MATERIALS AND METHODS

Study area

The study was conducted in the College Farm of Federal College of Wildlife Management, New Bussa, Niger state North Central Nigeria. New Bussa sits at 9° 53′N 4°31′E Coordinates: 9°53′N 4°31′E, and the original town of Bussa was located about 40 km North of New Bussa at 10°13′51″N 4°28′31″E (altitude 561 ft or 170 meters) (Fig. 1).

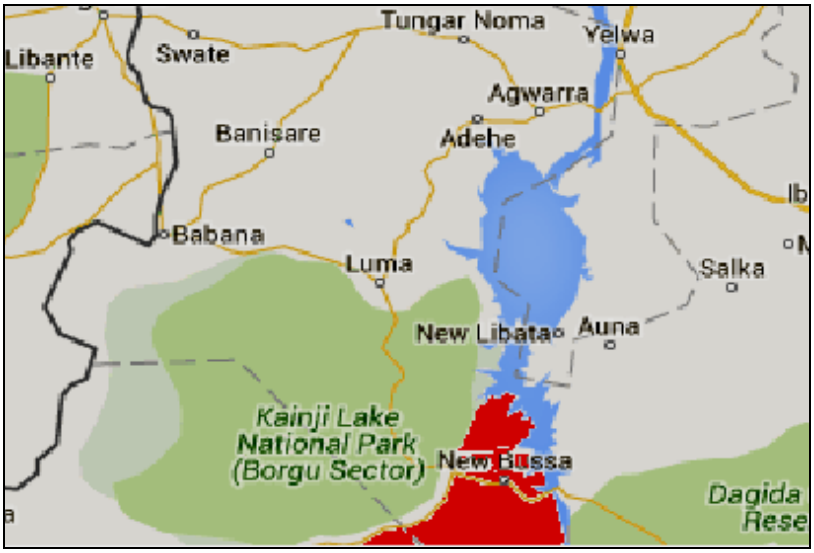

Fig. 1. Map of New Bussa (indicated red) the study area. Adopted and modified from http://www.postcodesdb.com/AlphabeticSearch.aspx? country=Nigeria&city=New% 20 Bussa &zip=912105.

It has a tropical continental climate characterized by a shorter wet season (May to September) and a longer dry season (October to April) with a temperature of 15ºC to nearly 40ºC. Annual rainfall is about 1000mm but there's considerable variation in amount and distribution of rainfall among years. Rainfall is concentrated in the months of June, July and August. The town is bordered by the Kainji Lake created by the damming of River Niger at Kainji. The vegetation in New Bussa is Guinea Savanna which is characterized by undistributed woodland with trees 15m – 18m tall (Nnaji and Omotugba, 2014).

Study population

Between January and August 2014, a total of 18 heads of cattle sampled from the college farm were subjected to detailed examination for the presence of ticks. Two breeds of cattle were identified in the college farm viz Fulani Breed and Sokoto Gudali. The Fulani Breed was further divided into; Colored and White.

Data collection

The survey was conducted over the course of two season's viz dry season (January- April) and wet season period (May-August). Ticks were collected three times in each month for both seasons. Eighteen heads of cattle were sampled out from the college farm and grouped into three, in each group six heads of cattle were sampled out at random and tagged as A (for Colored Fulani), B (for White Fulani) and C (for Sokoto Gudali). For the purpose of clarity, the animals were further labeled as A1-A6, B1-B6 and C1-C6 for the Colored Fulani, White Fulani and Sokoto Gudali respectively. The animals were physically restrained with strong rope. This is usually done with the help of herdsmen and the animals are physically inspected for complete deticking using a pair of hand forceps. Care was taken in removing the ticks intact to avoid the destruction of mouth parts. After each sample collection, the entire flock was fumigated with acaricide (Asuntol).

Ticks identification and preservation

Ticks were collected manually by hand picking from different parts of the cattle without damaging their mouth parts (Soulsby, 1982), identified and sorted out as Ixodidae (hard ticks) and Argasidae (soft ticks) using the standard taxonomic keys description by Walker *et al*. (2003). Ticks collected were preserved in sample bottles containing 70% alcohol solution and labeled according to the tags on the cattle and date of collection.

Data analysis

The data was subjected to statistical analysis using the chi-square to determine the significant level of the tick infestation in the study area; percentile was equally used to determine the group of cattle with high infirmity to tick infestation.

RESULTS AND DISCUSSION

Table 1 showed that the number of ticks collected from the various groups of cattle in dry season indicate that group A had a total of tick collection of 24, 20, 24 and 20 in the months of January, February, March and April respectively. Whereas group B had 24, 20, 26 and 6 respectively and group C had 18, 22, 19 and 10 for the respective months.

Table 2 showed that the number of ticks collected from the various groups of cattle in the wet season indicating

Table 1. Distribution of the collected ticks during the dry season.

	January	February	March	April	Total	%
A1-A6(Colored Fulani)	24	20	24	20	88	37.7
B1-B6(White Fulani)	24	20	26	6	76	32.62
C1-C6(Sokoto Gudali)	18	22	19	10	69	29.61

Table 2. Distribution of the collected ticks during the wet season.

	May	June	July	August	Total	%
A1-A6(Colored Fulani)	228	266	251	267	1012	50.35
B1-B6(White Fulani)	100	102	113	138	458	22.54
C1-C6(Sokoto Gudali)	117	133	149	146	645	27.11

that group A had 228, 266, 251 and 267 for the months of May, June, July and August respectively. Whilst group B had 100, 02, 113 and 138 and group C had 117, 133, 149 and 146 for the respective months.

Figure 2 shows the percentage distribution of ticks collected throughout the two periods of the study with soft ticks having 14.29% and hard ticks 85.71% during the dry season whilst during wet season had 93.39% and 6.61% for the soft and hard ticks respectively.

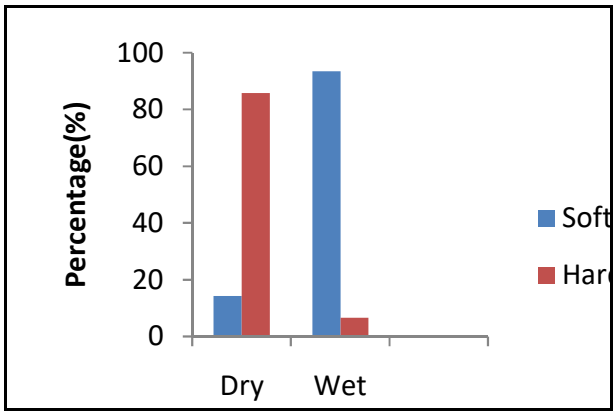

Fig. 2. Percentage distribution of ticks in the study area over the dry and wet seasons.

Figure 3 shows the percentage distribution of soft and hard ticks collected over the two seasons in respect to the two types of ticks. For the dry season, 140 (55.17%) soft ticks and 840 (44.83%) hard ticks whilst during the wet season 1,187 (55.17%) soft ticks and 84 (44.83%) hard ticks were recorded.

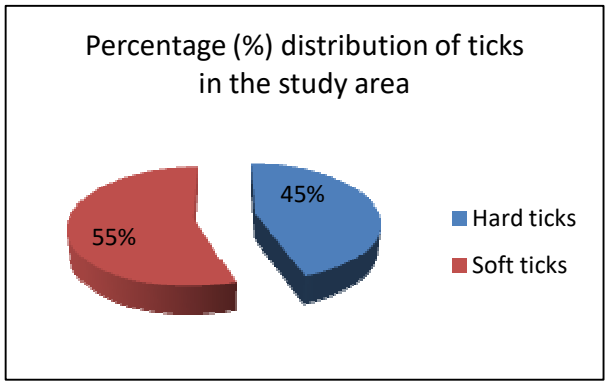

Fig. 3. Percentage distribution of the types of ticks in the study area.

Ticks are responsible for huge economic losses in livestock production through transmission of wide range of tick-borne diseases (TBD) and direct damage to hide and skin (Bedasso *et al.*, 2014; Gedilu *et al.*, 2014; Tamerat *et al.*, 2015). In the current study, it was revealed that cattle group A (Colored Fulani) had the highest affinity to ticks during the dry season period (37.77%) whilst C (Sokoto Gudali) has the lowest affinity to ticks (29.41%). During wet season, it was observed that cattle in group A (Colored Fulani) had the highest affinity to ticks with 50.35% followed by C (Sokoto Gudali) which has 27.11% and B (White Fulani) has the lowest tick affinity with 6.61%. During the dry season, hard ticks were more abundant with 85.71% compared to soft ticks which have 14.29%. During the wet season, soft ticks were more abundant than the hard ticks with 93.39% compared to soft ticks which were 6.61%. This is sequel to the fact that hard ticks are more resistant to dry season conditions of high temperature and high solar radiations are low. This concurs with the study of Okaeme, 1984. The abundance of hard ticks could also be attributed to the presence of their hard dorsal plate (Scutum) which

enables them to resist the harsh environmental dry season conditions. It was further revealed that soft ticks are the commonest (55.17%) of the samples collected on the college farm (Fig. 3).This could be attributed to the fact that the ticks need to hide whilst on the body of their hosts. Consequently, colored animals provide a good camouflage for the ticks.

CONCLUSIONS AND RECOMMENDATIONS

The present study revealed that cattle in the college farm are infested with different types of ticks which could be due to wide vegetation coverage of the study area, climatic and host factors. This potentially poses huge economical constraint to the college in particular and the extended community in the study area as a whole. Therefore, systematic intervention and control of tick infestation should be put in place to control the menace of ticks. Further research should be carried out to identify the various tick species in the study and possibly identify the various ticks' related diseases in the area.

REFERENCES

Abdela, N. 2016. Important Cattle Ticks and Tick Born Haemoparasitic Disease in Ethiopia: A Review. Acta Parasitologica Globalis. 7(1):12-20.

Agbede, RIS. 1981. A Survey of Ectoparasites and Parasitic conditions of animals in Zaria. Nigerian Journal of Animal Production Research 1:179-180.

Ahmed, A. and George, BDJ. 2002. Incidence of hard ticks (Ixodidae) on horses around Zaria, Nigeria. Nigerian Veterinary Journal. 23(1):70-74.

Alemu, G., Chanie, M., Mengesha, D. and Bogale, B. 2014. Prevalence of Ixodid Ticks on Cattle in Northwest Ethiopia. Acta Parasitologica Globalis. 5 (2):139-145.

Bedasso, M., Abebe, B. and Degefu, H. 2014. Species composition, prevalence and seasonal variations of ixodid cattle ticks in and around Haramaya town, Ethiopia. Journal of Veterinary Medicine and Animal Health. 6(5):131-137.

Brites-Neto, J., Duarte, KMR. and Martins, TF. 2015. Tick-borne infections in human and animal population worldwide. Veterinary World. 8(3):301-315.

Eyo, JE., Ekeh, FN., Ivoke, N., Atama, CI., Onah, IE., Ezenwaji, NE. and Ikele, CB. 2014. Survey of Tick Infestation of Cattle at Four Selected Grazing Sites in the Tropics. Global Veterinaria. 12 (4):479-486.

Gedilu, M., Mohamed, A. and Kechero, Y. 2014. Determination of the prevalence of ixodid ticks of cattle breeds, their predilection sites of variation and tick burden between different risk factors in Bahir Dar. Ethiopia. Glob. Vet. 13(4):520-529.

Girei, AA., Dire, B. and Bello, BH. 2013. Assessment of cost and returns of cattle marketing in central zone of Adamawa State, Nigeria. British Journal of Marketing Studies. 1(4):1-10.

Mohammed, AN. and Agbede, RIS. 1989. The Relevance of Effective Control of Ticks and Tick-Borne Diseases (TBD) in Livestock Production. Invited paper presented at the Symposium organized at the University of Sokoto. pp.13-19.

Mohammed, AN. and Agbede, RIS. 1980. Control of Ectoparasites of Ruminants in Nigeria –Invited paper. In: Proceedings or National Seminar on Current Problems Facing the Leather Industry in Nigeria held at Leather Research Institute of Nigeria (LERIN). Zaria. pp.21-27.

Nnaji, JC. and Omotugba, S. 2014. Physico-chemical Quality of Drinking Water in New Bussa, Niger State, Nigeria. International Research Journal of Pure & Applied Chemistry. 4(4):437-446.

Okaeme, AN. 1984. Prevalence of Skin Diseases of Cattle and Impact on leather Production in Nigeria. Journal of Leather Research. 2(55):16.

Patel, G., Shanker, D., Jaiswal, A. K., Sudan, V. and Verma, SK. 2015. Prevalence and Seasonal Variation in Ixodid Ticks on Buffaloes of Mathura District, Uttar Pradesh, India. International Buffalo Information Center (IBIC) Buffalo Bulletin. 34(1):21.

Periyaveeturaman, C., Selvaraju, D., Kinhekar, AS., Dutta, L. and Kumar, V. 2016. Community oriented ectoparasite intervention system: Concept s for on-farm application of indigenous veterinary medi cation. Adv. Anim. Vet. Sci. 4(1s):9-19.

Soulsby, EJI. 1982. Helminths, Arthropods and Protozoa of Domesticated Animals. (7th edi.). Bailliere Tidally and Cassel Limited, London.

Tamerat, N., Koroso,L., Mengistu, S. and Keffale, M. 2015. Prevalence and identification of ectoparasites fauna inMsmall ruminants in and around Adami Tulu, East Shawa Zone of Oromia, Ethiopia. Journal of Veterinary Medicine and Animal Health. 7: (In press).

Tongjura, JDC., Amuga, GA., Ombugadu, RJ., Azamu, Y. and Mafuiya, HB. 2012. Ectoparasites infesting livestock in three Local Government Areas (LGAS) of Nasarawa state, Nigeria. Science World Journal. 7(1):15-17.

Walker, AR., Bouattour, A., Camicas, JL., Estrada Peña, A., Horak, IG., Latif, AA., Pegram, RG. and Preston, PM. 2003. Ticks of Domestic Animals in Africa: a Guide to Identification of Species. Bioscience Reports. pp.227.

Received: June 8, 2016; Accepted: Oct 24, 2016

Canadian Journal of Pure and Applied Sciences
Vol. 11, No. 1, pp. 4091-4102, February 2017
Online ISSN: 1920-3853; Print ISSN: 1715-9997
Available online at www.cjpas.net

A REVIEW: VERTEBRATE BIODIVERSITY, ENVIRONMENTAL HAZARDS AND ECOLOGICAL CONDITION OF KEENJHAR LAKE, PAKISTAN

*Iqbal Saeed Khan[1], M Usman Ali Hashmi[2], Amtyaz Safi[3] and Tahira Abdul Latif[1]
[1]Wildlife Section, Department of Zoology, University of Karachi, Karachi-75270
[2]Department of Zoology, Dehli Government Science College, Hussainabad, Karachi-75950
[3]Department of Zoology, Sir Syed Government Girls College Nazimabad, Karachi-74600, Pakistan

ABSTRACT

Globally there are 2247 Ramsar sites with total area of 214,958,432 ha, including 19 sites of Pakistan. Keenjhar Lake is considered as one of largest freshwater lakes of Sindh, and it is the major source of water supply through different feeder canals to largest city of Karachi. There are 54 species of fishes, 121 species of birds, 25 species of mammals, two species of amphibian and 29 species of reptiles were reported. Aquatic ecosystem of the lake is under threat due to increased industrial and domestic effluent discharge via Kalri-Baghar Feeder Canal which carries contaminants from Kotri urban and Industrial area. KB Feeder Canal is the main source of pollution to Keenjhar Lake. Presently, industrial discharge from Kotri and Nooriabad industries are source for affecting water quality and health of this wetland, we also noted that eutrophication is also problem in the lake. Water samples collected from Keenjhar Lake found contained pesticides below the Maximum Acceptable Concentrations level.

Keywords: Keenjhar lake, vertebrate biodiversity, environment, threats.

INTRODUCTION

Wetland plays a vital role in ecological balance of an ecosystem. Significance of wetlands and their role in ecosystem management is well known but so many hazards are present which directly or indirectly affect the health of wetlands. Hazards are may be natural or artificial which are influenced by human activities. Sindh is the third largest province of Pakistan having a lot of diversity in ecosystems including mountains, deserts, grasslands, woodlands and variety of wetlands. Presently, Pakistan has 19 designated Ramsar Sites with the total area of 1,343,627 hectares, Convention entered into force in Pakistan on November 23, 1976 [(Table 1) (Ramsar Convention, 2017)].

Keenjhar Lake is located in Thatta District of Sindh (Fig. 1). It covers approximately 14,000 ha of area and having latitude and longitude of 68° 03'E and 24° 56'N. It is considered as one of largest fresh water lakes of Sindh and it is the major source of water supply through different feeder canals to Karachi city, Thatta city and Ketibunder. The main water supply to Keenjhar Lake comes from River Indus. The location of Keenjhar Lake is about 19km North and North East to Thatta District, while it is situated 113km away from Karachi city.

Many seepage lagoons and marshes are surrounding the Keekjhar Lake which is connected with semi deserted areas bearing limestone rock beds. This man made fresh water lake was formed in 1930 when two small lakes named Keenjhar and Kalri Lake were merged together after development of a dam at Bangla (Khan and Abbas, 2011).

The fish fauna of lake is diversified and contains a variety of fresh water fishes including Dahi (*Labeo calbasu*), Daya (*Oreochromis mossambicus*), Gandhan (*Chitala chitala*), Ganer (*Cirrhinus rebo*), Goj (*Mastacembelus armatus*), Jerki (*Wallago attu*), Kago (*Rita rita*), Kandar (*Chanda nama*), Luhr (*Heteropneustes fossillis*), Morakhi (*Cirrhinus mrigala*), Popri (*Puntius chola*), Palla (*Tenualosa ilisha*), Rohu (*Labeo rohita*), Sole (*Channa marulia*) and Thaila (*Gibelion catla*).

Birds mostly visit to Keenjhar Lake for many purposes like breeding and nesting grounds, roosting areas and for foraging purposes (Khan *et al*., 2012). The important breeding birds of the lake are Night Heron (*Nycticorax nycticorax*), Cotton Teal (*Nettapus coromondelianus*), Pheasant-tailed Jacana (*Hydrophasianus chirurgus*), Purple Moorhen (*Porphyrio porphyris*) and some passerine birds.

*Corresponding author email: iqbalsaeedkhan@gmail.com

Table 1. List Designated Ramsar Sites of Pakistan upto Jan 2017.

S. No.	Name	Province	Area hectares	Co-ordinates
1	Hub (Hab) Dam	Balochistan, Sindh	27,000	25°15'N 067°07'E
2	Astola (Haft Talar) Island	Balochistan	5,000	25°07'N 063°52'E
3	Jiwani Coastal Wetland	Balochistan	4,600	25°05'N 061°48'E
4	Miani Hor	Balochistan	55,000	25°24'N 066°06'E
5	Ormara Turtle Beaches	Balochistan	2,400	25°13'N 064°28'E
6	Chashma Barrage	Punjab	34,099	32º25'N 071º22'E
7	Taunsa Barrage	Punjab	6,576	30º42'N 070º50'E
8	Uchhali Complex (including Khabbaki, Uchhali and Jahlar Lakes)	Punjab	1,243	32º37'N 072º00'E
9	Tanda Dam	Khyber Pakhtunkhwa	405	33º35'N 071º22'E
10	Thanedar Wala	Khyber Pakhtunkhwa	4,047	32º37'N 071º05'E
11	Deh Akro-II Desert Wetland Complex	Sindh	20,500	26°50'N 068°20'E
12	Drigh Lake	Sindh	164	27º34'N 068º06'E
13	Haleji Lake	Sindh	1,704	24º47'N 067º46'E
14	Indus Delta	Sindh	472,800	24°06'N 067°42'E
15	Indus Dolphin Reserve	Sindh	125,000	28°01'N 069°15'E
16	Jubho Lagoon	Sindh	706	13,468 ha
17	Nurri Lagoon	Sindh	2,540	24°30'N 068°47'E
18	Runn of Kutch	Sindh	566,375	24°23'N 070°05'E
19	Kinjhar (Kalri) Lake	Sindh	13,468	24º56'N 068º03'E

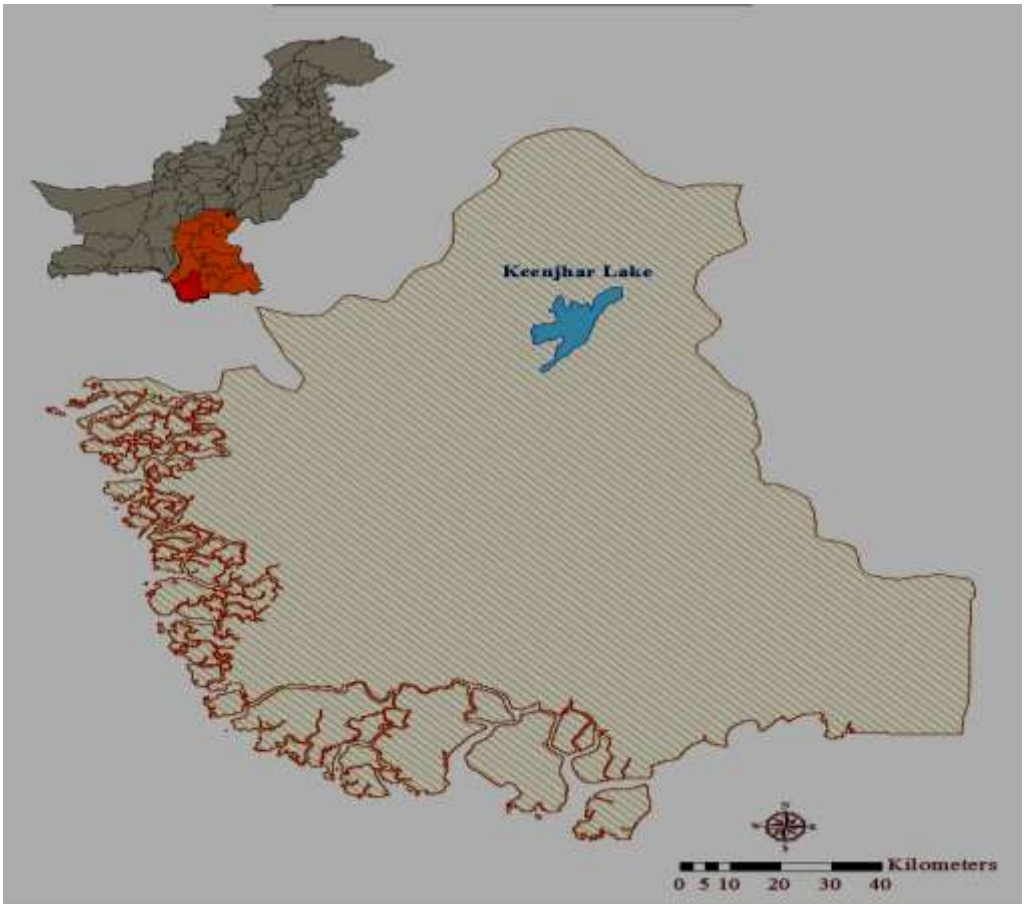

Fig. 1. Map of Pakistan with location of Keenjhar Lake.

Keenjhar Lake is playing a important role in providing the natural resources of livelihood to the local community consist of over 50 villages of Thatta district, and whole community are dependent on this lake for their survival (Khan and Abbas, 2011; Khan *et al*., 2012).

Keenjhar Lake also provides good habitat for various mammalian and reptilian species. Key species of mammals found in vicinity of Keenjhar Lakes includes Smooth-coated Otter (*Lutrogale perspicillatus*) and Fishing Cat (*Prionailurus viverrinus*). While important birds includes Cotton Teal (*Nettapus coromandelianus*) and Pallas's Fishing Eagle (*Haliacetus leucoryphus*). Reptiles includes Spiny-tailed Lizard (*Sara hardwickii*) and Indian Monitor Lizard (*Varanus bengalensis*).

Keenjhar Lake is contains a huge variety of water weeds and a complex network of aquatic vegetation in its depth. It also supports migratory birds annually as it offers an attractive habitat for aquatic migratory birds as their wintering area, staging and breeding grounds. The important species of birds includes European Wigeon (*Anas penelope*), Black Coot (*Fulica atra*) and Common Pochard (*Aythya ferina*) (Khan and Abbas, 2011; Khan *et al*., 2012).

Some work has been done by Ashraf *et al*., 1992; Baqai and Rehana, 1973; Baqai and Siddiqui, 1973; Baqai, 1974a,b; Conder, 1977; Durranee and Khan, 2008; Ghalib *et al*., 1981; Ghalib and Bhaagat, 2004; Ghalib *et al*., 2004, 2009; IFAP, 2009; IUCN, 2004; Jafri *et al*., 1999; Jehangir *et al*., 2000; Kazmi *et al*., 2006; Khan, 2005; Khan and Law, 2005; Khan and Ghalib, 2006; Khanum and Ahmed, 1991; Korai *et al*., 2008a,b; Korai *et al*., 2001; Korai *et al*., 2009; Khan and Abbas, 2011; Khan *et al*., 2012; Khan *et al*., 2015; Mahar *et al*., 2010; Nazneen, 1974, 1980; Nazneen and Begum, 1992; Roberts *et al*., 1986; Saqib *et al*., 2005; Scott, 1989; Scott and Poole, 1989 and Siddiqui *et al*., 1973. The aim of this paper is review the status of important vertebrate biodiversity, effects of environmental hazards and ecological condition of the lake.

DISCUSSION

The climate of Sindh is semiarid and the climatic studies of lake has revealed that lake being a individual ecosystem contains dry monsoonal fluctuating temperature with extreme hot weather during summers and moderately low temperatures in winter seasons. The average monsoonal rainfall measures about 175mm. The mean temperature during summers has been recorded as 47^0C, while in winters it is about 15^0C. Some adjacent small seasonal streams also supply water to the Keenjhar Lake from West and Northern sites. The lake is having one main canal which is called as Karli Bagri feeder Canal which is connected with the lake from North West site. Through South East site the only outlet of lake is Jam branch canal. Its length is about 24km, while its width is about 6km. Presently, depth of the lake is about 8m with the network of reef beds and aquatic weeds.

In the pre Monsoon period the minimum temperature of water of Keenjhar Lake was 28^0C, while the maximum temperature was about 33^0C and it was 16 to 20^0C during the post Monsoon. The air temperature was also monitored; during pre Monsoon it was recorded from 31 to 36^0C and it was from 18 to 24^0C in post Monsoon.

The conductivity was recorded as 453 to 742 mg/L, while, 243 to 492 mg/L was the value of total dissolved solids present in the lake, 6.81 to 8.31 was the value of pH recorded. 1.37 NTU to 12.6 NTU was the estimated turbidity level. Total alkalinity calculated from the values of 28 to 107 mg/L. 58 up to 144 mg/L was the value of total hardness present in lake. 0.21 to 1.9 mg/L was the recorded value of salinity. The BOD value ranged from 1.12 to 9.9 mg/L. The value of Carbon dioxide estimated from 1 up to 2 mg/L, while 28 to 87 mg/L was the value of calcium present in Lake. It was observed that 38 to 106 mg/L was the quantity of magnesium in Lake and the quantity of sulfate ranged from 18 to 156mg/L. The estimated range of chlorides was from 35.2 to 98 mg/L. While 0.006 to 0.28 mg/L was the quantity of phosphates in the Lake. The estimated amount of Cadmium was 0.00 to 1.32 mg/L, and the value of Chromium was from 0.00 to 1.01 mg/L. The quantity of Lead was from 0.00 to 0.01 mg/L, and the estimated amount of nickel recorded was 0.01 to 0.80 mg/L.

Vertebrate Biodiversity

Earlier studies regarding vertebrate biodiversity, Khan and Abbas (2011) and Khan *et al*. (2012) reported that there were twenty five species of mammals, and presently no change in the reported species (Table 2). The key species were Asiatic Jackal (*Canis aureus*), Bengal fox (*Vulpes bengalensis*), Desert Fox (*Vulpes vulpes*), Smooth-coated Otter (*Smooth-coated Otter*), Jungle Cat (*Felis chaus*), Fishing Cat (*Prionailurus viversina*), Grey Mongoose (*Herpestes edwardsi*), Small mongoose (*Herpestes javanicus*), Pangolin (*Manis crassicaudata*), Long-eared Hedgehog (*Hemiechinus collaris*) and Porcupine (*Hystrix indica*). There were 121 species of birds were identified from the Keenjhar Lake area (Table 3). The common birds present near lake were waterbirds, birds of prey, passerines and Grey Partridge (*Francolinus pondicerianus*).

While, Ferruginous Duck (*Aythya nyroca*), Dalmatian Pelican (*Pelecanus crispus*), Black-bellied Tern (*Sterna acuticauda*), Black-headed Ibis (*Threskiornis melanocephalus*), White Stork (*Ciconia ciconia*) and Cotton Teal (*Nettapus cormandelianus*) were noted as

Threatened or Near Threatened species (Figs. 2 - 6) and still these species observed as Threatened.

Fig. 2. Ferruginous Duck (*Aythya nyroca*) (Photo source: hotspotbirding.com).

Fig. 3. Dalmatian Pelican (*Pelecanus crispus*).

Fig. 4. Black-bellied Tern (*Sterna acuticauda*).

Fig. 5. Black-headed Ibis (*Threskiornis melanocephalus*)

Fig. 6. White Stork (*Ciconia ciconia*).

In a recent studies, Khan and Abbas (2011) and Khan *et al*. (2012) reported 29 species of reptiles and we observed that presently no change see Table 4, and still key species were Brilliant Agama (*Trapelus agilis*), Fat-tailed Gecko (*Eublepharis macularius*), Spiny-tailed Lizard (*Sara hardwickii*), Indian Monitor Lizard (*Varanus bengalensis*), Common Krait (*Bungarus caeruleus*), Indian Cobra (*Naja naja*), Oxus Cobra (*Naja oxiana*), Russel's Viper (*Daboia russelii*) and saw-scaled Viper (*Echis carinatus*). Two species of amphibian were observed from the study area which includes Skittering Frog (*Euphlyctis cyanophlyctis*) and Marbled Toad (*Bufo stomaticus*). We observed that in the recent years habitat degradation, habitat modification, disturbance by humans illegal hunting are important threats to the *Varanus* spp. and *S. hardwickii* in the areas surveyed.

Earlier studies was documented 54 fish species in the Keenjhar Lake, we reviewed that currently no change was reported regarding number of species, see Table 5.

Table 2. Mammals of Keenjhar Lake (Khan and Abbas, 2011; Khan *et al*., 2012)

S. No.	Scientific Name	Common Name	Status
1	*Canis aureas*	Asiatic Jackal	C
2	*Vulpes bengalensis*	Bengal Fox	S
3	*Vulpes vulpes*	Desert Fox	R
4	*Lutragale perspicillata*	Smooth-coated Otter	R
5	*Felis chaus*	Jungle Cat	S
6	*Prionailurus viverina*	Fishing Cat	S
7	*Herpestes edwardsi*	Grey Mongoose	LC
8	*Herpestes javanicus*	Small Indian Mongoose	LC
9	*Sus scrofa*	Indian Wild boar	LC
10	*Manis crassicaudata*	Indian Pangolin	R
11	*Hemiechinus collaris*	Long-eared Hedgehog	LC
12	*Hipposideros fulvus*	Leaf-nosed bat	LC
13	*Pipistrellus kuhlii*	Kuhls' bat	C
14	*Rhinopoma microphyllum*	Large mouse-tailed bat	LC
15	*Lepus nigricollis*	Desert Hare / Indian Hare	LC
16	*Funambulus pennant*	Palm squirrel	C
17	*Hystrix cristatus*	Indian crested porcupine	C
18	*Gerbillus nanus*	Balochistan Gerbil	C
19	*Bandicota bengalensis*	Indian Mole Rat	LC
20	*Meriones hurrianae*	Indian Desert Jird / Desert Gerbil	C
21	*Mus musculus*	House mouse	C
22	*Mus saxicola*	Grey spiny Mouse	LC
23	*Nesokia indica*	Short-tailed rat	LC
24	*Rattus rattus*	Common Rat	C
25	*Tatera indica*	Indian Gerbil	C

Table 3. Birds of Keenjhar Lake (Khan and Abbas, 2011; Khan *et al*., 2012).

S. No.	Scientific Name	Common Name	Status
1	*Tachybaptus ruficollis*	Little Grebe	C
2	*Phalacrocorax niger*	Little Cormorant	C
3	*Nycticorax nycticorax*	Night Heron	LC
4	*Ardeola grayii*	Indian Pond Heron	C
5	*Bubulcus ibis*	Cattle Egret	C
6	*Egretta garzeta*	Little Egret	C
7	*Egretta intermedia*	Intermediate Egret	C
8	*Egretta alba*	Great White Egret	C
9	*Ardea purpurea*	Purple Heron	LC
10	*Anas strepera*	Gadwall	C
11	*Anas crecca*	Common Teal	C
12	*Anas acuta*	Pintail	C
13	*Anas clypeata*	Shoveller	C
14	*Aythya ferina*	Common Pochard	C
15	*Aythya fuligula*	Tufted Duck	C
16	*Nettapus coromandelianus*	Cotton Teal	WV
17	*Elanus caeruleus*	Black-shouldered Kite	LC
18	*Milvus migrans*	Black Kite	C
19	*Haliastor indus*	Brahminy Kite	LC
20	*Haliaeetus leucoryphus*	Pallas's Fishing Eagle	S
21	*Gyps fulvus*	Eurasian Griffon Vulture	C
22	*Neophron perenopterus*	Egyptian Vulture	Ra
23	*Circus aeruginosus*	Marsh Harrier	C

24	*Aquila clanga*	Greater Spotted Eagle	LC
25	*Aquila nipalensis*	Steppe Eagle	C
26	*Circaetus gallicus*	Short-toed Eagle	Ra
27	*Pandion haliaetus*	Osprey	LC
28	*Falco tinnunculus*	Common Kestrel	LC
29	*Falco columbarius*	Merlin	Ra
30	*Francolinus pondicerianus*	Grey Partridge	C
31	*Amaurornis phoenicurus*	White-breasted Waterhen	LC
32	*Gallinula chloropus*	Common Moorhen	C
33	*Fulica atra*	Common Coot	C
34	*Hydrophasianus chirurgus*	Pheasant-tailed Jacana	LC
35	*Himantopus himantopus*	Black-winged Stilt	C
36	*Charadrius dubius*	Little-ringed Plover	LC
37	*Hoplopterus (vanellus) indicus*	Red-wattled Lapwing	C
38	*Chettusia (vanellus) leucurus*	White-tailed Lapwing	LC
39	*Calidris minutus*	Little Stint	C
40	*Gallinago (capella) gallinago*	Common Snipe	LC
41	*Tringa stagnatilis*	Marsh Sandpiper	LC
42	*Tringa totsnus*	Redshank	C
43	*Tringa nebularia*	Green Shank	LC
44	*Tringa ochropus*	Green Sandpiper	C
45	*Tringa glareola*	Wood Sandpiper	LC
46	*Actitis hypoleucos*	Common Sandpiper	LC
47	*Calidris temminckii*	Temminck’s Stint	C
48	*Calidris minuta*	Little Stint	C
49	*Larus ichthyaetus*	Great Black-headed Gull	C
50	*Larus ridibundus*	Black-headed Gull	C
51	*Larus argentatus*	Herring Gull	C
52	*Gelochelidon nilotica*	Gull-billed Tern	C
53	*Sterna aurantia*	River Tern	C
54	*Sterna albifrons*	Little Tern	C
55	*Chlidonias hybrid*	Whiskered Tern	C
56	*Sterna acuticauda*	Black-bellied Tern	S
57	*Columba livia*	Blue Rock Pigeon	C
58	*Pterocles exustus*	Chestnut-bellied Sandgrouse	LC
59	*Streptopelia decaocto*	Collared Dove	C
60	*Streptopelia senegalensis*	Little Brown Dove	C
61	*Psittacula krameri*	Rose-ringed Parakeet	LC
62	*Centropus sinensis*	Crow Pheasant	LC
63	*Endynamys scolopacea*	Common Koel	C
64	*Caprimulgus mahrattensis*	Syke’s Nightjar	LC
65	*Apus affinis*	House Swift	C
66	*Halcyon smyrnensis*	White-throated Kingfisher	C
67	*Alcedo atthis*	Common Kingfisher	LC
68	*Ceryle rudis*	Pied Kingfisher	C
69	*Merops orientalis*	Little Green Bee-eater	LC
70	*Coracias benghalensis*	Indian Roller	LC
71	*Upupa epops*	Hoopoe	LC
72	*Dinopium benghalensis*	Golden-backed Woodpecker	LC
73	*Eremopterix grisea*	Ashy-crowned Finch Lark	LC
74	*Eremopterix nigriceps*	Black-crowned Finch Lark	LC
75	*Ammomanes deserti*	Desert Finch Lark	LC
76	*Galerida cristata*	Crested Lark	C
77	*Alanda gulgula*	Oriental Sky Lark	C

78	*Riparia paludicola*	Plain Sand Martin	C
79	*Hirundo rustica*	Common Swallow	C
80	*Hirundu smithi*	Wire-tailed Swallow	C
81	*Lanius isabellinus*	Isabelline Shrike	LC
82	*Lanius vittatus*	Bay-backed Shrike	LC
83	*Lanius meridionalis*	Southern Grey Shrike	LC
84	*Dicrurus macrocercus*	Black Drongo	C
85	*Acridotheres tristis*	Common Myna	C
86	*Acridotheres ginginianus*	Bank Myna	C
87	*Stumus vulgaris*	Common Starling	C
88	*Dendrocitta vagabunda*	Indian Tree-pie	LC
89	*Corvus splendens*	Indian House crow	C
90	*Pycnonotus leucogenys*	White-cheeked Bulbul	A
91	*Pycnonotus cafer*	Red-vented Bulbul	LC
92	*Turdoides caudatus*	Common Babbler	C
93	*Turtoides earlei*	Striated Babbler	LC
94	*Turtoides striatus*	Jungle Babbler	LC
95	*Acrocephalus Agricola*	Paddy-field Warbler	S
96	*Acrocephalu neglectus*	Clamorous Reed Warbler	LC
97	*Cettia cetti*	Cettis Warbler	S
98	*Phylloscopus collybita*	Eurasian Chiffchaff	C
99	*Phylloscopus neglectus*	Plain Leaf Warbler	C
100	*Prinia inornata*	Plain Prinia	S
101	*Sylvia curruca*	Lesser Whitethroat	LC
102	*Rhipidura rhipidura*	White-browed Fantail Flycatcher	LC
103	*Prinia flaviventris*	Yellow-bellied Prinia	S
104	*Orthotomus suturius*	Common Tailor Bird	LC
105	*Luscinia svecica*	Blue-throat	LC
106	*Saxicola caprata*	Pied Bushchat	LC
107	*Oenanthe deserti*	Desert Wheatear	LC
108	*Oenanthe picata*	Eastern Pied Wheatear	LC
109	*Oenanthe alboniger*	Hume's Wheatear	LC
110	*Saxicoloides fulicat*	Indian Robin	C
111	*Anthus compestris*	Tawny Pipit	LC
112	*Anthus rufulus*	Paddy-field Pipit	C
113	*Motacilla flava*	Yellow Wagtail	C
114	*Motacilla alba*	White Wagtail	C
115	*Motacilla maderaspatensis*	White-bowed Pied Wagtail	LC
116	*Nectarina asiatica*	Purple Sunbird	LC
117	*Passer domesticus*	Indian House Sparrow	C
118	*Petronia xanthocollis*	Yellow-throated Sparrow	C
119	*Ploceus manyar*	Streaked Weaver	C
120	*Lonchura malabarica*	White-throated Munia	LC
121	*Emberiza stiolata*	House Bunting	LC

Table 4. Reptiles of Keenjhar Lake (Khan and Abbas, 2011; Khan *et al*., 2012).

S. No.	**Scientific Name**	**Common Name**
1.	*Calotes versicolor*	Indian Garden Lizard
2.	*Trapelus agilis*	Brilliant Agama
3.	*Trapelus megalonyx*	Afghan Ground Agama
4.	*Eublepharis macularius*	Fat-tailed Gecko
5.	*Cyrtopodion kachhensis*	Warty Rock Gecko

6.	*Cyrtopodian scaber*	Keeled Rock Gecko
7.	*Hemidactylus brookii*	Spotted Indian House Gecko
8.	*Hemidactylus flaviviridis*	Yellow-bellied House Gecko
9.	*Hemidactylus leschenaultii*	Bark Gecko
10.	*Acanthodactylus cantoris*	Indian Fringed-toed Sand Lizard
11.	*Ophisops jerdonii*	Punjab Snake-eyed Lacerta
12.	*Sara hardwickii*	Indian Spiny-tailed Lizard
13.	*Varanus bengalensis*	Indian Monitor Lizard
14.	*Eryx conicus*	Russel's Sand Boa
15.	*Coluber fasciolatus*	Banded Racer
16.	*Lycodon striatus*	Spotted Wolf Snake
17.	*Oligodon taeniolatus*	Streaked Kukri Snake
18.	*Platyceps rhodorachis*	Cliff Racer
19.	*Platyceps ventromaculatus*	Glossy-bellied Racer
20.	*Psammophis condanarus*	Pakistan Ribbon Snake
21.	*Psammophis leithii*	Indian Sand Sake
22.	*Ptyas mucosus*	Dhaman/Rope Snake
23.	*Spalerosophis diadema*	Royal Snake
24.	*Bungarus caeruleus*	Common Krait
25.	*Naja naja*	Indian Cobra
26.	*Naja oxiana*	Oxus Cobra/Brown Cobra
27.	*Daboia russelii*	Russel's Viper/ Chain Viper
28.	*Echis carinatus*	Saw-scaled Viper
29.	*Lissemys punctata*	Indian Flap-shelled Turtle

Table 5. Fishes of Keenjhar Lake (Khan and Abbas, 2011; Khan *et al*., 2012).

S. No.	**Species**
1	*Gadusia chapra*
2	*Notopterus chitala*
3	*N. notopterus*
4	*Chela cachius*
5	*Salmostoma bacaila*
6	*Securicula gora*
7	*Amblypharyngodon mola*
8	*Aspidoparia morar*
9	*Barilius vagra*
10	*Esomus danricus*
11	*Rasbora daniconius*
12	*Barbodes sarana*
13	*Catla catla*
14	*Cirrhinus mrigala*
15	*Cirrhinus reba*
16	*Labeo calbasu*
17	*Labeo dero*
18	*Labeo dyocheilus*
19	*Labeo gonius*
20	*Labeo rohita*
21	*Osteobrama cotio*
22	*Puntius chola*
23	*Puntius sophore*
24	*Puntius ticto*
25	*Cyprinus carpio*
26	*Ctenpharyngodon idella*
27	*Aristchthys nobilis*
28	*Hypophthalmichthys molitrix*
29	*Mystus bleekeri*
30	*Mystus cavasius*
31	*Mystus vittatus*
32	*Rita rita*
33	*Bagarius bagarius*
34	*Gagata cenia*
35	*Nangra nangra*
36	*Ompok bimaculatus*
37	*Wallago attu*
38	*Heteropneutes fossilis*
39	*Ailia coila*
40	*Clpisoma garua*
41	*Clpisoma naziri*
42	*Eutropiichthys vacha*
43	*Xenentodon cancila*
44	*Channa marulia*
45	*Channa punctata*
46	*Chanda nama*
47	*Parambassis baculis*
48	*Parambassis ranga*
49	*Sicamugil cascasia*
50	*Glossogobium giuris*
51	*Colisa fasciata*
52	*Colisa lalia*
53	*Oreochromis mossambicus*
54	*Mastacembelus armatus*

Pollution is considered as a major hazard for the water of Keenjhar Lake. It directly affects the quality of water and made it harmful for human consumption because of the addition of hazardous wastes from the industrial effluents of Kotri industrial area as well as Nooriabad industries (Fig. 7). The lake also serves a waste dumping area for at least 12 villages with a population of about over 1,500 people (Ilyas, 2015). Second major threat to ecology of Keenjhar Lake is Eutrophication (Fig. 8). This lake is also a hotspot of ecotourism. The main cause of its pollution is the arrival of above 15,000 visitors weekly which pose a serious risk to biodiversity of lake by polluting its water (see Figs. 9-12). Some people also used to wash their vehicles in the lake which resulted in the contamination of water with oil and fuels. Two types of system are followed in the lake for fishing practices, first one is Auction system and another one is License system but none of these are properly followed by fishermen and local people. There are so many disagreements based on these two systems in between Fisheries department and local fishermen. There are so many drawbacks developed in fisheries system of lake as there is no recruitment of new fish seeds in that lake and the continuous fishing practices has decreased the fisheries stock in this Lake. There is a major canal emerging from lake which supplies water to Karachi which is also an important source for exclusion of fish from the lake (Khan *et al*., 2012).

Fig. 7. Polluted water enter to Keenjhar Lake.

Fig. 8. A view of eutrophication in Keenjhar Lake.

There are five departments of Government which participates in the management of Keenjhar Lake. They includes Sindh Irrigation Department, Sindh Fisheries Department, Sindh Tourism Department, Sindh Wildlife Department and the Sindh Local Government Department. The problem is that these all departments are not working on collaboration with each other and that's the reason of mismanagement in the matters of lake`s development.

One example of this mismanagement is the introduction of *Tilapia* species on the lake which is a carnivorous fish. It is a predator species and has dominated over the native herbivorous species present in the lake such as Rohu, Thaila and Murakhi. Whereas, the introduced plant species have also invaded the whole open area in the lake. These introduces plants are *Eichhornia crassipes* (Water Hyacinth) and *Salvania molesta* (Water Fern).
These invasive aquatic weeds included Hyacinth (*Eichhornia crasspes*) and Water lettuce (*Pista stratiotes)* not only disturbs ecology of other aquatic vegetation but also obstruct water channels which are used for different purposes including commercial, recreational and household utilization. This eutrophication leads to habitat destruction and degradation, shortening of fishing sites and modification in infrastructure of fisheries system of the lake. These weeds also act as breeding grounds for mosquitoes and resulted in disastrous hazards for neighboring human populations. Exotic species not only disturb the ecology of the area but having severe effects on food chains and food web of that ecosystem. Interference of invasive species may results in disappearance of many native species from any ecosystem.

Fig. 9. Keenjhar Lake, a popular picnic point.

Fig. 10. Public disturbance at Keenjhar Lake.

Fig. 11. Oil pollution at Keenjhar Lake.

Fig. 12. Fishing activity in the Keenjhar Lake.

CONCLUSION

Based on this review, it is concluded that a more scientific detailed studies of Keenjhar Lake should be taken via academia and Sindh Wildlife Department with respect to habitat modifications due to environmental hazards present in the lake. The major threats should be point out and highlighted. All sources of pollution should be blocked including the industrial waste and agricultural waste. All projects including RBOD which is passing through Keenjhar and Haleji should be systematically monitored through Government of Sindh. The movements of migratory birds should be noted and there should be a check and balance on their population estimation. It should be ensured that there will be no illegal hunting of migratory species. The rare or vulnerable species should have special protection. There should be annual water bird census which will enable us to conserve them more effectively.

ACKNOWLEDGMENT

The authors would like to thank to Ms. Roohi Kanwal, Department of Zoology, University of Karachi for preparation of Keenjhar Lake figures.

REFERENCES

Ashraf, M., Jaffar, M. and Jaleel, T. 1992. Annual variation of Selected Trace metals in Freshwater Lake Fish, *Labeo rohita*, as an Environmental Pollution. Toxicol. Env. Chem. 35:1-7.

Baqai, IU. and Rehana, I. 1973. Seasonal Fluctuation of Freshwater Copepods of Kinjher Lake, Sindh and its correlation with Physcio-chemical factors. J. Zool. 5 (2):165-168.

Baqai, IU. and Siddiqui, PA. 1973. Problems of Freshwater fisheries in Sindh with special reference to Pollution and Eutrophication. Jadeed Sci. 14 (in Urdu).

Baqai, IU., M. Iqbal. and VA. Zuberi. 1974[a]. Limnological Studies of Kalri Lake. Agriculture Pakistan. 25 (2):119-135.

Baqai, IU., Siddiqui, PA. and Iqbal, M. 1974[b]. Limnological Studies of Haleji Lake. Agriculture Pakistan. 25(4):321-344.

Conder, PJ. 1977. Lake Haleji Wildlife Sanctuary Management Plan. (unpublished Report).

Durranee, J. and Khan, MZ. 2008. Birds of Keenjhar. Indus for All Program. WWF Pakistan, Karachi. pp.12.

Ghalib, SA., Rehman, H., Iffat, F. and Hasnain, SA. 1981. A Checklist of Reptiles of Pakistan. Rec. Zool. Sur. Pakistan. 8:37-59.

Ghalib, SA. and Bhaagat, HB. 2004. The Wetlands of Indus Delta Eco-region. In: Proceedings of Consultative Workshop on Indus Delta Eco-region (IDER). Eds. Ahmed, E., Omer, S. and Rasool, F. WWF-Pakistan. 117-142.

Ghalib, SA., Hasnain, SA. and Khan, AR. 2004. Current Status of the Mammals of Sindh. J. Nat. Hist. Wildl. 3(1):1-6.

Ghalib, SA., Rais, M., Abbas, D., Tabassum, F., Begum, A. and Jabeen, T. 2009. An Overview of the Status of Shorebirds and Internationally Important Sites in Pakistan. Pakistan. J. Zool. 41(3):165-172.

IFAP (Indus for All Program). 2009. Detailed Ecological Assessment of Fauna including Limnological Studies of Fauna at Keenjhar Lake, 2007-2008. WWF Pakistan, Karachi. pp.170. (unpublished).

IUCN. 2004. Sindh State of Environment and Development. Sindh Program Office. 18:423.Ilyas, F. 2015. Wastes, government neglect destroying Keenjhar lake. December 28th, 2015 http://www.dawn.com/news/1229061.

Jafri. SIH., Narejo, NT., Baloch, WA. and Saheto, GA. 1999. Studies on Land-locked Population of Palla, *Tenualosa ilisha* from Keenjhar Lake (Sindh), Pakistan. Pakistan J. Zool. 31:347-350.

Jehangir, TM., Khuhawar, SM., Leghari, SM., Baloch,, WA. and Leghari, A. 2000. Some Studies on Water Quality and Biological life at Kinjhar and Haleji Lakes of District Thatta, Sindh, Pakistan. Pakistan Journal of Biological Sciences. 3(11):65-72.

Kazmi, SJH., Qureshi, S., Siddiqui, MU. and Arsalan, MH. 2006. Depleting Wetlands of lower Sindh, Pakistan: A Spatio-Temporal Study through Satellite Remote Sensing Proceeding of the International Conference on advances in Space Technologies. (ICAST 2-3 Sept. 2006: Islamabad). 1-5.

Khan, MZ. 2005. Wetlands of Sindh with reference to Ramsar Sites. J. Nat. His. Wildl. 4(2):141-145.

Khan, MZ. and Law, FCP. 2005. Adverse Effects of Pesticides and related Chemicals on Enzyme andHormone Systems of Fish, Amphibians and Reptiles. Proc. Pakistan Acad. Sci. 42(4):315-323.

Khan, MZ. and Ghalib, SA. 2006. Birds Population and Threats to Some Selected Important Wetlands in Pakistan. J. Nat. Hist. Wildl. 5(2):209-215.

Khan, MZ. and Abbas, D. 2011. Aquatic Vertebrates of Haleji and Keenjhar Lakes. Lap Lambert Academic Publishing, Germany. pp.216.

Khan, MZ., Abbas, D., Ghalib, SA, Yasmeen, R., Siddiqui, S., Mehmood, N., Zehra., Begum, A., Jabeen, T., Yasmee, G. and Latif, T. 2012. Effects of Environmental Pollution on Aquatic Vertebrate and Inventories of Haleji and Keenjhar Lakes: Ramsar Sites. CJPAS. 6(1):1759-1783.

Khan, MZ., Khan, IS., Ghalib, SA., Hussain, SE., Ahmed, W., Siddiqui, S., Yasmeen, G., Zehra, A., Hussain, B., Kanwal, R., Latif, TA. and Iqbal, MA. 2015. Assessment of Water Quality of Nagiopeer and Dangewari Wetlands and Status of the Wildlife of Nara Game Reserve, Sindh, Pakistan. Canadian Journal of Pure and Applied Sciences. 9(2):3503-3512.

Khanum, Z. and Ahmed, M. 1991. A note on the birds of Haleji Area (Sindh-Pakistan). Zoolgica Pakistan. 2(1): 33-37.

Korai, AL. Sahato, GA. and Lashari, KH. 2008[a]. Fish Diversity in Relation to Physic-chemical Properties of Keenjhar Lake (District Thatta), Sindh, Pakistan. Research Journal of Fisheries and Hydrobiology. 3(1):1-10.

Korai, AL. Sahato, GA., Lashari, KH. and Arbani, SN. 2008[b]. Biodiversity in Relation to Physic-chemical Properties of Keenjhar Lake (District Thatta), Sindh, Pakistan. Turkish Journal of Fisheries and Aquatic Sciences. 8:259-268.

Lashari, KH. Sahato, GA. and Arbani. SN. 2001. Ecological Studies of Zooplankton in Keenjhar Lake, Sindh, Pakistan. Hamdard Medicus. 44(1):78-81.

Lashari, KH., Korai, AL., Sahato, GA. and Kazi, TG. 2009. Limnological Studies of Keenjhar Lake (District Thatta), Sindh, Pakistan. Pak. J. Anal. Environ. Chem. 10(1 and 2):39-47.

Mahar, MA., Larick, ZA., Narejo, NT. and Jafri, SIH. 2010. Limnological Study of Fishponds and Kalri Baghar Lower Canal at Chilya Fish Hatchery Thatta, Sindh, Pakistan. Pakistan J. Zool. 42(4):419-430.

Nazneen, S. 1974. Seasonal Distribution of Phytoplankton in Kinjhar (Kalri) Lake. Pak. J. Bot. 6:69-82.

Nazneen, S. 1980. Influence of Hydrological Factors on the Seasonal Abundance of Phytoplanktos in Keenjhar Lake, Pakistan. Inst. Rev. Ger. Hydrobiol. 65:269-285.

Nazneen, S. and Begum, F. 1992. Seasonal Distribution of Molluscs of Kinjhar Lake. Pakistan. J. Zool. 24(2):175-177.

Roberts, TJ., Passburg, R. and Van Zalinge, NP. 1986. A Checklist of Birds of Karachi and Lower Sind, Pakistan. World Wide Fund for Nature Pakistan.

Ramsar Convention. 2017. The List of Wetlands of International Importance. http://www.ramsar.org/accessed on Jan 2, 2017).

Saqib, T., Naqvi, SNH., Siddiqui, PA. and Azmi, MA. 2005. Detection of Pesticides in Muscles, Liver and Fat in three Species of *Labeo* found in Kalri and Haleji Lakes. Env. Biol. 26:433-448.

Scott, DA. (Ed.). 1989. A Directory of Asian Wetlands, Pakistan Section. IUCN, Gland, Switzerland. 295-365.

Scott, DA. and Poole, CM. 1989. A Status Overview of Asian Wetlands. Asian Wetland Bureau, Kuala Lumpur, Malaysia. pp.42.

Siddiqui, PA., IU. Baqai and Iqbal, M. 1973. Check List of Fishes of Kinjher (Kalri) Lake with Notes on Environmental Conditions and Fishes Potential. Agri. Pak. 24(2):201-220.

Received: Sept 20, 2016; Revised: Nov 2, 2016; Accepted: Jan 4, 2017

Canadian Journal of Pure and Applied Sciences
Vol. 11, No. 1, pp. 4103-4119, February 2017
Online ISSN: 1920-3853; Print ISSN: 1715-9997
Available online at www.cjpas.net

THE PROBLEM OF FINDING OF EIGENVECTORS FOR 4P-SH-SAW PROPAGATION IN 6 *mm* MEDIA

Aleksey Anatolievich Zakharenko
International Institute of Zakharenko Waves (IIZWs)
660014, ul. Chaikovskogo, 20-304, Krasnoyarsk, Russia

ABSTRACT

This theoretical report is pertinent to the mathematical problem of finding of all the possible eigenvectors for the four-potential shear-horizontal surface acoustic wave (4P-SH-SAW) propagation in suitable solids. In this case, the wave propagation is coupled with the four potentials, i.e. the electrical, magnetic, gravitational, and cogravitational ones. The taking into account these four potentials results in significant difficulties to find any eigenvector because the mathematical method is significantly complicated. To find all suitable eigenvectors is very important here because it will allow one in the future to theoretically disclose all suitable solutions of acoustic waves. This is applicable to the problem of finding of propagation velocities of the SH-SAWs, interfacial SH-waves, plate SH-waves, and more complicated cases. It is thought that all the effects (for instance, the gravitocogravitic, gravitoelectric, cogravitoelectric, gravitomagnetic, cogravitomagnetic effects) individually or collaboratively participating in the acoustic wave propagation can be vital for acoustic wave propagation that can be readily used for constitution of suitable technical devices. This fact must be first demonstrated theoretically for experimentalists and engineers working with the transmitting, detecting, and converting of the electromagnetic waves' signals. It is expected that the future communication technologies will also exploit gravitational waves for the new communication era based on some gravitational phenomena.

PACS: 51.40.+p, 62.65.+k, 68.35.Gy, 68.35.Iv, 68.60.Bs, 74.25.Ld, 74.25.Ha, 75.20.En, 75.80.+q, 81.70.Cv, 96.20.Jz, 04.30.-w, 04.90.+e, 95.30.Sf
Keywords: transversely isotropic solids, gravitational effects, magnetoelectric effect, eigenvector problem, four potential coupling problem.

INTRODUCTION

2016 was the jubilee year, namely the centenary celebration of the prediction of the existence of gravitational waves. This prediction was done by Albert Einstein (1916). Also, 2016 is the year when Einstein's prediction was experimentally confirmed by a team of more than thousand researchers (Abbott *et al*., 2016). They were working during several decades since 1970s for the purpose to detect the gravitational waves in space experiments called the LIGO (Laser Interferometer Gravitational-Wave Observatory). Using obtained data in the space experiments, they presented the first direct detection of gravitational waves and the first observation of a binary black hole merger. The black holes are famous invisible objects possessing very strong gravitational fields that are strong enough to capture even the electromagnetic waves propagating in a vacuum with the speed of light.

Corresponding author e-mail: aazaaz@inbox.ru

André Füzfa (2016) has reported his experimental realization when the magnetic and gravitational forces can interact: the magnetic field can control the gravitational field. He has described one revolutionary approach for the creation of gravitational fields from well-controlled magnetic fields and observing how these magnetic fields can bend space-time. He has proposed a theoretical device based on superconducting electromagnets for creation of detectable gravitational fields. He has also evaluated the coupling between the magnetic and gravitational fields in an order of ~ 10^{-35}. This leads to the generation of extremely weak gravitational redshift and gravitational attraction. Also, the atomic interferometry has been considered for the determination of the extremely faint change in the gravitational potential produced by small masses on matter waves. So, the amplitude of the extra gravitational acceleration artificially generated by the magnetic field of a single-layered solenoid is extremely weak but lies just a few orders of magnitude below the precision of atomic interferometry in the measurement of differential acceleration of 10^{-15} g. His pioneer work can

release many new applications concerning telecommunications with gravitational waves. The ability to produce, detect, and control gravitational fields can certainly be a major achievement in modern physics. Therefore, scientific interest in the problem of interactions between the gravitational and electromagnetic waves continuously increases.

The author of this report (Zakharenko, 2016) has developed the original theory concerning the four-potential shear-horizontal surface acoustic wave (4P-SH-SAW) propagation, i.e. the waves coupled with the electrical, magnetic, gravitational, and cogravitational potentials. This means that all five fields (elastic, electrical, magnetic, gravitational, and cogravitational) contribute to the wave motion. There are also interactions among and between each pair of the mechanical, electrical, magnetic, gravitational, and cogravitational subsystems in the common thermodynamic system. Theoretical work (Zakharenko, 2016) treats two extra subsystems (gravitational and cogravitational) to the thermodynamic system for piezoelectromagnetics (PEMs) in which mechanical, electrical, and magnetic subsystem contribute. The piezoelectromagnetics are a class of well-known magnetoelectric materials. The SH-SAW propagation coupled with the electrical and magnetic potentials in the 6 *mm* PEMs represented a great interest in the last decade. The transversely-isotropic 6 *mm* materials and suitable propagation directions (Gulyaev, 1998) for the acoustic waves are well known. There is single review (Zakharenko, 2013a) on the PEM-SH-SAWs and the disclosed peculiarities for the problem of the wave propagation are discussed in (Zakharenko, 2013b). There is also single book (Zakharenko, 2010) on some new PEM-SH-SAWs. The book was published in 2010 under the influence of the discoveries done by Melkumyan (2007). Some extra new PEM-SH-SAWs were recently discovered in (Zakharenko, 2013c) and (Zakharenko, 2015a) and some of the new waves were analytically studied in (Zakharenko, 2015b). It worth noting that Melkumyan (2007) has also discovered the new PEM-SH-SAW called the surface Bleustein-Gulyaev-Melkumyan wave in order to have an analogy with the surface Bleustein-Gulyaev wave. The later SH-SAW can propagate in pure piezoelectrics or pure piezomagnetics and was simultaneously discovered by Bleustein (1968) and Gulyaev (1969).

The wave propagation studied in (Zakharenko, 2016) is caused by the contribution of the following five fields: the elastic, electric, magnetic, gravitational, and cogravitational. The last two fields are respectively known as the gravitoelectric and gravitomagnetic ones in the theory of the gravitoelectromagnetism. Paper (Zakharenko, 2016) uses gravitational and cogravitational instead of gravitoelectric and gravitomagnetic because the last two words are naturally used for the corresponding exchange effects between the gravitational and electric (magnetic) subsystems, respectively. In this introductory part, it is possible to briefly review some studies on the cogravitational (gravitomagnetic) field because this field of five can be the most infamous for the reader.

Researchers specializing in general relativity, gravitational theories, and cosmology have formed the existence necessity of a magnetic-like gravitational field unknown in other domains of physics. Heaviside (1893) has first hypothesized the existence of the cogravitational (gravitomagnetic) field. This extra field predicted by general relativity was first formulated in Thirring (1918), Lense and Thirring (1918) and Thirring (1921). The translation of these papers was introduced by Mashhoon *et al*. (1984). Forward (1961) has first expressed the gravitational field equations (with the gravitomagnetic field called the prorotational field) in a vector form directly analogous and nearly identical to Maxwell's equations for electromagnetism. DeWitt (1966) has first identified the significance of gravitational effects in a superconductor and demonstrated that a magnetic-type gravitational field must result in the presence of fluxoid quantization. Ross (1983) has substantially expanded DeWitt's work.

In the early 1970s, Wallace has issued three patents (Wallace, 1971a; Wallace, 1971b; Wallace, 1974) for some unusual inventions relating to the gravitational field. He has also developed an experimental apparatus for generating and detecting a secondary gravitational field called the kinemassic field, i.e. the gravitomagnetic field. He has here described three different methods used for detection of the gravitomagnetic field: (1) change in the motion of a body on a pivot, (2) detection of a transverse voltage in a semiconductor crystal, and (3) a change in the specific heat of a crystal having spin-aligned nuclei. Also, he has shown an analogy between the un-paired angular momentum in some materials (elements and isotopes possessing an odd number of nucleons) and the un-paired magnetic moments of electrons in ferromagnetics. Wallace believed that a gravitational shield can be created: the gravitomagnetic field can create a secondary gravitoelectric field leading to exclusion of an existing primary background gravitoelectric field. However, these detected gravitational shielding effects are extremely small.

There is gravitational theoreticians' bible (Misner *et al*., 1973). This book presents gravitational field equations derived from general relativity in a form similar to Maxwell's equations along with many other theories. It is necessary to state that the Maxwell-like equations for gravitation are relatively simple and can have possible practical applications. Therefore, these equations must be perfectly described in any undergraduate physics textbook that is currently missing. Braginsky *et al*. (1977) have

written down gravitational field equations (with the gravitomagnetic field called the magnetic-type gravity) derived from the general relativity theory in a form similar to Maxwell's equations. A variety of experiments are proposed and analyzed for detecting the gravitomagnetic field. His further collaborative paper (Braginsky *et al*., 1984) analyses an experiment for detecting the earth's gravitomagnetic field. It is possible that the authors of papers (Braginsky *et al*., 1977; Braginsky *et al*., 1984) are the first who have utilized the terms "gravitoelectric" and "gravitomagnetic".

Bedford and Krumm (1985) have also derived the necessary existence of the gravitomagnetic field from arguments based on special relativity. Krumm and Bedford (1987) have also derived the gravitational Poynting vector and used the terms "gravinetic" and "gravistatic" for the gravitational fields. One year later, Kolbenstvedt (1988) has exploited the terms "gravielectric" and "gravimagnetic" for these fields and predicted the gravitomagnetic field existence using special relativity and time dilation. In the following year, Mashhoon *et al*. (1989) have provided a summary analysis of Maxwell's equations for gravitation and an in-depth analysis of the Gravity Probe-B orbital gyroscope experiment for detecting the earth's gravitomagnetic field. Harris (1991) has also composed Maxwell's equations for gravitation from general relativity in the case of nonrelativistic velocities and relatively weak field strengths.

In the book published by Jefimenko (1992), the electromagnetic field equations based on retarded sources (charges, moving charges, and accelerating charges) were derived and similar arguments to the gravitational field equations were applied. He also presents Maxwell's equations for gravitation and an unusual mass configuration relevant to an effect of change in gravity. Ciufolini and Wheeler (1995) have developed the electromagnetic analog of the gravitational field equations and provided an in-depth analysis of experiments for detecting the gravitomagnetic field. So, researchers (Misner *et al*., 1973; Braginsky *et al*., 1977; Braginsky *et al*., 1984; Bedford, and Krumm, 1985; Krumm and Bedford, 1987; Kolbenstvedt, 1988; Mashhoon *et al*., 1989; Harris, 1991; Jefimenko, 1992; Ciufolini and Wheeler, 1995) have demonstrated the necessary existence of the gravitomagnetic field, using arguments based on general relativity, special relativity, and the cause and effect relationship resulting from noninstantaneous propagation of energy (retardation).

Li and Torr (1991) have also presented Maxwell's equations for gravitation in a form where the gravitomagnetic permeability of a superconductor is different from the permeability of a vacuum (free space). They have derived an interrelationship between the magnetic and gravitomagnetic fields in a superconductor and established that an electrical current also results in a mass current. It is also found that the magnetic flux in a superconductor is a function of the gravitomagnetic permeability, and vice versa, and shown that the magnetically created gravitomagnetic field in a superconductor can be ~ 10^{11} times larger than the internal magnetic field. One year later, Li and Torr (1992) have discussed the interrelationship between the magnetic and cogravitational (gravitomagnetic) fields in superconductors, in which some spin alignment of the lattice ions can cause the later field. They have also estimated the propagation velocity of a gravitational wave in a superconductor: it is two orders of magnitude slower than the vacuum velocity. This allowed them to perform an estimation of the value of relative gravitomagnetic permeability of a superconductor: it is ~ 10,000 times larger than that for a vacuum. In the following year, Torr and Li (1993) have continued their analysis of gravitational effects in superconductors and shown a striking similarity to Wallace's ideas that the coherent alignment of lattice ion spins can generate detectable gravitomagnetic and gravitoelectric fields. Li *et al*. (1997) have described an experiment showing that the effect of change in gravity was very small, if it existed at all. In 1999, Li has left the University of Alabama and found her company AC Gravity LLC that remained listed as an "existent" business in 2014.

Nordtvedt (1988) has reported an indirect detection of the gravitomagnetic field by astronomical observations of the precession rate of the binary pulsar PSR 1913+16. Ciufolini *et al*. (1997) have reported that the gravitomagnetic field resulting from the earth's rotation was experimentally detected and measured by laser tracking of the LAGEOS II satellite. Their results agreed with the Lense-Thirring derivation from the general relativity theory. Ciufolini *et al*. (1998) have also reported a test of general relativity and measurement of the Lense-Thirring effect with two Earth satellites.

With a bulk $YBa_2Cu_3O_{7-x}$ superconductor, Podkletnov and Nieminen (1992) have described a possibility of gravitational force shielding when a 2% reduction in weight can be achieved in a mass suspended over a levitated and rotating toroidal-shaped type II superconductor disk. With the Meissner effect, constant vertical and time varying horizontal magnetic fields were applied for rapid rotation of the disk. Podkletnov's "gravity shielding" experiment at Tampere was replicated by the NASA and may also be an example of the effect described in Wallace's patents of the early 1970s claiming that a rotating object containing unpaired nuclear spins can modify gravity. It is a pleasure that an explanation in terms of a gravitational analogue to the magnetic field of electromagnetism is used.

Using the brief review written above, the reader is already familiar with the cogravitational (gravitomagnetic) field and different studies on the field. Therefore, it is possible to return to the problem of the acoustic wave propagation coupled with the four potentials (electric, magnetic, gravitational, and cogravitational). This theoretical report represents a complement to the previously published work Zakharenko (2016). Namely, it touches the very important mathematical problem of finding of the apt eigenvectors. To find all the possible eigenvectors is crucial because the utilization of different eigenvectors in coupe with different electrical, magnetic, gravitational, and cogravitational boundary conditions can lead to different formulas for calculation of propagation velocities of the acoustic wave. For instance, the four-potential shear-horizontal surface acoustic waves (4P-SH-SAWs) are the simplest example for the case. These 4P-SH-SAWs represent different mechanisms of instability of the corresponding bulk acoustic wave, i.e. 4P-SH-BAW. These different instability mechanisms can be caused even by extremely small exchange effects, for instance, the magnetoelectric, gravitocogravitic, gravitoelectric, cogravitoelectric, gravitomagnetic, and cogravitomagnetic effects. These effects represent an exchange between two corresponding subsystems of four: electric, magnetic, gravitational, and cogravitational.

This is possible that extremely weak effects can contribute in wave existence in a major way because the very weak magnetoelectric effect can be vital for the some acoustic wave propagation in piezoelectromagnetics (Zakharenko, 2010) in which the mechanical, electric, and magnetic subsystems interact. Therefore, let's resolve this mathematical problem concerning the finding of all possible eigenvectors. This represents a quite complicated mathematical task that will be demonstrated in the following sections.

The theory and the problem of finding of eigenvalues and eigenvectors

For the problem of acoustic wave propagation in solids, it is first necessary to resolve the equations of motion. This means that all suitable eigenvalues and corresponding eigenvectors must be disclosed. To resolve the equations of motion is a complicated task for the common case, for which they can be resolved only numerically. In the common case, the coupled equations of motion are written down in a tensor form representing the following compact form of the well-known Green-Christoffel equation (Zakharenko, 2016): $\left(GL_{IJ}-\delta_{IJ}\rho V_{ph}\right)U_I^0=0$, where the indices I and J run from 1 to 7 and ρ is the mass density. The phase velocity defined by $V_{ph}=\omega/k$ is proportional to the angular frequency ω and inversely proportional to the wavenumber k in the propagation direction. GL_{IJ} stands for the components of the modified symmetric tensor (Zakharenko, 2016) and δ_{IJ} represents the Kronecker delta-function with the following conditions: $\delta_{IJ}=1$ for $I=J<4$, $\delta_{IJ}=0$ for $I\neq J$, and $\delta_{44}=\delta_{55}=\delta_{66}=\delta_{77}=0$. Also, parameters U_I^0 represent the components of the eigenvector $\left(U_1^0,U_2^0,U_3^0,U_4^0,U_5^0,U_6^0,U_7^0\right)$. This compact tensor form of the coupled equations of motion represents the common problem for determination of the eigenvalues and eigenvectors.

However there are particular cases depending on the material symmetry and propagation directions when analytical solutions can be obtained. For the acoustic wave propagation in the transversely isotropic (6 *mm*) materials, the suitable propagation directions (Gulyaev, 1998; Dieulesaint and Royer, 1980; Auld, 1990) exist in many directions perpendicular to the sixfold symmetry axis. For this case, both the coupled equations of motion and the boundary conditions' determinant split into two independent parts. This allows one to separately study these two parts. The first part is for the case of the propagation of the purely mechanical wave, for instance, the surface Rayleigh type waves (Dieulesaint and Royer, 1980; Auld, 1990; Zakharenko, 2005). These acoustic waves with the in-plane polarization are famous and this work has no interest in their study. The second part is relevant to the propagation of the shear-horizontal (SH) acoustic wave with the anti-plane polarization. This case represents a great interest because the SH-wave propagation is couple with the electrical, magnetic, gravitational, and cogravitational potentials. This case was originally studied by Zakharenko (2016). To further develop the study by Zakharenko (2016), it is necessary to demonstrate all possible eigenvectors because each of them can lead to unique solution or the propagation velocity of the SH-wave.

Therefore, let's start to resolve the coupled equations of motion written down in the following tensor form (Zakharenko, 2016) for the case of the SH-wave propagation in the transversely isotropic (6 *mm*) materials:

$$\begin{pmatrix} C\left[m-\left(V_{ph}/V_{t4}\right)^2\right] & em & hm & gm & fm \\ em & -\varepsilon m & -\alpha m & -\zeta m & -\xi m \\ hm & -\alpha m & -\mu m & -\beta m & -\lambda m \\ gm & -\zeta m & -\beta m & -\gamma m & -\vartheta m \\ fm & -\xi m & -\lambda m & -\vartheta m & -\eta m \end{pmatrix} \begin{pmatrix} U^0 \\ \varphi^0 \\ \psi^0 \\ \Phi^0 \\ \Psi^0 \end{pmatrix} = \begin{pmatrix} 0 \\ 0 \\ 0 \\ 0 \\ 0 \end{pmatrix} \quad (1)$$

where $\left(U^0,\varphi^0,\psi^0,\Phi^0,\Psi^0\right) = \left(U_2^0,U_4^0,U_5^0,U_6^0,U_7^0\right)$, $m=1+n_3^2$, and $V_{t4}=\sqrt{C/\rho}$.

Table 1 lists all the material parameters present in equations (1). The values of the material parameters must be unique for each solid continuum. There is no necessity in this study to write down the values of the material parameters for a particular material. However, it is possible to provide the well-known vacuum material parameters listed in Table 2.

Table 1. The material parameters' dimensions.

Material parameter	Symbol	Dimension
Mass density	ρ	kg/m^3
Elastic stiffness constant	C	N/m^2
Piezoelectric constant	e	C/m^2
Piezomagnetic coefficient	h	T = N/(A×m)
Piezogravitic constant	g	kg/m^2
Piezocogravitic coefficient	f	rad/s
Electric constant	ε	F/m
Magnetic constant	μ	N×s^2/C^2
Electromagnetic constant	α	N×s/(V×C)
Gravitic constant	γ	kg^2/(N×m^2)
Cogravitic constant	η	m/kg
Gravitocogravitic constant	ϑ	s/m
Gravitoelectric constant	ζ	C×kg/(J×m)
Cogravitoelectric constant	ξ	m/Wb
Gravitomagnetic constant	β	T×kg×m/J
Cogravitomagnetic constant	λ	T×m^3/(C×Wb)

Table 2. The vacuum parameters (Yavorsky *et al*., 2006), where the value of the vacuum elastic constant was borrowed from work by Kiang and Tong (2010).

Vacuum parameter	Value
Elastic constant	$C_0 = 0.001$ [N/m^2]
Electric constant (dielectric permittivity constant)	$\varepsilon_0 = 0.08854187817 \times 10^{-10}$ [F/m]
Magnetic constant (magnetic permeability constant)	$\mu_0 = 1.25663706144 \times 10^{-6}$ [H/m]
Gravitic constant (gravitoelectric permittivity coefficient)	$\gamma_0 = 1.498334 \times 10^{10}$ [kg×s^2/m^3]
Cogravitic constant (gravitomagnetic permeability coefficient)	$\eta_0 = 0.0742592 \times 10^{-26}$ [m/kg]
Newtonian gravitational (gravitoelectric) constant	$G_0 = 1/\gamma_0 = 0.667408 \times 10^{-10}$ [m^3/(kg×s^2)]
Cogravitational (gravitomagnetic) constant	$M_0 = 1/\eta_0 = 13.46635 \times 10^{26}$ [kg/m]
Speed of light	$C_L = (G_0M_0)^{1/2} = (\gamma_0\eta_0)^{-1/2} = (\varepsilon_0\mu_0)^{-1/2} = 2.997924 \times 10^8$ [m/s]

This set (1) of five homogeneous equations allows one to determine all the eigenvalues n_3. With each of the found eigenvalues, it is possible to obtain the corresponding eigenvector $\left(U^0, \varphi^0, \psi^0, \Phi^0, \Psi^0\right)$. The suitable eigenvalues n_3 can be found when the determinant of the coefficient matrix in equations (1) is equal to zero. This determinant can be composed in the following convenient form consisting of five cofactors:

$$0 = m \times m \times m \times m \times \begin{vmatrix} C\left[m - \left(V_{ph}/V_{t4}\right)^2\right] & e & h & g & f \\ em & -\varepsilon & -\alpha & -\zeta & -\xi \\ hm & -\alpha & -\mu & -\beta & -\lambda \\ gm & -\zeta & -\beta & -\gamma & -\vartheta \\ fm & -\xi & -\lambda & -\vartheta & -\eta \end{vmatrix} \tag{2}$$

Therefore, these five factors in equation (2) give the following five pairs of the eigenvalues:

$$n_3^{(1,2)} = n_3^{(3,4)} = n_3^{(5,6)} = n_3^{(7,8)} = \mp \mathrm{j} \tag{3}$$

$$n_3^{(9,10)} = \mp \mathrm{j}\sqrt{1 - \left(V_{ph}/V_{temgc}\right)^2} \tag{4}$$

In equations (3) and (4), $\mathrm{j} = (-1)^{1/2}$ is the imaginary unity. Also, expression (4) introduces the velocity (V_{temgc}) of the shear-horizontal bulk acoustic wave (SH-BAW) coupled with the electrical, magnetic, gravitational, and cogravitational potentials, i.e. the 4P-SH-BAW speed. It is defined by

$$V_{temgc} = \sqrt{C\left(1 + K_{emgc}^2\right)/\rho} \tag{5}$$

In definition (5), K_{emgc}^2 defines the coefficient of the electromagnetogravitocogravitomechanical coupling (CEMGCMC). Its value can be calculated with the following formula:

$$K_{emgc}^2 = \frac{Z_1}{Z_2} \tag{6}$$

where

$$\begin{aligned} Z_1 = {} & e^2\left(\mu\gamma\eta + 2\beta\lambda\vartheta - \lambda^2\gamma - \beta^2\eta - \vartheta^2\mu\right) \\ & + h^2\left(\varepsilon\gamma\eta + 2\zeta\xi\vartheta - \vartheta^2\varepsilon - \zeta^2\eta - \xi^2\gamma\right) \\ & + g^2\left(\varepsilon\mu\eta + 2\alpha\xi\lambda - \lambda^2\varepsilon - \alpha^2\eta - \xi^2\mu\right) \\ & + f^2\left(\varepsilon\mu\gamma + 2\alpha\beta\zeta - \beta^2\varepsilon - \alpha^2\gamma - \zeta^2\mu\right) \\ & + 2eh\left(\vartheta^2\alpha + \zeta\beta\eta + \xi\gamma\lambda - \alpha\gamma\eta - \zeta\lambda\vartheta - \xi\beta\vartheta\right) \\ & + 2eg\left(\alpha\beta\eta + \lambda^2\zeta + \xi\vartheta\mu - \alpha\lambda\vartheta - \zeta\mu\eta - \xi\beta\lambda\right) \\ & + 2ef\left(\alpha\gamma\lambda + \zeta\vartheta\mu + \beta^2\xi - \alpha\beta\vartheta - \zeta\beta\lambda - \xi\mu\gamma\right) \\ & + 2hg\left(\varepsilon\lambda\vartheta + \zeta\alpha\eta + \xi^2\beta - \varepsilon\eta\beta - \zeta\lambda\xi - \xi\vartheta\alpha\right) \\ & + 2hf\left(\varepsilon\beta\vartheta + \zeta^2\lambda + \xi\alpha\gamma - \varepsilon\lambda\gamma - \zeta\vartheta\alpha - \xi\zeta\beta\right) \\ & + 2gf\left(\varepsilon\beta\lambda + \alpha^2\vartheta + \xi\mu\zeta - \varepsilon\mu\vartheta - \alpha\zeta\lambda - \alpha\beta\xi\right) \end{aligned} \tag{7}$$

$$\begin{aligned} Z_2 &= C(\varepsilon\mu-\alpha^2)(\gamma\eta-\vartheta^2) \\ &+ C(\beta^2\xi^2-\xi^2\mu\gamma-\beta^2\varepsilon\eta)+C(\lambda^2\zeta^2-\lambda^2\varepsilon\gamma-\zeta^2\mu\eta) \\ &+ 2C(\gamma\alpha\xi\lambda+\eta\alpha\beta\zeta+\varepsilon\beta\lambda\vartheta+\mu\zeta\xi\vartheta-\zeta\xi\beta\lambda-\alpha\zeta\lambda\vartheta-\alpha\beta\xi\vartheta) \end{aligned} \quad (8)$$

Thus, all the possible eigenvalues, namely the five pairs defined by expressions (3) and (4) are already obtained. Each found eigenvalue n_3 must be now used in equation (1) anew to determine the corresponding eigenvector $(U^0,\varphi^0,\psi^0,\Phi^0,\Psi^0)$. It is obvious that each of two eigenvalues in each pair of five provides the same eigenvector because equations (1) depend on n_3^2. Also, four pairs (3) are identical and therefore, they must give the same set of the eigenvector components. Fifth pair (4) can certainly provide a unique set of the eigenvector components different from those for eigenvalues (3). So, only two eigenvectors must be found: the first will correspond to each of eight eigenvalues (3) and the second will correspond to the last pair of eigenvalues (4). Probably, this peculiarity can significantly simplify the problem. The second peculiarity is the situation that any of the eigenvector components does not depend on the phase velocity V_{ph}. The reader can check this statement by using the final expressions for the eigenvector components obtained in the following six sections. It is worth noting that this second peculiarity exists only for the transversely isotropic (6 *mm*) materials and results in many possible solutions for the propagating velocity. A great interest represents to find some solutions with a dramatic dependence on (one of) the following extremely weak exchange effects: the gravitocogravitic, gravitoelectric, cogravitoelectric, gravitomagnetic, and cogravitomagnetic effects.

With equations (1), it is natural first to obtain common forms of the eigenvector components. Utilizing eigenvalue (3) or (4), these common forms will then give certain eigenvector components $(U^0,\varphi^0,\psi^0,\Phi^0,\Psi^0)$. It is natural to utilize the first equation in set (1) for determination of the eigenvector component U^0 as a function of the rest components φ^0, ψ^0, Φ^0, and Ψ^0. Consequently, this function reads:

$$U^0 = -m\left(e\varphi^0+h\psi^0+g\Phi^0+f\Psi^0\right)/CA \quad (9)$$

In definition (9), $m=1+n_3^2$ and the form of the parameter *A* depends on the form of the eigenvalue. For eigenvalues (3) and (4), the parameter *A* can respectively take the following forms:

$$A = m-\left(V_{ph}/V_{t4}\right)^2 = -\left(V_{ph}/V_{t4}\right)^2 \quad (10)$$

$$A = m-\left(V_{ph}/V_{t4}\right)^2 = -mK_{emgc}^2 \quad (11)$$

Exploitation of definition (9) for equations' set (1) allows exclusion of the eigenvector component U^0 from the further consideration and to deal with a reduced set of four equations. This is the usual mathematical procedure for finding of the unknowns for the set of five equations in five unknowns. Let's treat the six different cases that lead to different sets of the eigenvector components. It is convenient to use definitions (10) and (11) of the parameter *A* only in the final expressions for the eigenvector components in the common forms.

The first case

In this case, the new reduced set of four homogeneous equations can be written as follows:

$$\begin{aligned} &\varepsilon\left(1+mK_e^2/A\right)\varphi^0+\alpha\left(1+mK_\alpha^2/A\right)\psi^0 \\ &+\zeta\left(1+mK_\zeta^2/A\right)\Phi^0+\xi\left(1+mK_\xi^2/A\right)\Psi^0=0 \end{aligned} \quad (12)$$

$$\begin{aligned} &\alpha\left(1+mK_\alpha^2/A\right)\varphi^0+\mu\left(1+mK_m^2/A\right)\psi^0 \\ &+\beta\left(1+mK_\beta^2/A\right)\Phi^0+\lambda\left(1+mK_\lambda^2/A\right)\Psi^0=0 \end{aligned} \quad (13)$$

$$\begin{aligned} &\zeta\left(1+mK_\zeta^2/A\right)\varphi^0+\beta\left(1+mK_\beta^2/A\right)\psi^0 \\ &+\gamma\left(1+mK_g^2/A\right)\Phi^0+\vartheta\left(1+mK_\vartheta^2/A\right)\Psi^0=0 \end{aligned} \quad (14)$$

$$\begin{aligned} &\xi\left(1+mK_\xi^2/A\right)\varphi^0+\lambda\left(1+mK_\lambda^2/A\right)\psi^0 \\ &+\vartheta\left(1+mK_\vartheta^2/A\right)\Phi^0+\eta\left(1+mK_f^2/A\right)\Psi^0=0 \end{aligned} \quad (15)$$

where

$$K_e^2 = e^2/C\varepsilon \quad (16)$$

$$K_m^2 = h^2/C\mu \quad (17)$$

$$K_\alpha^2 = eh/C\alpha \quad (18)$$

$$K_g^2 = g^2/C\gamma \quad (19)$$

$$K_f^2 = f^2/C\eta \quad (20)$$

$$K_\vartheta^2 = gf/C\vartheta \quad (21)$$

$$K_\zeta^2 = eg/C\zeta \quad (22)$$

$$K_\xi^2 = ef/C\xi \quad (23)$$

$$K_\lambda^2 = hf/C\lambda \quad (24)$$

$$K_\beta^2 = hg/C\beta \quad (25)$$

Next, treating equation (12) it is possible to determine the second eigenvector component φ^0 as a function of the components ψ^0, Φ^0, and Ψ^0. It can be composed as follows:

$$\varphi^0 = -\frac{\alpha\left(A+mK_\alpha^2\right)}{\varepsilon\left(A+mK_e^2\right)}\psi^0-\frac{\zeta\left(A+mK_\zeta^2\right)}{\varepsilon\left(A+mK_e^2\right)}\Phi^0-\frac{\xi\left(A+mK_\xi^2\right)}{\varepsilon\left(A+mK_e^2\right)}\Psi^0 \quad (26)$$

Definition (26) for φ^0 can be then utilized in equations (13), (14), and (15) to reduce the set of four homogeneous equations in four undetermined. As a result, the new reduced set of three homogeneous equations with three unknown components ψ^0, Φ^0, and Ψ^0 can be composed as follows:

$$\begin{gathered}\left(\frac{\mu\left(A+mK_m^2\right)}{A}-\frac{\alpha^2\left(A+mK_\alpha^2\right)^2}{A\varepsilon\left(A+mK_e^2\right)}\right)\psi^0\\+\left(\frac{\beta\left(A+mK_\beta^2\right)}{A}-\frac{\alpha\zeta\left(A+mK_\alpha^2\right)\left(A+mK_\zeta^2\right)}{A\varepsilon\left(A+mK_e^2\right)}\right)\Phi^0\\+\left(\frac{\lambda\left(A+mK_\lambda^2\right)}{A}-\frac{\alpha\xi\left(A+mK_\alpha^2\right)\left(A+mK_\xi^2\right)}{A\varepsilon\left(A+mK_e^2\right)}\right)\Psi^0=0\end{gathered}\tag{27}$$

$$\begin{gathered}\left(\frac{\beta\left(A+mK_\beta^2\right)}{A}-\frac{\alpha\zeta\left(A+mK_\alpha^2\right)\left(A+mK_\zeta^2\right)}{A\varepsilon\left(A+mK_e^2\right)}\right)\psi^0\\+\left(\frac{\gamma\left(A+mK_g^2\right)}{A}-\frac{\zeta^2\left(A+mK_\zeta^2\right)^2}{A\varepsilon\left(A+mK_e^2\right)}\right)\Phi^0\\+\left(\frac{\vartheta\left(A+mK_\vartheta^2\right)}{A}-\frac{\xi\zeta\left(A+mK_\xi^2\right)\left(A+mK_\zeta^2\right)}{A\varepsilon\left(A+mK_e^2\right)}\right)\Psi^0=0\end{gathered}\tag{28}$$

$$\begin{gathered}\left(\frac{\lambda\left(A+mK_\lambda^2\right)}{A}-\frac{\alpha\xi\left(A+mK_\alpha^2\right)\left(A+mK_\xi^2\right)}{A\varepsilon\left(A+mK_e^2\right)}\right)\psi^0\\+\left(\frac{\vartheta\left(A+mK_\vartheta^2\right)}{A}-\frac{\xi\zeta\left(A+mK_\xi^2\right)\left(A+mK_\zeta^2\right)}{A\varepsilon\left(A+mK_e^2\right)}\right)\Phi^0\\+\left(\frac{\eta\left(A+mK_f^2\right)}{A}-\frac{\xi^2\left(A+mK_\xi^2\right)^2}{A\varepsilon\left(A+mK_e^2\right)}\right)\Psi^0=0\end{gathered}\tag{29}$$

Exploiting equation (27), the third eigenvector component ψ^0 represents the following function of the eigenvector components Φ^0 and Ψ^0:

$$\begin{gathered}\psi^0=-\frac{\beta\left(A+mK_\beta^2\right)-\dfrac{\alpha\zeta\left(A+mK_\alpha^2\right)\left(A+mK_\zeta^2\right)}{\varepsilon\left(A+mK_e^2\right)}}{\mu\left(A+mK_m^2\right)-\dfrac{\alpha^2\left(A+mK_\alpha^2\right)^2}{\varepsilon\left(A+mK_e^2\right)}}\Phi^0\\-\frac{\lambda\left(A+mK_\lambda^2\right)-\dfrac{\alpha\xi\left(A+mK_\alpha^2\right)\left(A+mK_\xi^2\right)}{\varepsilon\left(A+mK_e^2\right)}}{\mu\left(A+mK_m^2\right)-\dfrac{\alpha^2\left(A+mK_\alpha^2\right)^2}{\varepsilon\left(A+mK_e^2\right)}}\Psi^0\end{gathered}\tag{30}$$

Finally, definition (30) must be used for substitution in equations (28) and (29). This substitution results in the final two homogeneous equations in two unknowns: Φ^0 and Ψ^0. With these two equations, both Φ^0 and Ψ^0 can be readily defined. These two complicated equations can be composed in the following forms:

$$\begin{gathered}0=\left(\frac{\gamma\left(A+mK_g^2\right)}{A}-\frac{\zeta^2\left(A+mK_\zeta^2\right)^2}{A\varepsilon\left(A+mK_e^2\right)}-\frac{\left(\dfrac{\beta\left(A+mK_\beta^2\right)}{A}-\dfrac{\alpha\zeta\left(A+mK_\alpha^2\right)\left(A+mK_\zeta^2\right)}{A\varepsilon\left(A+mK_e^2\right)}\right)^2}{\dfrac{\mu\left(A+mK_m^2\right)}{A}-\dfrac{\alpha^2\left(A+mK_\alpha^2\right)^2}{A\varepsilon\left(A+mK_e^2\right)}}\right)\Phi^0\\+\left(\frac{\vartheta\left(A+mK_\vartheta^2\right)}{A}-\frac{\xi\zeta\left(A+mK_\xi^2\right)\left(A+mK_\zeta^2\right)}{A\varepsilon\left(A+mK_e^2\right)}\right)\Psi^0\\-\frac{\left(\dfrac{\beta\left(A+mK_\beta^2\right)}{A}-\dfrac{\alpha\zeta\left(A+mK_\alpha^2\right)\left(A+mK_\zeta^2\right)}{A\varepsilon\left(A+mK_e^2\right)}\right)\left(\lambda\left(A+mK_\lambda^2\right)-\dfrac{\alpha\xi\left(A+mK_\alpha^2\right)\left(A+mK_\xi^2\right)}{\varepsilon\left(A+mK_e^2\right)}\right)}{\mu\left(A+mK_m^2\right)-\dfrac{\alpha^2\left(A+mK_\alpha^2\right)^2}{\varepsilon\left(A+mK_e^2\right)}}\Psi^0\end{gathered}\tag{31}$$

$$\begin{gathered}0=\left(\frac{\vartheta\left(A+mK_\vartheta^2\right)}{A}-\frac{\xi\zeta\left(A+mK_\xi^2\right)\left(A+mK_\zeta^2\right)}{A\varepsilon\left(A+mK_e^2\right)}\right)\Phi^0\\-\frac{\left(\dfrac{\beta\left(A+mK_\beta^2\right)}{A}-\dfrac{\alpha\zeta\left(A+mK_\alpha^2\right)\left(A+mK_\zeta^2\right)}{A\varepsilon\left(A+mK_e^2\right)}\right)\left(\lambda\left(A+mK_\lambda^2\right)-\dfrac{\alpha\xi\left(A+mK_\alpha^2\right)\left(A+mK_\xi^2\right)}{\varepsilon\left(A+mK_e^2\right)}\right)}{\mu\left(A+mK_m^2\right)-\dfrac{\alpha^2\left(A+mK_\alpha^2\right)^2}{\varepsilon\left(A+mK_e^2\right)}}\Phi^0\\+\left(\frac{\eta\left(A+mK_f^2\right)}{A}-\frac{\xi^2\left(A+mK_\xi^2\right)^2}{A\varepsilon\left(A+mK_e^2\right)}-\frac{\left(\dfrac{\lambda\left(A+mK_\lambda^2\right)}{A}-\dfrac{\alpha\xi\left(A+mK_\alpha^2\right)\left(A+mK_\xi^2\right)}{A\varepsilon\left(A+mK_e^2\right)}\right)^2}{\dfrac{\mu\left(A+mK_m^2\right)}{A}-\dfrac{\alpha^2\left(A+mK_\alpha^2\right)^2}{A\varepsilon\left(A+mK_e^2\right)}}\right)\Psi^0\end{gathered}\tag{32}$$

Equations (31) and (32) represent a set of two homogeneous equations in two unknowns: Φ^0 and Ψ^0. This pair of equations can be schematically written as follows: $a_1x + by = 0$ and $bx + a_2y = 0$. Therefore, the unknowns x and y can be chosen in two different ways:

(1) $x = -b$ and $y = a_1$;
(2) $x = a_2$ and $y = -b$.

Taking into account this fact it is natural to write down below two different sets of the eigenvector components for this case. With equation (31) and definitions (9), (26), and (30), the first eigenvectors can be composed. For eigenvalues (3), $m = 0$ and therefore, the corresponding eigenvector components are relatively simple, i.e.

$$\begin{pmatrix}U^{0(1)}\\ \varphi^{0(1)}\\ \psi^{0(1)}\\ \Phi^{0(1)}\\ \Psi^{0(1)}\end{pmatrix}=\begin{pmatrix}U^{0(3)}\\ \varphi^{0(3)}\\ \psi^{0(3)}\\ \Phi^{0(3)}\\ \Psi^{0(3)}\end{pmatrix}=\begin{pmatrix}U^{0(5)}\\ \varphi^{0(5)}\\ \psi^{0(5)}\\ \Phi^{0(5)}\\ \Psi^{0(5)}\end{pmatrix}=\begin{pmatrix}U^{0(7)}\\ \varphi^{0(7)}\\ \psi^{0(7)}\\ \Phi^{0(7)}\\ \Psi^{0(7)}\end{pmatrix}=\begin{pmatrix}U^0=0\\ \varphi^0=-\dfrac{\alpha}{\varepsilon}\psi^0-\dfrac{\zeta}{\varepsilon}\Phi^0-\dfrac{\xi}{\varepsilon}\Psi^0\\ \psi^0=-\dfrac{\beta-\dfrac{\alpha\zeta}{\varepsilon}}{\mu-\dfrac{\alpha^2}{\varepsilon}}\Phi^0-\dfrac{\lambda-\dfrac{\alpha\xi}{\varepsilon}}{\mu-\dfrac{\alpha^2}{\varepsilon}}\Psi^0\\ =-\dfrac{\left(\beta-\dfrac{\alpha\zeta}{\varepsilon}\right)\left(\vartheta-\dfrac{\xi\zeta}{\varepsilon}\right)-\left(\lambda-\dfrac{\alpha\xi}{\varepsilon}\right)\left(\gamma-\dfrac{\zeta^2}{\varepsilon}\right)}{\mu-\dfrac{\alpha^2}{\varepsilon}}\\ \Phi^0=\vartheta-\dfrac{\xi\zeta}{\varepsilon}-\dfrac{\left(\beta-\dfrac{\alpha\zeta}{\varepsilon}\right)\left(\lambda-\dfrac{\alpha\xi}{\varepsilon}\right)}{\mu-\dfrac{\alpha^2}{\varepsilon}}\\ \Psi^0=-\gamma+\dfrac{\zeta^2}{\varepsilon}+\dfrac{\left(\beta-\dfrac{\alpha\zeta}{\varepsilon}\right)^2}{\mu-\dfrac{\alpha^2}{\varepsilon}}\end{pmatrix}\tag{33}$$

However, for eigenvalue (4) there is a more complicated eigenvector. For this case, the utilization of definition (11), equation (31), and definitions (9), (26), (30) leads to the following complicated eigenvector components:

$$\begin{pmatrix} U^{0(9)} \\ \varphi^{0(9)} \\ \psi^{0(9)} \\ \Phi^{0(9)} \\ \Psi^{0(9)} \end{pmatrix} = \begin{pmatrix} U^0 = \left(e\varphi^0 + h\psi^0 + g\Phi^0 + f\Psi^0\right)/\left(CK_{emgc}^2\right) \\ \varphi^0 = -\dfrac{\alpha K_A}{\varepsilon K_E}\psi^0 - \dfrac{\zeta K_Z}{\varepsilon K_E}\Phi^0 - \dfrac{\xi K_S}{\varepsilon K_E}\Psi^0 \\ \psi^0 = -\dfrac{\beta K_B - \dfrac{\alpha\zeta K_A K_Z}{\varepsilon K_E}}{\mu K_M - \dfrac{\alpha^2 K_A^{\,2}}{\varepsilon K_E}}\Phi^0 - \dfrac{\lambda K_L - \dfrac{\alpha\xi K_A K_S}{\varepsilon K_E}}{\mu K_M - \dfrac{\alpha^2 K_A^{\,2}}{\varepsilon K_E}}\Psi^0 \\ = -\dfrac{\left(\beta K_B - \dfrac{\alpha\zeta K_A K_Z}{\varepsilon K_E}\right)\left(\dfrac{\vartheta K_T}{K_{emgc}^2} - \dfrac{\xi\zeta K_S K_Z}{\varepsilon K_E K_{emgc}^2}\right) - \left(\lambda K_L - \dfrac{\alpha\xi K_A K_S}{\varepsilon K_E}\right)\left(\dfrac{\gamma K_G}{K_{emgc}^2} - \dfrac{\zeta^2 K_Z^{\,2}}{\varepsilon K_E K_{emgc}^2}\right)}{\mu K_M - \dfrac{\alpha^2 K_A^{\,2}}{\varepsilon K_E}} \\ \Phi^0 = \dfrac{\vartheta K_T}{K_{emgc}^2} - \dfrac{\xi\zeta K_S K_Z}{\varepsilon K_E K_{emgc}^2} - \dfrac{\left(\dfrac{\beta K_B}{K_{emgc}^2} - \dfrac{\alpha\zeta K_A K_Z}{\varepsilon K_E K_{emgc}^2}\right)\left(\lambda K_L - \dfrac{\alpha\xi K_A K_S}{\varepsilon K_E}\right)}{\mu K_M - \dfrac{\alpha^2 K_A^{\,2}}{\varepsilon K_E}} \\ \Psi^0 = -\dfrac{\gamma K_G}{K_{emgc}^2} + \dfrac{\zeta^2 K_Z^{\,2}}{\varepsilon K_E K_{emgc}^2} + \dfrac{\left(\dfrac{\beta K_B}{K_{emgc}^2} - \dfrac{\alpha\zeta K_A K_Z}{\varepsilon K_E K_{emgc}^2}\right)^2}{\dfrac{\mu K_M}{K_{emgc}^2} - \dfrac{\alpha^2 K_A^{\,2}}{\varepsilon K_E K_{emgc}^2}} \end{pmatrix} \tag{34}$$

where

$$K_M = K_{emgc}^2 - K_m^2 \tag{35}$$

$$K_E = K_{emgc}^2 - K_e^2 \tag{36}$$

$$K_F = K_{emgc}^2 - K_f^2 \tag{37}$$

$$K_G = K_{emgc}^2 - K_g^2 \tag{38}$$

$$K_T = K_{emgc}^2 - K_\vartheta^2 \tag{39}$$

$$K_A = K_{emgc}^2 - K_\alpha^2 \tag{40}$$

$$K_S = K_{emgc}^2 - K_\xi^2 \tag{41}$$

$$K_Z = K_{emgc}^2 - K_\zeta^2 \tag{42}$$

$$K_B = K_{emgc}^2 - K_\beta^2 \tag{43}$$

$$K_L = K_{emgc}^2 - K_\lambda^2 \tag{44}$$

To obtain the second eigenvectors, it is necessary to use equation (32). Therefore, two eigenvectors corresponding to eigenvalues (3) and (4) can be respectively inscribed as follows:

$$\begin{pmatrix} U^{0(1)} \\ \varphi^{0(1)} \\ \psi^{0(1)} \\ \Phi^{0(1)} \\ \Psi^{0(1)} \end{pmatrix} = \begin{pmatrix} U^{0(3)} \\ \varphi^{0(3)} \\ \psi^{0(3)} \\ \Phi^{0(3)} \\ \Psi^{0(3)} \end{pmatrix} = \begin{pmatrix} U^{0(5)} \\ \varphi^{0(5)} \\ \psi^{0(5)} \\ \Phi^{0(5)} \\ \Psi^{0(5)} \end{pmatrix} = \begin{pmatrix} U^{0(7)} \\ \varphi^{0(7)} \\ \psi^{0(7)} \\ \Phi^{0(7)} \\ \Psi^{0(7)} \end{pmatrix}$$

$$= \begin{pmatrix} U^0 = 0 \\ \varphi^0 = -\dfrac{\alpha}{\varepsilon}\psi^0 - \dfrac{\zeta}{\varepsilon}\Phi^0 - \dfrac{\xi}{\varepsilon}\Psi^0 \\ \psi^0 = -\dfrac{\beta - \dfrac{\alpha\zeta}{\varepsilon}}{\mu - \dfrac{\alpha^2}{\varepsilon}}\Phi^0 - \dfrac{\lambda - \dfrac{\alpha\xi}{\varepsilon}}{\mu - \dfrac{\alpha^2}{\varepsilon}}\Psi^0 \\ = \dfrac{\left(\beta - \dfrac{\alpha\zeta}{\varepsilon}\right)\left(\eta - \dfrac{\xi^2}{\varepsilon}\right) - \left(\lambda - \dfrac{\alpha\xi}{\varepsilon}\right)\left(\vartheta - \dfrac{\xi\zeta}{\varepsilon}\right)}{\mu - \dfrac{\alpha^2}{\varepsilon}} \\ \Phi^0 = -\eta + \dfrac{\xi^2}{\varepsilon} + \dfrac{\left(\lambda - \dfrac{\alpha\xi}{\varepsilon}\right)^2}{\mu - \dfrac{\alpha^2}{\varepsilon}} \\ \Psi^0 = \vartheta - \dfrac{\xi\zeta}{\varepsilon} - \dfrac{\left(\beta - \dfrac{\alpha\zeta}{\varepsilon}\right)\left(\lambda - \dfrac{\alpha\xi}{\varepsilon}\right)}{\mu - \dfrac{\alpha^2}{\varepsilon}} \end{pmatrix} \tag{45}$$

$$\begin{pmatrix} U^{0(9)} \\ \varphi^{0(9)} \\ \psi^{0(9)} \\ \Phi^{0(9)} \\ \Psi^{0(9)} \end{pmatrix} = \begin{pmatrix} U^0 = \left(e\varphi^0 + h\psi^0 + g\Phi^0 + f\Psi^0\right)/\left(CK_{emgc}^2\right) \\ \varphi^0 = -\dfrac{\alpha K_A}{\varepsilon K_E}\psi^0 - \dfrac{\zeta K_Z}{\varepsilon K_E}\Phi^0 - \dfrac{\xi K_S}{\varepsilon K_E}\Psi^0 \\ \psi^0 = -\dfrac{\beta K_B - \dfrac{\alpha\zeta K_A K_Z}{\varepsilon K_E}}{\mu K_M - \dfrac{\alpha^2 K_A^{\,2}}{\varepsilon K_E}}\Phi^0 - \dfrac{\lambda K_L - \dfrac{\alpha\xi K_A K_S}{\varepsilon K_E}}{\mu K_M - \dfrac{\alpha^2 K_A^{\,2}}{\varepsilon K_E}}\Psi^0 \\ = -\dfrac{\left(\beta K_B - \dfrac{\alpha\zeta K_A K_Z}{\varepsilon K_E}\right)\left(\dfrac{\eta K_F}{K_{emgc}^2} - \dfrac{\xi^2 K_S^{\,2}}{\varepsilon K_E K_{emgc}^2}\right) - \left(\lambda K_L - \dfrac{\alpha\xi K_A K_S}{\varepsilon K_E}\right)\left(\dfrac{\vartheta K_T}{K_{emgc}^2} - \dfrac{\xi\zeta K_S K_Z}{\varepsilon K_E K_{emgc}^2}\right)}{\mu K_M - \dfrac{\alpha^2 K_A^{\,2}}{\varepsilon K_E}} \\ \Phi^0 = -\dfrac{\eta K_F}{K_{emgc}^2} + \dfrac{\xi^2 K_S^{\,2}}{\varepsilon K_E K_{emgc}^2} + \dfrac{\left(\dfrac{\lambda K_L}{K_{emgc}^2} - \dfrac{\alpha\xi K_A K_S}{\varepsilon K_E K_{emgc}^2}\right)^2}{\dfrac{\mu K_M}{K_{emgc}^2} - \dfrac{\alpha^2 K_A^{\,2}}{\varepsilon K_E K_{emgc}^2}} \\ \Psi^0 = \dfrac{\vartheta K_T}{K_{emgc}^2} - \dfrac{\xi\zeta K_S K_Z}{\varepsilon K_E K_{emgc}^2} - \dfrac{\left(\dfrac{\beta K_B}{K_{emgc}^2} - \dfrac{\alpha\zeta K_A K_Z}{\varepsilon K_E K_{emgc}^2}\right)\left(\lambda K_L - \dfrac{\alpha\xi K_A K_S}{\varepsilon K_E}\right)}{\mu K_M - \dfrac{\alpha^2 K_A^{\,2}}{\varepsilon K_E}} \end{pmatrix} \tag{46}$$

One can find that obtained eigenvectors (33), (34), (45), and (46) depend only on the material parameters and do not depend on the phase velocity V_{ph}. All the material parameters are listed in table 1.

The second case

It is also possible to regroup equations (12), (13), (14), (15) and then to find new sets of the eigenvector components. So, the new regrouped set of four homogeneous equations can be written as follows:

$$\begin{cases} \varepsilon\left(1+mK_e^2/A\right)\varphi^0+\zeta\left(1+mK_\zeta^2/A\right)\Phi^0 \\ +\alpha\left(1+mK_\alpha^2/A\right)\psi^0+\xi\left(1+mK_\xi^2/A\right)\Psi^0=0 \\ \zeta\left(1+mK_\zeta^2/A\right)\varphi^0+\gamma\left(1+mK_g^2/A\right)\Phi^0 \\ +\beta\left(1+mK_\beta^2/A\right)\psi^0+\vartheta\left(1+mK_\vartheta^2/A\right)\Psi^0=0 \\ \alpha\left(1+mK_\alpha^2/A\right)\varphi^0+\beta\left(1+mK_\beta^2/A\right)\Phi^0 \\ +\mu\left(1+mK_m^2/A\right)\psi^0+\lambda\left(1+mK_\lambda^2/A\right)\Psi^0=0 \\ \xi\left(1+mK_\xi^2/A\right)\varphi^0+\vartheta\left(1+mK_\vartheta^2/A\right)\Phi^0 \\ +\lambda\left(1+mK_\lambda^2/A\right)\psi^0+\eta\left(1+mK_f^2/A\right)\Psi^0=0 \end{cases} \tag{47}$$

Similarly, from the first equation in set (47) it can be written the following dependence:

$$\varphi^0=-\frac{\zeta\left(A+mK_\zeta^2\right)}{\varepsilon\left(A+mK_e^2\right)}\Phi^0 -\frac{\alpha\left(A+mK_\alpha^2\right)}{\varepsilon\left(A+mK_e^2\right)}\psi^0-\frac{\xi\left(A+mK_\xi^2\right)}{\varepsilon\left(A+mK_e^2\right)}\Psi^0 \tag{48}$$

Using definition (48) for the second, third, and fourth equations in set (47), one can get the following reduced set of three homogeneous equations:

$$\begin{cases} \left(\frac{\gamma\left(A+mK_g^2\right)}{A}-\frac{\zeta^2\left(A+mK_\zeta^2\right)^2}{A\varepsilon\left(A+mK_e^2\right)}\right)\Phi^0+\left(\frac{\beta\left(A+mK_\beta^2\right)}{A}-\frac{\alpha\zeta\left(A+mK_\alpha^2\right)\left(A+mK_\zeta^2\right)}{A\varepsilon\left(A+mK_e^2\right)}\right)\psi^0 \\ +\left(\frac{\vartheta\left(A+mK_\vartheta^2\right)}{A}-\frac{\xi\zeta\left(A+mK_\xi^2\right)\left(A+mK_\zeta^2\right)}{A\varepsilon\left(A+mK_e^2\right)}\right)\Psi^0=0 \\ \left(\frac{\beta\left(A+mK_\beta^2\right)}{A}-\frac{\alpha\zeta\left(A+mK_\alpha^2\right)\left(A+mK_\zeta^2\right)}{A\varepsilon\left(A+mK_e^2\right)}\right)\Phi^0+\left(\frac{\mu\left(A+mK_m^2\right)}{A}-\frac{\alpha^2\left(A+mK_\alpha^2\right)^2}{A\varepsilon\left(A+mK_e^2\right)}\right)\psi^0 \\ +\left(\frac{\lambda\left(A+mK_\lambda^2\right)}{A}-\frac{\alpha\xi\left(A+mK_\alpha^2\right)\left(A+mK_\xi^2\right)}{A\varepsilon\left(A+mK_e^2\right)}\right)\Psi^0=0 \\ \left(\frac{\vartheta\left(A+mK_\vartheta^2\right)}{A}-\frac{\xi\zeta\left(A+mK_\xi^2\right)\left(A+mK_\zeta^2\right)}{A\varepsilon\left(A+mK_e^2\right)}\right)\Phi^0+\left(\frac{\lambda\left(A+mK_\lambda^2\right)}{A}-\frac{\alpha\xi\left(A+mK_\alpha^2\right)\left(A+mK_\xi^2\right)}{A\varepsilon\left(A+mK_e^2\right)}\right)\psi^0 \\ +\left(\frac{\eta\left(A+mK_f^2\right)}{A}-\frac{\xi^2\left(A+mK_\xi^2\right)^2}{A\varepsilon\left(A+mK_e^2\right)}\right)\Psi^0=0 \end{cases} \tag{49}$$

It is natural to exploit the first equation in set (49) for the determination of the eigenvector component Φ^0. It is defined by

$$\Phi^0=-\frac{\beta\left(A+mK_\beta^2\right)-\frac{\alpha\zeta\left(A+mK_\alpha^2\right)\left(A+mK_\zeta^2\right)}{\varepsilon\left(A+mK_e^2\right)}}{\gamma\left(A+mK_g^2\right)-\frac{\zeta^2\left(A+mK_\zeta^2\right)^2}{\varepsilon\left(A+mK_e^2\right)}}\psi^0 -\frac{\vartheta\left(A+mK_\vartheta^2\right)-\frac{\xi\zeta\left(A+mK_\xi^2\right)\left(A+mK_\zeta^2\right)}{\varepsilon\left(A+mK_e^2\right)}}{\gamma\left(A+mK_g^2\right)-\frac{\zeta^2\left(A+mK_\zeta^2\right)^2}{\varepsilon\left(A+mK_e^2\right)}}\Psi^0 \tag{50}$$

A substitution of the eigenvector component Φ^0 defined by (50) in the second and third equations in set (49) leads to the following final two homogeneous equation, with which it is already possible to soundly determine the rest two eigenvector components ψ^0 and Ψ^0:

$$\begin{cases} 0=\left(\frac{\mu\left(A+mK_m^2\right)}{A}-\frac{\alpha^2\left(A+mK_\alpha^2\right)^2}{A\varepsilon\left(A+mK_e^2\right)}-\frac{\left(\frac{\beta\left(A+mK_\beta^2\right)}{A}-\frac{\alpha\zeta\left(A+mK_\alpha^2\right)\left(A+mK_\zeta^2\right)}{A\varepsilon\left(A+mK_e^2\right)}\right)^2}{\frac{\gamma\left(A+mK_g^2\right)}{A}-\frac{\zeta^2\left(A+mK_\zeta^2\right)^2}{A\varepsilon\left(A+mK_e^2\right)}}\right)\psi^0 \\ +\left(\frac{\lambda\left(A+mK_\lambda^2\right)}{A}-\frac{\alpha\xi\left(A+mK_\alpha^2\right)\left(A+mK_\xi^2\right)}{A\varepsilon\left(A+mK_e^2\right)}\right)\Psi^0 \\ -\left(\frac{\beta\left(A+mK_\beta^2\right)}{A}-\frac{\alpha\zeta\left(A+mK_\alpha^2\right)\left(A+mK_\zeta^2\right)}{A\varepsilon\left(A+mK_e^2\right)}\right)\frac{\vartheta\left(A+mK_\vartheta^2\right)-\frac{\xi\zeta\left(A+mK_\xi^2\right)\left(A+mK_\zeta^2\right)}{\varepsilon\left(A+mK_e^2\right)}}{\gamma\left(A+mK_g^2\right)-\frac{\zeta^2\left(A+mK_\zeta^2\right)^2}{\varepsilon\left(A+mK_e^2\right)}}\Psi^0 \\ 0=\left(\frac{\lambda\left(A+mK_\lambda^2\right)}{A}-\frac{\alpha\xi\left(A+mK_\alpha^2\right)\left(A+mK_\xi^2\right)}{A\varepsilon\left(A+mK_e^2\right)}\right)\psi^0 \\ -\left(\frac{\beta\left(A+mK_\beta^2\right)}{A}-\frac{\alpha\zeta\left(A+mK_\alpha^2\right)\left(A+mK_\zeta^2\right)}{A\varepsilon\left(A+mK_e^2\right)}\right)\frac{\vartheta\left(A+mK_\vartheta^2\right)-\frac{\xi\zeta\left(A+mK_\xi^2\right)\left(A+mK_\zeta^2\right)}{\varepsilon\left(A+mK_e^2\right)}}{\gamma\left(A+mK_g^2\right)-\frac{\zeta^2\left(A+mK_\zeta^2\right)^2}{\varepsilon\left(A+mK_e^2\right)}}\Psi^0 \\ +\left(\frac{\eta\left(A+mK_f^2\right)}{A}-\frac{\xi^2\left(A+mK_\xi^2\right)^2}{A\varepsilon\left(A+mK_e^2\right)}-\frac{\left(\frac{\vartheta\left(A+mK_\vartheta^2\right)}{A}-\frac{\xi\zeta\left(A+mK_\xi^2\right)\left(A+mK_\zeta^2\right)}{A\varepsilon\left(A+mK_e^2\right)}\right)^2}{\frac{\gamma\left(A+mK_g^2\right)}{A}-\frac{\zeta^2\left(A+mK_\zeta^2\right)^2}{A\varepsilon\left(A+mK_e^2\right)}}\right)\Psi^0 \end{cases} \tag{51}$$

Using the first of two equations in (51), the first pair of the eigenvectors can be composed. Therefore, they read:

$$\begin{pmatrix} U^{0(1)} \\ \varphi^{0(1)} \\ \psi^{0(1)} \\ \Phi^{0(1)} \\ \Psi^{0(1)} \end{pmatrix}=\begin{pmatrix} U^{0(3)} \\ \varphi^{0(3)} \\ \psi^{0(3)} \\ \Phi^{0(3)} \\ \Psi^{0(3)} \end{pmatrix}=\begin{pmatrix} U^{0(5)} \\ \varphi^{0(5)} \\ \psi^{0(5)} \\ \Phi^{0(5)} \\ \Psi^{0(5)} \end{pmatrix}=\begin{pmatrix} U^{0(7)} \\ \varphi^{0(7)} \\ \psi^{0(7)} \\ \Phi^{0(7)} \\ \Psi^{0(7)} \end{pmatrix}=\begin{pmatrix} U^0=0 \\ \varphi^0=-\frac{\zeta}{\varepsilon}\Phi^0-\frac{\alpha}{\varepsilon}\psi^0-\frac{\xi}{\varepsilon}\Psi^0 \\ \psi^0=\lambda-\frac{\alpha\xi}{\varepsilon}-\frac{\left(\beta-\frac{\alpha\zeta}{\varepsilon}\right)\left(\vartheta-\frac{\xi\zeta}{\varepsilon}\right)}{\gamma-\frac{\zeta^2}{\varepsilon}} \\ \Phi^0=-\frac{\beta-\frac{\alpha\zeta}{\varepsilon}}{\gamma-\frac{\zeta^2}{\varepsilon}}\psi^0-\frac{\vartheta-\frac{\xi\zeta}{\varepsilon}}{\gamma-\frac{\zeta^2}{\varepsilon}}\Psi^0 \\ \Psi^0=-\mu+\frac{\alpha^2}{\varepsilon}+\frac{\left(\beta-\frac{\alpha\zeta}{\varepsilon}\right)^2}{\gamma-\frac{\zeta^2}{\varepsilon}} \end{pmatrix} \tag{52}$$

$$\begin{pmatrix} U^{0(9)} \\ \varphi^{0(9)} \\ \psi^{0(9)} \\ \Phi^{0(9)} \\ \Psi^{0(9)} \end{pmatrix}=\begin{pmatrix} U^0=\left(e\varphi^0+h\psi^0+g\Phi^0+f\Psi^0\right)/CK_{emgc}^2 \\ \varphi^0=-\frac{\zeta K_Z}{\varepsilon K_E}\Phi^0-\frac{\alpha K_A}{\varepsilon K_E}\psi^0-\frac{\xi K_S}{\varepsilon K_E}\Psi^0 \\ \psi^0=\frac{\lambda K_L}{K_{emgc}^2}-\frac{\alpha\xi K_A K_S}{\varepsilon K_E K_{emgc}^2}-\frac{\left(\frac{\beta K_B}{K_{emgc}^2}-\frac{\alpha\zeta K_A K_Z}{\varepsilon K_E K_{emgc}^2}\right)\left(\vartheta K_T-\frac{\xi\zeta K_S K_Z}{\varepsilon K_E}\right)}{\gamma K_G-\frac{\zeta^2 K_Z{}^2}{\varepsilon K_E}} \\ \Phi^0=-\frac{\beta K_B-\frac{\alpha\zeta K_A K_Z}{\varepsilon K_E}}{\gamma K_G-\frac{\zeta^2 K_Z{}^2}{\varepsilon K_E}}\psi^0-\frac{\vartheta K_T-\frac{\xi\zeta K_S K_Z}{\varepsilon K_E}}{\gamma K_G-\frac{\zeta^2 K_Z{}^2}{\varepsilon K_E}}\Psi^0 \\ \Psi^0=-\frac{\mu K_M}{K_{emgc}^2}+\frac{\alpha^2 K_A{}^2}{\varepsilon K_E K_{emgc}^2}+\frac{\left(\frac{\beta K_B}{K_{emgc}^2}-\frac{\alpha\zeta K_A K_Z}{\varepsilon K_E K_{emgc}^2}\right)^2}{\frac{\gamma K_G}{K_{emgc}^2}-\frac{\zeta^2 K_Z{}^2}{\varepsilon K_E K_{emgc}^2}} \end{pmatrix} \tag{53}$$

The utilization of the second equation in (51) results in the second pair of the eigenvectors. They can be naturally written down as follows:

$$\begin{pmatrix} U^{0(1)} \\ \varphi^{0(1)} \\ \psi^{0(1)} \\ \Phi^{0(1)} \\ \Psi^{0(1)} \end{pmatrix} = \begin{pmatrix} U^{0(3)} \\ \varphi^{0(3)} \\ \psi^{0(3)} \\ \Phi^{0(3)} \\ \Psi^{0(3)} \end{pmatrix} = \begin{pmatrix} U^{0(5)} \\ \varphi^{0(5)} \\ \psi^{0(5)} \\ \Phi^{0(5)} \\ \Psi^{0(5)} \end{pmatrix} = \begin{pmatrix} U^{0(7)} \\ \varphi^{0(7)} \\ \psi^{0(7)} \\ \Phi^{0(7)} \\ \Psi^{0(7)} \end{pmatrix} = \begin{pmatrix} U^0 = 0 \\ \varphi^0 = -\dfrac{\zeta}{\varepsilon}\Phi^0 - \dfrac{\alpha}{\varepsilon}\psi^0 - \dfrac{\xi}{\varepsilon}\Psi^0 \\ \psi^0 = -\eta + \dfrac{\xi^2}{\varepsilon} + \dfrac{\left(\vartheta - \dfrac{\xi\zeta}{\varepsilon}\right)^2}{\gamma - \dfrac{\zeta^2}{\varepsilon}} \\ \Phi^0 = -\dfrac{\beta - \dfrac{\alpha\zeta}{\varepsilon}}{\gamma - \dfrac{\zeta^2}{\varepsilon}}\psi^0 - \dfrac{\vartheta - \dfrac{\xi\zeta}{\varepsilon}}{\gamma - \dfrac{\zeta^2}{\varepsilon}}\Psi^0 \\ \Psi^0 = \lambda - \dfrac{\alpha\xi}{\varepsilon} - \dfrac{\left(\beta - \dfrac{\alpha\zeta}{\varepsilon}\right)\left(\vartheta - \dfrac{\xi\zeta}{\varepsilon}\right)}{\gamma - \dfrac{\zeta^2}{\varepsilon}} \end{pmatrix} \tag{54}$$

$$\begin{pmatrix} U^{0(9)} \\ \varphi^{0(9)} \\ \psi^{0(9)} \\ \Phi^{0(9)} \\ \Psi^{0(9)} \end{pmatrix} = \begin{pmatrix} U^0 = \left(e\varphi^0 + h\psi^0 + g\Phi^0 + f\Psi^0\right) / CK_{emgc}^2 \\ \varphi^0 = -\dfrac{\zeta K_Z}{\varepsilon K_E}\Phi^0 - \dfrac{\alpha K_A}{\varepsilon K_E}\psi^0 - \dfrac{\xi K_S}{\varepsilon K_E}\Psi^0 \\ \psi^0 = -\dfrac{\eta K_F}{K_{emgc}^2} + \dfrac{\xi^2 K_S^{\,2}}{\varepsilon K_E K_{emgc}^2} + \dfrac{\left(\dfrac{\vartheta K_T}{K_{emgc}^2} - \dfrac{\xi\zeta K_S K_Z}{\varepsilon K_E K_{emgc}^2}\right)^2}{\gamma K_G - \dfrac{\zeta^2 K_Z^{\,2}}{\varepsilon K_E}} \\ \Phi^0 = -\dfrac{\beta K_B - \dfrac{\alpha\zeta K_A K_Z}{\varepsilon K_E}}{\gamma K_G - \dfrac{\zeta^2 K_Z^{\,2}}{\varepsilon K_E}}\psi^0 - \dfrac{\vartheta K_T - \dfrac{\xi\zeta K_S K_Z}{\varepsilon K_E}}{\gamma K_G - \dfrac{\zeta^2 K_Z^{\,2}}{\varepsilon K_E}}\Psi^0 \\ \Psi^0 = \dfrac{\lambda K_L}{K_{emgc}^2} - \dfrac{\alpha\xi K_A K_S}{\varepsilon K_E K_{emgc}^2} - \dfrac{\left(\dfrac{\beta K_B}{K_{emgc}^2} - \dfrac{\alpha\zeta K_A K_Z}{\varepsilon K_E K_{emgc}^2}\right)\left(\vartheta K_T - \dfrac{\xi\zeta K_S K_Z}{\varepsilon K_E}\right)}{\gamma K_G - \dfrac{\zeta^2 K_Z^{\,2}}{\varepsilon K_E}} \end{pmatrix} \tag{55}$$

The third case

For the third case, the new regrouped set of four homogeneous equations (47) can be introduced as follows:

$$\begin{cases} \varepsilon\left(1 + mK_e^2/A\right)\varphi^0 + \xi\left(1 + mK_\xi^2/A\right)\Psi^0 \\ + \alpha\left(1 + mK_\alpha^2/A\right)\psi^0 + \zeta\left(1 + mK_\zeta^2/A\right)\Phi^0 = 0 \\ \xi\left(1 + mK_\xi^2/A\right)\varphi^0 + \eta\left(1 + mK_f^2/A\right)\Psi^0 \\ + \lambda\left(1 + mK_\lambda^2/A\right)\psi^0 + \vartheta\left(1 + mK_\vartheta^2/A\right)\Phi^0 = 0 \\ \alpha\left(1 + mK_\alpha^2/A\right)\varphi^0 + \lambda\left(1 + mK_\lambda^2/A\right)\Psi^0 \\ + \mu\left(1 + mK_m^2/A\right)\psi^0 + \beta\left(1 + mK_\beta^2/A\right)\Phi^0 = 0 \\ \zeta\left(1 + mK_\zeta^2/A\right)\varphi^0 + \vartheta\left(1 + mK_\vartheta^2/A\right)\Psi^0 \\ + \beta\left(1 + mK_\beta^2/A\right)\psi^0 + \gamma\left(1 + mK_g^2/A\right)\Phi^0 = 0 \end{cases} \tag{56}$$

Indeed, the fist equation in set (56) defines the eigenvector component φ^0 as a function of the rest components Ψ^0, ψ^0, and Φ^0. This dependence reads:

$$\varphi^0 = -\frac{\xi\left(A + mK_\xi^2\right)}{\varepsilon\left(A + mK_e^2\right)}\Psi^0 - \frac{\alpha\left(A + mK_\alpha^2\right)}{\varepsilon\left(A + mK_e^2\right)}\psi^0 - \frac{\zeta\left(A + mK_\zeta^2\right)}{\varepsilon\left(A + mK_e^2\right)}\Phi^0 \tag{57}$$

Using definition (57) for the standard mathematical procedure, the unknown φ^0 can be excluded for the further treatment and therefore, one can deal already with the following reduced set of three homogeneous equations:

$$\begin{cases} \left(\dfrac{\eta\left(A + mK_f^2\right)}{A} - \dfrac{\xi^2\left(A + mK_\xi^2\right)^2}{A\varepsilon\left(A + mK_e^2\right)}\right)\Psi^0 + \left(\dfrac{\lambda\left(A + mK_\lambda^2\right)}{A} - \dfrac{\alpha\xi\left(A + mK_\alpha^2\right)\left(A + mK_\xi^2\right)}{A\varepsilon\left(A + mK_e^2\right)}\right)\psi^0 \\ + \left(\dfrac{\vartheta\left(A + mK_\vartheta^2\right)}{A} - \dfrac{\xi\zeta\left(A + mK_\xi^2\right)\left(A + mK_\zeta^2\right)}{A\varepsilon\left(A + mK_e^2\right)}\right)\Phi^0 = 0 \\ \left(\dfrac{\lambda\left(A + mK_\lambda^2\right)}{A} - \dfrac{\alpha\xi\left(A + mK_\alpha^2\right)\left(A + mK_\xi^2\right)}{A\varepsilon\left(A + mK_e^2\right)}\right)\Psi^0 + \left(\dfrac{\mu\left(A + mK_m^2\right)}{A} - \dfrac{\alpha^2\left(A + mK_\alpha^2\right)^2}{A\varepsilon\left(A + mK_e^2\right)}\right)\psi^0 \\ + \left(\dfrac{\beta\left(A + mK_\beta^2\right)}{A} - \dfrac{\alpha\zeta\left(A + mK_\alpha^2\right)\left(A + mK_\zeta^2\right)}{A\varepsilon\left(A + mK_e^2\right)}\right)\Phi^0 = 0 \\ \left(\dfrac{\vartheta\left(A + mK_\vartheta^2\right)}{A} - \dfrac{\xi\zeta\left(A + mK_\xi^2\right)\left(A + mK_\zeta^2\right)}{A\varepsilon\left(A + mK_e^2\right)}\right)\Psi^0 + \left(\dfrac{\beta\left(A + mK_\beta^2\right)}{A} - \dfrac{\alpha\zeta\left(A + mK_\alpha^2\right)\left(A + mK_\zeta^2\right)}{A\varepsilon\left(A + mK_e^2\right)}\right)\psi^0 \\ + \left(\dfrac{\gamma\left(A + mK_g^2\right)}{A} - \dfrac{\zeta^2\left(A + mK_\zeta^2\right)^2}{A\varepsilon\left(A + mK_e^2\right)}\right)\Phi^0 = 0 \end{cases} \tag{58}$$

Analogically, the first equation in set (58) defines the eigenvector component Ψ^0 by

$$\Psi^0 = -\frac{\lambda\left(A + mK_\lambda^2\right) - \dfrac{\alpha\xi\left(A + mK_\alpha^2\right)\left(A + mK_\xi^2\right)}{\varepsilon\left(A + mK_e^2\right)}}{\eta\left(A + mK_f^2\right) - \dfrac{\xi^2\left(A + mK_\xi^2\right)^2}{\varepsilon\left(A + mK_e^2\right)}}\psi^0 - \frac{\vartheta\left(A + mK_\vartheta^2\right) - \dfrac{\xi\zeta\left(A + mK_\xi^2\right)\left(A + mK_\zeta^2\right)}{\varepsilon\left(A + mK_e^2\right)}}{\eta\left(A + mK_f^2\right) - \dfrac{\xi^2\left(A + mK_\xi^2\right)^2}{\varepsilon\left(A + mK_e^2\right)}}\Phi^0 \tag{59}$$

The application of definition (59) for substitution in the second and third equations in set (58) can provide the final set of two homogeneous equations. These two equations can be exposed in the following form:

$$\begin{cases} \left(\dfrac{\mu\left(A + mK_m^2\right)}{A} - \dfrac{\alpha^2\left(A + mK_\alpha^2\right)^2}{A\varepsilon\left(A + mK_e^2\right)} - \dfrac{\left(\dfrac{\lambda\left(A + mK_\lambda^2\right)}{A} - \dfrac{\alpha\xi\left(A + mK_\alpha^2\right)\left(A + mK_\xi^2\right)}{A\varepsilon\left(A + mK_e^2\right)}\right)^2}{\dfrac{\eta\left(A + mK_f^2\right)}{A} - \dfrac{\xi^2\left(A + mK_\xi^2\right)^2}{A\varepsilon\left(A + mK_e^2\right)}}\right)\psi^0 \\ - \left(\dfrac{\lambda\left(A + mK_\lambda^2\right)}{A} - \dfrac{\alpha\xi\left(A + mK_\alpha^2\right)\left(A + mK_\xi^2\right)}{A\varepsilon\left(A + mK_e^2\right)}\right)\dfrac{\vartheta\left(A + mK_\vartheta^2\right) - \dfrac{\xi\zeta\left(A + mK_\xi^2\right)\left(A + mK_\zeta^2\right)}{\varepsilon\left(A + mK_e^2\right)}}{\eta\left(A + mK_f^2\right) - \dfrac{\xi^2\left(A + mK_\xi^2\right)^2}{\varepsilon\left(A + mK_e^2\right)}}\Phi^0 \\ + \left(\dfrac{\beta\left(A + mK_\beta^2\right)}{A} - \dfrac{\alpha\zeta\left(A + mK_\alpha^2\right)\left(A + mK_\zeta^2\right)}{A\varepsilon\left(A + mK_e^2\right)}\right)\Phi^0 = 0 \\ - \left(\dfrac{\lambda\left(A + mK_\lambda^2\right)}{A} - \dfrac{\alpha\xi\left(A + mK_\alpha^2\right)\left(A + mK_\xi^2\right)}{A\varepsilon\left(A + mK_e^2\right)}\right)\dfrac{\vartheta\left(A + mK_\vartheta^2\right) - \dfrac{\xi\zeta\left(A + mK_\xi^2\right)\left(A + mK_\zeta^2\right)}{\varepsilon\left(A + mK_e^2\right)}}{\eta\left(A + mK_f^2\right) - \dfrac{\xi^2\left(A + mK_\xi^2\right)^2}{\varepsilon\left(A + mK_e^2\right)}}\psi^0 \\ + \left(\dfrac{\beta\left(A + mK_\beta^2\right)}{A} - \dfrac{\alpha\zeta\left(A + mK_\alpha^2\right)\left(A + mK_\zeta^2\right)}{A\varepsilon\left(A + mK_e^2\right)}\right)\psi^0 \\ + \left(\dfrac{\gamma\left(A + mK_g^2\right)}{A} - \dfrac{\zeta^2\left(A + mK_\zeta^2\right)^2}{A\varepsilon\left(A + mK_e^2\right)} - \dfrac{\left(\dfrac{\vartheta\left(A + mK_\vartheta^2\right)}{A} - \dfrac{\xi\zeta\left(A + mK_\xi^2\right)\left(A + mK_\zeta^2\right)}{A\varepsilon\left(A + mK_e^2\right)}\right)^2}{\dfrac{\eta\left(A + mK_f^2\right)}{A} - \dfrac{\xi^2\left(A + mK_\xi^2\right)^2}{A\varepsilon\left(A + mK_e^2\right)}}\right)\Phi^0 = 0 \end{cases} \tag{60}$$

Using the first equation in set (60), the first eigenvectors read:

$$\begin{pmatrix} U^{0(1)} \\ \varphi^{0(1)} \\ \psi^{0(1)} \\ \Phi^{0(1)} \\ \Psi^{0(1)} \end{pmatrix} = \begin{pmatrix} U^{0(3)} \\ \varphi^{0(3)} \\ \psi^{0(3)} \\ \Phi^{0(3)} \\ \Psi^{0(3)} \end{pmatrix} = \begin{pmatrix} U^{0(5)} \\ \varphi^{0(5)} \\ \psi^{0(5)} \\ \Phi^{0(5)} \\ \Psi^{0(5)} \end{pmatrix} = \begin{pmatrix} U^{0(7)} \\ \varphi^{0(7)} \\ \psi^{0(7)} \\ \Phi^{0(7)} \\ \Psi^{0(7)} \end{pmatrix} = \begin{pmatrix} U^0 = 0 \\ \varphi^0 = -\dfrac{\xi}{\varepsilon}\Psi^0 - \dfrac{\alpha}{\varepsilon}\psi^0 - \dfrac{\zeta}{\varepsilon}\Phi^0 \\ \psi^0 = \beta - \dfrac{\alpha\zeta}{\varepsilon} - \dfrac{\left(\lambda - \dfrac{\alpha\xi}{\varepsilon}\right)\left(\vartheta - \dfrac{\xi\zeta}{\varepsilon}\right)}{\eta - \dfrac{\xi^2}{\varepsilon}} \\ \Phi^0 = -\mu + \dfrac{\alpha^2}{\varepsilon} + \dfrac{\left(\lambda - \dfrac{\alpha\xi}{\varepsilon}\right)^2}{\eta - \dfrac{\xi^2}{\varepsilon}} \\ \Psi^0 = -\dfrac{\lambda - \dfrac{\alpha\xi}{\varepsilon}}{\eta - \dfrac{\xi^2}{\varepsilon}}\psi^0 - \dfrac{\vartheta - \dfrac{\xi\zeta}{\varepsilon}}{\eta - \dfrac{\xi^2}{\varepsilon}}\Phi^0 \end{pmatrix} \tag{61}$$

$$\begin{pmatrix} U^{0(9)} \\ \varphi^{0(9)} \\ \psi^{0(9)} \\ \Phi^{0(9)} \\ \Psi^{0(9)} \end{pmatrix} = \begin{pmatrix} U^0 = \left(e\varphi^0 + h\psi^0 + g\Phi^0 + f\Psi^0\right)\Big/ CK_{emgc}^2 \\ \varphi^0 = -\dfrac{\xi K_S}{\varepsilon K_E}\Psi^0 - \dfrac{\alpha K_A}{\varepsilon K_E}\psi^0 - \dfrac{\zeta K_Z}{\varepsilon K_E}\Phi^0 \\ \psi^0 = \dfrac{\beta K_B}{K_{emgc}^2} - \dfrac{\alpha\zeta K_A K_Z}{\varepsilon K_E K_{emgc}^2} - \left(\dfrac{\lambda K_L}{K_{emgc}^2} - \dfrac{\alpha\xi K_A K_S}{\varepsilon K_E K_{emgc}^2}\right)\dfrac{\vartheta K_T - \dfrac{\xi\zeta K_S K_Z}{\varepsilon K_E}}{\eta K_F - \dfrac{\xi^2 K_S{}^2}{\varepsilon K_E}} \\ \Phi^0 = -\dfrac{\mu K_M}{K_{emgc}^2} + \dfrac{\alpha^2 K_A{}^2}{\varepsilon K_E K_{emgc}^2} + \dfrac{\left(\dfrac{\lambda K_L}{K_{emgc}^2} - \dfrac{\alpha\xi K_A K_S}{\varepsilon K_E K_{emgc}^2}\right)^2}{\dfrac{\eta K_F}{K_{emgc}^2} - \dfrac{\xi^2 K_S{}^2}{\varepsilon K_E K_{emgc}^2}} \\ \Psi^0 = -\dfrac{\lambda K_L - \dfrac{\alpha\xi K_A K_S}{\varepsilon K_E}}{\eta K_F - \dfrac{\xi^2 K_S{}^2}{\varepsilon K_E}}\psi^0 - \dfrac{\vartheta K_T - \dfrac{\xi\zeta K_S K_Z}{\varepsilon K_E}}{\eta K_F - \dfrac{\xi^2 K_S{}^2}{\varepsilon K_E}}\Phi^0 \end{pmatrix} \tag{62}$$

The second eigenvectors can be obtained by the use of the second equation in set (60). Their components can be written down as follows:

$$\begin{pmatrix} U^{0(1)} \\ \varphi^{0(1)} \\ \psi^{0(1)} \\ \Phi^{0(1)} \\ \Psi^{0(1)} \end{pmatrix} = \begin{pmatrix} U^{0(3)} \\ \varphi^{0(3)} \\ \psi^{0(3)} \\ \Phi^{0(3)} \\ \Psi^{0(3)} \end{pmatrix} = \begin{pmatrix} U^{0(5)} \\ \varphi^{0(5)} \\ \psi^{0(5)} \\ \Phi^{0(5)} \\ \Psi^{0(5)} \end{pmatrix} = \begin{pmatrix} U^{0(7)} \\ \varphi^{0(7)} \\ \psi^{0(7)} \\ \Phi^{0(7)} \\ \Psi^{0(7)} \end{pmatrix} = \begin{pmatrix} U^0 = 0 \\ \varphi^0 = -\dfrac{\xi}{\varepsilon}\Psi^0 - \dfrac{\alpha}{\varepsilon}\psi^0 - \dfrac{\zeta}{\varepsilon}\Phi^0 \\ \psi^0 = -\gamma + \dfrac{\zeta^2}{\varepsilon} + \dfrac{\left(\vartheta - \dfrac{\xi\zeta}{\varepsilon}\right)^2}{\eta - \dfrac{\xi^2}{\varepsilon}} \\ \Phi^0 = \beta - \dfrac{\alpha\zeta}{\varepsilon} - \dfrac{\left(\lambda - \dfrac{\alpha\xi}{\varepsilon}\right)\left(\vartheta - \dfrac{\xi\zeta}{\varepsilon}\right)}{\eta - \dfrac{\xi^2}{\varepsilon}} \\ \Psi^0 = -\dfrac{\lambda - \dfrac{\alpha\xi}{\varepsilon}}{\eta - \dfrac{\xi^2}{\varepsilon}}\psi^0 - \dfrac{\vartheta - \dfrac{\xi\zeta}{\varepsilon}}{\eta - \dfrac{\xi^2}{\varepsilon}}\Phi^0 \end{pmatrix} \tag{63}$$

$$\begin{pmatrix} U^{0(9)} \\ \varphi^{0(9)} \\ \psi^{0(9)} \\ \Phi^{0(9)} \\ \Psi^{0(9)} \end{pmatrix} = \begin{pmatrix} U^0 = \left(e\varphi^0 + h\psi^0 + g\Phi^0 + f\Psi^0\right)\Big/ CK_{emgc}^2 \\ \varphi^0 = -\dfrac{\xi K_S}{\varepsilon K_E}\Psi^0 - \dfrac{\alpha K_A}{\varepsilon K_E}\psi^0 - \dfrac{\zeta K_Z}{\varepsilon K_E}\Phi^0 \\ \psi^0 = -\dfrac{\gamma K_G}{K_{emgc}^2} + \dfrac{\zeta^2 K_Z{}^2}{\varepsilon K_E K_{emgc}^2} + \dfrac{\left(\dfrac{\vartheta K_T}{K_{emgc}^2} - \dfrac{\xi\zeta K_S K_Z}{\varepsilon K_E K_{emgc}^2}\right)^2}{\dfrac{\eta K_F}{K_{emgc}^2} - \dfrac{\xi^2 K_S{}^2}{\varepsilon K_E K_{emgc}^2}} \\ \Phi^0 = \dfrac{\beta K_B}{K_{emgc}^2} - \dfrac{\alpha\zeta K_A K_Z}{\varepsilon K_E K_{emgc}^2} - \left(\dfrac{\lambda K_L}{K_{emgc}^2} - \dfrac{\alpha\xi K_A K_S}{\varepsilon K_E K_{emgc}^2}\right)\dfrac{\vartheta K_T - \dfrac{\xi\zeta K_S K_Z}{\varepsilon K_E}}{\eta K_F - \dfrac{\xi^2 K_S{}^2}{\varepsilon K_E}} \\ \Psi^0 = -\dfrac{\lambda K_L - \dfrac{\alpha\xi K_A K_S}{\varepsilon K_E}}{\eta K_F - \dfrac{\xi^2 K_S{}^2}{\varepsilon K_E}}\psi^0 - \dfrac{\vartheta K_T - \dfrac{\xi\zeta K_S K_Z}{\varepsilon K_E}}{\eta K_F - \dfrac{\xi^2 K_S{}^2}{\varepsilon K_E}}\Phi^0 \end{pmatrix} \tag{64}$$

The fourth case

In order to obtain the other possible forms of the eigenvectors it is possible to treat the following order of equations (47):

$$\begin{cases} \mu\left(1 + mK_m^2/A\right)\psi^0 + \beta\left(1 + mK_\beta^2/A\right)\Phi^0 \\ + \alpha\left(1 + mK_\alpha^2/A\right)\varphi^0 + \lambda\left(1 + mK_\lambda^2/A\right)\Psi^0 = 0 \\ \beta\left(1 + mK_\beta^2/A\right)\psi^0 + \gamma\left(1 + mK_g^2/A\right)\Phi^0 \\ + \zeta\left(1 + mK_\zeta^2/A\right)\varphi^0 + \vartheta\left(1 + mK_\vartheta^2/A\right)\Psi^0 = 0 \\ \alpha\left(1 + mK_\alpha^2/A\right)\psi^0 + \zeta\left(1 + mK_\zeta^2/A\right)\Phi^0 \\ + \varepsilon\left(1 + mK_e^2/A\right)\varphi^0 + \xi\left(1 + mK_\xi^2/A\right)\Psi^0 = 0 \\ \lambda\left(1 + mK_\lambda^2/A\right)\psi^0 + \vartheta\left(1 + mK_\vartheta^2/A\right)\Phi^0 \\ + \xi\left(1 + mK_\xi^2/A\right)\varphi^0 + \eta\left(1 + mK_f^2/A\right)\Psi^0 = 0 \end{cases} \tag{65}$$

It is natural to exploit the first equation in set (65) to determine the eigenvector component ψ^0 as a function of the components Φ^0, φ^0, and Ψ^0. Therefore, this dependence can be introduced as follows:

$$\begin{aligned} \psi^0 = &-\frac{\beta\left(A + mK_\beta^2\right)}{\mu\left(A + mK_m^2\right)}\Phi^0 \\ &-\frac{\alpha\left(A + mK_\alpha^2\right)}{\mu\left(A + mK_m^2\right)}\varphi^0 - \frac{\lambda\left(A + mK_\lambda^2\right)}{\mu\left(A + mK_m^2\right)}\Psi^0 \end{aligned} \tag{66}$$

A substitution of definition (66) into equations (65), but the first equation in set (65), leads to the homogeneous set of three equations in three unknowns representing the eigenvector components Φ^0, φ^0, and Ψ^0. These three complicated equations are inscribed as follows:

$$\begin{cases}\left(\dfrac{\gamma\left(A+mK_g^2\right)}{A}-\dfrac{\beta^2\left(A+mK_\beta^2\right)^2}{A\mu\left(A+mK_m^2\right)}\right)\Phi^0+\left(\dfrac{\zeta\left(A+mK_\zeta^2\right)}{A}-\dfrac{\alpha\beta\left(A+mK_\alpha^2\right)\left(A+mK_\beta^2\right)}{A\mu\left(A+mK_m^2\right)}\right)\varphi^0 \\ +\left(\dfrac{\vartheta\left(A+mK_\vartheta^2\right)}{A}-\dfrac{\beta\lambda\left(A+mK_\beta^2\right)\left(A+mK_\lambda^2\right)}{A\mu\left(A+mK_m^2\right)}\right)\Psi^0=0 \\ \left(\dfrac{\zeta\left(A+mK_\zeta^2\right)}{A}-\dfrac{\alpha\beta\left(A+mK_\alpha^2\right)\left(A+mK_\beta^2\right)}{A\mu\left(A+mK_m^2\right)}\right)\Phi^0+\left(\dfrac{\varepsilon\left(A+mK_e^2\right)}{A}-\dfrac{\alpha^2\left(A+mK_\alpha^2\right)^2}{A\mu\left(A+mK_m^2\right)}\right)\varphi^0 \\ +\left(\dfrac{\xi\left(A+mK_\xi^2\right)}{A}-\dfrac{\alpha\lambda\left(A+mK_\alpha^2\right)\left(A+mK_\lambda^2\right)}{A\mu\left(A+mK_m^2\right)}\right)\Psi^0=0 \\ \left(\dfrac{\vartheta\left(A+mK_\vartheta^2\right)}{A}-\dfrac{\beta\lambda\left(A+mK_\beta^2\right)\left(A+mK_\lambda^2\right)}{A\mu\left(A+mK_m^2\right)}\right)\Phi^0+\left(\dfrac{\xi\left(A+mK_\xi^2\right)}{A}-\dfrac{\alpha\lambda\left(A+mK_\alpha^2\right)\left(A+mK_\lambda^2\right)}{A\mu\left(A+mK_m^2\right)}\right)\varphi^0 \\ +\left(\dfrac{\eta\left(A+mK_\eta^2\right)}{A}-\dfrac{\lambda^2\left(A+mK_\lambda^2\right)^2}{A\mu\left(A+mK_m^2\right)}\right)\Psi^0=0\end{cases} \tag{67}$$

Next, let's use the first equation in set (67) for definition of the eigenvector component Φ^0. Thus, it is defined by

$$\Phi^0=-\frac{\zeta\left(A+mK_\zeta^2\right)-\dfrac{\alpha\beta\left(A+mK_\alpha^2\right)\left(A+mK_\beta^2\right)}{\mu\left(A+mK_m^2\right)}}{\gamma\left(A+mK_g^2\right)-\dfrac{\beta^2\left(A+mK_\beta^2\right)^2}{\mu\left(A+mK_m^2\right)}}\varphi^0 -\frac{\vartheta\left(A+mK_\vartheta^2\right)-\dfrac{\beta\lambda\left(A+mK_\beta^2\right)\left(A+mK_\lambda^2\right)}{\mu\left(A+mK_m^2\right)}}{\gamma\left(A+mK_g^2\right)-\dfrac{\beta^2\left(A+mK_\beta^2\right)^2}{\mu\left(A+mK_m^2\right)}}\Psi^0 \tag{68}$$

Two homogeneous equations can be finally written and used for determination of the eigenvector components φ^0 and Ψ^0. These final equations are

$$\begin{cases}0=\left(\dfrac{\varepsilon\left(A+mK_\varepsilon^2\right)}{A}-\dfrac{\alpha^2\left(A+mK_\alpha^2\right)^2}{A\mu\left(A+mK_m^2\right)}-\dfrac{\left(\dfrac{\zeta\left(A+mK_\zeta^2\right)}{A}-\dfrac{\alpha\beta\left(A+mK_\alpha^2\right)\left(A+mK_\beta^2\right)}{A\mu\left(A+mK_m^2\right)}\right)^2}{\dfrac{\gamma\left(A+mK_g^2\right)}{A}-\dfrac{\beta^2\left(A+mK_\beta^2\right)^2}{A\mu\left(A+mK_m^2\right)}}\right)\varphi^0 \\ +\left(\dfrac{\xi\left(A+mK_\xi^2\right)}{A}-\dfrac{\alpha\lambda\left(A+mK_\alpha^2\right)\left(A+mK_\lambda^2\right)}{A\mu\left(A+mK_m^2\right)}\right)\Psi^0 \\ -\left(\dfrac{\zeta\left(A+mK_\zeta^2\right)}{A}-\dfrac{\alpha\beta\left(A+mK_\alpha^2\right)\left(A+mK_\beta^2\right)}{A\mu\left(A+mK_m^2\right)}\right)\dfrac{\vartheta\left(A+mK_\vartheta^2\right)-\dfrac{\beta\lambda\left(A+mK_\beta^2\right)\left(A+mK_\lambda^2\right)}{\mu\left(A+mK_m^2\right)}}{\gamma\left(A+mK_g^2\right)-\dfrac{\beta^2\left(A+mK_\beta^2\right)^2}{\mu\left(A+mK_m^2\right)}}\Psi^0 \\ 0=\left(\dfrac{\xi\left(A+mK_\xi^2\right)}{A}-\dfrac{\alpha\lambda\left(A+mK_\alpha^2\right)\left(A+mK_\lambda^2\right)}{A\mu\left(A+mK_m^2\right)}\right)\varphi^0 \\ -\left(\dfrac{\zeta\left(A+mK_\zeta^2\right)}{A}-\dfrac{\alpha\beta\left(A+mK_\alpha^2\right)\left(A+mK_\beta^2\right)}{A\mu\left(A+mK_m^2\right)}\right)\dfrac{\vartheta\left(A+mK_\vartheta^2\right)-\dfrac{\beta\lambda\left(A+mK_\beta^2\right)\left(A+mK_\lambda^2\right)}{\mu\left(A+mK_m^2\right)}}{\gamma\left(A+mK_g^2\right)-\dfrac{\beta^2\left(A+mK_\beta^2\right)^2}{\mu\left(A+mK_m^2\right)}}\varphi^0 \\ +\left(\dfrac{\eta\left(A+mK_\eta^2\right)}{A}-\dfrac{\lambda^2\left(A+mK_\lambda^2\right)^2}{A\mu\left(A+mK_m^2\right)}-\dfrac{\left(\dfrac{\vartheta\left(A+mK_\vartheta^2\right)}{A}-\dfrac{\beta\lambda\left(A+mK_\beta^2\right)\left(A+mK_\lambda^2\right)}{A\mu\left(A+mK_m^2\right)}\right)^2}{\dfrac{\gamma\left(A+mK_g^2\right)}{A}-\dfrac{\beta^2\left(A+mK_\beta^2\right)^2}{A\mu\left(A+mK_m^2\right)}}\right)\Psi^0\end{cases} \tag{69}$$

The utilization of the first of two equations (69) provides the following first eigenvectors:

$$\begin{pmatrix}U^{0(1)}\\ \varphi^{0(1)}\\ \psi^{0(1)}\\ \Phi^{0(1)}\\ \Psi^{0(1)}\end{pmatrix}=\begin{pmatrix}U^{0(3)}\\ \varphi^{0(3)}\\ \psi^{0(3)}\\ \Phi^{0(3)}\\ \Psi^{0(3)}\end{pmatrix}=\begin{pmatrix}U^{0(5)}\\ \varphi^{0(5)}\\ \psi^{0(5)}\\ \Phi^{0(5)}\\ \Psi^{0(5)}\end{pmatrix}=\begin{pmatrix}U^{0(7)}\\ \varphi^{0(7)}\\ \psi^{0(7)}\\ \Phi^{0(7)}\\ \Psi^{0(7)}\end{pmatrix}=\begin{pmatrix}U^0=0\\ \varphi^0=\xi-\dfrac{\alpha\lambda}{\mu}-\dfrac{\left(\zeta-\dfrac{\alpha\beta}{\mu}\right)\left(\vartheta-\dfrac{\beta\lambda}{\mu}\right)}{\gamma-\dfrac{\beta^2}{\mu}}\\ \psi^0=-\dfrac{\beta}{\mu}\Phi^0-\dfrac{\alpha}{\mu}\varphi^0-\dfrac{\lambda}{\mu}\Psi^0\\ \Phi^0=-\dfrac{\zeta-\dfrac{\alpha\beta}{\mu}}{\gamma-\dfrac{\beta^2}{\mu}}\varphi^0-\dfrac{\vartheta-\dfrac{\beta\lambda}{\mu}}{\gamma-\dfrac{\beta^2}{\mu}}\Psi^0\\ \Psi^0=-\varepsilon+\dfrac{\alpha^2}{\mu}+\dfrac{\left(\zeta-\dfrac{\alpha\beta}{\mu}\right)^2}{\gamma-\dfrac{\beta^2}{\mu}}\end{pmatrix} \tag{70}$$

$$\begin{pmatrix}U^{0(9)}\\ \varphi^{0(9)}\\ \psi^{0(9)}\\ \Phi^{0(9)}\\ \Psi^{0(9)}\end{pmatrix}=\begin{pmatrix}U^0=\left(e\varphi^0+h\psi^0+g\Phi^0+f\Psi^0\right)/CK_{emgc}^2\\ \varphi^0=\dfrac{\xi K_S}{K_{emgc}^2}-\dfrac{\alpha\lambda K_A K_L}{\mu K_M K_{emgc}^2}-\left(\dfrac{\zeta K_Z}{K_{emgc}^2}-\dfrac{\alpha\beta K_A K_B}{\mu K_M K_{emgc}^2}\right)\dfrac{\vartheta K_T-\dfrac{\beta\lambda K_B K_L}{\mu K_M}}{\gamma K_G-\dfrac{\beta^2 K_B{}^2}{\mu K_M}}\\ \psi^0=-\dfrac{\beta K_B}{\mu K_M}\Phi^0-\dfrac{\alpha K_A}{\mu K_M}\varphi^0-\dfrac{\lambda K_L}{\mu K_M}\Psi^0\\ \Phi^0=-\dfrac{\zeta K_Z-\dfrac{\alpha\beta K_A K_B}{\mu K_M}}{\gamma K_G-\dfrac{\beta^2 K_B{}^2}{\mu K_M}}\varphi^0-\dfrac{\vartheta K_T-\dfrac{\beta\lambda K_B K_L}{\mu K_M}}{\gamma K_G-\dfrac{\beta^2 K_B{}^2}{\mu K_M}}\Psi^0\\ \Psi^0=-\dfrac{\varepsilon K_E}{K_{emgc}^2}+\dfrac{\alpha^2 K_A{}^2}{\mu K_M K_{emgc}^2}+\dfrac{\left(\dfrac{\zeta K_Z}{K_{emgc}^2}-\dfrac{\alpha\beta K_A K_B}{\mu K_M K_{emgc}^2}\right)^2}{\dfrac{\gamma K_G}{K_{emgc}^2}-\dfrac{\beta^2 K_B{}^2}{\mu K_M K_{emgc}^2}}\end{pmatrix} \tag{71}$$

The second eigenvectors for this case can be obtained by using the second equation in set (69). They are defined by

$$\begin{pmatrix}U^{0(1)}\\ \varphi^{0(1)}\\ \psi^{0(1)}\\ \Phi^{0(1)}\\ \Psi^{0(1)}\end{pmatrix}=\begin{pmatrix}U^{0(3)}\\ \varphi^{0(3)}\\ \psi^{0(3)}\\ \Phi^{0(3)}\\ \Psi^{0(3)}\end{pmatrix}=\begin{pmatrix}U^{0(5)}\\ \varphi^{0(5)}\\ \psi^{0(5)}\\ \Phi^{0(5)}\\ \Psi^{0(5)}\end{pmatrix}=\begin{pmatrix}U^{0(7)}\\ \varphi^{0(7)}\\ \psi^{0(7)}\\ \Phi^{0(7)}\\ \Psi^{0(7)}\end{pmatrix}$$

$$=\begin{pmatrix}U^0=0\\ \varphi^0=-\eta+\dfrac{\lambda^2}{\mu}+\dfrac{\left(\vartheta-\dfrac{\beta\lambda}{\mu}\right)^2}{\gamma-\dfrac{\beta^2}{\mu}}\\ \psi^0=-\dfrac{\beta}{\mu}\Phi^0-\dfrac{\alpha}{\mu}\varphi^0-\dfrac{\lambda}{\mu}\Psi^0\\ \Phi^0=-\dfrac{\zeta-\dfrac{\alpha\beta}{\mu}}{\gamma-\dfrac{\beta^2}{\mu}}\varphi^0-\dfrac{\vartheta-\dfrac{\beta\lambda}{\mu}}{\gamma-\dfrac{\beta^2}{\mu}}\Psi^0\\ \Psi^0=\xi-\dfrac{\alpha\lambda}{\mu}-\dfrac{\left(\zeta-\dfrac{\alpha\beta}{\mu}\right)\left(\vartheta-\dfrac{\beta\lambda}{\mu}\right)}{\gamma-\dfrac{\beta^2}{\mu}}\end{pmatrix} \tag{72}$$

$$\begin{pmatrix} U^{0(9)} \\ \varphi^{0(9)} \\ \psi^{0(9)} \\ \Phi^{0(9)} \\ \Psi^{0(9)} \end{pmatrix} = \begin{pmatrix} U^0 = \left(e\varphi^0 + h\psi^0 + g\Phi^0 + f\Psi^0\right) / CK_{emgc}^2 \\ \varphi^0 = -\dfrac{\eta K_F}{K_{emgc}^2} + \dfrac{\lambda^2 K_L^{\,2}}{\mu K_M K_{emgc}^2} + \dfrac{\left(\dfrac{\vartheta K_T}{K_{emgc}^2} - \dfrac{\beta\lambda K_B K_L}{\mu K_M K_{emgc}^2}\right)^2}{\dfrac{\gamma K_G}{K_{emgc}^2} - \dfrac{\beta^2 K_B^{\,2}}{\mu K_M K_{emgc}^2}} \\ \psi^0 = -\dfrac{\beta K_B}{\mu K_M}\Phi^0 - \dfrac{\alpha K_A}{\mu K_M}\varphi^0 - \dfrac{\lambda K_L}{\mu K_M}\Psi^0 \\ \Phi^0 = -\dfrac{\zeta K_Z - \dfrac{\alpha\beta K_A K_B}{\mu K_M}}{\gamma K_G - \dfrac{\beta^2 K_B^{\,2}}{\mu K_M}}\varphi^0 - \dfrac{\vartheta K_T - \dfrac{\beta\lambda K_B K_L}{\mu K_M}}{\gamma K_G - \dfrac{\beta^2 K_B^{\,2}}{\mu K_M}}\Psi^0 \\ \Psi^0 = \dfrac{\xi K_S}{K_{emgc}^2} - \dfrac{\alpha\lambda K_A K_L}{\mu K_M K_{emgc}^2} - \left(\dfrac{\zeta K_Z}{K_{emgc}^2} - \dfrac{\alpha\beta K_A K_B}{\mu K_M K_{emgc}^2}\right)\dfrac{\vartheta K_T - \dfrac{\beta\lambda K_B K_L}{\mu K_M}}{\gamma K_G - \dfrac{\beta^2 K_B^{\,2}}{\mu K_M}} \end{pmatrix} \tag{73}$$

The fifth case

Four homogeneous equations (47) can be also rewritten in the following order to get the other set of the eigenvector components:

$$\begin{cases} \mu\left(1+mK_m^2/A\right)\psi^0 + \lambda\left(1+mK_\lambda^2/A\right)\Psi^0 \\ +\alpha\left(1+mK_\alpha^2/A\right)\varphi^0 + \beta\left(1+mK_\beta^2/A\right)\Phi^0 = 0 \\ \lambda\left(1+mK_\lambda^2/A\right)\psi^0 + \eta\left(1+mK_f^2/A\right)\Psi^0 \\ +\xi\left(1+mK_\xi^2/A\right)\varphi^0 + \vartheta\left(1+mK_\vartheta^2/A\right)\Phi^0 = 0 \\ \alpha\left(1+mK_\alpha^2/A\right)\psi^0 + \xi\left(1+mK_\xi^2/A\right)\Psi^0 \\ +\varepsilon\left(1+mK_e^2/A\right)\varphi^0 + \zeta\left(1+mK_\zeta^2/A\right)\Phi^0 = 0 \\ \beta\left(1+mK_\beta^2/A\right)\psi^0 + \vartheta\left(1+mK_\vartheta^2/A\right)\Psi^0 \\ +\zeta\left(1+mK_\zeta^2/A\right)\varphi^0 + \gamma\left(1+mK_g^2/A\right)\Phi^0 = 0 \end{cases} \tag{74}$$

As a result, the firs equation in set (74) can provide the eigenvector component ψ^0 as the following function of the eigenvector components Ψ^0, φ^0, and Φ^0:

$$\psi^0 = -\frac{\lambda\left(A+mK_\lambda^2\right)}{\mu\left(A+mK_m^2\right)}\Psi^0 - \frac{\alpha\left(A+mK_\alpha^2\right)}{\mu\left(A+mK_m^2\right)}\varphi^0 - \frac{\beta\left(A+mK_\beta^2\right)}{\mu\left(A+mK_m^2\right)}\Phi^0 \tag{75}$$

So, equation (75) must be used for set (74) to reduce it. The following set of three homogeneous equations can be then obtained:

$$\begin{cases} \left(\dfrac{\eta\left(A+mK_f^2\right)}{A} - \dfrac{\lambda^2\left(A+mK_\lambda^2\right)^2}{A\mu\left(A+mK_m^2\right)}\right)\Psi^0 + \left(\dfrac{\xi\left(A+mK_\xi^2\right)}{A} - \dfrac{\alpha\lambda\left(A+mK_\alpha^2\right)\left(A+mK_\lambda^2\right)}{A\mu\left(A+mK_m^2\right)}\right)\varphi^0 \\ +\left(\dfrac{\vartheta\left(A+mK_\vartheta^2\right)}{A} - \dfrac{\beta\lambda\left(A+mK_\beta^2\right)\left(A+mK_\lambda^2\right)}{A\mu\left(A+mK_m^2\right)}\right)\Phi^0 = 0 \\ \left(\dfrac{\xi\left(A+mK_\xi^2\right)}{A} - \dfrac{\alpha\lambda\left(A+mK_\alpha^2\right)\left(A+mK_\lambda^2\right)}{A\mu\left(A+mK_m^2\right)}\right)\Psi^0 + \left(\dfrac{\varepsilon\left(A+mK_e^2\right)}{A} - \dfrac{\alpha^2\left(A+mK_\alpha^2\right)^2}{A\mu\left(A+mK_m^2\right)}\right)\varphi^0 \\ +\left(\dfrac{\zeta\left(A+mK_\zeta^2\right)}{A} - \dfrac{\alpha\beta\left(A+mK_\alpha^2\right)\left(A+mK_\beta^2\right)}{A\mu\left(A+mK_m^2\right)}\right)\Phi^0 = 0 \\ \left(\dfrac{\vartheta\left(A+mK_\vartheta^2\right)}{A} - \dfrac{\beta\lambda\left(A+mK_\beta^2\right)\left(A+mK_\lambda^2\right)}{A\mu\left(A+mK_m^2\right)}\right)\Psi^0 + \left(\dfrac{\zeta\left(A+mK_\zeta^2\right)}{A} - \dfrac{\alpha\beta\left(A+mK_\alpha^2\right)\left(A+mK_\beta^2\right)}{A\mu\left(A+mK_m^2\right)}\right)\varphi^0 \\ +\left(\dfrac{\gamma\left(A+mK_g^2\right)}{A} - \dfrac{\beta^2\left(A+mK_\beta^2\right)^2}{A\mu\left(A+mK_m^2\right)}\right)\Phi^0 = 0 \end{cases} \tag{76}$$

The first equation in set (76) defines the eigenvector component Ψ^0 as follows:

$$\Psi^0 = -\frac{\xi\left(A+mK_\xi^2\right) - \dfrac{\alpha\lambda\left(A+mK_\alpha^2\right)\left(A+mK_\lambda^2\right)}{\mu\left(A+mK_m^2\right)}}{\eta\left(A+mK_f^2\right) - \dfrac{\lambda^2\left(A+mK_\lambda^2\right)^2}{\mu\left(A+mK_m^2\right)}}\varphi^0 - \frac{\vartheta\left(A+mK_\vartheta^2\right) - \dfrac{\beta\lambda\left(A+mK_\beta^2\right)\left(A+mK_\lambda^2\right)}{\mu\left(A+mK_m^2\right)}}{\eta\left(A+mK_f^2\right) - \dfrac{\lambda^2\left(A+mK_\lambda^2\right)^2}{\mu\left(A+mK_m^2\right)}}\Phi^0 \tag{77}$$

The deployment of definition (77) for set (76) leads to the following two final equations, with which it is already possible to obtain the values of the eigenvector components φ^0 and Φ^0 in explicit forms. These two final equations can be formed as follows:

$$\begin{cases} 0 = \left(\dfrac{\varepsilon\left(A+mK_e^2\right)}{A} - \dfrac{\alpha^2\left(A+mK_\alpha^2\right)^2}{A\mu\left(A+mK_m^2\right)} - \dfrac{\left(\dfrac{\xi\left(A+mK_\xi^2\right)}{A} - \dfrac{\alpha\lambda\left(A+mK_\alpha^2\right)\left(A+mK_\lambda^2\right)}{A\mu\left(A+mK_m^2\right)}\right)^2}{\dfrac{\eta\left(A+mK_f^2\right)}{A} - \dfrac{\lambda^2\left(A+mK_\lambda^2\right)^2}{A\mu\left(A+mK_m^2\right)}}\right)\varphi^0 \\ +\left(\dfrac{\zeta\left(A+mK_\zeta^2\right)}{A} - \dfrac{\alpha\beta\left(A+mK_\alpha^2\right)\left(A+mK_\beta^2\right)}{A\mu\left(A+mK_m^2\right)}\right)\Phi^0 \\ -\left(\dfrac{\xi\left(A+mK_\xi^2\right)}{A} - \dfrac{\alpha\lambda\left(A+mK_\alpha^2\right)\left(A+mK_\lambda^2\right)}{A\mu\left(A+mK_m^2\right)}\right)\dfrac{\vartheta\left(A+mK_\vartheta^2\right) - \dfrac{\beta\lambda\left(A+mK_\beta^2\right)\left(A+mK_\lambda^2\right)}{\mu\left(A+mK_m^2\right)}}{\eta\left(A+mK_f^2\right) - \dfrac{\lambda^2\left(A+mK_\lambda^2\right)^2}{\mu\left(A+mK_m^2\right)}}\Phi^0 \\ 0 = \left(\dfrac{\zeta\left(A+mK_\zeta^2\right)}{A} - \dfrac{\alpha\beta\left(A+mK_\alpha^2\right)\left(A+mK_\beta^2\right)}{A\mu\left(A+mK_m^2\right)}\right)\varphi^0 \\ -\left(\dfrac{\xi\left(A+mK_\xi^2\right)}{A} - \dfrac{\alpha\lambda\left(A+mK_\alpha^2\right)\left(A+mK_\lambda^2\right)}{A\mu\left(A+mK_m^2\right)}\right)\dfrac{\vartheta\left(A+mK_\vartheta^2\right) - \dfrac{\beta\lambda\left(A+mK_\beta^2\right)\left(A+mK_\lambda^2\right)}{\mu\left(A+mK_m^2\right)}}{\eta\left(A+mK_f^2\right) - \dfrac{\lambda^2\left(A+mK_\lambda^2\right)^2}{\mu\left(A+mK_m^2\right)}}\varphi^0 \\ +\left(\dfrac{\gamma\left(A+mK_g^2\right)}{A} - \dfrac{\beta^2\left(A+mK_\beta^2\right)^2}{A\mu\left(A+mK_m^2\right)} - \dfrac{\left(\vartheta\left(A+mK_\vartheta^2\right) - \dfrac{\beta\lambda\left(A+mK_\beta^2\right)\left(A+mK_\lambda^2\right)}{\mu\left(A+mK_m^2\right)}\right)^2}{\eta\left(A+mK_f^2\right) - \dfrac{\lambda^2\left(A+mK_\lambda^2\right)^2}{\mu\left(A+mK_m^2\right)}}\right)\Phi^0 \end{cases} \tag{78}$$

The first equation in set (78) determines the first eigenvectors. Their components take the following forms:

$$\begin{pmatrix} U^{0(1)} \\ \varphi^{0(1)} \\ \psi^{0(1)} \\ \Phi^{0(1)} \\ \Psi^{0(1)} \end{pmatrix} = \begin{pmatrix} U^{0(3)} \\ \varphi^{0(3)} \\ \psi^{0(3)} \\ \Phi^{0(3)} \\ \Psi^{0(3)} \end{pmatrix} = \begin{pmatrix} U^{0(5)} \\ \varphi^{0(5)} \\ \psi^{0(5)} \\ \Phi^{0(5)} \\ \Psi^{0(5)} \end{pmatrix} = \begin{pmatrix} U^{0(7)} \\ \varphi^{0(7)} \\ \psi^{0(7)} \\ \Phi^{0(7)} \\ \Psi^{0(7)} \end{pmatrix} = \begin{pmatrix} U^0 = 0 \\ \varphi^0 = \zeta - \dfrac{\alpha\beta}{\mu} - \dfrac{\left(\xi - \dfrac{\alpha\lambda}{\mu}\right)\left(\vartheta - \dfrac{\beta\lambda}{\mu}\right)}{\eta - \dfrac{\lambda^2}{\mu}} \\ \psi^0 = -\dfrac{\lambda}{\mu}\Psi^0 - \dfrac{\alpha}{\mu}\varphi^0 - \dfrac{\beta}{\mu}\Phi^0 \\ \Phi^0 = -\varepsilon + \dfrac{\alpha^2}{\mu} + \dfrac{\left(\xi - \dfrac{\alpha\lambda}{\mu}\right)^2}{\eta - \dfrac{\lambda^2}{\mu}} \\ \Psi^0 = -\dfrac{\xi - \dfrac{\alpha\lambda}{\mu}}{\eta - \dfrac{\lambda^2}{\mu}}\varphi^0 - \dfrac{\vartheta - \dfrac{\beta\lambda}{\mu}}{\eta - \dfrac{\lambda^2}{\mu}}\Phi^0 \end{pmatrix} \tag{79}$$

$$\begin{pmatrix} U^{0(9)} \\ \varphi^{0(9)} \\ \psi^{0(9)} \\ \Phi^{0(9)} \\ \Psi^{0(9)} \end{pmatrix} = \begin{pmatrix} U^0 = \left(e\varphi^0 + h\psi^0 + g\Phi^0 + f\Psi^0\right) / CK_{emgc}^2 \\ \varphi^0 = \dfrac{\zeta K_Z}{K_{emgc}^2} - \dfrac{\alpha\beta K_A K_B}{\mu K_M K_{emgc}^2} - \left(\dfrac{\xi K_S}{K_{emgc}^2} - \dfrac{\alpha\lambda K_A K_L}{\mu K_M K_{emgc}^2}\right) \dfrac{\vartheta K_T - \dfrac{\beta\lambda K_B K_L}{\mu K_M}}{\eta K_F - \dfrac{\lambda^2 K_L^{\,2}}{\mu K_M}} \\ \psi^0 = -\dfrac{\lambda K_L}{\mu K_M}\Psi^0 - \dfrac{\alpha K_A}{\mu K_M}\varphi^0 - \dfrac{\beta K_B}{\mu K_M}\Phi^0 \\ \Phi^0 = -\dfrac{\varepsilon K_E}{K_{emgc}^2} + \dfrac{\alpha^2 K_A^{\,2}}{\mu K_M K_{emgc}^2} + \dfrac{\left(\dfrac{\xi K_S}{K_{emgc}^2} - \dfrac{\alpha\lambda K_A K_L}{\mu K_M K_{emgc}^2}\right)^2}{\dfrac{\eta K_F}{K_{emgc}^2} - \dfrac{\lambda^2 K_L^{\,2}}{\mu K_M K_{emgc}^2}} \\ \Psi^0 = -\dfrac{\xi K_S - \dfrac{\alpha\lambda K_A K_L}{\mu K_M}}{\eta K_F - \dfrac{\lambda^2 K_L^{\,2}}{\mu K_M}}\varphi^0 - \dfrac{\vartheta K_T - \dfrac{\beta\lambda K_B K_L}{\mu K_M}}{\eta K_F - \dfrac{\lambda^2 K_L^{\,2}}{\mu K_M}}\Phi^0 \end{pmatrix} \tag{80}$$

The second equation in set (78) is responsible for the existence of the second eigenvectors. Their components can be composed as follows:

$$\begin{pmatrix} U^{0(1)} \\ \varphi^{0(1)} \\ \psi^{0(1)} \\ \Phi^{0(1)} \\ \Psi^{0(1)} \end{pmatrix} = \begin{pmatrix} U^{0(3)} \\ \varphi^{0(3)} \\ \psi^{0(3)} \\ \Phi^{0(3)} \\ \Psi^{0(3)} \end{pmatrix} = \begin{pmatrix} U^{0(5)} \\ \varphi^{0(5)} \\ \psi^{0(5)} \\ \Phi^{0(5)} \\ \Psi^{0(5)} \end{pmatrix} = \begin{pmatrix} U^{0(7)} \\ \varphi^{0(7)} \\ \psi^{0(7)} \\ \Phi^{0(7)} \\ \Psi^{0(7)} \end{pmatrix} = \begin{pmatrix} U^0 = 0 \\ \varphi^0 = -\gamma + \dfrac{\beta^2}{\mu} + \dfrac{\left(\vartheta - \dfrac{\beta\lambda}{\mu}\right)^2}{\eta - \dfrac{\lambda^2}{\mu}} \\ \psi^0 = -\dfrac{\lambda}{\mu}\Psi^0 - \dfrac{\alpha}{\mu}\varphi^0 - \dfrac{\beta}{\mu}\Phi^0 \\ \Phi^0 = \zeta - \dfrac{\alpha\beta}{\mu} - \dfrac{\left(\xi - \dfrac{\alpha\lambda}{\mu}\right)\left(\vartheta - \dfrac{\beta\lambda}{\mu}\right)}{\eta - \dfrac{\lambda^2}{\mu}} \\ \Psi^0 = -\dfrac{\xi - \dfrac{\alpha\lambda}{\mu}}{\eta - \dfrac{\lambda^2}{\mu}}\varphi^0 - \dfrac{\vartheta - \dfrac{\beta\lambda}{\mu}}{\eta - \dfrac{\lambda^2}{\mu}}\Phi^0 \end{pmatrix} \tag{81}$$

$$\begin{pmatrix} U^{0(9)} \\ \varphi^{0(9)} \\ \psi^{0(9)} \\ \Phi^{0(9)} \\ \Psi^{0(9)} \end{pmatrix} = \begin{pmatrix} U^0 = \left(e\varphi^0 + h\psi^0 + g\Phi^0 + f\Psi^0\right) / CK_{emgc}^2 \\ \varphi^0 = -\dfrac{\gamma K_G}{K_{emgc}^2} + \dfrac{\beta^2 K_B^{\,2}}{\mu K_M K_{emgc}^2} + \dfrac{\left(\dfrac{\vartheta K_T}{K_{emgc}^2} - \dfrac{\beta\lambda K_B K_L}{\mu K_M K_{emgc}^2}\right)^2}{\dfrac{\eta K_F}{K_{emgc}^2} - \dfrac{\lambda^2 K_L^{\,2}}{\mu K_M K_{emgc}^2}} \\ \psi^0 = \psi^0 = -\dfrac{\lambda K_L}{\mu K_M}\Psi^0 - \dfrac{\alpha K_A}{\mu K_M}\varphi^0 - \dfrac{\beta K_B}{\mu K_M}\Phi^0 \\ \Phi^0 = \dfrac{\zeta K_Z}{K_{emgc}^2} - \dfrac{\alpha\beta K_A K_B}{\mu K_M K_{emgc}^2} - \left(\dfrac{\xi K_S}{K_{emgc}^2} - \dfrac{\alpha\lambda K_A K_L}{\mu K_M K_{emgc}^2}\right) \dfrac{\vartheta K_T - \dfrac{\beta\lambda K_B K_L}{\mu K_M}}{\eta K_F - \dfrac{\lambda^2 K_L^{\,2}}{\mu K_M}} \\ \Psi^0 = -\dfrac{\xi K_S - \dfrac{\alpha\lambda K_A K_L}{\mu K_M}}{\eta K_F - \dfrac{\lambda^2 K_L^{\,2}}{\mu K_M}}\varphi^0 - \dfrac{\vartheta K_T - \dfrac{\beta\lambda K_B K_L}{\mu K_M}}{\eta K_F - \dfrac{\lambda^2 K_L^{\,2}}{\mu K_M}}\Phi^0 \end{pmatrix} \tag{82}$$

The sixth case

Note that equations (47) can be also rewritten in the other possible forms that are different from the six case treated below. However, this order of equations is final for this research. The reader can also have some practice in mathematics to obtain the other possible forms if they exist. So, one can also regroup equations (47) as follows:

$$\begin{cases} \gamma\left(1 + mK_g^2/A\right)\Phi^0 + \vartheta\left(1 + mK_\vartheta^2/A\right)\Psi^0 \\ + \zeta\left(1 + mK_\zeta^2/A\right)\varphi^0 + \beta\left(1 + mK_\beta^2/A\right)\psi^0 = 0 \\ \vartheta\left(1 + mK_\vartheta^2/A\right)\Phi^0 + \eta\left(1 + mK_f^2/A\right)\Psi^0 \\ + \xi\left(1 + mK_\xi^2/A\right)\varphi^0 + \lambda\left(1 + mK_\lambda^2/A\right)\psi^0 = 0 \\ \zeta\left(1 + mK_\zeta^2/A\right)\Phi^0 + \xi\left(1 + mK_\xi^2/A\right)\Psi^0 \\ + \varepsilon\left(1 + mK_e^2/A\right)\varphi^0 + \alpha\left(1 + mK_\alpha^2/A\right)\psi^0 = 0 \\ \beta\left(1 + mK_\beta^2/A\right)\Phi^0 + \lambda\left(1 + mK_\lambda^2/A\right)\Psi^0 \\ + \alpha\left(1 + mK_\alpha^2/A\right)\varphi^0 + \mu\left(1 + mK_m^2/A\right)\psi^0 = 0 \end{cases} \tag{83}$$

The first equation in set (83) gives the following definition:

$$\begin{aligned} \Phi^0 = &-\frac{\vartheta\left(A + mK_\vartheta^2\right)}{\gamma\left(A + mK_g^2\right)}\Psi^0 \\ &-\frac{\zeta\left(A + mK_\zeta^2\right)}{\gamma\left(A + mK_g^2\right)}\varphi^0 - \frac{\beta\left(A + mK_\beta^2\right)}{\gamma\left(A + mK_g^2\right)}\psi^0 \end{aligned} \tag{84}$$

Definition (84) is then used in set (83) to reduce this set of four equations and afterward to deal with the following set of three homogeneous equations:

$$\begin{cases} \left(\dfrac{\eta\left(A + mK_f^2\right)}{A} - \dfrac{\vartheta^2\left(A + mK_\vartheta^2\right)^2}{A\gamma\left(A + mK_g^2\right)}\right)\Psi^0 + \left(\dfrac{\xi\left(A + mK_\xi^2\right)}{A} - \dfrac{\vartheta\zeta\left(A + mK_\zeta^2\right)\left(A + mK_\vartheta^2\right)}{A\gamma\left(A + mK_g^2\right)}\right)\varphi^0 \\ + \left(\dfrac{\lambda\left(A + mK_\lambda^2\right)}{A} - \dfrac{\beta\vartheta\left(A + mK_\beta^2\right)\left(A + mK_\vartheta^2\right)}{A\gamma\left(A + mK_g^2\right)}\right)\psi^0 = 0 \\ \left(\dfrac{\xi\left(A + mK_\xi^2\right)}{A} - \dfrac{\vartheta\zeta\left(A + mK_\zeta^2\right)\left(A + mK_\vartheta^2\right)}{A\gamma\left(A + mK_g^2\right)}\right)\Psi^0 + \left(\dfrac{\varepsilon\left(A + mK_e^2\right)}{A} - \dfrac{\zeta^2\left(A + mK_\zeta^2\right)^2}{A\gamma\left(A + mK_g^2\right)}\right)\varphi^0 \\ + \left(\dfrac{\alpha\left(A + mK_\alpha^2\right)}{A} - \dfrac{\beta\zeta\left(A + mK_\beta^2\right)\left(A + mK_\zeta^2\right)}{A\gamma\left(A + mK_g^2\right)}\right)\psi^0 = 0 \\ \left(\dfrac{\lambda\left(A + mK_\lambda^2\right)}{A} - \dfrac{\beta\vartheta\left(A + mK_\beta^2\right)\left(A + mK_\vartheta^2\right)}{A\gamma\left(A + mK_g^2\right)}\right)\Psi^0 + \left(\dfrac{\alpha\left(A + mK_\alpha^2\right)}{A} - \dfrac{\beta\zeta\left(A + mK_\beta^2\right)\left(A + mK_\zeta^2\right)}{A\gamma\left(A + mK_g^2\right)}\right)\varphi^0 \\ + \left(\dfrac{\mu\left(A + mK_m^2\right)}{A} - \dfrac{\beta^2\left(A + mK_\beta^2\right)^2}{A\gamma\left(A + mK_g^2\right)}\right)\psi^0 = 0 \end{cases} \tag{85}$$

It is convenient to exploit the first equation in set (85) for determination of the eigenvector component Ψ^0. It is defined by

$$\begin{aligned} \Psi^0 = &-\frac{\xi\left(A + mK_\xi^2\right) - \dfrac{\vartheta\zeta\left(A + mK_\zeta^2\right)\left(A + mK_\vartheta^2\right)}{\gamma\left(A + mK_g^2\right)}}{\eta\left(A + mK_f^2\right) - \dfrac{\vartheta^2\left(A + mK_\vartheta^2\right)^2}{\gamma\left(A + mK_g^2\right)}}\varphi^0 \\ &-\frac{\lambda\left(A + mK_\lambda^2\right) - \dfrac{\beta\vartheta\left(A + mK_\beta^2\right)\left(A + mK_\vartheta^2\right)}{\gamma\left(A + mK_g^2\right)}}{\eta\left(A + mK_f^2\right) - \dfrac{\vartheta^2\left(A + mK_\vartheta^2\right)^2}{\gamma\left(A + mK_g^2\right)}}\psi^0 \end{aligned} \tag{86}$$

In the final accord, definition (86) is used for reduction of equations' set (85). The reduced set of equations represents two homogeneous equations that can be expressed in the following form:

$$\begin{cases} 0=\left(\dfrac{\varepsilon\left(A+mK_{\varepsilon}^{2}\right)}{A}-\dfrac{\zeta^{2}\left(A+mK_{\zeta}^{2}\right)^{2}}{A\gamma\left(A+mK_{g}^{2}\right)}-\dfrac{\left(\dfrac{\xi\left(A+mK_{\xi}^{2}\right)}{A}-\dfrac{\vartheta\zeta\left(A+mK_{\zeta}^{2}\right)\left(A+mK_{\vartheta}^{2}\right)}{A\gamma\left(A+mK_{g}^{2}\right)}\right)^{2}}{\dfrac{\eta\left(A+mK_{f}^{2}\right)}{A}-\dfrac{\vartheta^{2}\left(A+mK_{g}^{2}\right)^{2}}{A\gamma\left(A+mK_{g}^{2}\right)}}\right)\varphi^{0} \\ +\left(\dfrac{\alpha\left(A+mK_{\alpha}^{2}\right)}{A}-\dfrac{\beta\zeta\left(A+mK_{\beta}^{2}\right)\left(A+mK_{\zeta}^{2}\right)}{A\gamma\left(A+mK_{g}^{2}\right)}\right)\psi^{0} \\ -\left(\dfrac{\xi\left(A+mK_{\xi}^{2}\right)}{A}-\dfrac{\vartheta\zeta\left(A+mK_{\zeta}^{2}\right)\left(A+mK_{\vartheta}^{2}\right)}{A\gamma\left(A+mK_{g}^{2}\right)}\right)\dfrac{\lambda\left(A+mK_{\lambda}^{2}\right)-\dfrac{\beta\vartheta\left(A+mK_{\beta}^{2}\right)\left(A+mK_{\vartheta}^{2}\right)}{\gamma\left(A+mK_{g}^{2}\right)}}{\eta\left(A+mK_{f}^{2}\right)-\dfrac{\vartheta^{2}\left(A+mK_{g}^{2}\right)^{2}}{\gamma\left(A+mK_{g}^{2}\right)}}\psi^{0} \\ 0=\left(\dfrac{\alpha\left(A+mK_{\alpha}^{2}\right)}{A}-\dfrac{\beta\zeta\left(A+mK_{\beta}^{2}\right)\left(A+mK_{\zeta}^{2}\right)}{A\gamma\left(A+mK_{g}^{2}\right)}\right)\varphi^{0} \\ -\left(\dfrac{\xi\left(A+mK_{\xi}^{2}\right)}{A}-\dfrac{\vartheta\zeta\left(A+mK_{\zeta}^{2}\right)\left(A+mK_{\vartheta}^{2}\right)}{A\gamma\left(A+mK_{g}^{2}\right)}\right)\dfrac{\lambda\left(A+mK_{\lambda}^{2}\right)-\dfrac{\beta\vartheta\left(A+mK_{\beta}^{2}\right)\left(A+mK_{\vartheta}^{2}\right)}{\gamma\left(A+mK_{g}^{2}\right)}}{\eta\left(A+mK_{f}^{2}\right)-\dfrac{\vartheta^{2}\left(A+mK_{g}^{2}\right)^{2}}{\gamma\left(A+mK_{g}^{2}\right)}}\varphi^{0} \\ +\left(\dfrac{\mu\left(A+mK_{m}^{2}\right)}{A}-\dfrac{\beta^{2}\left(A+mK_{\beta}^{2}\right)^{2}}{A\gamma\left(A+mK_{g}^{2}\right)}-\dfrac{\left(\dfrac{\lambda\left(A+mK_{\lambda}^{2}\right)}{A}-\dfrac{\beta\vartheta\left(A+mK_{\beta}^{2}\right)\left(A+mK_{\vartheta}^{2}\right)}{A\gamma\left(A+mK_{g}^{2}\right)}\right)^{2}}{\dfrac{\eta\left(A+mK_{f}^{2}\right)}{A}-\dfrac{\vartheta^{2}\left(A+mK_{g}^{2}\right)^{2}}{A\gamma\left(A+mK_{g}^{2}\right)}}\right)\psi^{0} \end{cases} \tag{87}$$

Final equations' set (87) allows one to obtain all possible eigenvectors. With the first equation in the set, one can find that the first eigenvectors can be exposed in the following explicit forms:

$$\begin{pmatrix} U^{0(1)} \\ \varphi^{0(1)} \\ \psi^{0(1)} \\ \Phi^{0(1)} \\ \Psi^{0(1)} \end{pmatrix}=\begin{pmatrix} U^{0(3)} \\ \varphi^{0(3)} \\ \psi^{0(3)} \\ \Phi^{0(3)} \\ \Psi^{0(3)} \end{pmatrix}=\begin{pmatrix} U^{0(5)} \\ \varphi^{0(5)} \\ \psi^{0(5)} \\ \Phi^{0(5)} \\ \Psi^{0(5)} \end{pmatrix}=\begin{pmatrix} U^{0(7)} \\ \varphi^{0(7)} \\ \psi^{0(7)} \\ \Phi^{0(7)} \\ \Psi^{0(7)} \end{pmatrix}$$

$$=\begin{pmatrix} U^{0}=0 \\ \varphi^{0}=\alpha-\dfrac{\beta\zeta}{\gamma}-\dfrac{\left(\xi-\dfrac{\vartheta\zeta}{\gamma}\right)\left(\lambda-\dfrac{\beta\vartheta}{\gamma}\right)}{\eta-\dfrac{\vartheta^{2}}{\gamma}} \\ \psi^{0}=-\varepsilon+\dfrac{\zeta^{2}}{\gamma}+\dfrac{\left(\xi-\dfrac{\vartheta\zeta}{\gamma}\right)^{2}}{\eta-\dfrac{\vartheta^{2}}{\gamma}} \\ \Phi^{0}=-\dfrac{\vartheta}{\gamma}\Psi^{0}-\dfrac{\zeta}{\gamma}\varphi^{0}-\dfrac{\beta}{\gamma}\psi^{0} \\ \Psi^{0}=-\dfrac{\xi-\dfrac{\vartheta\zeta}{\gamma}}{\eta-\dfrac{\vartheta^{2}}{\gamma}}\varphi^{0}-\dfrac{\lambda-\dfrac{\beta\vartheta}{\gamma}}{\eta-\dfrac{\vartheta^{2}}{\gamma}}\psi^{0} \end{pmatrix} \tag{88}$$

$$\begin{pmatrix} U^{0(9)} \\ \varphi^{0(9)} \\ \psi^{0(9)} \\ \Phi^{0(9)} \\ \Psi^{0(9)} \end{pmatrix}=\begin{pmatrix} U^{0}=\left(e\varphi^{0}+h\psi^{0}+g\Phi^{0}+f\Psi^{0}\right)\Big/CK_{emgc}^{2} \\ \varphi^{0}=\dfrac{\alpha K_{A}}{K_{emgc}^{2}}-\dfrac{\beta\zeta K_{B}K_{Z}}{\gamma K_{G}K_{emgc}^{2}}-\left(\dfrac{\xi K_{S}}{K_{emgc}^{2}}-\dfrac{\vartheta\zeta K_{T}K_{Z}}{\gamma K_{G}K_{emgc}^{2}}\right)\dfrac{\lambda K_{L}-\dfrac{\beta\vartheta K_{B}K_{T}}{\gamma K_{G}}}{\eta K_{F}-\dfrac{\vartheta^{2}K_{T}{}^{2}}{\gamma K_{G}}} \\ \psi^{0}=-\dfrac{\varepsilon K_{E}}{K_{emgc}^{2}}+\dfrac{\zeta^{2}K_{Z}{}^{2}}{\gamma K_{G}K_{emgc}^{2}}+\dfrac{\left(\dfrac{\xi K_{S}}{K_{emgc}^{2}}-\dfrac{\vartheta\zeta K_{T}K_{Z}}{\gamma K_{G}K_{emgc}^{2}}\right)^{2}}{\dfrac{\eta K_{F}}{K_{emgc}^{2}}-\dfrac{\vartheta^{2}K_{T}{}^{2}}{\gamma K_{G}K_{emgc}^{2}}} \\ \Phi^{0}=-\dfrac{\vartheta K_{T}}{\gamma K_{G}}\psi^{0}-\dfrac{\zeta K_{Z}}{\gamma K_{G}}\varphi^{0}-\dfrac{\beta K_{B}}{\gamma K_{G}}\psi^{0} \\ \Psi^{0}=-\dfrac{\xi K_{S}-\dfrac{\vartheta\zeta K_{T}K_{Z}}{\gamma K_{G}}}{\eta K_{F}-\dfrac{\vartheta^{2}K_{T}{}^{2}}{\gamma K_{G}}}\varphi^{0}-\dfrac{\lambda K_{L}-\dfrac{\beta\vartheta K_{B}K_{T}}{\gamma K_{G}}}{\eta K_{F}-\dfrac{\vartheta^{2}K_{T}{}^{2}}{\gamma K_{G}}}\psi^{0} \end{pmatrix} \tag{89}$$

With the second equation in set (87), one can obtain the second eigenvectors. Their explicit forms can be demonstrated as follows:

$$\begin{pmatrix} U^{0(1)} \\ \varphi^{0(1)} \\ \psi^{0(1)} \\ \Phi^{0(1)} \\ \Psi^{0(1)} \end{pmatrix}=\begin{pmatrix} U^{0(3)} \\ \varphi^{0(3)} \\ \psi^{0(3)} \\ \Phi^{0(3)} \\ \Psi^{0(3)} \end{pmatrix}=\begin{pmatrix} U^{0(5)} \\ \varphi^{0(5)} \\ \psi^{0(5)} \\ \Phi^{0(5)} \\ \Psi^{0(5)} \end{pmatrix}=\begin{pmatrix} U^{0(7)} \\ \varphi^{0(7)} \\ \psi^{0(7)} \\ \Phi^{0(7)} \\ \Psi^{0(7)} \end{pmatrix}=\begin{pmatrix} U^{0}=0 \\ \varphi^{0}=-\mu+\dfrac{\beta^{2}}{\gamma}+\dfrac{\left(\lambda-\dfrac{\beta\vartheta}{\gamma}\right)^{2}}{\eta-\dfrac{\vartheta^{2}}{\gamma}} \\ \psi^{0}=\alpha-\dfrac{\beta\zeta}{\gamma}-\dfrac{\left(\xi-\dfrac{\vartheta\zeta}{\gamma}\right)\left(\lambda-\dfrac{\beta\vartheta}{\gamma}\right)}{\eta-\dfrac{\vartheta^{2}}{\gamma}} \\ \Phi^{0}=-\dfrac{\vartheta}{\gamma}\psi^{0}-\dfrac{\zeta}{\gamma}\varphi^{0}-\dfrac{\beta}{\gamma}\psi^{0} \\ \Psi^{0}=-\dfrac{\xi-\dfrac{\vartheta\zeta}{\gamma}}{\eta-\dfrac{\vartheta^{2}}{\gamma}}\varphi^{0}-\dfrac{\lambda-\dfrac{\beta\vartheta}{\gamma}}{\eta-\dfrac{\vartheta^{2}}{\gamma}}\psi^{0} \end{pmatrix} \tag{90}$$

$$\begin{pmatrix} U^{0(9)} \\ \varphi^{0(9)} \\ \psi^{0(9)} \\ \Phi^{0(9)} \\ \Psi^{0(9)} \end{pmatrix}=\begin{pmatrix} U^{0}=\left(e\varphi^{0}+h\psi^{0}+g\Phi^{0}+f\Psi^{0}\right)\Big/CK_{emgc}^{2} \\ \varphi^{0}=-\dfrac{\mu K_{M}}{K_{emgc}^{2}}+\dfrac{\beta^{2}K_{B}{}^{2}}{\gamma K_{G}K_{emgc}^{2}}+\dfrac{\left(\dfrac{\lambda K_{L}}{K_{emgc}^{2}}-\dfrac{\beta\vartheta K_{B}K_{T}}{\gamma K_{G}K_{emgc}^{2}}\right)^{2}}{\dfrac{\eta K_{F}}{K_{emgc}^{2}}-\dfrac{\vartheta^{2}K_{T}{}^{2}}{\gamma K_{G}K_{emgc}^{2}}} \\ \psi^{0}=\dfrac{\alpha K_{A}}{K_{emgc}^{2}}-\dfrac{\beta\zeta K_{B}K_{Z}}{\gamma K_{G}K_{emgc}^{2}}-\left(\dfrac{\xi K_{S}}{K_{emgc}^{2}}-\dfrac{\vartheta\zeta K_{T}K_{Z}}{\gamma K_{G}K_{emgc}^{2}}\right)\dfrac{\lambda K_{L}-\dfrac{\beta\vartheta K_{B}K_{T}}{\gamma K_{G}}}{\eta K_{F}-\dfrac{\vartheta^{2}K_{T}{}^{2}}{\gamma K_{G}}} \\ \Phi^{0}=-\dfrac{\vartheta K_{T}}{\gamma K_{G}}\psi^{0}-\dfrac{\zeta K_{Z}}{\gamma K_{G}}\varphi^{0}-\dfrac{\beta K_{B}}{\gamma K_{G}}\psi^{0} \\ \Psi^{0}=-\dfrac{\xi K_{S}-\dfrac{\vartheta\zeta K_{T}K_{Z}}{\gamma K_{G}}}{\eta K_{F}-\dfrac{\vartheta^{2}K_{T}{}^{2}}{\gamma K_{G}}}\varphi^{0}-\dfrac{\lambda K_{L}-\dfrac{\beta\vartheta K_{B}K_{T}}{\gamma K_{G}}}{\eta K_{F}-\dfrac{\vartheta^{2}K_{T}{}^{2}}{\gamma K_{G}}}\psi^{0} \end{pmatrix} \tag{91}$$

The reader can find that all the obtained eigenvector components do not depend on the phase velocity. This is true for all the treated six cases. This peculiarity can be further used for finding the propagation velocity of the acoustic wave when different boundary conditions will be applied.

CONCLUSION

This analysis has demonstrated that many possible eigenvectors can be revealed for the problem of the shear-horizontal acoustic wave propagation coupled with the electrical, magnetic, gravitational, and cogravitational potentials. This can be explained by the fact that in this case, any found apt eigenvector does not depend on the phase velocity. This peculiarity exists in certain directions of the transversely isotropic (6 *mm*) continua. Exploitation of each found eigenvector can give an unique solution for the propagation velocity of the acoustic wave. The existence of some found unique acoustic waves can dramatically depend on one of the extremely weak exchange effects: the magnetoelectric, gravitocogravitic, gravitoelectric, cogravitoelectric, gravitomagnetic, cogravitomagnetic effects. This possibility must be analytically demonstrated in the future, using the found eigenvectors. The obtained analytical results can be readily used for finding the propagation velocities of the acoustic waves managed by the solid surface, common interface between two solids, waveguide consisting of this film (plate), and more complicated configurations. Therefore, the obtained results can stimulate constitution of suitable technical devices based on some gravitation phenomena by experimentalists and engineers working with the transmitting, detecting, and converting of the electromagnetic waves' signals.

REFERENCES

Abbott, BP., Abbott, R., Abbott, TD., Abernathy, MR., Acernese, F., Ackley, K., Adams, C., Adams, T., Addesso, P., Adhikari, RX. *et al*. 2016. Observation of gravitational waves from a binary black hole merger. Physical Review Letters. 116(6):061102. pp.16.

Auld, BA. 1990. Acoustic Fields and Waves in Solids. Krieger Publishing Company (vol. I and II, 2nd ed.). pp.878.

Bedford, D. and Krumm, P. 1985. On relativistic gravitation. American Journal of Physics. 53(9):889-890.

Bleustein, JL. 1968. A new surface wave in piezoelectric materials. Applied Physics Letters. 13(12):412-413.

Braginsky, VB., Caves, CM. and Thorne, KS. 1977. Laboratory experiments to test relativistic gravity. Physical Review D. 15(8):2047-2068.

Braginsky, V., Polnarev, A. and Thorne, K. 1984. Foucault pendulum at the south pole: Proposal for an experiment to detect the Earth's general relativistic gravitomagnetic field. Physical Review Letters. 53(9):863-866.

Ciufolini, I. and Wheeler, J. 1995. The gravitomagnetic field and its measurement. Chapter 6 in: Gravitation and Inertia, Princeton Series in Physics. Princeton University Press, New Jersey, USA.

Ciufolini, I., Chieppa, F., Lucchesi, D. and Vespe, F. 1997. Test of the Lense-Thirring orbital shift due to spin. Classical and Quantum Gravitation. 14(10):2701-2726.

Ciufolini, I., Pavlis, E., Chieppa, F., Fernandes-Vieira, E. and Perez-Mercader, J. 1998. Test of general relativity and measurement of the Lense-Thirring effect with two Earth satellites. Science. 279(5359):2100-2103.

DeWitt, BS. 1966. Superconductors and gravitational drag. Physical Review Letters. 16(24):1092-1093.

Dieulesaint, E. and Royer, D. 1980. Elastic waves in solids: Applications to signal processing. J. Wiley, New York, USA. (Translated by Bastin, A. and Motz, M., Chichester). pp.511.

Einstein, A. 1916. Die Grundlage der allgemeinen Relativitätstheorie. Annalen der Physik. 4(49):769-822.

Forward, RL. 1961. General relativity for the experimentalist. The Proceedings of the Institute of Radio Engineers-IRE. 49(5):892-904.

Füzfa, A. 2016. How current loops and solenoids curve space-time. Physical Review D. 93(2):024014. pp.5.

Gulyaev, YuV. 1969. Electroacoustic surface waves in solids. Soviet Physics Journal of Experimental and Theoretical Physics Letters. 9(1):37-38.

Gulyaev, Yu V. 1998. Review of shear surface acoustic waves in solids. IEEE Transactions on Ultrasonics, Ferroelectrics, and Frequency Control. 45(4):935-938.

Harris, EG. 1991. Analogy between general relativity and electromagnetism for slowly moving particles in weak gravitational fields. American Journal of Physics. 59(5):421-425.

Heaviside, O. 1893. A gravitational and electromagnetic analogy. The Electrician. 31(Part I):281-282 and 359.

Jefimenko, OD. 1992. Causality, electromagnetic induction, and gravitation: a different approach to the theory of electromagnetic and gravitational fields. Electret Scientific Publishing, USA. pp.180.

Kiang, J. and Tong, L. 2010. Nonlinear magneto-mechanical finite element analysis of Ni-Mn-Ga single crystals. Smart Materials and Structures. 19(1):015017. pp.17.

Kolbenstvedt, H. 1988. Gravitomagnetism in special relativity. American Journal of Physics. 56(6):523-524.

Krumm, P. and Bedford, D. 1987. The gravitational Poynting vector and energy transfer. American Journal of Physics. 55(4):362-363.

Lense, J. and Thirring, H. 1918. Über den Einfluss der Eigenrotation der Zentralkörper auf die Bewegung der Planeten und Monde nach der Einsteinschen Gravitationstheorie. Physikalische Zeitschrift. 19:156-163.

Li, N. and Torr, DG. 1991. Effects of a gravitomagnetic field on pure superconductors. Physical Review D. 43(2):457-459.

Li, N. and Torr, DG. 1992. Gravitational effects on the magnetic attenuation of superconductors. Physical Review B. 64(9):5489-5495.

Li, N., Noever, D., Robertson, T., Koczor, R. and Brantley, W. 1997. Static test for a gravitational force coupled to type II YBCO superconductors. Physica C: Superconductivity and its Applications. 281(2-3):260-267.

Mashhoon, B., Hehl, FW. and Theiss, DS. 1984. On the Gravitational Effects of Rotating Masses: The Lense-Thirring Papers Translated. General Relativity and Gravitation. 16(8):711-750.

Mashhoon, B., Paik, HJ. and Will, CM. 1989. Detection of the gravitomagnetic field using an orbiting superconducting gravity gradiometer: Theoretical principles. Physical Review D. 39(10):2825-2838.

Melkumyan, A. 2007. Twelve shear surface waves guided by clamped/free boundaries in magneto-electro-elastic materials. International Journal of Solids and Structures. 44(10):3594-3599.

Misner, CW., Thorne, KS. and Wheeler, JA. 1973. Gravitation. Freeman Publishing, San Francisco. pp1215.

Nordtvedt, K. 1988. Existence of the gravitomagnetic interaction. International Journal of Theoretical Physics. 27(11):1395-1404.

Podkletnov, E. and Nieminen, R. 1992. A possibility of gravitational force shielding by bulk $YBa_2Cu_3O_{7-x}$ superconductor. Physica C: Superconductivity. 203(3-4):441-444.

Ross, DK. 1983. The London equations for superconductors in a gravitational field. Journal of Physics A: Mathematical and General. 16(6):1331-1335.

Thirring, H. 1918. Über die Wirkung rotierender ferner Massen in der Einsteinschen Gravitationstheorie. Physikalische Zeitschrift. 19:33-39.

Thirring, H. 1921. Berichtigung zu meiner Arbeit: "Über die Wirkung rotierender Massen in der Einsteinschen Gravitationstheorie". Physikalische Zeitschrift. 22:29.

Torr, DG. and Li, N. 1993. Gravitoelectric-electric coupling via superconductivity. Foundations of Physics Letters. 6(4):371-383.

Wallace, HW. 1971[a]. Method and apparatus for generating a secondary gravitational force field. US Patent No 3626605, Ardmore PA, December 14.

Wallace, HW. 1971[b]. Method and apparatus for generating a dynamic force field. US Patent No 3626606, Ardmore PA, December 14.

Wallace, HW. 1974. Heat pump. US Patent No 3823570, 60 Oxford Drive, Freeport NY, July 16.

Yavorsky, BM., Detlaf, AA. and Lebedev, AK. 2006. The text-book on physics for engineers and student of the higher education. ONICS Publishers, Moscow (8th ed.). pp.1054.

Zakharenko, AA. 2005. Dispersive Rayleigh type waves in layered systems consisting of piezoelectric crystals bismuth silicate and bismuth germinate. Acta Acustica united with Acustica. 91(4):708-715.

Zakharenko, AA. 2010. Propagation of seven new SH-SAWs in piezoelectromagnetics of class 6 *mm*. LAP LAMBERT Academic Publishing GmbH & Co. KG, Saarbruecken-Krasnoyarsk. pp.84.

Zakharenko, AA. 2013[a]. Piezoelectromagnetic SH-SAWs: A review. Canadian Journal of Pure and Applied Sciences. 7(1):2227-2240.

Zakharenko, AA. 2013[b]. Peculiarities study of acoustic waves' propagation in piezoelectromagnetic (composite) materials. Canadian Journal of Pure and Applied Sciences. 7(2):2459-2461.

Zakharenko, AA. 2013[c]. New nondispersive SH-SAWs guided by the surface of piezoelectromagnetics. Canadian Journal of Pure and Applied Sciences. 7(3):2557-2570.

Zakharenko, AA. 2015[a]. A study of new nondispersive SH-SAWs in magnetoelectroelastic medium of symmetry class 6 *mm*. Open Journal of Acoustics. 5(3):95-111.

Zakharenko, AA. 2015[b]. Dramatic influence of the magnetoelectric effect on the existence of the new SH-SAWs propagating in magnetoelectroelastic composites. Open Journal of Acoustics. 5(3):73-87.

Zakharenko, AA. 2016. On piezogravitocogravitoelectro-magnetic shear-horizontal acoustic waves. Canadian Journal of Pure and Applied Sciences. 10(3):4011-4028.

Received: Nov 29, 2016; Accepted: Jan 5, 2017

Canadian Journal of Pure and Applied Sciences
Vol. 11, No. 1, pp. 4121-4130, February 2017
Online ISSN: 1920-3853; Print ISSN: 1715-9997
Available online at www.cjpas.net

RADIOACTIVE POLLUTION AND EXCESS LIFETIME CANCER RISK DUE TO GAMMA EXPOSURE OF SOIL AND GROUND WATER AROUND OPEN LANDFILLS IN RIVERS STATE, NIGERIA

*Ononugbo C.P[1], Avwiri G.O[1] and Agbalagba, E.O[2]
[1]Department of Physics, University of Port Harcourt, Port Harcourt R/State
[2]Department of Physics, Federal University of Technology, Warri, Nigeria

ABSTRACT

The objective of present study was to evaluate the activity concentrations of ^{238}U, ^{232}Th and ^{40}K and excess lifetime cancer risk due to gamma exposure of soil and ground water around open landfills in Rivers State, Nigeria. A total of 21 soil and 17 ground water samples were collected around Aluu and Rumuolumeni landfills. Soil and water samples were analyzed using a well calibrated gamma-ray spectrometry (NaI (Tl)) detector system after they have reached radiogenic equilibrium. The mean specific activity concentration of ^{238}U, ^{232}Th and ^{40}K for soil samples were 48.44± 4.08 $Bqkg^{-1}$, 39.68±2.48$Bqkg^{-1}$ and 416.48±11.23$Bqkg^{-1}$ in Aluu landfill and 22.99± 1.04$Bqkg^{-1}$, 12.94± 0.84$Bqkg^{-1}$ and 169.11±5.46$Bqkg^{-1}$ in the Rumuolumeni landfill respectively, while in water they were 10.58± 1.09Bql^{-1}, 10.30±1.02 Bql^{-1} and 173. 78±21.32Bql^{-1} in Aluu landfill and 11.01±3.44Bql^{-1}, 16.26± 3.77Bql^{-1} and 225.88± 36.10Bql^{-1}in Rumuolumeni landfill respectively. The mean activity concentration of ^{238}U, ^{232}Th and ^{40}K around Aluu landfill were higher than the permissible values. The radiation hazard indices calculated for the soil samples around Aluu landfill were higher than their permissible values. All other radiation hazard indices calculated in all the samples (soil and ground water) from both Aluu and Rumuolumeni landfill were below unity. Based on our present study, we concluded that activity concentration of ^{238}U, ^{232}Th and ^{40}K in soil and ground water samples were high and Excess lifetime cancer risk calculated for all the samples analyzed were higher than the safe limits, therefore long term radiation exposure of the residents around Aluu and Rumuolumeni landfill will pose significant health threat, thus the ground water from these study areas should be treated for radionuclide before ingestion to reduce the radiation risk .

Keywords: River State, radioactivity, health impacts, soil and water land filling, spectrometer.

INTRODUCTION

Humans are usually exposed to some levels of environmental radiation of terrestrial origin. Terrestrial radiation mainly originate from radionuclides which exists naturally in air, water , soil, rocks and building materials depending on the geological and geographical features of the region (Avwiri *et al*., 2011). Dumping of industrial, medical and domestic wastes such as phosphogypsum, alum shale, scraps from oil and gas plants and so on can contaminate the soil, surface and underground water resources (Olubosede *et al*., 2012). In Nigeria, landfills are usually an unlined shallow pits (oftennot deeper than 50cm) where wastes are dumped. Another study, Odunaike *et al*. (2008) defined it as dumps which receives solid wastes in an uncontrolled manner and allows free access to scavengers. Studies have shown that soil from landfills and water resources near landfills contains high activity concentration of radionuclides (Oladapo *et al*., 2012; Innocent *et al*., 2013).

Hazards posed by such dumpsites are not only in terms of odour or presence of disease vectors, but can also arise from the radiation exposure (Ojoawo *et al*., 2011). Natural radionuclides constitute a treat to humans when ingested or inhaled in the body, either through drinking water or food chain (Ononugbo *et al*., 2013; Uosif *et al*., 2012). Ingested, radionuclide could be concentrated in certain parts of the body according to the metabolism involved (Ajayi *et al*., 2009). The effect can be chronic such as lung disease, acute leucopenia, anemia or death (Avwiri *et al*., 2013; Ramasamy *et al*., 2009).

Various radioactivity measurements carried out in many countries especially in Nigeria have shown the existence of natural radionuclides in several matrices like soil, water, foods (Jibril *et al*., 2007; Tchokossa *et al*., 2012). All these are contained in the domestic, industrial and medical wastes which are indiscriminately dumped in open pits fields (Ojoawo *et al*., 2011) and farm soils

*Corresponding author e-mail: onochinyere@yahoo.co.uk

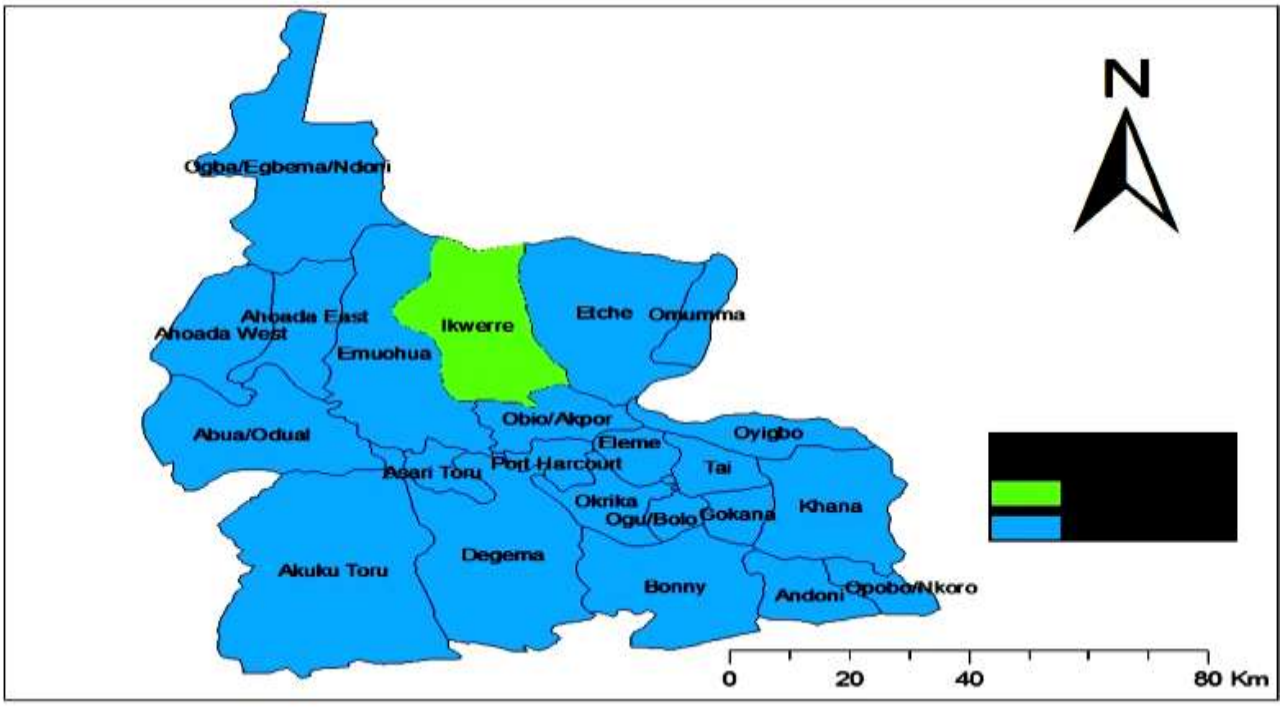

Fig. 1. Rivers State map showing Ikwerre LGA.

(Alatise *et al*., 2008). In Nigeria, unprotected, unlined landfill and open dumping are the available options for solid waste disposal. Aluu and Rumu-olumeni landfills in Rivers state are not exempted from poor environmental management. These wastes range from chemical toxic, hazardous industrial, medical, metal scraps and other debris, which are not separated from the municipal solid wastes disposed of at the Aluu and Rumuolumeni landfills. The potential environmental and health hazards could be deleterious if not properly handled (Eja *et al*., 2010; Longe and Kehinde, 2005; WHO, 2011). Hence this work aimed at evaluating the radiation emanating from these dumpsites/open landfills in order to provide accurate data and scientific information on the radiological health implications of such exposure.

MATERIALS AND METHODS

Study Area

The study area lies within latitude $04^0$53'14" N and $04^0$55'20"N and longitude $06^0$55'08"E and $06^0$55'58"E situated at the western Niger Delta region of Nigeria as shown in Figure 1. It comprises the Aluu and Rumuolumeni towns of Obio-Akpor local Government Area of Rivers State. These landfills have received more than 50% of the total refuse in Rivers area since 1989. The state has a population of 5 million and an annual growth rate of 3.6% (NPC, 2006; Avwiri *et al*., 2011).

Sample Preparation

Twenty-one soil and seventeen ground water samples of different wasteland were collected randomly to spatially cover the selected landfills. Soil were air-dried in the laboratory to a constant weight, crushed and made to pass through a 0.5 mm mesh sieve. Tap water was acidified with 11 M HCl at the rate of 10 ml per litre immediately after collection to avoid adsorption of radionuclide on the walls of the container (IAEA, 1999). The sample container were previously washed with dilute tetraoxosulphate (VI) acid and dried to avoid contamination. All the samples were sealed, labeled and stored in cylindrical named Marinelli beaker for at least 28 days before counting in order to attain a state of secular radioactive equilibrium among the radionuclide present and their progeny (Veiga *et al*., 2006) before the γ-ray counting.

Gamma Counting

The counting used a Sodium Iodide (NaI(Tl) gamma ray spectrometer system coupled to an electronic set. It has an energy resolution of 2.0 KeV and relative efficiency of 33% at 1.33 MeV and is encapsulated in a 15 cm thick cylindrical lead shield with a 10 cm thick cover at the top. The counting time was 10,000 seconds. The calibrations were carried out using a standard radioactive mixed sources supplied by the International Atomic Energy Agency (IAEA). The photo peaks corresponding to

Table 1. Location of the sampling point's and the Activity concentration of ^{238}U, ^{232}Th and ^{40}K in Soil Samples (Bqkg^{-1}).

S/N	Sample Code	Activity Concentration (Bqkg^{-1})		
		^{40}K (Bqkg^{-1})	^{238}U (Bqkg^{-1})	^{232}Th (Bqkg^{-1})
1.	SALU1	470.06±89.51	38.08 ± 13.32	21.75± 7.86
2.	SALU2	390.86± 78.75	41.36± 14.56	40.94± 12.08
3.	SALU3	497.41± 91.83	33.19± 9.31	44.65± 11.87
4.	SALU4	457.35± 102.08	44.68± 16.20	38.96± 10.69
5.	SALU5	379.86± 72.28	43.20± 11.31	39.84± 10.02
6.	SALU6	420.9± 68.37	47.74± 12.37	40.81± 13.03
7.	SALU7	298.69± 53.74	51.32± 18.06	45.72± 20.11
8.	SALU8	347.57± 97.37	39.78± 10.41	37.24± 9.20
9.	SALU9	603.77± 129.35	37.53± 8.95	41.95±16.89
10.	SALU10	342.52± 81.13	51.21± 16.40	45.67± 20.03
11.	SALU11	467.48± 117.46	47.73± 12.32	39.89± 17.18
12.	SALU12	316.69± 99.84	43.62± 15.18	38.77± 14.97
13.	SREP1	197.88± 87.51	33.23± 12.36	25.54± 8.79
14.	SREP2	156.49± 49.26	29.31±9.12	16.21±5.81
15.	SREP3	174.46± 53.32	22.55± 7.38	9.56± 3.10
16.	SREP4	162.72± 42.85	19.87± 8.29	7.98± 2.34
17.	SREP5	110.85± 36.84	23.53± 6.88	8.95± 3.01
18.	SREP6	168.76± 45.37	21.98±9.02	7.62±2.71
19.	SREP7	130.44±29.74	17.09± 6.34	15.14± 4.17
20.	SREP8	159.86± 46.89	19.14 ±8.49	13.84± 3.19
21.	SREP9	260.55± 72.47	20.19± 7.03	11.59± 4.01
Mean		**310.25±68.30**	**34.59**± 11.12	**27.27± 7.89**
Standard		**400**	**35**	**30**

gamma lines at 1460.30, 1764.5 (^{214}Bi) and 2614.5 (^{208}Tl) KeV were used to identify ^{40}K, ^{238}U and ^{232}Th respectively (IAEA, 1999; Yussuf *et al*., 2012; Ramasamy *et al*., 2009).

The activity concentration (C) of the radionuclide was calculated after subtracting decay correction using the following expression;

$$C_S = \frac{C_a}{P_\gamma (M_s / V_s)\varepsilon_\gamma t_c} \text{ (Bq kg}^{-1} \text{ or Bq l}^{-1}\text{)} \quad (1)$$

Where C_S = Sample concentration, C_a = net peak area of a peak at energy, ε_γ = Efficiency of the detector for a γ-energy of interest, M_S/V_s= sample mass/volume for soil/water, t_c = total counting time, P_γ is the abundance of the γ-line in a radionuclide.

Radiological Risk Parameters

In order to quantify the radiation hazard posed on the populace that are exposed to these radionuclides due to their use of the soil for building and consumption of water from resources near the landfills, some radiological parameters were estimated:

Radium Equivalent Activity (Ra_{eq})

The radium equivalent (Ra_{eq}) activity represents a weighted sum of activities of ^{238}U, ^{232}Th and ^{40}K. It is based on the estimation that 1 Bq kg^{-1} of ^{238}U, 0.7 Bq kg^{-1} of ^{232}Th and 13 Bq kg^{-1} of ^{40}K produce the same radiation dose rates. The radium equivalent activity index was estimated using the relation (Avwiri et al., 2013).

$$Ra_{eq} = C_{U+} 1.43C_{Th} + 0.077C_K \quad (2)$$

Where C_u, C_{Th} and C_K are the activity concentration in Bqkg^{-1} or Bql^{-1} of ^{238}U, ^{232}Th and ^{40}K.

Absorbed Dose rate (D)

The absorbed dose rate (D) was computed using the following expression[23].

$$D = 0.462C_{Ra+}0.604C_{Th} + 0.0417C_K \quad (3)$$

Where, D is the absorbed dose rate in nGy hr^{-1}, C_U, C_{Th}, and C_K are the concentrations of uranium, thorium and potassium respectively.

Annual Gonadal Equivalent Dose (AGED)

An increase in AGED has been known to affect the bone marrow, causing destruction of the red blood cells that are then replaced by white blood cells. This situation results in a blood cancer called leukemia which is fatal. The

AGED for the resident using such material for building were evaluated using the equation (UNSCEAR, 2000).

$$AGED\ (Sv/yr) = 3.09C_{Ra} + 4.18C_{Th} + 0.314C_K \quad (4)$$

Where C_{Ra}, C_{Th} and C_K are the activity concentration of ^{226}Ra, ^{232}Th and ^{40}K in soil samples or water samples.

the absorbed dose emitted from radionuclide in the environment such as ^{226}Ra, ^{232}Th and ^{40}K.

The annual effective dose resulting from the ingestion of water was estimated based on the assumption that a daily intake of water per person is 2 l d^{-1} from the following expression (WHO, 2011; Avwiri *et al*., 2013).

Table 2. Location of the sampling point's and the Activity concentration of ^{238}U, ^{232}Th and ^{40}K in Water Samples.

S/N	Sample Code	Activity Concentration (Bql^{-1})		
		$^{40}K(Bql^{-1})$	$^{238}U(Bql^{-1})$	$^{232}Th(Bql^{-1})$
1.	WALU1	125.30**±** **2**9.35	14.25 ± 5.66	17.27± 5.34
2.	WALU2	246.38± 68.75	16.79± 7.15	12.65± 3.09
3.	WALU3	245.73± 57.32	10.58±4.12	9.07± 2.87
4.	WALU4	179.18± 7.85	7.85± 3.53	10.99± 3.65
5.	WALU5	120.82±33.62	9.07± 2.87	8.52± 2.87
6.	WALU6	141.98±45.30	8.10± 4.11	7.53± 2.19
7.	WALU7	211.95± 68.48	9.96± 3.21	8.46± 3.16
8.	WALU8	118.91± 42.52	8.02± 3.11	7.92±3.10
9.	WREP1	118.74± 31.93	13.50± 3.19	18.72± 6.82
10.	WREP2	246.01± 91.12	12.03±4.21	15.70±5.93
11.	WREP3	244.77± 69.46	14.23± 5.13	21.62± 7.32
12.	WREP4	222.98±46.39	11.48± 3.17	14.24± 6.07
13.	WREP5	226.60± 50.01	8.61± 2.34	22.30± 8.11
14.	WREP6	137.41± 37.62	7.86±3.09	14.02±4.21
15.	WREP7	226.60±74.92	9.25± 2.18	17.28± 6.09
16.	WREP8	217.16± 46.58	8.99±3.29	13.02± 4.21
17.	WREP9	392.66± 97.23	13.15± 4.11	9.46± 3.21
Mean		**170.19±55.28**	**10.81± 3.67**	**13.49± 4.60**
WHO, 2011 standard		**10**	**10.0**	**1.0**

Representative Gamma Index (I_γ)

This is used to estimate the gamma radiation hazard associated with the natural radionuclides in the investigated samples. The representative gamma index was estimated as follows[11].

$$I_\gamma = C_{Ra}/150 + CTh/100 + CK/1500 \leq 1 \quad (5)$$

Annual Effective Dose Equivalent (AEDE)

The annual effective dose equivalent received by a member of the public is calculated from the absorbed dose rate by applying dose conversion factor of 0.7Sv/Gy and occupancy factor for outdoor and indoor was 0.2 and 0.8 respectively[21]. AEDE is determined using the following equations (Veiga *et al*., 2006).

$$AEDE_{(outdoor)}\ (\mu Sv/y) = \text{Absorbed dose D (nGy/h) x } 8760h \text{ x } 0.7Sv/Gy \text{ x } 0.2 \text{ x} 10^{-3} \quad (6)$$

$$AEDE_{(indoor)}(\mu Sv/y) = \text{Absorbed dose D (nGy/h) x } 8760h \text{ x } 0.7Sv/Gy \text{ x } 0.8 \text{ x} 10^{-3} \quad (7)$$

The AEDE indoor occurs within a house whereby the radiation risks due to building materials are taken into consideration. AEDE outdoor involves a consideration of

$$AEDE = I \text{ x } A \text{ x } C \times 365 \quad (8)$$

Where AEDE is the annual effective dose, I is the water intake per day, A is the daily intake of radionuclide and C is the ingestion coefficient of the specific radionuclide.

Excess Lifetime Cancer Risk (ELCR)

The Excess Lifetime cancer risk (ELCR) was calculated using the following equation (Jankowski *et al*., 2011).

$$ELCR = AEDE \times DL \times RF \quad (9)$$

Where AEDE is the Annual Equivalent Dose Equivalent, DL is the average duration of life (estimated to be 70 years), and RF is the Risk Factor (Sv^{-1}), i.e. fatal cancer risk per Sievert. For stochastic effects, ICRP uses RF as 0.05 for public.

Hazard Indices (H_{ex} and H_{in})

The external hazard (H_{ex}) and internal hazard (H_{in}) indices were evaluated using the relations (Ramasamy *et al*., 2009).

$$H_{ex} = C_{Ra}/370 + C_{Th}/259 + C_K/4810 \leq 1 \quad (11a)$$

$$H_{in} = C_{Ra}/185 + C_{Th}/259 + C_K/4810 < 1 \quad (11b)$$

Table 3. Hazard Indices and Excess lifetime Cancer Risk for soil Samples.

Sample code	D(nGy/h)	Ra_{eq} ($Bqkg^{-1}$)	AGED $mSvy^{-1}$	$AEDE_{outdoor}$ μSvy^{-1}	$AEDE_{indoor}$ μSvy^{-1}	H_{in}	H_{ex}	Iγ	ELCR X 10^{-3}
SALU1	50.33	178.21	356.18	63.62	246.90	0.29	0.39	0.79	0.86
SALU2	60.13	130.00	421.66	73.74	294.34	0.35	0.46	0.95	1.03
SALU3	63.04	135.34	345.81	77.30	309.25	0.37	0.46	1.00	1.08
SALU4	63.25	135.61	444.52	77.60	310.28	0.37	0.49	0.99	1.09
SALU5	59.86	129.42	419.30	73.41	293.65	0.35	0.47	0.94	1.03
SALU6	64.26	138.51	450.27	78.81	315.23	0.37	0.50	1.01	1.10
SALU7	63.78	139.70	443.48	78.22	312.88	0.32	0.52	1.00	1.10
SALU8	55.36	120.02	387.72	67.89	271.57	0.32	0.43	0.87	0.95
SALU9	67.86	144.01	480.90	83.22	332.89	0.39	0.49	1.07	1.17
SALU10	65.52	142.89	456.69	80.37	321.46	0.39	0.52	1.03	1.13
SALU11	65.64	140.77	461.01	30.50	322.00	0.38	0.51	1.03	1.13
SALU12	56.76	123.45	396.29	69.61	278.44	0.33	0.45	0.89	0.97
SREP1	39.03	59.52	271.57	47.87	191.47	0.23	0.32	0.41	0.67
SREP2	29.86	64.54	207.46	36.62	146.40	0.17	0.25	0.46	0.51
SREP3	23.47	29.65	164.42	28.78	115.13	0.10	0.20	0.36	0.40
SREP4	20.79	43.81	145.84	25.50	101.99	0.12	0.17	0.32	0.36
SREP5	20.90	44.86	144.93	25.63	102.53	0.12	0.19	0.25	0.36
SREP6	21.79	45.87	157.48	26.72	106.89	0.12	0.18	0.34	0.37
SREP7	22.48	48.78	157.05	27.57	110.28	0.13	0.18	0.35	0.39
SREP8	23.87	37.40	167.99	29.27	117.10	0.14	0.19	0.37	0.41
SREP9	27.19	36.83	147.37	33.35	133.38	0.15	0.21	0.33	0.47
Mean	45.96	93.77	315.61	47.06	213.49	0.26	0.36	0.70	0.79

Where, C_{Ra}, C_{Th} and $C_K$are the radioactivity concentration in Bq/kg (or Bq/l) of ^{226}Ra, ^{232}Th, and ^{40}K respectively

Correlation between ^{238}U and ^{232}Th, ^{238}U and ^{40}K and ^{232}Th and ^{40}K

The elemental concentrations of Uranium-238 (in ppm), Thorium-232 (in ppm) and Potassium (in %) were calculated from the measured activity concentrations of ^{238}U, ^{232}Th and ^{40}K in $Bqkg^{-1}$ using the conversion factors recommended by the IAEA Technical Report No 1363.The correlation of the radionuclide was performed to ascertain their relationship.

RESULTS AND DISCUSSION

The results of the gamma ray spectrometry of various samples are presented in Table 1 and Table 2. The radionuclide observed with reliable regularity belonged to the decay series chain headed by ^{238}U and ^{232}Th as well as the non- series ^{40}K.

The activity concentration of all the radionuclides (^{238}U, ^{232}Th and ^{40}K) in soil samples collected around the Aluu landfill is considerably higher than that from the Rumu-olumeni landfill as shown in Table 1. This is an indication that the wastes in the Aluu landfill are rich in radionuclide as a result of the medical wastes from the teaching hospital and Health centre within the vicinity of the landfill. In all the sampling sites, mean activity concentration is of the order ^{232}Th $<^{238}$U $<^{40}$K in particular SALU7 and SALU10, the activity concentration of ^{238}U is high, which may be due to solubility and mobility of $U(VI)O_2$ (Ibe and Njoku, 1999).

However, increasing concentration of ^{232}Th and ^{40}K may be due to the high content of monazite (Ramasamy *et al*., 2009) while that of ^{40}K is due to presence of loamy and clay sediments and the composition of the landfill. The concentration of ^{238}U, ^{232}Th and ^{40}K in all the measured soil samples from the Aluu landfill except one spot exceeded the world average values which are 35.0Bq kg^{-1}, 30.0 Bq kg^{-1} and 400.0Bq kg^{-1} for ^{238}U, ^{232}Th and ^{40}K is respectively. While the activity concentrations of ^{238}U, ^{232}Th and ^{40}K in soil from Rumu-olumeni landfill is within the world average values. The values of ^{238}U, ^{232}Th and ^{40}K obtained from Aluu landfill were higher than the values reported in other works in a similar environment (Faweya and Babalola, 2010). This may be due the volume and variation in the compositions of the un-segregated wastes in the landfill.

The activity concentration of ^{238}U, ^{232}Th and ^{40}K in all the water samples follow the same trend as in soil and exceeds the World Health Organization [18] standard for drinking water of 10.0, 1.0 and 10.0 Bq l^{-1} for ^{238}U, ^{232}Th and ^{40}K respectively as shown in Table 2. This is due to the infiltration of radionuclide from medical sources along with other hazardous wastes from landfill in the Aluu and industries in Rumu-olumeni. This compared well with the work done by Ibe and Njoku (1999) which presented variability of ^{226}Ra to ^{228}Ra concentration ratio content.

Table 4. Estimated daily intake and Annual Effective Dose from ingestion of water.

Sample Code	Daily intake per person (Bq d^{-1})		Annual Effective Dose (AEDE)(mSv y^{-1}) Ingestion dose Coefficient (Sv Bq^{-1}) (WHO, 2011)				
	6.2×10^{-9} for ^{40}K			4.5×10^{-8} for ^{238}U	$2.3\times$ 10-7 for ^{232}Th		
	^{40}K	^{238}U	^{232}Th	^{40}K	^{238}U	^{232}Th	Total	AEDE
WALU1	125.30± 29.35	14.25 ± 5.66	17.27± 5.34	0.57	0.47	2.90	3.94	
WALU2	246.38± 68.75	16.79± 7.15	12.65± 3.09	1.12	0.55	2.06	3.73	
WALU3	245.73± 57.32	10.58±4.12	9.07± 2.87	1.11	0.35	1.52	2.98	
WALU4	179.18± 7.85	7.85± 3.53	10.99± 3.65	0.81	0.26	1.85	2.92	
WALU5	120.82±33.62	9.07± 2.87	8.52± 2.87	0.55	0.30	1.43	2.28	
WALU6	141.98±45.30	8.10± 4.11	7.53± 2.19	0.64	0.27	1.26	2.17	
WALU7	211.95± 68.48	9.96± 3.21	8.46± 3.16	0.96	0.33	1.42	2.71	
WALU8	118.91± 42.52	8.02± 3.11	7.92±3.10	0.54	0.26	1.33	2.13	
WREP1	118.74± 31.93	13.50± 3.19	18.72± 6.82	0.54	0.44	3.14	4.12	
WREP2	246.01± 91.12	12.03±4.21	15.70±5.93	1.11	0.40	2.64	4.15	
WREP3	244.77± 69.46	14.23± 5.13	21.62± 7.32	1.11	0.47	3.63	5.21	
WREP4	222.98±46.39	11.48± 3.17	14.24± 6.07	1.01	0.38	2.39	3.78	
WREP5	226.60± 50.01	8.61± 2.34	22.30± 8.11	1.03	0.28	3.74	5.05	
WREP6	137.41± 37.62	7.86±3.09	14.02±4.21	0.62	0.26	2.35	3.23	
WREP7	226.60±74.92	9.25± 2.18	17.28± 6.09	1.03	0.30	2.90	4.23	
WREP8	217.16± 46.58	8.99±3.29	13.02± 4.21	0.98	0.30	2.19	3.47	
WREP9	392.66± 97.23	13.15± 4.11	9.46± 3.21	1.78	0.43	1.59	3.80	
Total	**170.19±55.28**	**10.81± 3.67**	**13.49± 4.60**	**1.20**	**0.36**	**2.26**	**3.52**	

All the radiological hazard indices calculated in soil samples from Aluu and Rumu-olumeni landfill are presented in Table 3.The radium equivalent doses calculated for soil from the Aluu and Rumu-olumeni landfill are within the world average value of 370.0 Bq kg^{-1}. The results show that the mean absorbed dose in soil from Aluu landfill is higher than the world average value of 55 nGy h^{-1} and also other reported works (Baykara *et al*., 2005; Tchokossa *et al*., 2012). The annual effective dose (outdoor) for soil from Aluu landfill is higher than the world average value of 70.0 μSvy^{-1}. The mean annual effective dose (indoor) in soil from the two landfill namely Aluu and Rumu-olumeniwere lower than the world permissible value of 450 μSv y^{-1}(Ramasamy *et al*., 2009) but still within the range obtained by other workers (Innocent *et al*., 2013).

The average annual gonadal dose equivalent of soil from Aluu landfillis higher than the permissible value of 300 mSv y^{-1}as shown in Figure 3. This may pose a threat to the bone marrow and the bone surface cells of persons exposed by the use of soil from the Aluu landfill since the landfill is situated in farmland. Also, the external hazard index, internal hazard index and representative gamma index are less than the world permissible value of unity (Avwiri *et al*., 2013) though the gamma index exceeded at four sampling points. This indicates that the immediate radiation hazard could not be noticeable but might have long term impact. The average excess lifetime cancer risk (ELCR) for soil samples from Aluu and Rumu-olumeni landfill are 0.79×10^{-3} and 0.44×10^{-3} respectively and is shown in Figure 2. For the ground water samples ELCR for Aluu and Rumu-olumeni landfill are 0.33×10^{-3} and 0.38×10^{-3}respectively. These values are slightly higher than the world average of 0.29×10^{-3}as shown in Figure 4. This implies that the chances of having cancer by populace that use the water and soil from the area of study are significant.

The estimated daily intake of radionuclide and annual effective dose from ingestion of water as presented in Table 4 are higher than the values reported by other researchers (Baykara *et al*., 2005; Adewole, 2009) due to variation in the composition of the landfills. The absorbed dose rate due to ingestion of water from Aluu and Rumu-olumeni landfill as presented in Table 5 are within the safe limits. There is no significant difference in radionuclide concentration shown by the water samples from the two landfills. This is due to frequent migration of radionuclides in the direction of flow of water. These radionuclides deposited over a period of time are infiltrated from the landfill via the soil and contaminate groundwater which then migrates following the direction of flow. The mean value of the annual effective dose of water samples from Aluu landfill and Rumuolumeni are above the recommended value of 1.0 $mSvyr^{-1}$due to borehole water only and 0.1 mSv yr^{-1} for drinking water (WHO, 2011). Also, external hazard index, internal hazard index and representative gamma index are less than the world permissible value of unity as shown in Table 5. The excess life time cancer risk in all the water

Table 5. Hazard Indices and Excess lifetime Cancer Risk for Water Samples.

Sample	**D**	**Ra_{eq} (nGy h^{-1})**	**AGED (Bq l^{-1})**	**$H_{ex}H_{in}$ (mSv y^{-1})**	**I_γ × 10^{-3}**	**ELCR**	code
WALU1	22.24	48.84	137.85	0.13	0.17	0.51	0.47
WALU2	25.67	36.90	136.14	0.15	0.15	0.29	0.44
WALU3	20.61	42.47	105.01	0.12	0.14	0.33	0.35
WALU4	17.74	37.36	126.46	0.10	0.12	0.28	0.31
WALU5	14.37	30.56	101.57	0.08	0.11	0.23	0.25
WALU6	14.21	29.80	101.09	0.08	0.10	0.22	0.24
WALU7	18.55	32.99	137.69	0.10	0.13	0.17	0.32
WALU8	13.47	28.47	95.23	0.08	0.10	0.21	0.23
WREP1	22.50	41.71	157.25	0.13	0.17	0.08	0.39
WREP2	20.22	39.12	180.05	0.14	0.18	0.40	0.35
WREP3	29.84	63.99	217.56	0.17	0.21	0.47	0.51
WREP4	14.03	49.01	165.01	0.13	0.16	0.37	0.24
WREP5	26.90	42.55	190.97	0.16	0.18	0.23	0.46
WREP6	17.83	38.46	126.04	0.10	0.13	0.28	0.31
WREP7	16.13	51.41	171.97	0.14	0.16	0.39	0.28
WREP8	21.07	44.33	150.39	0.12	0.14	0.34	0.36
WREP9	28.16	56.91	203.47	0.15	0.19	0.44	0.48
Mean	**20.21**	**59.70**	**147.28**	**0.12**	**0.15**	**0.43**	**0.35**

samples exceeded the world accepted safe limit (Udom and Esu, 2004).

The ranges of the calculated elemental activity concentrations in all soil samples are found to be between 1.38 ± 0.03 and 4.16 ± 0.04 ppm for uranium, 1.88 ± 0.01 and 11.26 ± 0.05 ppm for thorium and 0.15 ± 0.001 to 1.6 ± 0.02 % for potassium with an arithmetic mean of 2.90±0.03ppm, 6.86±0.05ppm and 0.94±0.002% respectively. It can be seen that there is a good correlation between Uranium and thorium with a correlation coefficient of 0.797. The relationship between U and Th can be considered in terms of the Th/U ratio. In the current study, the obtained result of elemental ratios for Th/U varies from 1.06 to 4.09, with an arithmetic mean of 2.34 which is lower than the theoretical value of 3.0. A relatively high or low value of the ratio as measured in some studied locations may be an indicative of an enrichment of Thorium or depletion of Uranium of which may be due to alteration or natural processes in that area (Ononugbo *et al*., 2013; USEPA, 2012).

The activity concentrations of natural radionuclides and their associated radiological health risk parameters determined in the two landfills are high when compared with other works done in similar environment. This is an indication that the environment has been contaminated by the un-segregated wastes which may contain some radioelements. Therefore, residents, Scavengers and workers of the landfills areas may be exposed daily to different doses of radiation which may result to health problems such as radiation poisoning, cancer and cell mutation for a long exposure.

CONCLUSION

The activity concentration of ^{238}U, ^{232}Th and ^{40}K in soil and ground water from the two landfills has been studied with the aid of a well calibrated Gamma ray spectrometry and was found to be high compared to results of other works done in a similar environment and their stipulated world safe limit. The annual gonad equivalent dose and excess lifetime cancer risk calculated from the activity concentration of these radionuclides exceeded the permissible values of 300 $mSvy^{-1}$ and 0.29 × 10^{-3} respectively in soil samples. The mean absorbed dose of radiation calculated from soil samples from Aluu landfill is higher than the world value of 55 $nGyh^{-1}$ and also other values reported from a similar environment. The estimated daily intake of radionuclides and the AEDE from ingestion of those radionuclides are higher than the values reported in other works and also the world accepted safe limits.

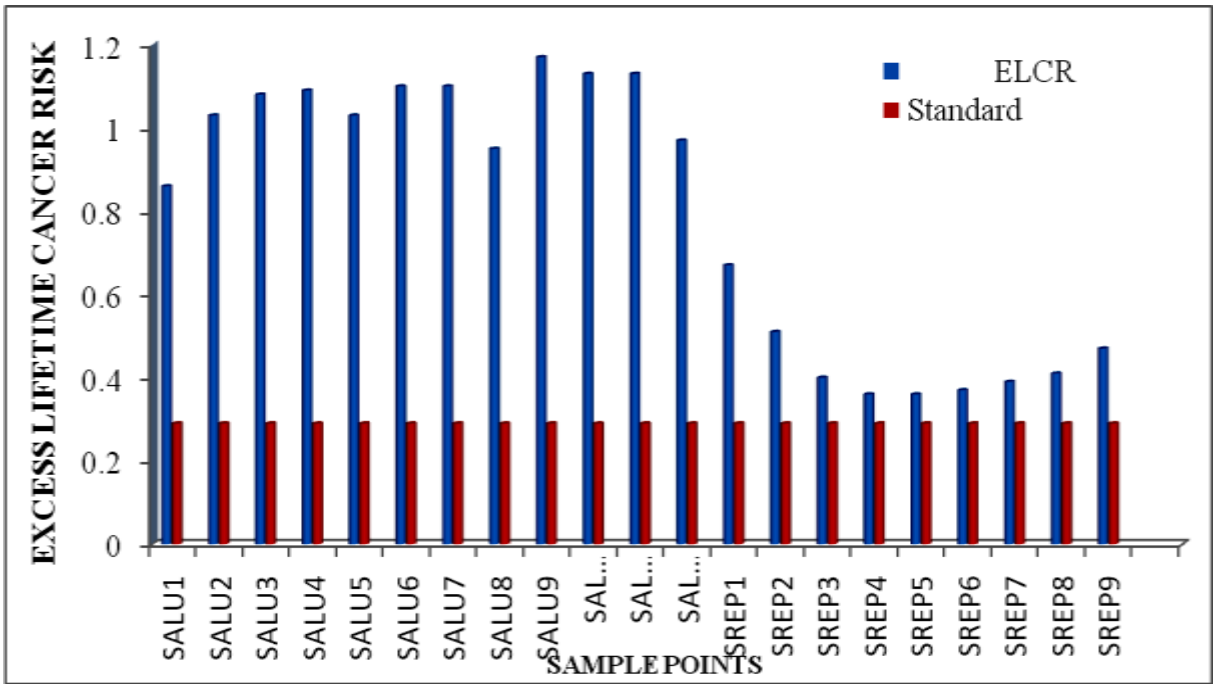

Fig. 2. Comparison of ELCR in soil with UNSCEAR, 2000 Threshold.

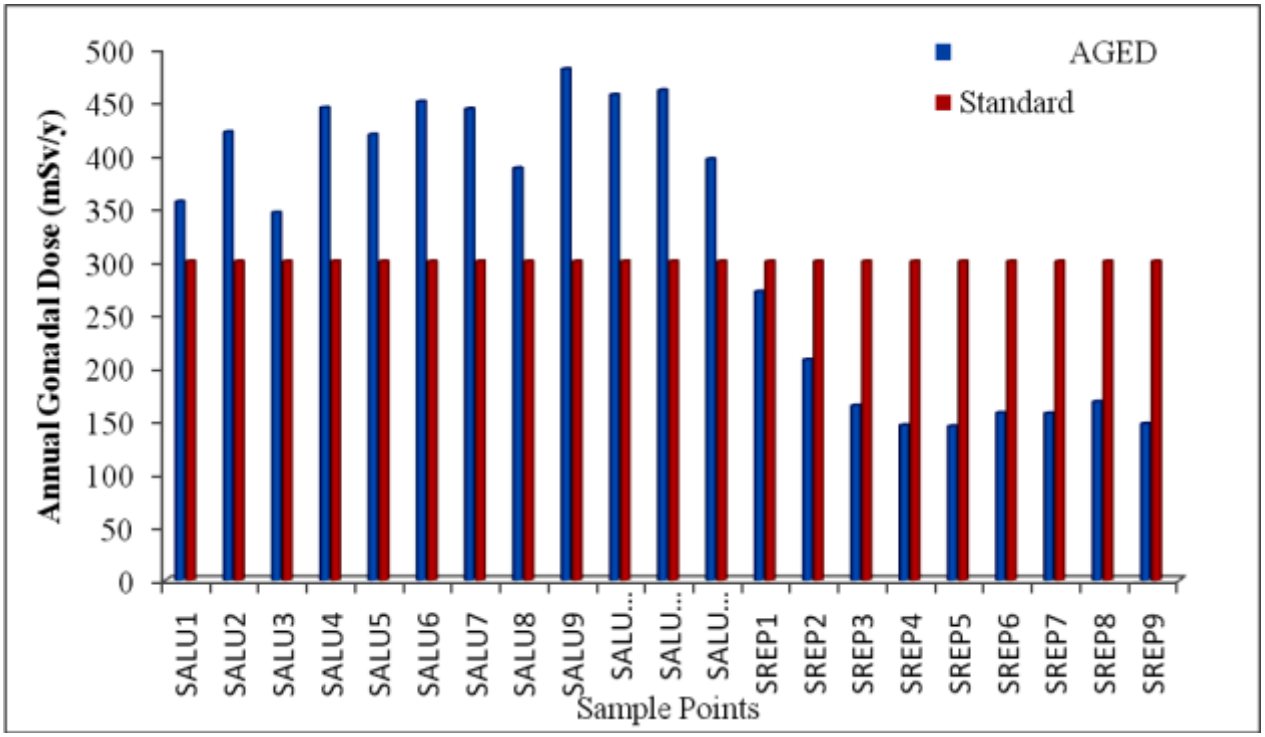

Fig. 3. Comparison of Annual Gonad dose in soil with UNSCEAR, 2000 Standard.

The study therefore conclude that the area have been radiologically polluted by the waste dumps in both landfills , therefore residents, scavengers and workers of the landfill are exposed to varying doses of radiation which could lead to radiation related health hazard for long term exposure. We therefore recommend that the wastes be sorted out from domestic wastes and appropriate disposal option be adopted to help safeguard

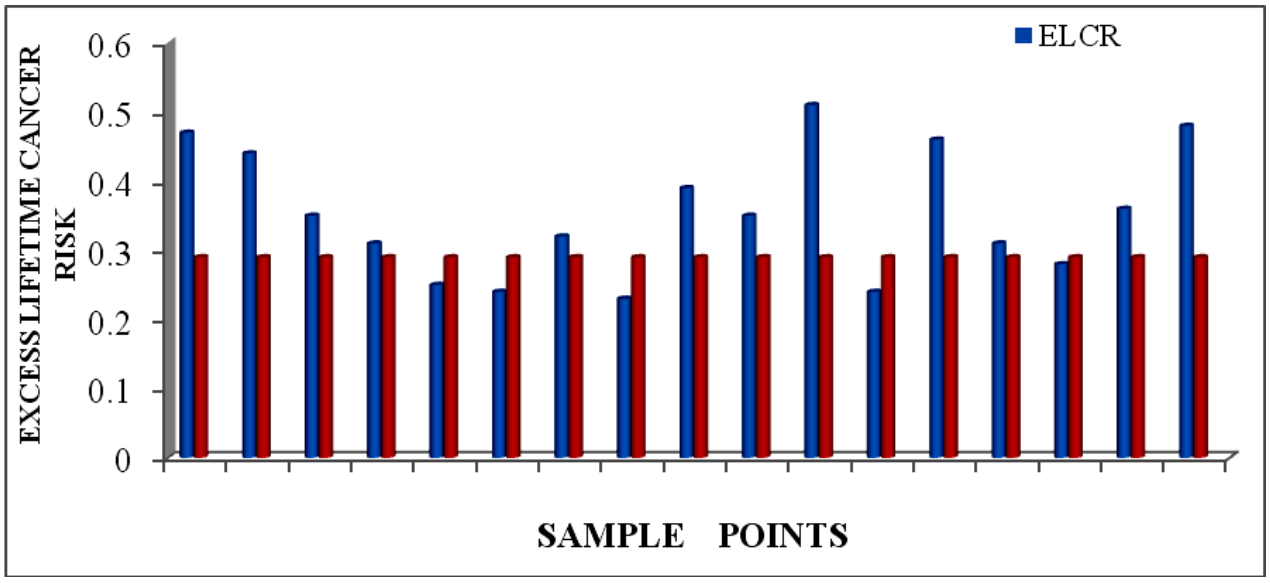

Fig. 4. Comparison of ELCR in water with UNSCEAR, 2000 Threshold.

the lives of the people residing close to the landfills and their environment. Also, boreholes in the area should incorporate ion exchange of reverse osmosis technology in order to eliminate the radionuclides from the water before consumption.

ACKNOWLEDGEMENTS

The authors are thankful to the management of National Institute for Radiation Protection and Research (NIRPR) for permission to use their facilities and also Mr. Jafaru Egeiya and Mrs. Mary Ajibode for their contribution during the field work and sample preparation.

REFERENCES

Adewole, AT. 2009. Waste management towards sustainable development in Nigeria: A case study of Lagos state. Int. NGO J. (3):45-57.

Ajayi, TR., Torto, N., Tchokossa, P. and Akinlua, A. 2009. Natural Radioactivity and Trace Metals in Crude Oils: Implication for Health. Environ Geochem Health. 31:61-69.

Alatise, OO., Babalola, IA. and Olawofela, JA. 2008. Distribution of some Natural Gamma Emitting Radionuclides in the Soils of the Coastal areas of Nigeria. Journal of Environmental Radioactivity. 99(11):1746-1749.

Avwiri, GO., Nte, FU. and Olanrewaju, AI. 2011. Determination of Radionuclide Concentration of Landfill at Eliozu, Port Harcourt, Rivers State. Scientia Africana. 10(1):46-57.

Avwiri, GO., Egieya, JM. and Ononugbo, CP. 2013. Radiometric Survey of Aluu landfill in Rivers State, Nigeria. J. Advanced in Physics Theories and Application. 22:24-29.

Baykara, O., Hasar, H., Obek, E. and Dogru, E. 2005. Determination of Radioactive Pollution from an Open Landfill. Journal of Radioanalytical and Nuclear Chemistry. 265(1):95-99.

Eja, MK., Alobi, NO., Ikpeme, EM., Ogiri, OR. and Iyang, AO. 2010. Environmental and public Health related assessment of solid waste Management in Uyo, Akwa-Ibom State, Nigeria. World Journal of Applied Science and Technology. 2(1):110-123.

Faweya, EB. and Babalola, S. 2010. Radiological Safety Assessment and Occurrence of Heavy Metals in Soils from Designated waste dumpsites used for building and composting in South Western Nigeria. The Arabic Journal for Science and Engineering. 35(2):219-225.

Ibe, KM. and Njoku, JC. 1999. Migration of Contaminants in ground water at a landfill site. Nigerian Journal of Environmental Hydrology. 7(8):1-9.

Innocent, AJ., Onimisi, MY. and Jonah, SA. 2013. Evaluation of naturally occurring Radionuclide Materials in Soil samples collected from some mining sites in Zamfara State, Nigeria. British Journal of Applied Science and Technology. 3(4):684-692.

International Atomic Energy Agency (IAEA). 1999. Safety Report on Radiation Protection and the Management of a Radioactive Waste in mine, oil and gas industries. New York, USA.

Jankowski, J., Chuscielewski, W., Kamimski, Z. and Zak, A. 2011. Natural Radioactivity of underground water supplies in the Region laulz in Poland. In Proceedings of the IRPA 10 on Scientific Topics-1Natural.

Jibril, NN., Farai, IP. and Alausa, SK. 2007. Activity Concentration of ^{226}Ra,^{232}Th and ^{40}K in different food crops form a high background radiation area in Bisichi, Jos Plateau state, Nigeria. Radiat Environ. Biophysics. 46:53-59.

Longe, EO. and Kehinde, MO. 2005. Investigation of potential ground water impact at an unlined waste disposal site in Agege, Lagos Nigeria. Proc 3rd Faculty of Engineering International Conference, University of Lagos, Nigeria.

NPC. 2006. National Population Commission of Nigeria: Provisional Census Result of Federal Republic of Nigeria.

Olubosede, O., Akinnagbe, OB. and Adekoya, E. 2012. Assessment of Radiation Emission from waste Dumpsite in Lagos State of Nigeria. International Journal of Computational Engineering Research. 2(3):806-811.

Odunaike, R.K., Laoye, JA. ,Alausa, SK., Ijeoma, GC. and Aelaja, AD. 2008. Radiation Emission Characterization of waste Dumpsites in the city of Ibadan in Oyo State of Nigeria. Research Journal of Environmental Toxicology. (2):100-103.

Oladapo, OO., Oni, EA., Olawoyin, AA., Akereke, OO. and Tijani, SA. 2012. Assessment of Natural Radionuclides levels in Wasteland Soils around Olusosun Dumpsite Lagos. Nigerian Journal of Applied Physics. 2(3):38-43.

Ojoawo, S., Agbeole, O. and Sangodoyin, S. 2011. A. Physical Composition of solid wastes in selected Dumpsites of Ogbomoso land, South-Western Nigeria. Journal of water Resources and protection. (3):661-661.

Ononugbo, CP., Avwiri, GO. and Egieya, JM. 2013. Evaluation of Natural Radionuclide Content in Surface and Ground Water and Excess Lifetime Cancer Risk Due To Gamma Radioactivity. Academic Research International. 4(6):636-647.

Ramasamy, V., Suresh, G., Meenakshisundaram, V. and Gajendran, V. 2009. Evaluation of Natural Radionuclide content in River sediments and excess lifetime cancer Risk due to Gamma Radioactivity. Research J. of Environmental and Earth Sciences. 1(1):6-10.

Tchokossa, P., Olomo, JB., Balogun, FA. and Adesanmi, CA. 2012. Radiological Study of Soils in Oils and Gas Producing Areas in Delta State, Nigeria. Radiation Protection Dosimetry. 1-6. doi:10.1093/rpd/nsc101

Taskin, H., Karavus, M., Ay, P., Topuzoglu, S., Hindiroglu, N. and Karahan, G. 2009. Radionuclide Concentrations in soil and Lifetime cancer risk due to the gamma radioactivity in Kirklareli, Turkey. J. of Environmental Radioactivity. 100:49-53.

Udom, GJ. and Esu, EO. 2004. A preliminary assessment of the impact of solid wastes on soil and ground water system in parts of Port Harcourt city and its Environs, Nigeria. 4(1):23-32.

Uosif, MA., Mahmond, T., Shams, AM. and Reds, E. 2012. Naturally Occurring Radionuclides in Sludge samples from some Egyptian Drinking water Purification Stations. International Journal of Advanced Science and Technology. 42:69-81.

United Nations Scientific Committee on Effect of Atomic Radiation. (UNSCEAR). 2000. Report to the general assembly Annex B: exposure from natural radiation source.

United States Environmental Protection Agency (UNSEPA). 2012. Edition of the Drinking water Standards and Health Advisories. Spring.

Veiga, RG., Sanches, N. and Anjos, RM. 2006. Measurement of natural radioactivity in Brazilizn beach sands. Radiation Measurements. 41:189-196.

World Health Organization (WHO). 2011. Guidelines for Drinking Water Quality. (4th edi.). Incorporating the 1st and 2nd Agenda vol.1 Recommendations, Geneva.

Yussuf, NM., Hossain, I. and Wagiran, H. 2012. Natural Radioactivity in Drinking and Mineral water in Johor Bahru (Malaysia). Scientific Research and Essays. 7(9):1070-1075.

Received: March 24, 2016; Revised: Dec 13, 2016;
Dec 19, 2016

Canadian Journal of Pure and Applied Sciences
Vol. 11, No. 1, pp. 4131-4140, February 2017
Online ISSN: 1920-3853; Print ISSN: 1715-9997
Available online at www.cjpas.net

REMOVAL OF MICRO POLLUTANTS FROM AQUEOUS SOLUTION USING ACTIVATED CARBONS FROM PET WASTE

*Abdoul Ntieche Rahman[1], Abdoul Wahabou[1], Patrick Mountapmbeme Kouotou[2,3], Abdelaziz Bacaoui[4], Kouotou Daouda[5] and Abdelrani Yaacoubi[4]
[1]Higher Teachers' Training College, University of Maroua, PO Box 55, Maroua, Cameroon
[2]Higher Institute of the Sahel, University of Maroua, PO Box 46, Maroua, Cameroon
[3]Institute of Engineering Thermophysics, Chinese Academy of Sciences, Beisihuanxi 11, 100190 Beijing, China
[4]Department of Chemistry, Faculty of Science Semlalia, University of Cady Ayyad, Marrakech, Morocco
[5]Department of Inorganic Chemistry, Faculty of Science, University of Yaoundé I, PO Box 812, Yaoundé, Cameroon

ABSTRACT

The aim of this study was the production of activated carbons (ACs) starting from urban plastics waste that is the post-consumer bottles made of polyethylene terephtalate (PET) as raw material, the characterization and the investigation of their efficiency in the removal of micro-pollutants such as chloro- and nitro-phenolic compounds from an aqueous solution. Plastics waste were carbonized at 600°C in an inert N_2 atmosphere and the resulting char was subjected to the physical and physico-chemical activation at 850ºC. The ACs prepared by this method were characterized in terms of structure, pore texture, microstructure and surface functional groups. Finally, the ACs prepared were successfully tested as adsorbent in the removal of 4-chlorophenol and 4-nitrophenol from an aqueous solution. The influence of the activation method on the performance of the so-prepared ACs was investigated and discussed. On the basis of the results obtained the greatest performance in the removal performance of 4-chlorophenol and 4-nitrophenol was observed with the sample obtained from physico-chemical activation. It was thus suggested that the physico-chemical activation leads to the formation of chemical bond at the surface of the adsorbent so prepared, showing that the impregnation of char with KOH before physical activation enhance the formation of functional groups necessary for chemisorption.

Keywords: Urban plastics waste, activated carbon, adsorption, phenolic compounds, wastewater.

INTRODUCTION

World increasing population and industrialization have resulted in a large increase in public demand of consumer goods. The industrial and agricultural activities carried out with a view of meeting this demand involve the use of many different chemicals which are subsequently released to various extents in the effluents from such industries. As these wastes are by and large discharged through aquatic route, they are detected as water pollutants and over the years, this has grown to a widespread contamination of surface and ground waters by various organic and inorganic compounds. In particular, huge quantities of phenolic, chloro and nitro aromatic compounds used as raw materials in many industrial processes are disposed as waste by petrochemical, pharmaceutical, agribusiness, polymer, textile and paper industries. There is consequently a growing public concern about this environmental pollution which has led to the instatement by global organizations such as the World Health Organization (WHO) of stringent worldwide regulations to be abided with by industry (Tonni *et al*., 2006).

In order to comply with the stringent contaminant limit set forth by environmental protection institutions, industrialists have been resorting to various technologies developed over the years to remove pollutants from water such as chemical precipitation, electro flotation, ion exchange, reverse osmosis and adsorption on activated carbon (CPC). Among these, adsorption on activated carbon has become commonplace as compared to other physico-chemical techniques owing to its simplicity, low price, ease to scale-up and its high efficiency in removing low substance concentrations even at part per million levels (Goyal, 2005). Most importantly, activated carbon has been widely used in water treatments because of its high specific surface area, well-developed micropores, chemical stability and durability (Goyal, 2005).

The economic advantage of the use of activated carbons in water treatments based on adsorption processes can be enhanced by exploring new synthetic routes or using non

*Corresponding author e-mail: rahmino@gmail.com

valuable by-products, residues or post-consumer waste materials as precursors for their preparation. In addition, the utilization of by-products, residues or post-consumer waste materials as precursors of carbon adsorbents appears to be a valuable strategy to deal with the problem of urban wastes disposal and recycling (Arenillas *et al*., 2005). In recent years a lot of research has been reported on the use of miscellaneous residues as starting materials in the preparation of activated carbons for the adsorption of micro pollutants (Laszlo, 1997), including waste materials of agricultural origin (Boumaza, 2012), agricultural waste (Bharathi, 2013), agricultural by-products (Ahmedna *et al*., 1997), olive mill solid residue (Nameri *et al*., 2000), cork waste (Carvalho *et al*., 2003), waste apricot (Önal, 2006), olive-seed waste residue (Stavropoulos, 2005), coir pith (Namasivayam, 2002), oil palm shell (PoedjiLoekitowati Hariani, 2013), corn cobs (Leelavathy, 2015), grapefruit peel (Huang *et al*., 2014), coconut shell waste (Kurniawan *et al*., 2011), biogas residue (Xiangzheng Yuan *et al*., 2011), waste newspaper (Kiyoshi Okada *et al*., 2003), waste tyres(Mui, 2004), city wastes (Tamon, 1998). From among the potential residues candidates, Polyethylene terephthalate (PET) captures a great attention (Miroslaw Marzec *et al*., 1999). Researchers in the developing countries are working hard to reduce environmental pollution caused by non-biodegradable plastics waste (i.e. post-consumer products like plastics bottles, plastic bags, plastic floor tiles, window and door frames in the construction industry), through their transformation to a biodegradable materials such as activated carbon, well known as useful material for the wastewater treatment. Although the effectiveness of the application of activated carbon made of plastics materials for the treatment of contaminated water have been demonstrated, up to date, just few works are reported in the literature (Parra *et al*., 2004; Kartel*et al*., 2006; Ania *et al*., 2007). Another study, Parra *et al*. (2004) prepared activated carbons from post-consumer waste using physical activation at 400°C in a nitrogen atmosphere followed by activation of the char with carbon dioxide at 925°C. The obtained AC had a composite porous structure. Two years later Kartel *et al.* (2006) obtained from the same precursor an AC prepared by physical activation with steam, precursor material which was at first treated with sulfuric acid and the resulting AC had a surface area of 1030 m^2/g and an effective pore size of 1.8 nm. The preparation of low-cost adsorbents from waste materials presents several advantages, mainly with regard to economic and environmental aspects. The transformation of plastic wastes to activated carbon (AC), appears as a means to solve the pollution problem caused by plastic wastes. Therefore, the transformation of plastic wastes to activated carbon is considered as one of the concrete and immediate contribution to the alleviation of environmental pollution.

The present study focused on the preparation, the characterization and the evaluation of the adsorption properties of ACs obtained from post-consumer plastics and prepared using both physical and physico-chemical activation methods. The adsorption properties of the ACs obtained were studied using the Langmuir and Freundlich isotherms.

MATERIALS AND METHODS

Preparation of activated carbon

The polyethylene terephtalate (PET) polymer plastics from post-consumer soft-drink bottles used as the raw material were collected from the municipal waste. They were cut down to desirable particle sizes and dried under sunlight for 05hrs before carbonization process. 20 g of the polymer plastics were loaded in the furnace and heated from room temperature (18°C) with a temperature increment rate of 10°C/min up to a final temperature of 600°C. The heating process was stabilized with nitrogen at a flow rate of about 100 $mL.min^{-1}$. The residence time of the samples at the final stabilized temperature of 600°C was 03 hours. After the heat treatment, the nitrogen flow was stopped and the char obtained was cooled down to the room temperature**.** Two samples of char (5g of each carbonized sample) were subjected to physical activation with steam of nitrogen at the rate of 0,13mL/min by increasing the temperature up to 850°C at a heating rate of $10°C.min^{-1}$, with a residence time of 2 and 3 hours respectively. The sample of char (5g) was also used for physico-chemical activation, the carbonized samples were mixed with the potassium hydroxyl (KOH) in the ratio 1:2 (char/KOH) and dried in the oven overnight at 110ºC and then heated in the same condition as described above for the physical method. The resulting activated carbons were grinded and sieved to a particle size < 150 µm. The activated carbon obtained by the physico-chemical activation method was firstly washed with distilled water then dried in the oven overnight at 110°C before it was grinded and sieved into particles of size < 150 µm. The activated carbons obtained by physical activation during 2 and 3h are referred as **PET1** and **PET2,** respectively, in relation to the raw material PET, whereas the activated carbon produced by physico-chemical activation is referred as **PETA**.

Characterization

The textural characteristics of the activated carbon were obtained using a chemisorption and physisorption surface area analyzer (Micromeritics TriStar 3000). The activated carbons were out-gassed in vacuum at 353K and 5µm Hg during 6h prior to measurement. The surface areas of activated carbons were estimated by BET (Brunauer–Emmett–Teller) model with the assumption of the adsorbed nitrogen molecule having a cross sectional area of 0.162 nm^2, while the total pore volume was determined at the relative pressures of 0.01–0.30. The micro pore

volume and external surface areas were obtained from the t-plot method. The mesopore volume was calculated by subtracting the micropore volume from the total pore volume and the average pore width could be roughly calculated from the BET surface area and the total pore volume. The adsorptive property of the activated carbon in liquid phase was determined by iodine and methylene blue adsorption capacities. The surface functional groups of the obtained samples were determined by Fourier transform infrared (FTIR) analysis using FT-IR (SPECTRUM ONE brand). The wave number was varied between 4000 and 450 cm^{-1}. The micro-structural morphology was investigated using the Transmission electron microscopy (TEM) (A JEM 100s, an FEI Tecnai G2 Spirit and an FEI Tecnai F20 X-Twin at 200 kV FEG with an Oxford EDS system). For TEM analysis, all samples were ultrasonically suspended in the methanol and a drop of the suspension was transferred to a copper grid and allowed to dry before the TEM analysis. XRD was also carried out to study of crystalline structure of the carbon using the diffractometer Bruker D8 X-ray FOCUS. Raman spectroscopy is often used to reveal fine structural information of the carbon material. In this work Raman spectra were obtained with a T6400 Raman Spectrometer (JOBIN/YVON).

Batch Equilibrium Experiments

The adsorption equilibrium studies were performed using isotherm technique. 10 mg of the adsorbent were mixed with 100 mL of each aqueous solution (4-chlorophenol and 2-nitrophenol) with initial concentration in the range of (11-72 mg/L). Each solution was shaken vigorously at the rate of 200 rpm at room temperature for 4 hours. At the end of the adsorption process, the solutions were filtered and the equilibrium concentrations were determined by spectrophotometric analysis. Q_e the quantity of phenolic compounds adsorbed per gram of adsorbent was determined using the following formula:

$$\boldsymbol{Q_e = (C_0 - C_e)V/m} \quad \ldots\ldots\ldots\ldots\ldots\ldots\ldots\ldots\ldots\ldots (1)$$

where, C_0 and C_e are respectively the initial and equilibrium concentration (mg/L), of phenolic compounds in solution; V the volume (L), and *m* is the weight (g) of the adsorbent.

RESULTS AND DISCUSSION

The polyethylene terephthalate (PET) from post-consumer soft drink bottle was used as the raw material for the production of an adsorbent. After the carbonization process, the samples were first subjected to physical activation with two different residence time and then different burn-off which lead to the ACs, PET1 and PET2. Another sample PETA was prepared by the physico-chemical activation process. The burn-off and the yield of activated carbons are listed in Table 1. It can be seen that the activated carbons obtained from post-consumer plastics give a low yield; this is directly due to the structure of raw material. The raw material is constituted of volatile compounds which escape during the carbonization, the departure of volatile compounds leaves pores, which are developed during activation process (Harry Marsh, 2006) The burn-off shows that the sample PET1 and PETA are micro and mesoporous (burn-off between 50-70%), for PET2 the burn off is less than 50% mainly microporous. This can be explained by the higher degradation of the material by steam water during the activation process.

Characterization of activated carbon

The characterization is an important tool that helps to understand the properties of carbon that may affect the removal of micro pollutants in aqueous solution. The Figure 1 shows typical N_2 adsorption-desorption isotherms of the activated carbons obtained from both physical activation and physic-chemical activation. All the samples exhibited the development of both micropores and mesopores. We observed an inflection at low relative pressure $P/P^o > 0.1$ and at high relative pressure of $P/P^o > 0.9$ where extents of adsorption rise very rapidly. The differences in the shape of the three isotherms are not very significant at relative pressure $P/P° < 0.9$. The samples presented greater adsorption capacities at low pressures, indicating the presence of a more developed micropores structure. The sample obtained from physico-chemical activation PETA exhibited a higher quantity of mesopores (63.45%), they allow the rapid filling of micropores before the beginning of filling by capillary condensation in mesopore. According to the IUPAC classification (Goyal, 2005), these activated carbons can be described under type II isotherm with type H3 hysteresis, which is associated with a narrow pore size distribution of microporous material. For all the samples the pronounced intensity of hysteresis implies the presence of a more extensively developed pore network wherein the fraction of larger pores trapped within the network of smaller pores is much higher

Table 1. Characteristics of different ACs obtained and their adsorptions test capacities.

Activated carbons	Activation time (hours)	Yields (%)		Burn-off (%)	$Q_{(ads)}$MB (mol/g)	$Q_{(ads)}I_2$ (mol/g)
		Carbonization	Activation			
PET1	*2*	15	65,46	61.4	272.8	1110,4
PET2	3	15	61.4	38.6	386.0	1237,3
PETA	2	15	33,33	67.6	276 .0	1181.8

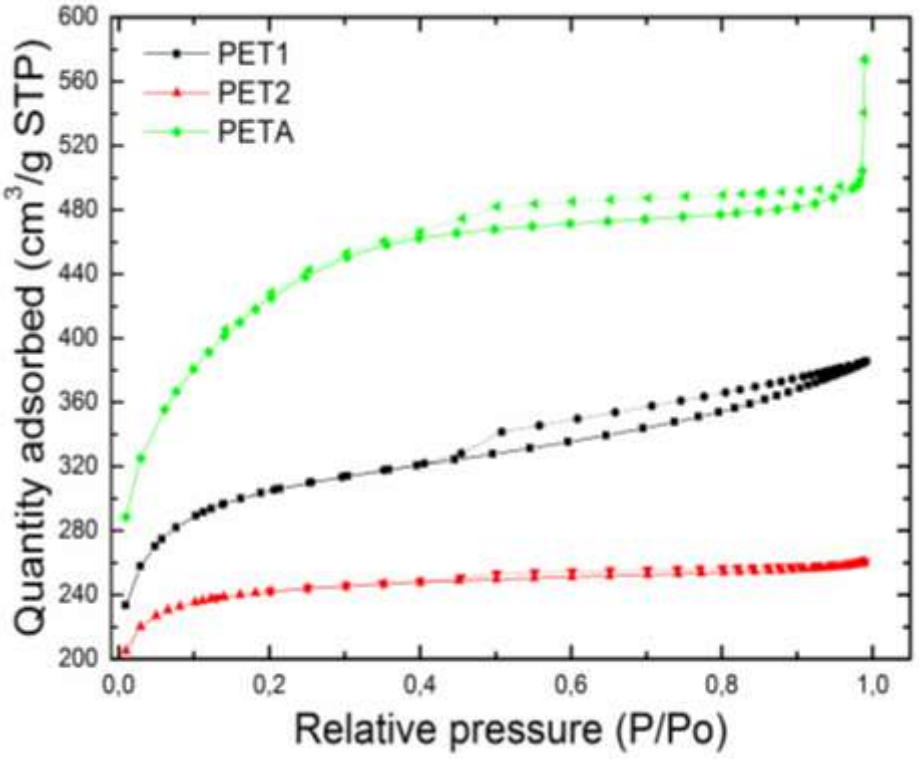

Fig. 1. Adsorption–desorption N_2 isotherm of ACs prepared by physical activation at 800°C under H_2O flow and by physico-chemical activation at 850°C using KOH under H_2O flow.

Table 2 shows that sample prepared by physico-chemical activation PETA presents higher surface area (1412.9 m^2/g) compared to those obtained by physical activation. This means that impregnation of carbonation material with KOH increases considerably the formation of pore network into the carbon. But in the depth analysis, the percentage of micropores in sample PET2 is higher, this means that the increase of the residence time during the activation process opens the external pores and gives access to more micropores, this is shown well by the transmission electron microscopy (TEM) images (Fig. 2). The average pore diameters were between 1.9 nm and 2.4 nm, indicating its microporous character. It appeared that all the samples of activated carbons were predominantly microporous.

The FTIR is mainly used for the study of the surface chemical functional groups on activated carbon. The carbon materials are black materials thus they absorb the radiations almost in the visible spectrum and the peaks obtained in the FTIR are commonly a sum of interactions of different types of groups. The Figure 3 shows the FTIR spectra of carbons prepared by physical and physico-chemical activation with nitrogen atmosphere and by impregnation with KOH, respectively. The samples show the band around 3437 cm^{-1} assigned to the O–H stretching mode of hydroxyl groups and adsorbed water. The spectra show that for carbon obtained by impregnation with KOH the degree of oxidation enhances absorption bands at 1563 cm^{-1}, 1082 cm^{-1} and even at 3437 cm^{-1}. The 1563 cm^{-1} band observed only on PETA spectrum is attributed to aromatic structures, also at unconjugated carbonyl groups obtained after acetylating of C–C with KOH. The 1082 cm^{-1} can be attributed to C–O vibrational stretch.

Raman spectra of PETA sample (Fig. 4) obtained from physico-chemical activation show a line at 1350 cm^{-1} in addition to the line near 1600 cm^{-1}. It has been shown that the peak at 1600 cm^{-1} named G-band (G = graphite) corresponds to an E2g mode of hexagonal graphite and is related to the vibration of sp2 hybridized carbon networks in a graphite layer. The D-band (D = disorder) at about 1343 cm^{-1} is due to the breathing modes of six-atom rings and requires a defect for its activation. The presence of defects improves the performance of carbon materials because of the high anisotropy of the mechanical strength or the electrical conductivity between the in-plane and out-of-plane direction.

The diffractograms of sample PETA is shown in Figure 5. The XRD spectra of AC sample exhibits an intense peak at $2\theta = 36.27°$. This peak is assigned to the turbostratic structure of the carbon.

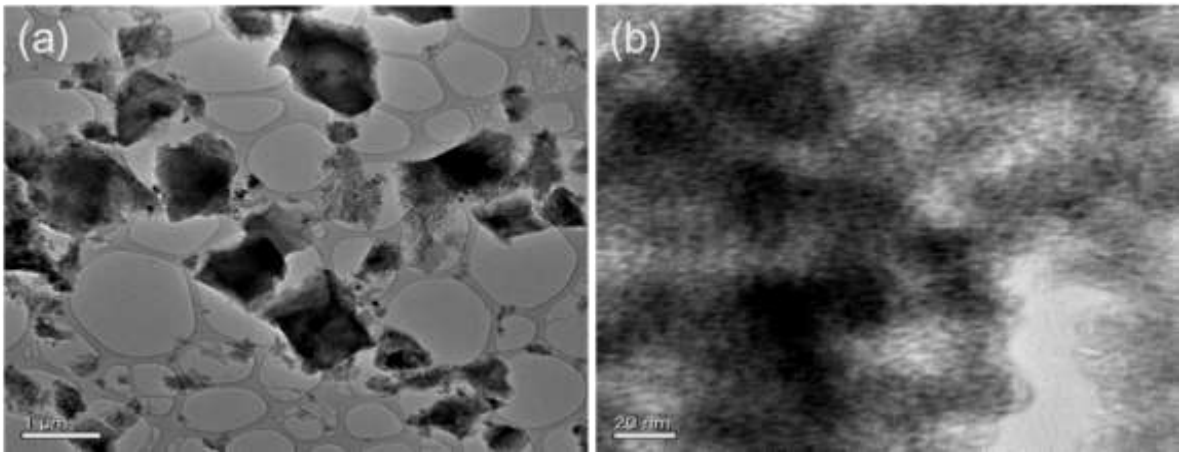

Fig. 2. Higher and low magnification TEM image of AC prepared by physical activation PET2: (a)at 1 µm **(b)** at 20nm.

Table 2. Porous parameters of the activated carbons.

Samples	$^{a}S_{BET}$ (m^2/g)	$^{b}S_{Langmuir}$ (m^2/g)	$^{c}S_{mic}$ (m^2/g)	$^{d}S_{ext}$ (m^2/g)	Pores sizes (nm)				Pores Volumes (cm^3/g)
					BET_{ads}	BJH_{des}	BJH_{ads}	V_{mic}	v_{cum}
PET1	1063.5	1293.934	753.9	309.6	2.238	4.190	3.874	0.335	0.595
PET2	849.2	1041.815	703.268	145.891	1.8929	3.095	3.331	0.3104	0.4018
PETA	1412.9	1566.70	516.714	896.144	22.084	36.253	37.252	0.2634	0.4553

[a]BET surface ; [b]Langmuir surface ; [c]micropore surface ; [d]External surface

SEM analysis of the activated carbons

The Scanning electron microscopy (SEM) technique was used to observe the morphology of the surface of the activated carbon obtained from plastics. The Figure 6 shows the cavities of different sizes and different shapes on the external surface of carbons.

Application of prepared activated carbon to liquid phase adsorption

Adsorption isotherms

The equilibrium adsorption isotherms are usually used to determine the relationship between liquid phase and the adsorbents. The Figure 7 shows adsorption isotherms of 4-clorophenol and 2-nitrophenol on the three samples of activated carbon PET1, PET2 and PETA. The shape of the 4-chlorophenol and 2-nitrophenol adsorption isotherms appears to be type I characteristic of a medium containing mainly micropores. The isotherms show rapid adsorption at the beginning for all the samples, the number of adsorption sites available reduces when the concentration of the phenolic compound increases, indicating that there is a strong adsorption between the active sites of the activated carbon and the molecules of phenolic compounds. The amount adsorbed steadily increases and the adsorption isotherms display a plateau indicating the formation of a complete monolayer. It can be seen that the highest uptake was obtained for PETA, which is normal because PETA has larger surface area with an important quantity of mesopores which act like gateway for micropores. The higher adsorption of phenolic compounds on PETA can also be attributed to the higher quantities of functional groups on the surface, mainly carbonyls functions which may establish the hydrogen bonds with OH function of phenolic compounds.

The experimental data were simulated with the Langmuir ($\boldsymbol{1/Q_e = 1/q_m kC_e + 1/Q_m}$) and Freundlich ($\boldsymbol{lnQ_e = lnK_F + lnC_e}$) models (Figs. 8 and 9), where Q_e(mg/g) is the adsorption density at the equilibrium, C_e is the equilibrium concentration of adsorbate in solution (mg/L), $Q_{max}$is the maximum adsorption capacity corresponding to complete monolayer coverage, K_L is the Langmuir constant related to energy of adsorption (L/mg), K_F is the Freundlich constant, 1/n is the heterogeneity factor which is related to the capacity and intensity of the adsorption.

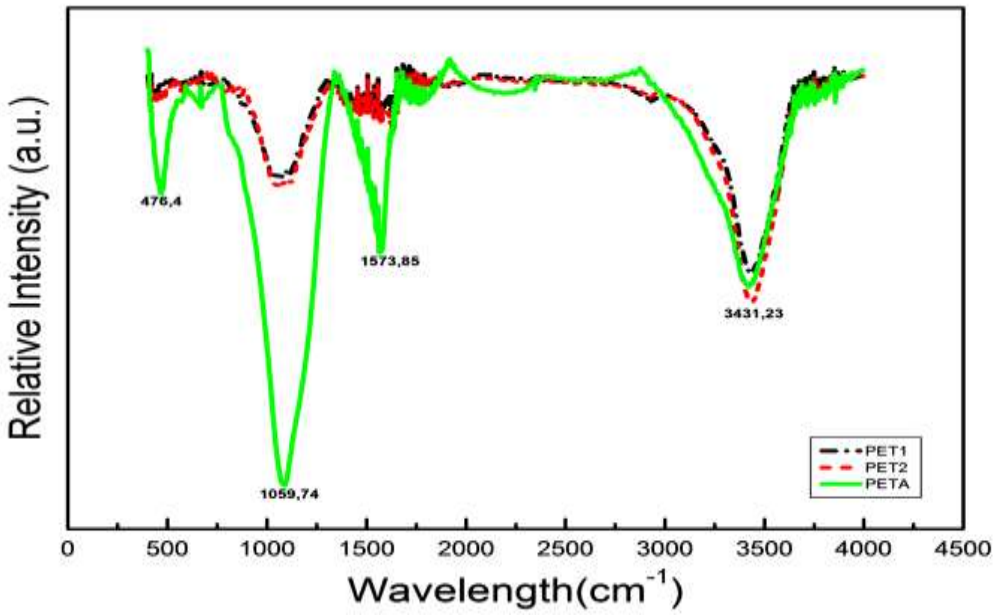

Fig. 3. FTIR spectra of three Activated Carbons obtained by physical activation and physico-chemical activation.

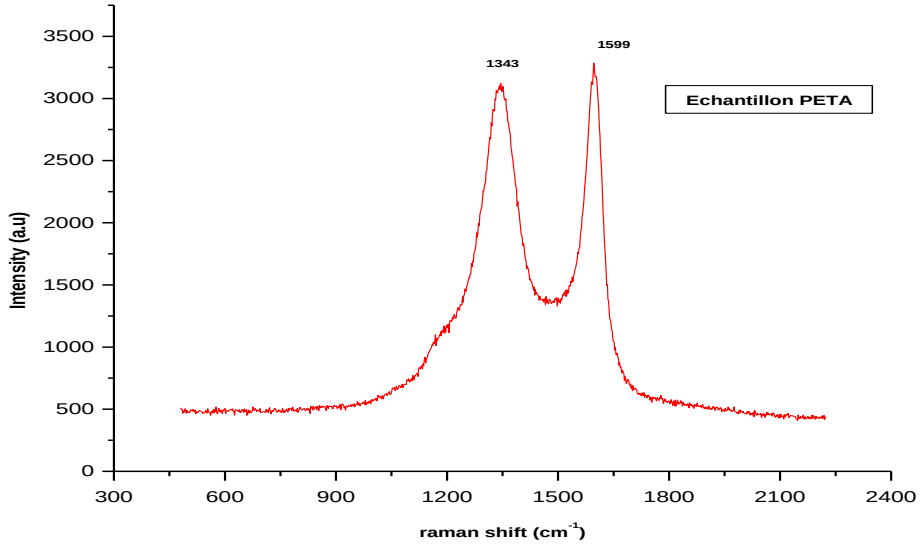

Fig.4.The Raman spectrum of PETA sample prepared by physico-chemical activation showing disordered sp2 bonded graphite.

The Table 3 provides a compilation of the main parameters obtained from the fittings to both equations, along with the correlation coefficients. The constant of Langmuir, K_L measures the intensity of adsorption. In fact, the higher the K_L value the stronger the affinity between the phenolic compounds and the activated carbon. Thus, it comes out from results that PET1 has stronger affinity for 4-Chlorophenol adsorption than PET2 and PETA. In contrast the sample PETA prepared by physico-chemical activation has stronger affinity for adsorption of 2-nitrophenol than PET2 and PET1. Despite the values obtained for constants K_L, the values of the monolayer adsorption capacity (Q_m) of PET1 is larger than PET2 and PETA for 2-nitrophenol adsorption, as already noticed for values of K_L, this values of Q_m is in contrast larger for PETA than PET2 and PET1 for 4-chlorophenol adsorption. This can be explained by the fact that the sample PETA has a great amount of micropores and the existent of mesopores act only as the gateway of micropores (the functional group at the

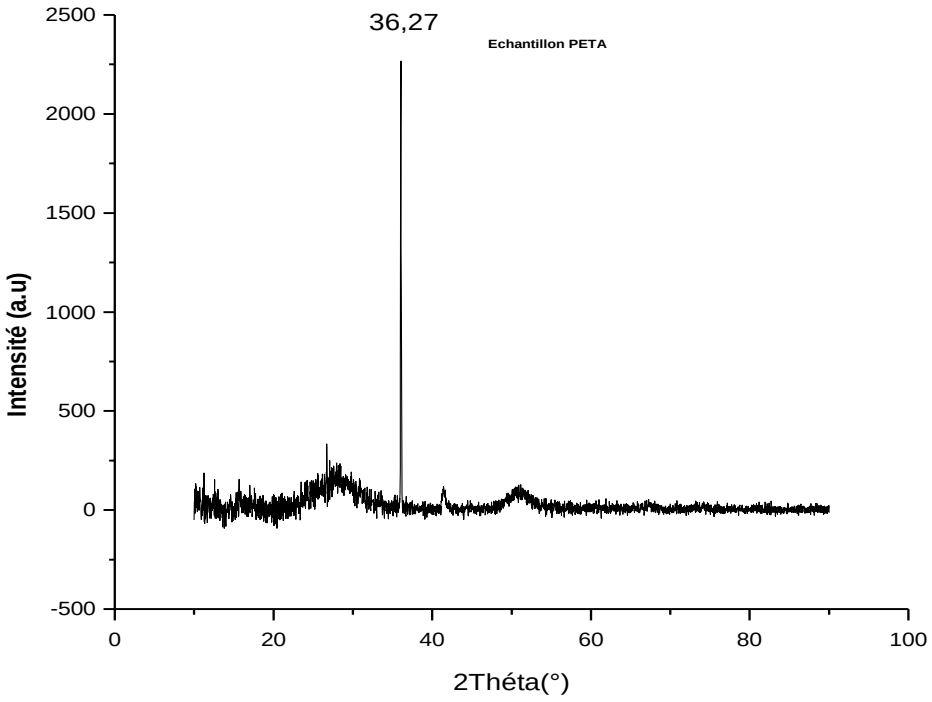

Fig. 5. X-ray diffractogram for activated carbon obtained by physico-chemical activation (PETA).

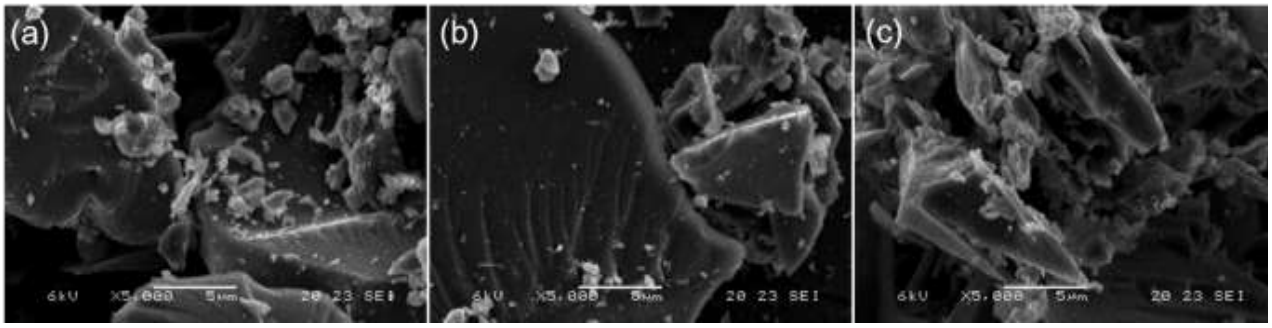

Fig. 6. SEM images of the three Activated Carbons: (a) PET1, (b) PET2 and (C) PETA.

surface of activated carbon). In addition, the linear correlation coefficients R^2 for this model are all higher than 0.96 making the Langmuir model suitable to explain the adsorption of micropollutants onto activated carbon prepared from post-consumer plastics.

The values of the Freundlich constants n lie between 1 and 10 and vary in the interval 1.107 - 4.098 showing that the phenolic compounds adsorption on the activated carbon is favourable. However, the Freundlich model has values of correlation coefficient lower than 0.96, which restricts the utility of the model to describe the phenolic compounds adsorption on these samples.

CONCLUSION

The adsorption capacities of three activated carbons obtained from post-consumer plastics using both physical and physico-chemical activation for the removal of phenolic compounds were investigated. The characterization of the materials revealed that the adsorption of phenolic compounds is favorable and depends of the structure of adsorbent. It was observed that there are good interactions between the adsorbate and the adsorbent. The adsorption capacity was higher for the sample PETA prepared by physico-chemical activation compared to others obtained by physical activation, due to higherquantity of hydroxyl and carboxylic functional

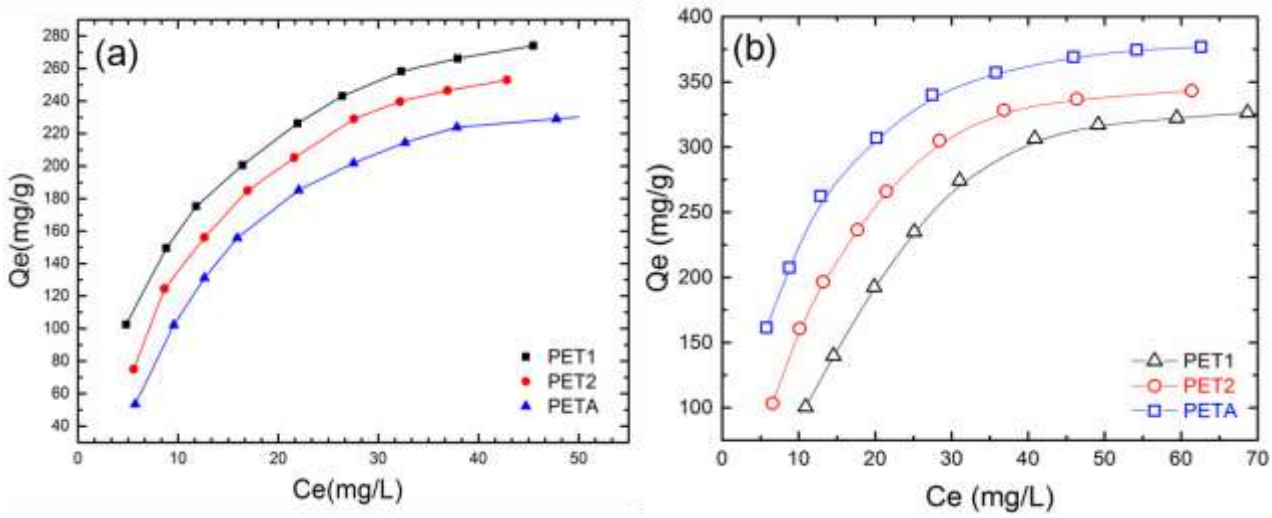

Fig. 7. Adsorption isotherms of (a) 4-chlorophenol and 2-nitrophenol on the three ACs samples from PET wastes.

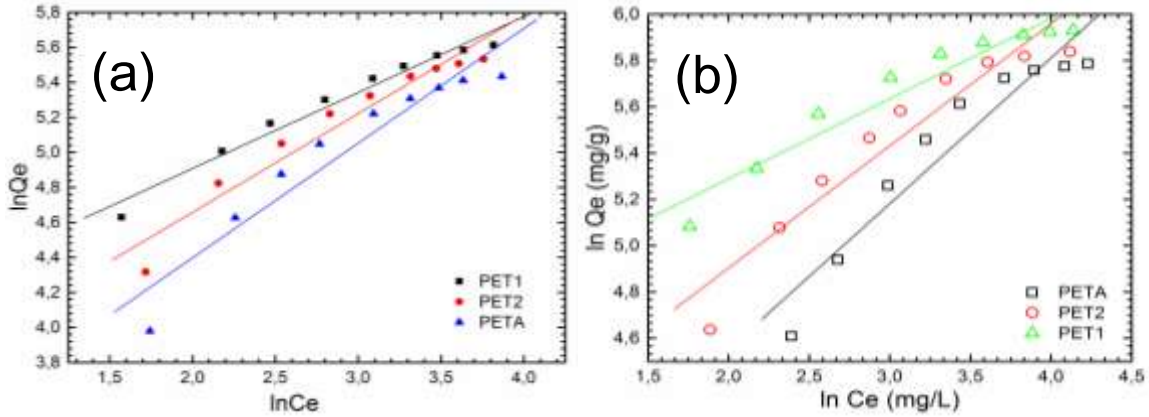

Fig. 8. Linear transforms of Langmuir isotherm for (a) 4-chlorophenol and 2-nitrophenol on the three samples of AC from post-consumer plastics.

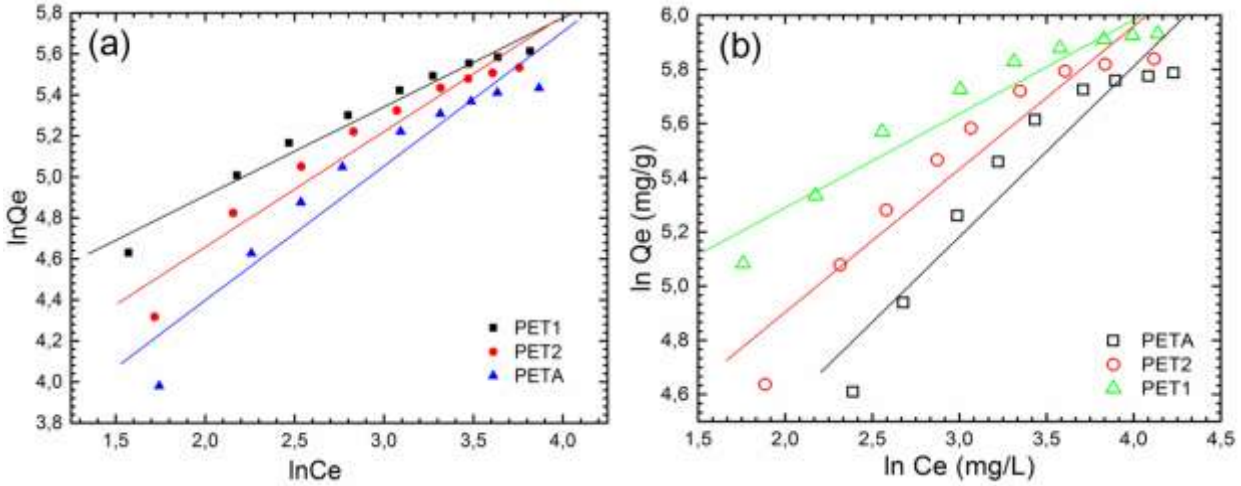

Fig. 9. Linear transforms of Freundlich isotherm of (a) 4-chlorophenol and 2-nitrophenol on the three samples of AC from post-consumer plastics.

Table 3. Fitting parameters of the equilibrium adsorption isotherms to the Langmuir and Freundlich models.

Adsorbates	Adsorbents	Langmuir			Freundlich		
		K_L	Q_m	R^2	K_F	1/n	R^2
2-nitrophenol	PET1	0.01361	826.446	0.983	26.936	0.6296	0.952
	PET2	0.03288	609.756	0.989	46.894	0.5280	0.953
	PETA	0.09491	458.716	0.998	99.066	0.3467	0.943
4-chlorophenol	PET1	0.08756	344.828	0.9998	56.818	0.4339	0.985
	PET2	0.03828	450.451	0.988	34.174	0.5632	0.970
	PETA	0.01648	666.667	0.981	21.891	0.6555	0.956

groups on the surface that interact with adsorbate. Therefore, the ACs prepared are mainly microporous with a greater adsorption capacity thus they can be used as low-cost adsorbents and as an alternative for environmental pollution remediation.

ACKNOWLEDGEMENTS

The authors are grateful to University of Maroua, Cameroon for financial support.

REFERENCES

Arenillas, A., Parra, JB., Ania, CO. and Pis, JJ. 2005. Surface modification of low cost carbons for their application in the environmental protection. Applied Surface Science. 252:6. oi:10.1016/j.apsusc.2005.02.076.

Ahmedna, M., Johns, MM., Clarke, SJ., Marshall, WE. and Rao, RM. 1997. Potential of Agricultural By-Product-Based Activated Carbons for Use in Raw Sugar Decolourisation. J Sci Food Agric. 75:8.

Ania, CO. and TJB. 2006. Metal-loaded polystyrene-based activated carbons as dibenzothiophene removal media via reactive adsorption. Carbon. 44(9):2404–2412. doi:10.1016/j.carbon.2006.05.016.

Ania, CO., Pevida, BC., Arenillas, A., Parra, JB., Rubiera, F. and Pis, JJ. 2007. Removal of naphthalene from aqueous solution on chemically modified activated carbons. Water Research. 41:8. doi:10.1016/j.watres.2006.10.016

Bharathi, KS. and Ramesh, ST. 2013. Removal of dyes using agricultural waste as low-cost adsorbents: a review. Appl Water Sci. 3:773. doi. 10.1007/s13201-013-0117-y.

Boumaza, S., Kaouah, F., Berrama, T., Trari, M. and Bendjama, Z. 2012. Optimization of preparation conditions for activated carbon from waste materials of agricultural origin for the removal of basic red 46. Chemometrics and Intelligent Laboratory Systems.118:311-316.

Carvalho, AP., Cardoso, B., Pires, J. and Brotas de Carvalho, M. 2003. Preparation of activated carbons from cork waste by chemical activation with KOH. Carbon 41(12):2873-2884.

CPC, P. 1986. Removal of cadmium from wastewaters. In: Cadmium in the environment. Eds. Mislin, H. and Ravera, O. Basel. Birkhauser, Switzerland. 46-55.

Harry, M. and Francisco, RR. 2006. Activated Carbon. Elsevier Science & Technology Books. 36-52.

Huang, H., Luo, L., Zhang, Hua, Lu, Y. and Zhang, D. 2014. Adsorption of Congo red from aqueous solutions by the activated carbons prepared from grapefruit peel. Applied Mechanics and Materials. 529:5.

Kiyoshi Okada, NY., Yoshikazu, K. and Atsuo, Y. 2003. Adsorption properties of activated carbon from waste newspaper prepared by chemical and physical activation. Journal of Colloid and Interface Science. 262:6.

Kartel, MT., N, VS., Tsyba, MM. and Strelko, VV. 2006. Preparation of porous carbons by chemical activation of polyethyleneterephthalate. Carbon, 441013-1024. doi:10.1016/j.carbon.2005.10.031

Kurniawan, TA., Lo, WH. and Sillanpää, ME. 2011. Treatment of Contaminated Water Laden with 4-Chlorophenol using Coconut Shell Waste-Based Activated Carbon Modified with Chemical Agents. Separation Science and Technology. 46:13.

Laszlo, K., Bota, A. and Nagy, LG. 1997. Characterization of activated carbons from waste materials by adsorption from aqueous solutions. Carbon. 35(5)6:593-598.

Leelavathy, KR., Nageshwaran, V. and Bharathi, M. 2015. Comparative Study on Commercial and Corn Cobs Activated Carbon for Removal of Congo Red Dye. Applied Mechanics and Materials. 787:5.

Miroslaw Marzec, BT., Ryszard, JK. and Antoni, WM. 1999. Poly(ethylene terephthalate) as a Source of Activated Carbon. Polym. Adv. Techno. 10:8.

Mui, ELK., Ko, DCK. and McKay, G. 2004. Production of active carbon from waste tyres – a review. Carbon 42:2789-2805.

Namasivayam, CKD. 2002. Removal of Congo Red from water by adsorption onto activated carbon prepared from coir pith, an agricultural solid waste. Dyes and Pigments, 54:12.

Nameri, N., Aioueche, F., Belhocine, D., Grib, H., Lounici, H. Piron, DL. and Yahiat, Y. 2000. Preparation of activated carbon from olive mill solid residue. J Chem Technol Biotechnol. 75:7.

Önal, Y. 2006. Kinetics of adsorption of dyes from aqueous solution using activated carbon prepared from waste apricot. Journal of Hazardous Materials. 137:12.

Parra, JB., Arenillas, A., Rubiera, F., Palacios, JM. and Pis, JJ. 2004. Textural development and hydrogen adsorption of carbon materials from PET waste. Journal of Alloys and Compounds. 379:280-289. doi:10.1016/j.jallcom.2004.02.044.

PoedjiLoekitowati Hariani, M. F., Ridwan, Marsi. and Dedi, S. 2013. Characterization of Activated Carbon from Oil Palm Shell Prepared by H3PO4 for Procion Red Dye Removal. Applied Mechanics and Materials. 391:51-55.

Roop, CB. and Goyal, Meenakshi, G. 2005. Activated carbon adsorption. Taylor & Francis Group. 11-41.

Stavropoulos, GG. and Z, AA. 2005. Production and characterization of activated carbons from olive-seed waste residue. Microporous and Mesoporous Materials. 82:7.

Tamon, H. 1998. Preparation of activated carbon from city wastes. Kemikaru Enjiniyaringu. 43(9):6.

Tonni Agustiono Kurniawan, GYS. C., Wai-Hung Lo. and Sandhya, B. 2006. Physico–chemical treatment techniques for wastewater laden with heavy metals. Chemical Engineering Journal. 118:16.

Xiangzheng Yuan, XS., Shujuan Zeng. and Yueli, W. 2011. Activated carbons prepared from biogas residue: characterization and methylene blue adsorption capacity. J Chem Technol Biotechnol. 86:6.

Received: Oct 11, 2016; Revised: Nov 7, 2016; Accepted: Nov 11, 2016

Canadian Journal of Pure and Applied Sciences
Vol. 11, No. 1, pp. 4141-4149, February 2017
Online ISSN: 1920-3853; Print ISSN: 1715-9997
Available online at www.cjpas.net

TOTAL ELECTRON CONTENT VARIATIONS DURING DIFFERENT GEOMAGNETIC ACTIVITIES IN ILE-IFE, NIGERIA

EI Akintufede[1], *LG Olatunbosun[2], AO Olabode[1], AB Babinisi[1] and EA. Ariyibi[1]
[1]Department of Physics and Engineering Physics, Obafemi Awolowo University, Ile-Ife, Nigeria
[2]Department of Science and Technology, Federal Polytechnic, Ado-Ekiti, Nigeria

ABSTRACT

GPS-derived vertical Total Electron content (TEC) recorded at Ile-Ife (Mlat. 7.52^{o}N and Mlong. 4.28^{o}E), Nigeria during the year 2011 for different geomagnetic activities was analyzed to investigate TEC variations. The results showed that TEC exhibit diurnal and seasonal variations, with equinoctial season recording the highest TEC during the daytime maximum. Winter anomaly was absent. Comparative results revealed that IRI-2012 underestimates measured TEC during the different geomagnetic activities in Ile-Ife. An average value of about 40% deviation between the modeled and measured TEC was obtained during moderate and intense geomagnetic activities, while that during low geomagnetic activities was about 11%.

Keywords: Equatorial ionisation anomaly, vertical TEC, global positioning system, international reference ionosphere.

INTRODUCTION

The ionosphere is an important error source for the signal of the Global Positioning System (GPS).GPS satellites are at an altitude of about 20,200km and transmit signals through the ionosphere to the receiver on the earth surface. As the global positioning system signal propagate through the ionosphere, the carrier experiences a phase advance and the code experiences a group delay due to total number of free electrons along the path of the signals from the satellite to the receiver. The ionospheric effects during geomagnetic activities on navigational control application, satellite tracking, positioning and communication and time information depends on the variations in the Total Electron Content (TEC) in the ionosphere. The TEC provides an overall description of the ionization in the ionosphere during different geomagnetic activities and so forms important ionospheric parameters for several practical purposes.

The extensive study of the geomagnetic activities in the ionosphere has revealed the primary physical mechanisms responsible for generating the large disturbances that are observed to occur in the ionosphere. Ariyibi *et al*. (2013b) interpreted the data records in Ile-Ife station (TEC and S4 index) from 4 - 6 April, 2010 and used it to study the effects of geomagnetic storms on TEC in African ionosphere and the scintillation variations during the storms. The ionospheric condition during low geomagnetic activity period and their seasonal dependence was also discussed. The dependence of TEC on level of geomagnetic activity, time and seasons of the year was observed. TEC was enhanced during the daytime and was highest during the equinoctial months. Scintillation occurrence was closely linked to TEC depletion and not necessarily geomagnetic storms in the station. Olatunbosun and Ariyibi (2015) also combined GPS data from three stations of Ile-Ife, Addis Ababa and Bangalore to draw comparative results in TEC variations in the stations. It was found that Ile-Ife station had the least diurnal and seasonal TEC variations. Jimoh *et al.* (2016) also used GPS data obtained from Ile-Ife to study the effect of geomagnetic storm on TEC variations. It was observed significant enhancement in TEC during geomagnetic storms. Fayose *et al*. (2012) studied the diurnal and seasonal variations of vertical TEC at Akure, Nigeria using GPS data. They observed that the mean TEC varies from pre-dawn minimum to a maximum during the afternoon and then decreases. The low values of TEC are observed in winter and high values observed in equinox.

Among the different sources of global positioning system positional errors, ionospheric delay, which is proportional to the TEC, is the highest contributor. Therefore in order to get better accuracy, it is necessary to have a precise knowledge of the accurate value and the variations of the TEC measured at different geomagnetic activities. This research work therefore studies the variations of TEC during different geomagnetic activities in low latitude

*Corresponding author e-mail: lilianola@yahoo.com

station over Ile-Ife. The measured TEC was compared with modelled TEC for better reproduction of IRI models.

MATERIALS AND METHODS

Methodology

The data obtained from the dual frequency SCINDA NovAtel GSV 4004B GPS receiver installed at Department of Physics and Engineering Physics, Obafemi Awolowo University, Ile- Ife, Nigeria (geographical Latitude 7º 33^1 N and Longitude 4º 33^1 E and geomagnetic dipole coordinate of Latitude 9.84ºN and Longitude 77.25ºE) were processed using GPS-TEC analysis software developed by Gopi (2010). The application gave the slant total electron content (STEC) which is dependent on elevation angle. The geomagnetic indices of Disturbance storm index (Dst) and planetary K index (Kp) obtained from World Data Center (WDC) for geomagnetism was used to identify and classify the storm events. The IMF-Bz and plasma speed (Vp) was used to describe the condition of the ionosphere. The model TEC data from International Reference Ionosphere (IRI) of 2012 version were obtained from OMNI web (omniweb.gsfc.nasa.gov/vitmo/iri_vitmo.html) for different geomagnetic conditions. These were plotted alongside the measured TEC for comparison. The location of the study area in the Nigeria map is shown in the Figure 1. It lies within the equatorial ionisation anomaly (EIA) zone.

The GPS receiver measures the pseudoranges using the coarse acquisition code on L_1 and the precise (P) code on L_2.The slant TEC (STEC) is obtained according to Langley (2000) and Fedrizzi *et al*. (2005). It is related to the calibrated $TEC_{BE}$and the dual frequency code measurements by:

$$STEC = \frac{1}{40.3} \times \left(\frac{1}{L_1^2} - \frac{1}{L_2^2}\right)^{-1} \times (P_1 - P_2) + TEC_{BE} \quad (1)$$

where P_1 = Pseudo range at L_1, P_2 = Pseudo range at L_2 and TEC_{BE} is the bias error correction, which is different for different satellite – receiver pairs (Bagiya *et al*., 2009). The vertical TEC (VTEC) therefore, is obtained by taking the projection from the slant to the vertical using the thin shell model assuming a height of 350km, following the technique given by Klobuchar (1986).

$$VTEC = STEC \times Cos\left[Sin^{-1}\left(\frac{R_E\, Cos\, e}{R_E + h_{max}}\right)\right] \quad (2)$$

where the radius of the Earth, R_e = 6378km, the height to the pierce point, h_{max} = 350km, and z = elevation angle at the ground station, as depicted in Figure 2. VTEC is in TEC units (TECu) and 1TECu = 10^{16} electrons/m^2.

RESULTS AND DISCUSSION

Classification of geomagnetic activities

The geomagnetic activities were classified as low, moderate, intense and quiet conditions. These classifications were informed based on the geomagnetic indices of Dst, Kp and Ap. While Dst index was used to identify the geomagnetic conditions, Kp and Ap indices were used to ascertain the level of severity of the geomagnetic activities. The summary of the classification of the geomagnetic activities considered in this paper is shown in Table 1.

Solar Interplanetary Condition

The condition of the ionosphere during the different geomagnetic conditions were investigated using ionospheric parameters of Interplanetary Magnetic Field of Z-component (IMF-Bz) and plasma speed (Vp), in conjunction with the geomagnetic indices. Figures 1 – 3 show the interplanetary conditions during the different classes of geomagnetic activities. The intense storm on 26 September and the moderate storm on 10 -11 March was marked with storm sudden commencement (SSC) when the IMF-Bz suddenly turned southward. A positive phase of IMF-Bz observed indicates compression in earth's magnetic field. This is an indication that the factors generating the positive phase have a bearing on the southward turning of the IMF-Bz. The plasma speed abruptly increased during the main phase of the storm. The ionospheric condition was different during the low storm event on 28 July, with IMF-Bz remaining northward and low value of plasma speed.

Rapidly decreasing IMF-Bz during the intense and moderate storms caused a sudden increase in polar cap potential, resulting in the generation of sudden region-1 currents which could not be shielded by the region-2 currents. This caused the high latitude electric potential (normally shielded by the region-2 currents) to reach the lower latitudes (Peymirat *et al*., 2000).

TEC variations

Diurnal variations of TEC

The diurnal variations of vertical TEC during the different geomagnetic activities were investigated using GPS- and IRI- derived TEC. In the day-to-day variations as represented in Figure 4, different geomagnetic conditions were represented. The results showed that TEC varies diurnally, with maximum values attained during the daytime (11:00 – 18:00 LT). The TEC variations were also found to be dependent on geomagnetic conditions, with enhanced TEC maximum corresponding to low Dst values. The results also revealed that IRI model underestimates the measured TEC in Ile-Ife station during all the geomagnetic conditions. The underestimation was more during the high geomagnetic activities, with average deviation of about 40%.

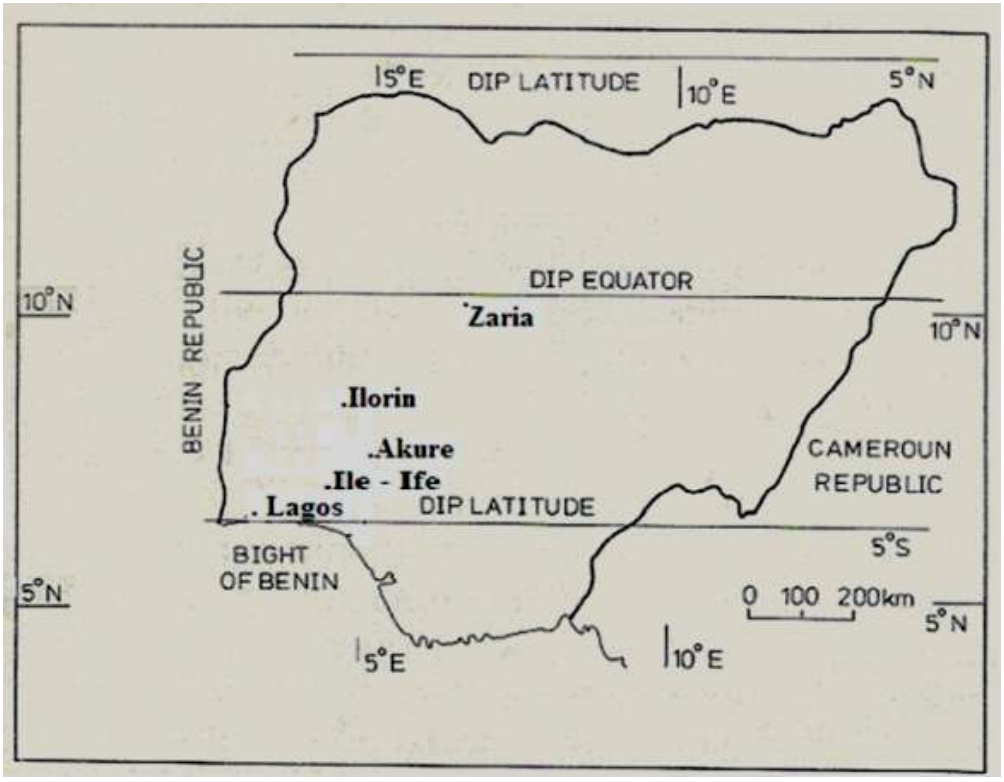

Fig. 1. Map of Nigeria showing the location of Ile-Ife GPS receiver station (After Ogunade, 1987).

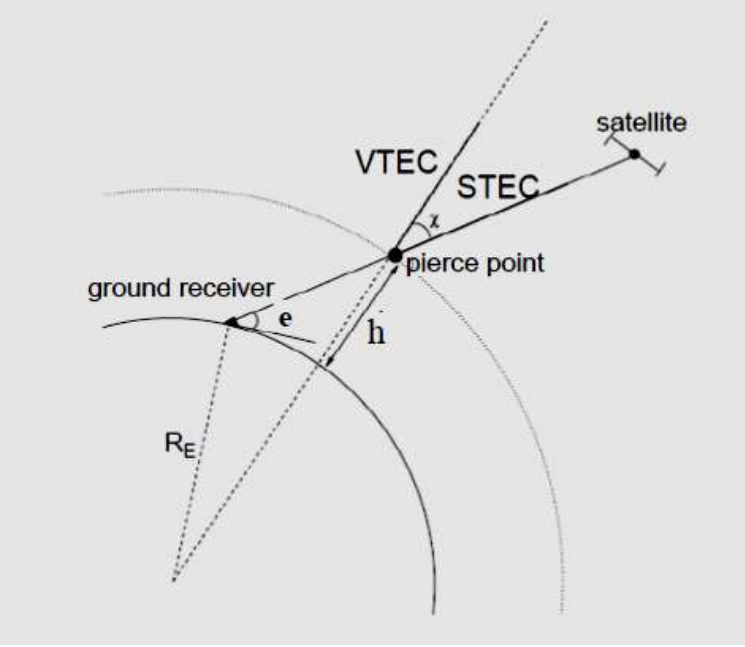

Fig. 2. Geometry for the conversion of slant TEC to vertical TEC.

Seasonal variations of TEC

TEC was further investigated for seasonal dependence. This was done by grouping the monthly mean into three seasons of Equinox (March, April, September and October), Winter (January, February, November and December) and Summer (May, June, July and August). From Figure 5, it was obvious that TEC variations were dependent on seasons of the year. The equinoctial season

Table 1. The classifications of geomagnetic activities in 2011 (From WDC Kyoto, Japan).

Days of the Year	Geomagnetic Indices			
	Maximum Kp	Dst (nT)	Maximum Ap	Class of storms
A. Disturbed days in 2011				
1. May 2nd	3 +4 4 +3 3 3 +3 +3	-49	18 27 32 15 15 1818 15	Low
2. March 10th 11th	2 2 +4 +4 -3 -2 4 5 5 5 +4 +2 2 -4 +5 6	-60 -83	9 32 22 12 7 27 39 56 32 7 6 32 48 67	Moderate
3. August 6th 4. September 26th 5. October 25th	6 +5 4 -4 4 -3 +1 +3 1 +1 -7 +6 -5 -3 3 2 1 +1 1 1 +5 -6 +6 +5	-107 -101 -132	94 48 22 27 22 18 5 15 5 3 4 5 39 94 94 56 154 67 39 15 15 7 5 3	Intense
B. Quiet Day in 2011				
1. July 28th 2. August 4th	1 -1 +0 +0 +0 +0 +1-1	≤-3 ≤-4	3 5 2 2 2 2 3 5	Quiet

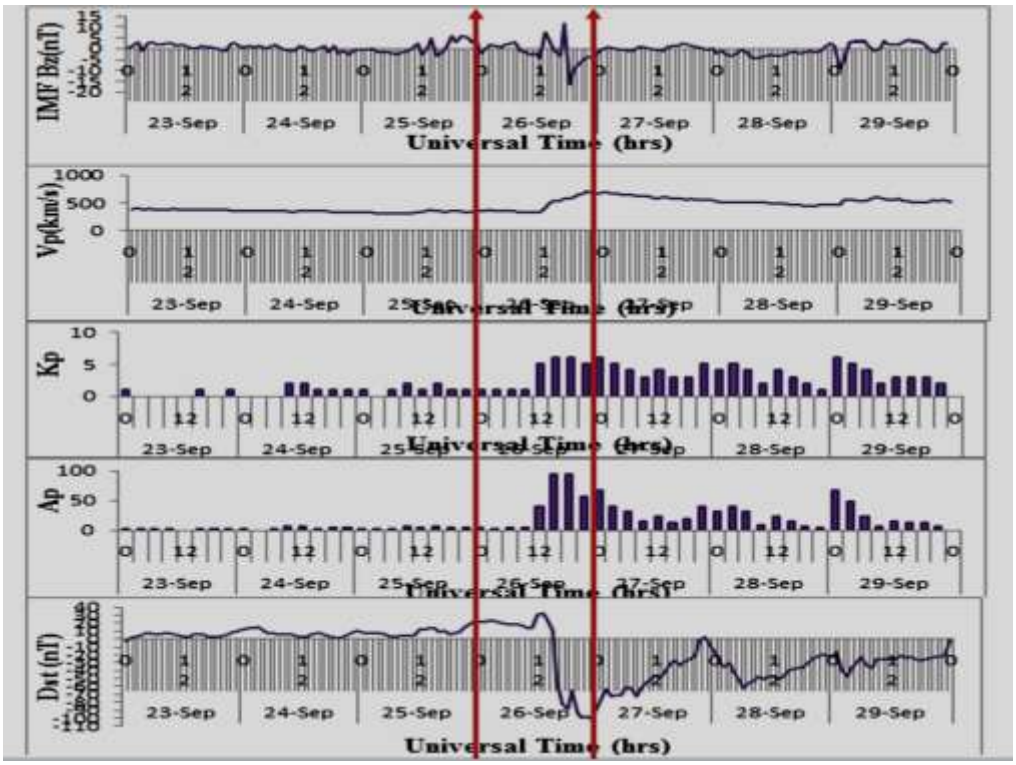

Fig. 1. Solar Interplanetary Condition for intense storm on 26 September 2011.

recorded the highest value of TEC during the daytime plateau, followed by the summer and winter seasons. The seasonal variation of TEC can be explained using thermospheric neutral composition phenomenon. Rishbeth and Setty (1961) suggested that the seasonal changes result from changes in ratio of the concentration of atomic oxygen and molecular nitrogen in the F-region. During the daytime, the equator is hotter than the pole, therefore meridional wind flows towards the pole from the equator. This flow of meridional wind changes the neutral composition and O/N_2 decreases at equatorial and low latitude stations. The decrease is maxima in equinoctial seasons. Also, at 350 km altitude (F2-layer), N_2 dissociation is the major process which removes ambient electrons. Hence, the decrease in O/N_2 ratio will result in higher electron density and comparative results showed that IRI underestimates measured TEC during the daytime in all seasons. The IRI maximum TEC values are about 34, 32 and 24 TECu and GPS maximum TEC values are about 49, 35 and 35 TECu for equinox, summer and winter seasons, respectively. It became obvious that the underestimation was more during high geomagnetic activities, with equinox and winter seasons having the highest deviation of about 31% each, while the summer season recorded the least deviation of about 9%.

Many comparisons of observed F region parameters, such as TEC at low latitudes with IRI predicted values have

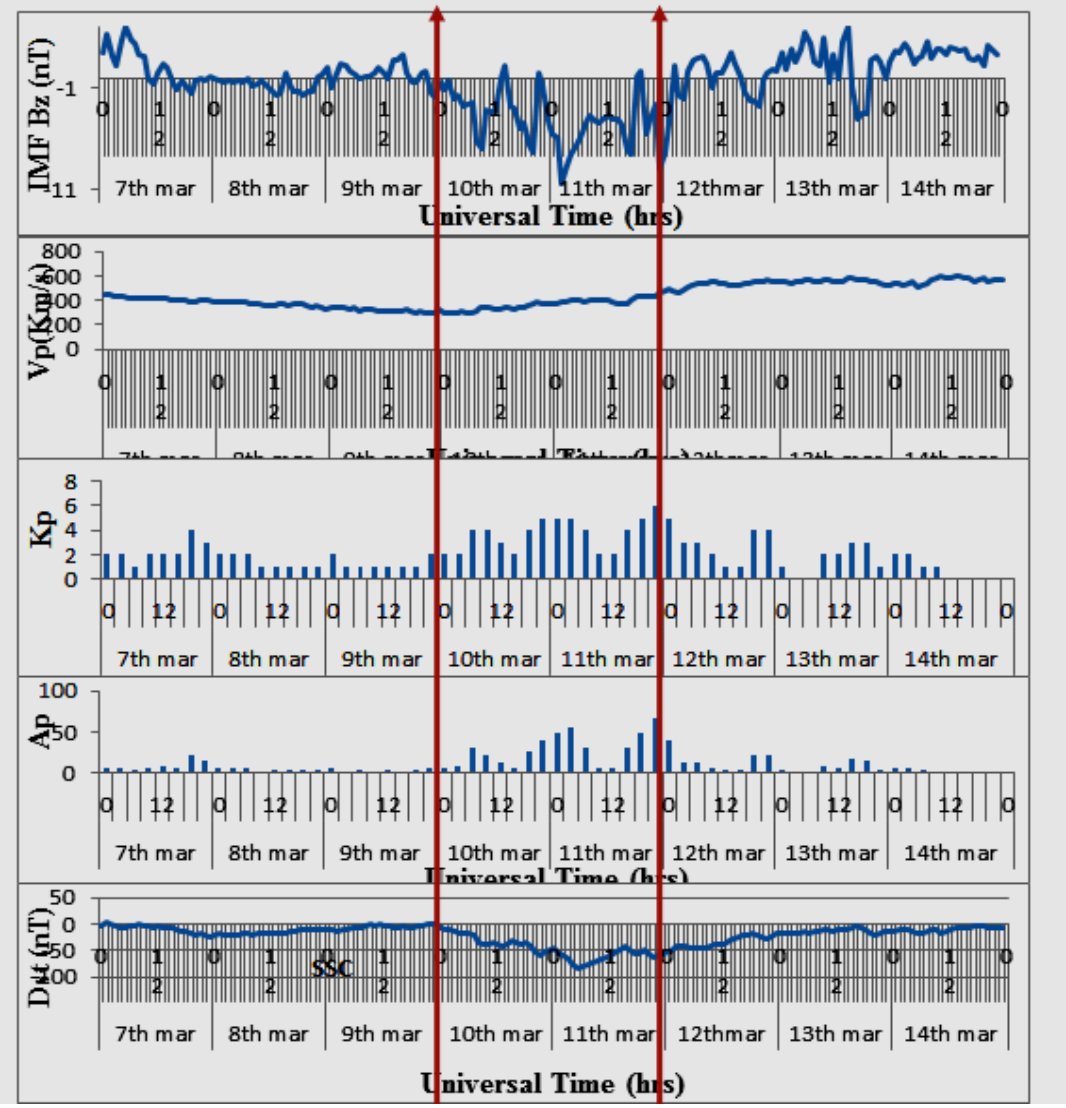

Fig. 2. The Solar Interplanetary Condition for moderate storm periods of 7-14 March, 2011.

been made by many research in different locations. For example, Ezquer *et al.* (1995) used GPS measurement over Tucuman (24.9°S, 294.6°E, geomagnetic latitude 15.45°S) during high solar activity year of 1982. Their results showed that IRI-90 overestimates the TEC measured over the station during hours of minimum TEC (00:00–10:00 LT) and underestimated it during hours of maximum TEC (12:00–18:00 LT). Also, Abdu *et al.* (1996) compared the IRI-90 predictions and observed F-region parameters, e.g., foF2, hmF2, and TEC for the equatorial anomaly region in the Brazilian sector. The results were also compared with those obtained from the Asian and Indian longitude sectors. They found that the TEC predicted by the IRI shows good agreement with observation at intermediate solar activities. IRI overestimates the TEC during solar minimum in the Brazilian and Asian longitude sectors. Contrarily, IRI tends to underestimate the anomaly region TEC during solar maximum in both longitude sectors. Shastri *et al.* (1996) made a study of the performance of the IRI-90 in the Indian sector from a comparison of foF2 observed at four locations and found that the IRI in general overestimates the observed peak density at all solar activity levels. The difference between observation and prediction varies with local time and location. On the other hand, Iyer *et al.* (1996) have shown that the IRI overestimates TEC during low solar activity and under estimates it in high solar activity at the crest of the anomaly both in the Indian and East Asian longitude sectors. However, this is the first comparative result of modelled TEC and measured TEC in Ile-Ife, Nigeria. Our result showed that IRI-2012 underestimates TEC during the different geomagnetic conditions and was more during high solar activities. The underestimation was during the

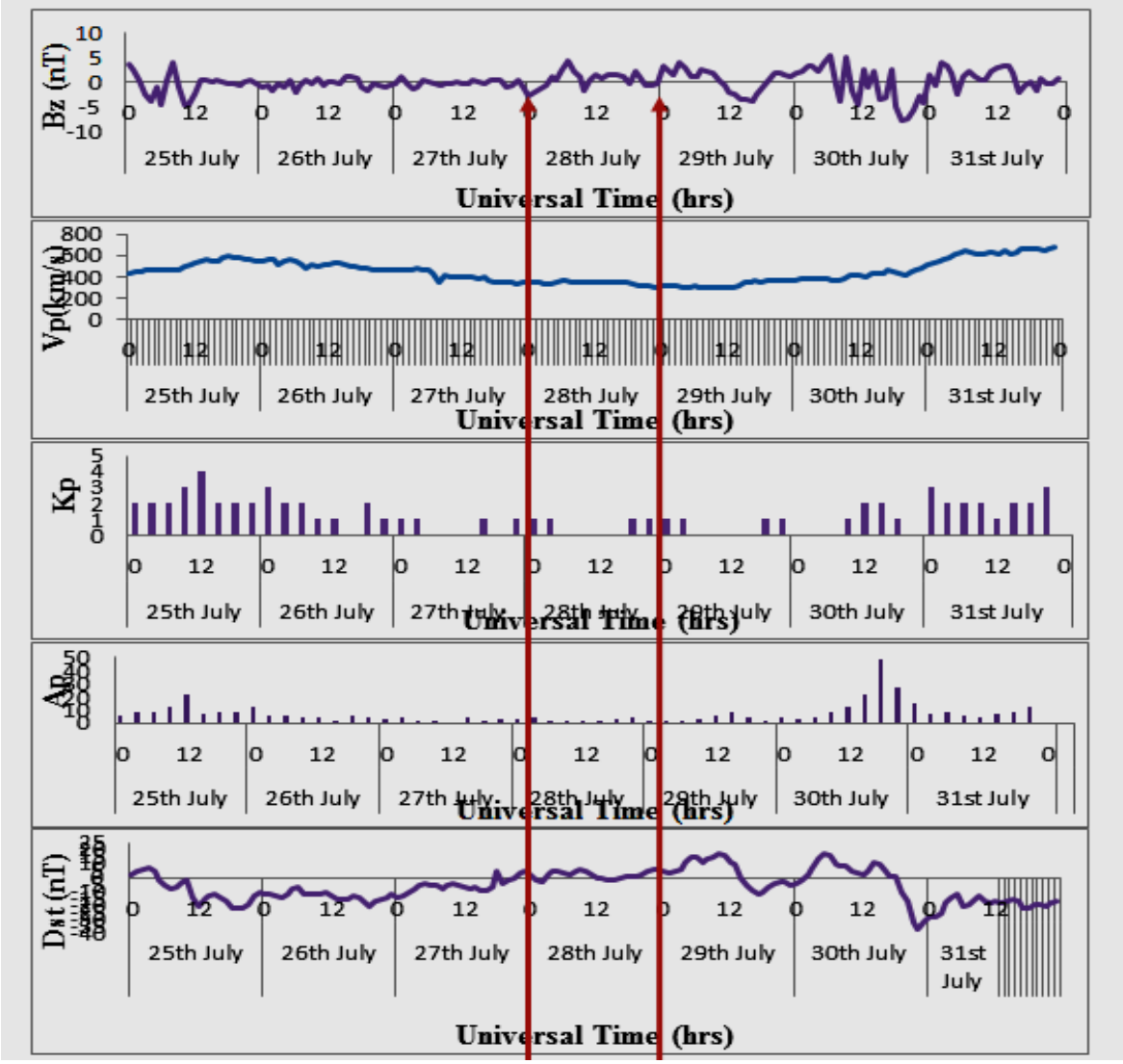

Fig. 3. The Solar Interplanetary Condition for quiet days from 25-31 July, 2011.

daytime plateau and the build-up region. However, it averagely overestimated the measured TEC during the decay region.

Correlation of TEC with geomagnetic activities

The summary of the geomagnetic indices and solar interplanetary parameters during quiet, low, moderate and intense storm days is presented in Table 2. Visible in the table was the dependent of TEC values along the equatorial ionosphere on not only the Dst values, but also on factors such as IMF- Bz and Kp. The 28 July for instance recorded the lowest Dst value of -3 nT and also had IMF-Bz pointing northward with maximum value of 4.3 nT. In terms of TEC variations, it recorded the least value of TEC variation. This was not the same during increased geomagnetic activities where the Dst values were lowest at -107, -101, -83, and -60 nT. The IMF-Bz pointed southward in all the days and also had enhanced TEC variation, which was dependent on season. The Kp values ranged between 1(quiet day) to 6 (intense storm day) and correspondingly have 37 TECu and 60 TECu. The variation of TEC with Kp was similar to its variation with Dst. The behaviour of the Ap values are similar to that of Kp variations and so can be used in place of one another. The variation of Vp values with TEC was such that an abrupt increase in Vp resulted to enhanced TEC, which was also dependent on seasons.

CONCLUSION

TEC variations during different geomagnetic activities revealed day-to-day, monthly and seasonal variations. The amplitude of TEC is dependent on time of the day and the activity of the Sun. Geomagnetic storm enhances the TEC

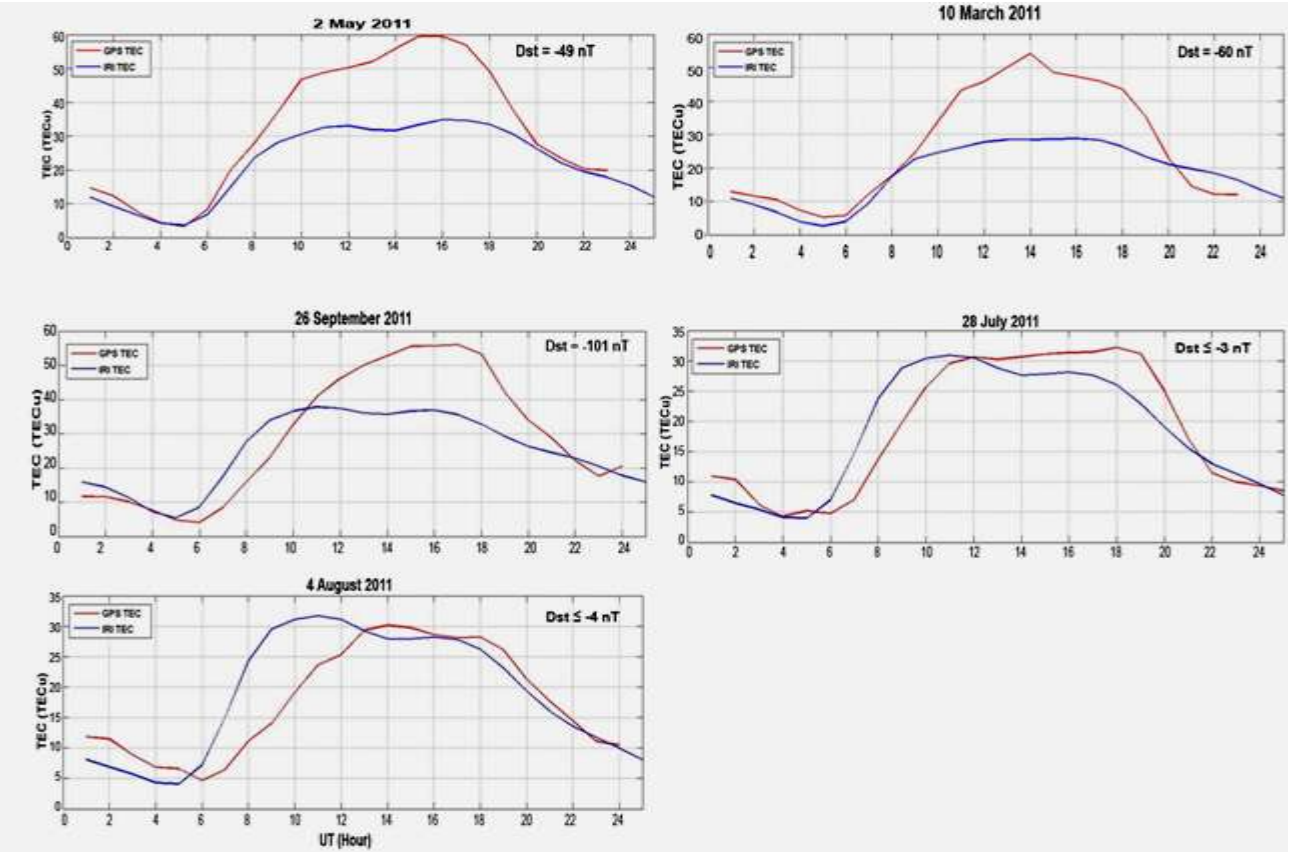

Fig. 4. Diurnal Variation of GPS and IRI TEC during different geomagnetic activities.

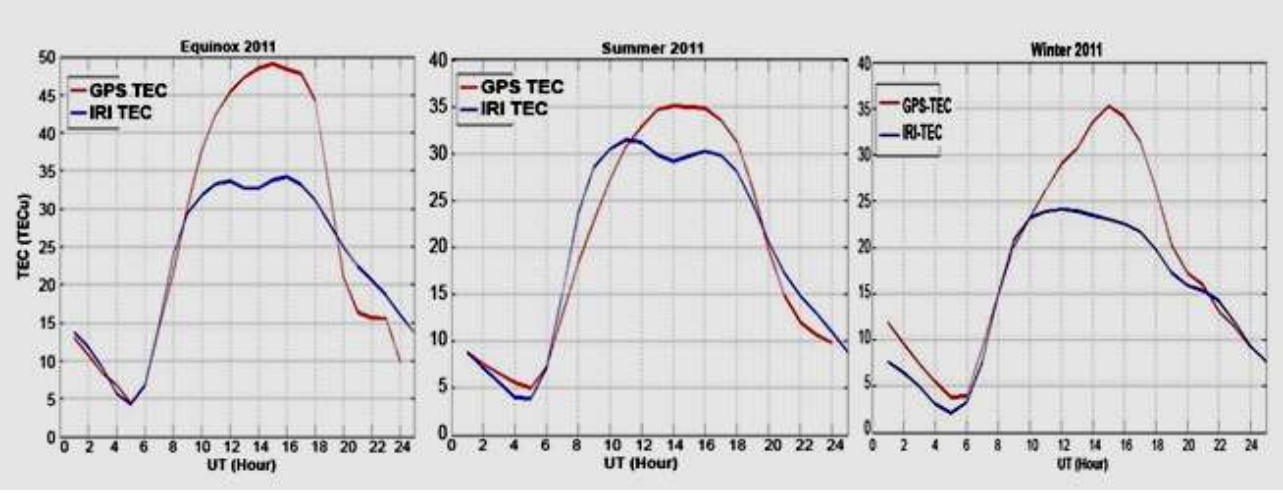

Fig. 5. The Seasonal Variation of GPS-derived and IRI-derived TEC in Ile-Ife.

variations. Comparative results between GPS- and IRI-derived TEC showed similar pattern of diurnal variations. The TEC increases gradually from hours of minimum TEC (06:00 – 07:00 LT) during all seasons, reaching maximum during the day (11:00 – 18:00 LT). At sunset, the TEC values decreased, reaching minimum at about sunrise. The study also revealed that IRI-2012 underestimates the GPS TEC in all seasons during the daytime plateau. The underestimation was highest during the effort by International Geophysical Year (IGY) through coordinated global observations has yielded in increased ionospheric research to primarily help in the design and operation of HF radio wave communication systems. The African region covers a highly variable part

Table 2. The Correlation of geomagnetic indices with TEC variations during different geomagnetic activities.

Storm	Dst (nT)	Max. Kp	Max. Ap	Max. Vp (km/s)	Max. IMF-Bz(nT)	Max. TEC (TECu)
Quiet day (July 28)	-3	1	5	360	+4.3	37
Low Storm (May 2)	-49	4	32	700	-3.2	64
Moderate Storm	-60	4	39	300	-7.3	59
(a) March 10	-83	6	67	400	-10.5	60
(b) March 11						
Intense storm						
(a) August 6	-107	6	94	600	-7.0	48
(b) September 26	-101	6	94	700	-16.4	60

of the equatorial electrojet and EIA (Equatorial Ionisation Anomaly) phenomena making its predictability difficult. The need for accurate ionospheric TEC (Total Electron Content) models at global and regional scales has also been stressed. The results of this research have revealed the need for adjustment in the IRI-2012 for better representation of low-latitude ionosphere, more especially Ile-Ife, Nigeria.

ACKNOWLEDGEMENT

The authors are grateful to the World Data Centre for Geomagnetism, Kyoto University, Japan, and OMNI centre for the provision of data used in this research. We acknowledge Prof. P. Doherty of the Institute of Scientific Research, Boston College, USA, and the Air Force Research Laboratory (AFRL), USA, for making available the GPS device for research in the Department of Physics and Engineering Physics, Obafemi Awolowo University, Ile- Ife, Nigeria. We also thank G.K. Seemala for making available the GPS TEC software.

REFERENCES

Abdu, MA., Batista, IS. and de Souza, JR. 1996. An overview of IRI-observational data comparison in America (Brazilian) sector low latitude ionosphere. Adv. Space Res. 18:13-22.

Ariyibi, EA., Joshua, EO. and Rabiu, AB. 2013[b]. Studies of Ionospheric Variations during Geomagnetic Activities at the Low-Latitude Station, Ile-Ife, Nigeria. Acta Geophys. 61(1):223-229, DOI: 10.2478/s11600-012-0039-3.

Bagiya, S., Mala, JHP., Iyer, KN., Aggarwal, M., Ravindran, S. and Pathan, BM. 2009. TEC variations during low solar activity period (2005-2007) near the Equatorial Ionospheric Anomaly Crest Region in India. Annales Geophysicae. 27:1047-1057. http://dx.doi.org/10.5194/angeo-27-1047-2009.

Ezquer, RG., Ortiz de Adler, N., Radicella, SM., Mosert, M. and Manzano, JR. 1995. IRI and BPM total electron content predictions for Tucuman. Adv. Space Res. 15:121-124.

Fayose, RS., Rabiu, AB., Oladosu, O. and Groves, K. 2012. Variation of Total Electron Content and Their Effect on GNSS over Akure, Nigeria. J. Appl. Res. 4**(**2): doi:10.5539/apr.4(2), 105.

Fedrizzi, M., de Paula, ER., Langley, RB., Komjathy, A. and Batista, IS. and Kantor, IJ 2005. Study of March 31, 2001 magnetic storm effects on the ionosphere using GPS data. Advances in Space Research. 36(3):534-545.

Gopi, S. 2010. Rinex GPS-TEC program, version 1.45. Boston College.

Iyer, KN., Joshi, HP., Jivarajani, RD. and Arvindakshan, P. 1996. Comparative study of TEC near the crest of the equatorial anomaly with IRI model for solar minimum to solar maximum. Adv. Space Res. 18(6):233-236.

Jimoh, OE., Yesufu, TK. and Ariyibi, EA. 2016. Investigation of Ionospheric Response to Geomagnetic Storms over a Low Latitude Station, Ile-Ife, Nigeria. Acta Geophysica. DOI: 10.1515/acgeo-2016-0013.

Klobuchar, J. 1986. Design and characteristics of the GPS ionospheric time-delay algorithm for single frequency users, in: Proceedings of PLANS'86 – Position Location and Navigation Symposium, Las Vegas, Nevada. 4(7):280-286.

Langley, RB. 2000. GPS, the ionosphereand the solar maximum. GPS World. 44-49.

Ogunade, SO. 1987. Geomagnetic variations in south western – Nigeria: Preliminary results. Ann Geophys. 06 B. 607-611.

Olatunbosun, LG. and Ariyibi, EA. 2015. Studies of Total Electron Content variations at low-latitude stations within the Equatorial Ionization Anomaly zone. IOSR Journal of Applied Physics. 7(5):12-24.

Peymirat, C., Richmond, AD. and Kobea, AT. 2000. Electrodynamic coupling of high and low latitudes: Simulations of shielding/overshielding effects. J. Geophys. Res. 105(A10): 22,991–23,003, doi:10.1029/2000JA000057.

Rishbeth, H. and Setty, CSGK. 1961. The F-layer at sunrise. J. Atmos. Terr. Phys. 20:263.

Shastri, S., Aggarwal, S. and Sethi, NK. 1996. Performance of IRI model prediction of F-region for Indian latitude. Adv. Space Res. 18(6):41-44.

Received: Nov 30, 2016; Accepted: Dec 20, 2016

Canadian Journal of Pure and Applied Sciences
Vol. 11, No. 1, pp. 4151-4156, February 2017
Online ISSN: 1920-3853; Print ISSN: 1715-9997
Available online at www.cjpas.net

OPTICAL ANALYSIS OF ISOTACTIC POLYPROPYLENE: CHARACTERIZE THE TYPES OF ISOTACTIC POLYPROPYLENE SPHERULITES α AND β, AND THEIR OPTICAL PROPERTIES

*Sokainah Rawashdeh[1] and Ayed Alsharafat[2]
[1]Department of Physics and Applied Science, Faculty of Engineering Technology
Al-Balqa' Applied University, Al-Salt, Jordan
[2]Department of Physics, Faculty of Science, Jordan University, Amman, Jordan

ABSTRACT

The optical properties of isotactic polypropylene were studied according to different crystallization temperatures. Early beginning of growth of isotactic polypropylene were observed at different stages of growth, where the structures begins with primary nuclei developed through isolated single lamella, then develops into a lamellar sheaves and finally attains the spherulitic structure. Two main types of spherulites, α and β spherulites appears for the isotactic polypropylene over a wide range of crystallization temperature. However, the difference between spherulites types appears due to the difference in its contents of radial lamellae and cross hatching beside the difference in crystallization temperature and melting points.

Keywords: Isotactic polypropylene, fiber morphology crystallization, spherulites, optical properties.

INTRODUCTION

Polypropylene is one of very important polymers , it has double forms; plastic and fiber. Isotactic polypropylene is known to exhibit in several crystalline forms, the monoclinic α-form, the hexagonal β-form, and the triclinic γ-form (Norton and Keller, 1985; Varga, 1992). While, α-form is the stable and is also the most prevalent one. The β-form is observed occasionally during crystallization and it appears as a minority constituent of the isotactic polypropylene. Under special crystallization conditions or when selective β-nucleates are used, higher levels of the β-form can be produced (Tjong *et al*., 1996). The microstructures and mechanical properties of α-form isotactic polypropylene have been investigated extensively. In contrast, fewer studies have been made on the morphology and mechanical behavior of the β-form isotactic polypropylene. Another study, Jeffery *et al*. (2000) have reported different levels of the β-form by adding a small amount of a quinacridone dye nucleation agent. They also reported that isotactic polypropylene which contains high levels of the β-form exhibits lower values of the modulus and yield stress but higher elongation at break. Pawel (1994) investigated that a high purity of the β-phase can be formed in isotactic polypropylene by adding a specific biocomponent β-nucleator consisting of equal amounts of pimelic acid and calcium stearate . The relative β-phase content can reach as high as 94% by adding only 0.001 of such β-nucleates. Clark and Hoffman, (1984) studies the existence of two crystal growth regimes. The occurrence of a regime III/II transition would exhibit a downward change in the slope with increasing crystallization temperature. The regime III to regime II transition occurred near 137˚C. Earlier study, Allen and Mandelkern (1987) reported a regime II/I transition at about 152˚C. They found that the regimes do not serve as boundaries between distinct morphological textures. Sadler (1987) found that low molecular mass ipp fractions, the presence of a regime II/I transition is well-defined by both observations from linear crystal growth and overall crystallization measurements. Data from morphological observations carried out from solutions and from the melt (Khoury, 1966) show a three dimensional array of a nearly orthogonal cross-hatched lamellar texture. Solution crystallization studies have elucidated the basic morphology as being lath line chain-folded lamellar crystals. These crystals formed relatively open networks in solution –grown aggregates, while tightly interwoven textures appeared during melt crystallization. It has been observed that such lamellar branching is characterized by the constant angle between daughter and mother lamellae (80˚ or 100˚). From the two orthogonal components of the cross-hatch, the radial lamellae (mother lamellae) by themselves would generate negatively birefrengent spherulites as in β-form spherulites. The tangential lamellae (daughter lamellae)

*Corresponding author e-mail: sokainahrawashdeh@yahoo.com

would generate their own positive birefringence. However, the latter occurs in combination with the radial lamellae. The presence of the tangential lamellae reduces the negative birefringence and if in sufficient quantity, may actually impart their own sign, rendering the spherulite positively birefringent. From the previous studies, there appears to be no morphological distinct stage where birefringence changes from positive to negative during isothermal crystallization or heating. In this work, particular attention is served to crystallization conditions and their influences on the melting behavior and morphological change in the isotactic polypropylene. Van der Meer (2003) found that the isotactic polypropylenes synthesized by metallocene catalysts show unique properties in the sense that the system allows us to study the influence of two different kinds of defects on the crystallization.

In this study we want to characterize the types of isotactic polypropylene spherulites α and β, and their optical properties.

MATERIALS AND METHODS

During this study the used materials are a homopolymer of isotactic polypropylene originally supplied by (PSCC) at RAPRA, SHAWBURY, SHOPSHIRE, UK. Its molecular mass has been measured by PSCC to be Mn=4.7 × 104 and Mw= 4.2 × 105. The samples were used in the pellets form.

Optical Microscopy

In the present study, the sample was placed on a Nikon microscope type (FX-35DX) with cross polarization condition. The sample is in the hot stage above the melting point of ipp at 200°C, and then it was cooled to different crystallization temperatures. The spherulitic growth at crystallization temperature was monitored in most cases and the resulting spherulites were photographed by Nikon 35 mm, the Nikon microscope was connected to photo monitor to measure the transmitted light intensity of spherulites.

RESULTS AND DISCUSSION

In our study for the α-phase the melting is associated with a continuous decrease of the relative light intensity until 145°C, above that temperature there is an increase in the relative light intensity associated due to the melting and recrystallizing of the cross-hatched lamellae which are thin to form more radial perfect lamellae, at crystallization temperature 140°C the form α- spherulites has mixed from α_1 and α_2-spherulites, so that there is a slight increase in the light intensity which is transmitted from the mixed α- spherulites (Zhang *et al.*, 1996).

As we see that the scanning electron micrograph given in Figure 1, shows embryos appearing as 100 nm dots in many regions as shown in the optical micrograph of isotactic polypropylene crystallized from the melt, after several minutes from the isothermal crystallization at 125°C. The observations demonstrate that an embryo below a critical size disintegrates. The embryos can be seen in the regions A and B. In Figure 2. These embryos have growing fronts where polymer chain segments fold into the crystal lattice. Eventually, similar embryo grows into a founding lamella as shown in region A Figure 3.

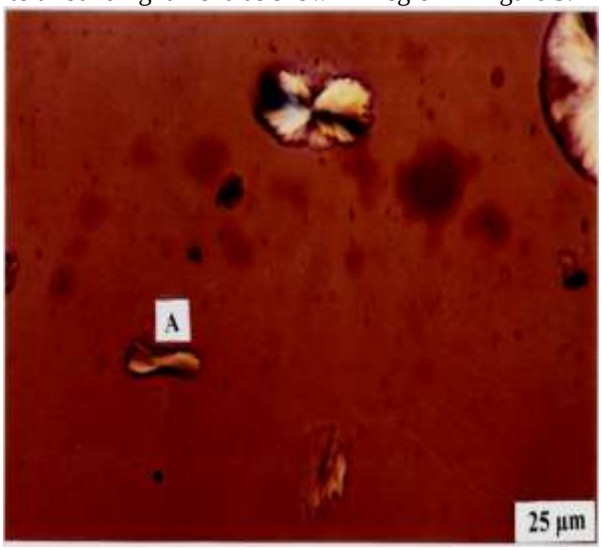

Fig. 1. Optical photograph of isotactic polypropylene crystallized from the melt at 125°C, under crossed polarization conditions showing the beginning of embryos appearance as a dots in many places in addition to other objects as growing lamellae as shown in region A.

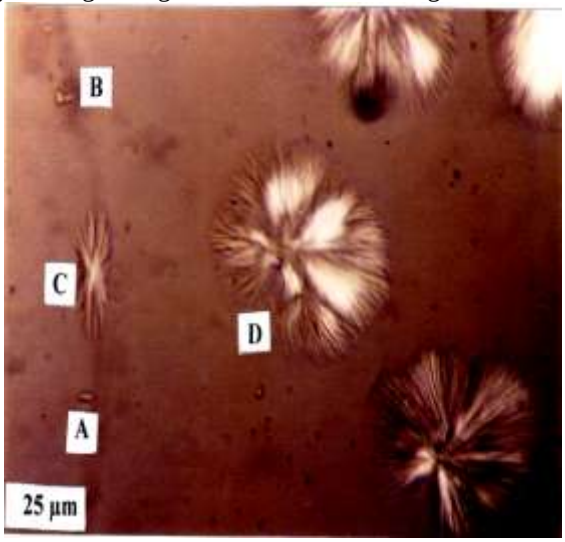

Fig. 2. Optical photograph of dots embryos of isotactic polypropylene in different places in addition to isolated lamellae as shown in region A and B. the figure shows also more advanced growing objects such as the multilayer branching region C and sheaf-like object region D. the crystallization temperature is 125°C.

Another embryo can be found in the middle of Figure 4, this embryo appears to integrate to form an isolated single lamella. An embryo below a critical size is not stable, so that it can disintegrate. Once an embryo grows larger than the critical size, as predicated by the thermodynamics keynities, it can grow continuously at both ends and develop into a single lamella as shown in Figure 3 region A.

There is a founding lamella in Figure 1 region A. this founding lamella grows in two directions. Branching occurs in the middle of founding lamella, so that an induced nucleus formed next to the founding lamella, developed into a subsidiary lamella.

Fig. 3. Optical photograph of isotactic polypropylene, crystallized at T = 125°C. showing isolated single lamellae region A and different orientation of the a sheaf-like object region B.

Fig. 4. Optical photograph of isolated single lamella of isotactic polypropylene which crystallized at Tc= 125°C.

Such subsidiary lamella then grows both forward and backward. Therefore, other subsidiary lamella is formed at both sides of the founding lamella as shown in region C Figure 2. Branching and splaying continue, so that, as can be seen for similar founding lamella, the structure develops into a lamellar sheaf consisting of many lamella as shown in region B Figure 3. High degraded isotactic polypropylene can be produced when the sample of ipp crystallized from melt has low thickness, as shown in Figure 5 highly degraded sample shows positive α-spherulites independently of the crystallization temperature, where monofibrils and small angle branches of fibrils became visible even by optical microscopy.

At the edges of the specimen where it's crystallized from the melt, there is a lack of crystallization of isotactic polypropylene. This can be seen in Figure 6. In this figure the sample was crystallized isothermally at 145°C, where it can be seen to be a composite structure of narrow central thread strung with small platelets. This behavior is similar to the narrow fibrils which become overgrown with platelets in the characteristic fashion when they are allowed to nucleate from polymer solution (Al-Raheil *et al*., 1998a). In short, this fiber morphology is regarded as it clearly obvious, as a nucleation of fibril followed by epitaxial overgrowth of lamellae sharing a common chain axis orientation along the fiber. The fiber itself results from strain-induced crystallization, which means that, from distorted molecular conformations in which chains have been brought and maintained parallel for long enough to nucleate crystallites. The circumstances where such fiber to occur, is probably involvement of some stresses on partly melted molecules as the growth moves through the melted polymers in convective flow. The fiber growth in the molten polymer has a great technical importance, being related to processes of molding and extrusion.

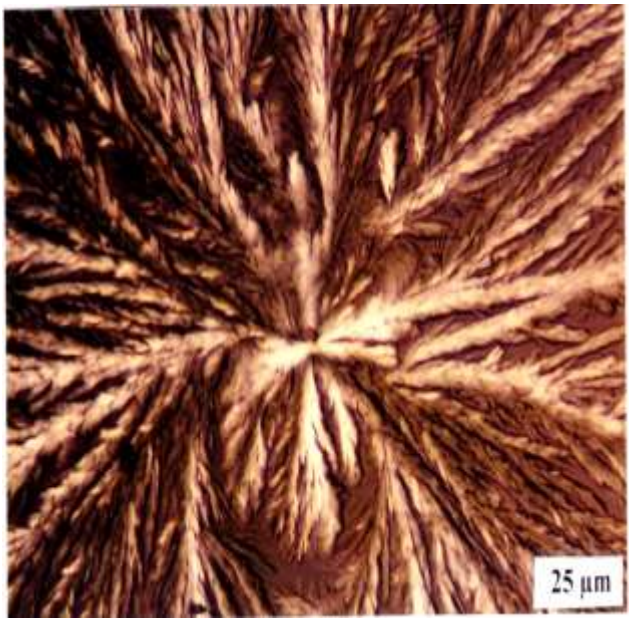

Fig. 5. Optical photograph of highly degraded α-spherulites, Tc= 135°C.

It is now possible a more informed look at row nucleation in crystallization of isotactic polypropylene from the melt as exemplified by Figure 7. When the melt is under strain the probability of bringing chains parallel for long enough to nucleate a crystal embryo will increase.

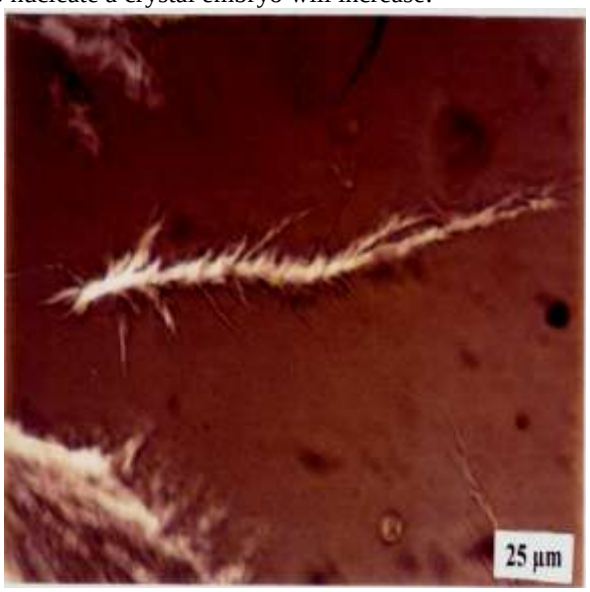

Fig. 6. Optical photograph of fiber morphology crystallization of isotactic polypropylene at the edge of specimen, Tc=145°C.

As it does for fiber morphology, once a crystallite has formed, the chance of generating a row nucleus in this way will increase with strain and with crystallization temperature. After a row nucleus has formed it is likely to initiate transverse growth perpendicular to the direction of strain. The reason for this row nucleation is that molecular conformations are being drawn out, the more so far longer molecules. Moreover, the extension in the flow field will tend to form a series of nuclei in a row positively discourage molecular back folding. One expects therefore, row nuclei containing reasonably chain-extended molecules on which may deposits, under suitable conditions of low temperatures and modified flow, lamellar overgrowths.

Figure 8 shows an intermediate stage of growth in a different part of specimen for isotactic polypropylene crystallized from melt at 125°C. This figure shows two kinds of spherulites, the first is α-type spherulites and exhibits a dark contrast, the second is a β-spherulites having a bright contrast. In all observations which were carried out on the crystallization of this polymer at 125°C , the measurements indicates that the growth of β-type spherulites is slower than α-type spherulites, with an agreement with the results obtained previously by Al-Raheil *at el*. (1998b), where they found that β-type spherulites appear to be slower in growth than α-type spherulites up to 142°C, and above 142°C the α-type spherulites has higher growth due to low temperature melting of β-spherulites. They found also the β-spherulites usually form only when the crystallization temperature is below 132°C. To measure the growth rate of β-spherulites above 132°C the procedure is to make two step crystallization. The first step is to crystallize the specimen of isotactic polypropylene at temperature below 132°C. Once the β-spherulites appear in the specimen at the early stages of growth, the temperature of the specimen can be raised to higher crystallization temperature more than 132°C; therefore the growth of β-spherulites can be measured at the new temperature, as a second step of crystallization.

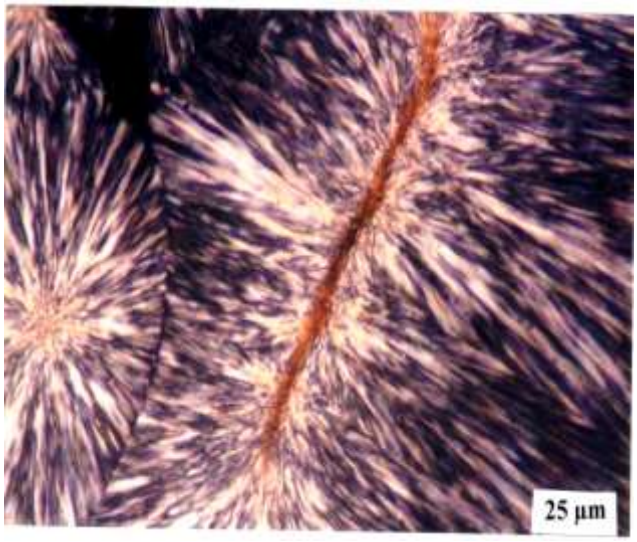

Fig. 7. Optical photograph of row nucleation in crystallization of polypropylene which crystallized at Tc=128°C.

However, it was found in the present results, the proportions of β-spherulites are much less than α-spherulites for samples which contain both modifications, the proportions of β-type spherulites decreases with increasing the crystallization temperature, and it cease, completely to be appeared above 132°C crystallization temperature, if the crystallization was carried by one step above the mentioned temperature. However in most cases, the β-form does not exceed 15% of the crystallization material. Figure 9 shows a region of isothermally crystallized sample of 128°C. In this figure two modification of α and β spherulites can be identified. In general, the β-spherulites have a larger size than α-spherulites, despite the fact that β-phase occupies, on the whole, a smaller fraction. It can be seen that inter-spherulitic boundary between boundary the α and β-types is always curved, with the concavity oriented towards the α-phase. The reason for the concavity is due to the higher crystallization growth of β-spherulites at that temperature. Upon heating, the β-phase melts at 152 °C leaving the α-spherulites alone as shown in Figure 9 and 10. The contrast of α-type spherulites can be seen in Figure 9 as dark region with positive birefringence due to high

density of cross-hatching lamellae. The α-spherulite in Figure 9 can be identified as α_1-type. With increasing the temperature, the cross-hatching lamellae start to melt gradually. Therefore, the dark contrast of α_1-type spherulite changes to bright with negative birefringence due to the melting of tangential lamellae as shown in Figure 10. According to that there is a transformation from type α_1 to α_2 spherulites, and the α-spherulites which can be seen after melting of β-spherulites in Figure 10 can be considered as α_2-type. In fact, the two types of α-spherulites (Padden and Keith, 1959) are distinguishable by the different degrees of cross-hatching. Hence, without the cross-hatched lamellae, the spherulite should be a type α_2.

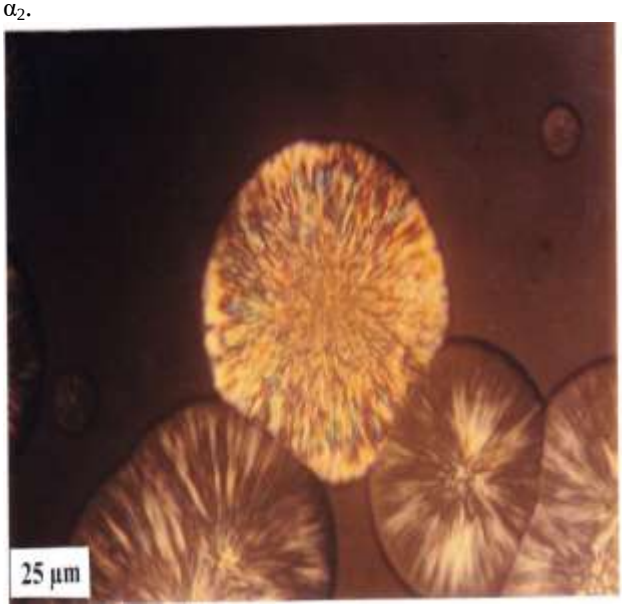

Fig, 8. Optical photograph of two types of spherulites α-spherulites and β-type spherulites, the β-spherulites is bright while the α-spherulites have a dark appearance, Tc=125°C.

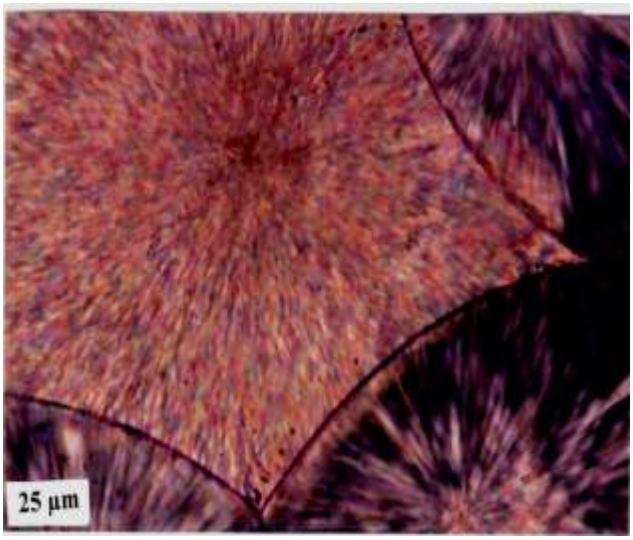

Fig. 9. Optical photograph of α-spherulites and β-spherulites, Tc=128°C.

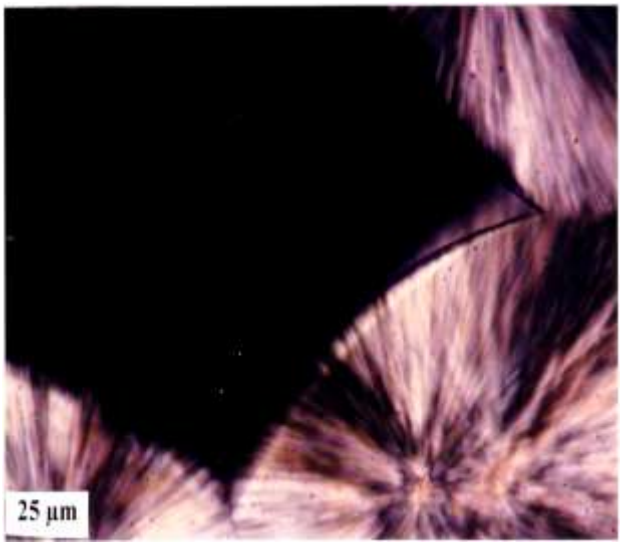

Fig. 10. Optical photograph of melting of β-spherulites at T_m=152°C, T_c=128°C.

CONCLUSION

According to the above results, it's clear that the isotactic polypropylene is crystallized from melt. Four types of spherulites were identified; β-spherulite, α_1-spherulites, α_2-spherulites and mixed α-spherulite. β-spherulites and α_1-spherulites form below 132°C, mixed α-spherulites grows in temperature range 132-145°C, while α_2-spherulite forms at high crystallization temperature above 145°C.α_1-spherulites contains two types of lamellae cross-hatch and redial lamellae, but α_2-spherulites contains only the radial lamellae, so that the mixed α-spherulites has lower contents of cross-hatch lamellae comparing with pure α_1-spherulite. For sample contains two modifications of α and β-spherulites, it was observed that β-spherulites melts first at 152°C while α-spherulites melts at 167°C. Sometimes if there are induced strains in the melt crystallized isotactic polypropylene fibril structures and row nucleation may be observed.

REFERENCES

Allen, RC. and Mandelkern, L. 1987. Structure of poly carpolactam obtained in anionic bulk polymerization. Polymer. 17 (22):473.

Al-Raheil, IA, Qudah, AM. and Al-share, M. 1998[a]. Isotactic polypropylene crystallized from the melt. I. Morphological study. Journal of Applied Polymer Science. (67):1259.

Al-Raheil, IA., Qudah, AM. and Al-share, M. 1998[b]. Reproductive toxicity and infertility effect of ferula hormonis extracts in mice. Journal of Applied Polymer Science. (67):1267.

Clark, EJ. and Hoffmann, JD. 1984. Crystallization and morphology of poly ethylene oxide crystallized from melt. Macromolecules. 10(17):878.

Jeffery, LH. and John, B. 2000. Banded spherulitic growth in liquid crystal. Journal of Crystal of Growth. 4 (217):332-343.

Khoury, FJ. 1966. The spherulitic crystallization of isotactic polypropylene from solution: On the evolution of monoclinic spherulites from dendritic chain-folded crystal precursors. J. Res. nati. bur. stand**.** (70A):29.

Norton, DR. and Keller, A. 1985. The spherulitic and Iamellar morphology of melt-crystallized isotactic polypropylene. Polymer**.** (26):704.

Padden, FJ. and Keith, HD. 1959. Spherulitic Crystallization in Polymers. J. Appl. Physics**.** (30):1479.

Sadler, DM. 1987. On surface morphology and drawing of polypropylene films. Polymer. 13 (28):1440.

Tjong, SC., Shen, JS. and Li, RKY. 1996. Crystallinity in the polypropylene and crystallization conditions. Polymer. 10(12):2309.

Van der Meer, DW. 2003. Structure-Property Relationships in Isotactic Polypropylene. Netherlands: Twente University Press.

Varga. 1992. Super molecular structure of isotactic polypropylene. J. Materials Sci. 10 2557-2579.

Zhang, SC., Shen, JS. and Li, RKY. 1996. Morphological behavior and instrumented dart impact properties of β - crystalline-phase polypropylene. Polymer**.** (12):2309.

Received: Sept 9, 2016; Revised: Dec 31, 2016; Accepted: Jan 2, 2017